A NONLINEAR THEORY OF COSSERAT ELASTIC PLATES USING THE VARIATIONAL-ASYMPTOTIC METHOD

A Thesis
Presented to
The Academic Faculty

by

Ravi Kumar Kovvali

In Partial Fulfillment
of the Requirements for the Degree
Doctor of Philosophy in the
School of Aerospace Engineering

Georgia Institute of Technology
December 2015

A NONLINEAR THEORY OF COSSERAT ELASTIC PLATES USING THE VARIATIONAL-ASYMPTOTIC METHOD

Approved by:

Professor Dewey H. Hodges, Advisor
School of Aerospace Engineering
Georgia Institute of Technology

Professor Graeme J. Kennedy
School of Aerospace Engineering
Georgia Institute of Technology

Professor Massimo Ruzzene
School of Aerospace Engineering
Georgia Institute of Technology

Professor Michael J. Leamy
School of Mechanical Engineering
Georgia Institute of Technology

Professor Julian J. Rimoli
School of Aerospace Engineering
Georgia Institute of Technology

Date Approved: 18 August 2015

DEDICATION

To my incredible parents,

Drs. Vijaya Lakshmi & Bala Subrahmanyam Kovvali.

Your love and affection has kept me going.

ACKNOWLEDGEMENTS

It is an absolute pleasure to express my profound gratitude to all those who have made everything that follows in this dissertation possible.

No words I write here can do justice to express how thankful I am to be given the opportunity to have Prof. Dewey H. Hodges as my doctoral advisor. His guidance and motivation have always been immensely valuable and often exceeded what I could have hoped for. Beyond his sheer brilliance made obvious by an impressive body of work, I am certain I have had the pleasure to work with the most wonderful human being I have ever come across. I will forever remember and cherish everything he taught me.

I would like to sincerely thank the members of my thesis advisory committee, Drs. Massimo Ruzzene, Julian Rimoli and Graeme Kennedy, for your enthusiasm and providing valuable feedback. In addition, I would also like to thank Dr. Michael Leamy for serving on my final doctoral examination committee.

A person's interest in a particular field of study is often the result of exemplary teachers. My interest in the general area of solid mechanics was sparked by Prof. K. Bhaskar (IIT Madras). The lectures by Prof. Olivier Bauchau (Georgia Tech) that I was fortunate to attend only served to greatly increase my fascination of the subject. I must also wholeheartedly thank Prof. Dineshkumar Harursampath (IISc. Bangalore) for encouraging me to pursue graduate studies – it is very likely I would not be writing this dissertation if it was not for the stimulating interactions we have had.

To the set of excellent individuals that I had the opportunity to work with during my time at Georgia Tech, I owe you a lot. I would especially like to thank Dr. Anurag

Rajagopal, Dr. Zahra Sotoudeh and Mohit Gupta for the innumerable discussions, technical and otherwise!

An excellent set of friends made my days in Atlanta that much sweeter. I am greatly indebted to Shilpa Mahamulkar, who has been an unbelievable source of support for me during the past few years. Thank you for your constant love and affection. To Sandeep, Sravani, Sampath, Balachandra, Bhanu, Bhuvana and Uma, I thank you for your friendship and will always treasure the times we spent together.

On a rather peculiar note, I would like to thank Apple Inc. for the truly amazing products they create. It is no joke when i say that part of the motivation to sit and work at a computer all day has been because of their Macintoshes. They remind me everyday strive to be the best I can and, of course, think different.

Last, but in no way the least, I would like to express my deepest gratitude towards my family: my mother, Dr. Vijaya Lakshmi Kovvali, my father, Dr. Bala Subrahmanyam Kovvali, and my sister, Jayasri Kovvali. You have always showered me with immense love, trusted my choices and believed in my abilities. For that, I am truly thankful from the bottom of my heart and I dedicate this thesis to you. None of my accomplishments would have been possible without your blessings.

TABLE OF CONTENTS

LIST OF TABLES

LIST OF FIGURES

SUMMARY

One of the most important branches of applied mechanics is the theory of plates - defined to be plane structural elements whose thickness is very small when compared to the two planar dimensions. There is an abundance of plate theories in the literature modeling classical elastic solids that fit this description. Recently, however, there has been a steady growth of interest in modeling materials with microstructures that exhibit length-scale dependent behavior, generally known as Cosserat elastic materials. Concurrently, there has also been an increased interest in the construction of reduced dimensional models of such materials owing to advantages like reduced computational effort and a simpler, yet elegant, resulting mathematical formulation.

The objective of this work is the formulation and implementation of a theory of elastic plates with microstructure. The mathematical underpinning of the approach used is the Variational Asymptotic Method (VAM), a powerful tool used to construct asymptotically correct plate models. Unlike existing Cosserat plate models in the literature, the VAM allows for a plate formulation that is free of a priori assumptions regarding the kinematics. The result is a systematic derivation of the two-dimensional constitutive relations and a set of geometrically-exact, fully intrinsic equations governing the motion of a plate. An important consequence is the extraction of the drilling degree of freedom and the associated stiffness. Finally, a Galerkin approach for the solution of the fully-intrinsic formulation will be developed for a Cosserat surface analysis which will also be compatible with more traditional plate solvers based on the classical theory of elasticity. Results and validation are presented from linear static and dynamic analyses, along with a discussion on some challenges and solution techniques for nonlinear problems.

CHAPTER I

INTRODUCTION

1.1 An Overview of Higher-Order Elasticity Theories

A Cosserat or micropolar continuum can be defined as one in which each material particle has six degrees of freedom, with three independent rotational degrees of freedom along with three translational degrees of freedom associated with a classical (or Cauchy) continuum. Although the concepts leading to the development of generalized continuum models were discussed as early as the late nineteenth century by Voigt [153], Kelvin, Helmholtz, Duhem and others, it was the seminal work of E. and F. Cosserat [25] in 1909 that presented the governing equations for a three-dimensional Cosserat continuum, as well as a two-dimensional analogue called a Cosserat surface, that were nonlinear and geometrically-exact. Such a Cosserat continuum also postulates the independent existence of forces and moments (or force stresses and couple stresses) along with independence of translations and rotations. However, these initial efforts by the Cosserats did not address how the constitutive laws for such a theory could be established, limiting its use.

After being forgotten for nearly half a century, there was a revival of interest in the use of generalized continuum models starting in the late fifties to explain the discrepancy between the results of classical elasticity and experiments in cases where the microstructure of the body is significant – in the neighborhoods of cracks and notches with appreciable strain gradients, and in granular media. Notable amongst these are the works by Günther [58], Truesdell and Toupin [150, 148], Grioli [57], Aero and Kuvshinskii [1, 87], Mindlin and Tiersten [101], Koiter [81], Palmov [111], all of whom developed a linear Cosserat theory called a Couple-Stress Theory. Common

to all these higher-order elasticity theories is the appearance of a material-dependent length-scale parameter that is thought to be microstructure-dependent. This also led to the prediction of several non-classical phenomena: for example, Mindlin [100] predicted that the stress concentration factor for a circular hole would be smaller than the classical value, and is dependent on the size of the hole itself. Also, the flexural rigidity of very thin plates was predicted to be higher than those from a classical Kirchhoff-Love theory. However, in a couple-stress theory, despite the continuum being able to support couple stresses, the rotation of each material point, called the *microrotation*, was not independent and taken to be the *macrorotation* of the medium (and hence determined by the displacement field).

Shortly, Eringen [38] developed what was termed as a linear theory of micropolar elasticity. The term micropolar, coined by Eringen, implied that the microrotation of each material point was distinct from the macrorotation while also including effects of rotary inertia. The previous couple-stress theory was now termed indeterminate because the antisymmetric part of the stress tensor could no longer be determined solely by constitutive relations. Later, a nonlinear theory of micropolar media was developed by Kafadar and Eringen [79]. Problems involving finite deformations were also studied by Grioli [57], Toupin [149], Nowacki [107], Besdo [11] and Reissner [124, 126, 127]. A more exhaustive set of references highlighting the development of micropolar[1] elasticity in this period can be found in the excellent review article by Altenbach et al. [3].

It is interesting to note that most of the modeling efforts in literature deal with isotropic polar media. While it is possible that these efforts have concentrated only on applications where material isotropy was present (despite microstructures like rigid inclusions and voids), another practical reason can be understood by looking at the

[1]For the sake of brevity, the words *Cosserat*, *micropolar* and *polar* will be used interchangeably henceforth.

three-dimensional constitutive law for an isotropic micropolar material (using the symbols for the constants used by Eringen [38]):

$$\begin{aligned} \sigma_{ij} &= \lambda \Gamma_{kk} \delta_{ij} + (\mu + \kappa) \Gamma_{ij} + \mu \Gamma_{ji} \\ \mu_{ij} &= \alpha X_{kk} \delta_{ij} + \beta X_{ji} + \gamma X_{ij} \end{aligned} \tag{1}$$

where $\sigma_{ij}, \Gamma_{ij}, \mu_{ij}, X_{ij}$ are the measure numbers of the Jaumann stress tensor, the Jaumann strain tensor,[2] the couple-stress tensor and the wryness tensor[3].

It is immediately clear that we are faced with a problem of identifying *six* parameters for a micropolar material. Classical elasticity for small strain only needed two Lamé moduli to be determined. If one were to look at a fully anisotropic material instead, a staggering 90 material constants would have to be identified! In such cases, one must resort to homogenization techniques [51] or numerical techniques [77] as experimental determination becomes impractical. Nevertheless, some solutions for anisotropic bodies have been developed assuming one had knowledge of these constants (for example, see works by Ieşan [73, 75, 74, 76], Kumar and Choudary [86]).

Fortunately, as will be seen, many engineering applications involving materials with microstructure can be considered isotropic, for which identifying the six parameters will suffice. Before proceeding further, it is necessary to address the following question: How does one experimentally determine these micropolar elastic constants? At a more fundamental level, what is the evidence of this length-scale dependent behavior that the micropolar theory of elasticity seeks to model?

1.2 Evidence of Micropolar Effects and Applications

In 1937, Neuber [106] developed an empirical approach that predicted a reduction of stress-concentration factor below that predicted by classical elasticity in regions of

[2]Since we plan to restrict ourselves to small strain for the present purposes, we choose to work with the mathematically-simpler Jaumann strain tensor.

[3]There are various definitions of the wryness tensor used in literature, a comparative review of which has been conducted by Pietrasczkiewicz [118].

high strain gradients. This has since been confirmed experimentally by Peterson [117], Kuhn and Figge [84] and others. Most of the earlier works discussing micropolar or couple-stress theories could also model the non-classical effects mentioned previously, but did so without experimentally confirming their validity.

In 1966, Schijve [134] was one of the first to attempt experimental validation: testing on aluminum alloy sheet specimens, he concluded that no significant couple-stress effects were present. Ellis and Smith [35] carried out cylindrical bending tests on aluminum and low-carbon steel sheets and concluded that Mindlin's couple-stress theory was inadequate in explaining these phenomena, and that grain size of the material was unrelated to the length-scale parameter present in the theory.

On the other hand, Perkins and Thompson [116] were able to experimentally observe an increase in the shear modulus of a polyvinyl chloride foam plastic as the specimen's thickness diminished as predicted by theory.

Gauthier and Jahsman [47, 48] prepared a composite material with aluminum shot uniformly distributed throughout an epoxy matrix to represent rigid microelements in a deformable continuum. While static torsion tests indicated that the material developed behaved as a classical elastic solid, dynamic tests performed later by Gauthier [46] were successful in determining the micropolar elastic moduli. Importantly, the characteristic length of the material turned out to be very close to the radius of the aluminum particles.

Yang and Lakes [158, 159], Lakes [91, 92, 89] and Park and Lakes [112] determined the elastic properties of porous solids like foams and human bone and interpreted their results in terms of a micropolar theory, noting that characteristic length-scale parameter was close to the size of structural elements in these materials. For a detailed discussion about experimental methods for studying generalized elastic continua, the reader may consult the book chapter by Lakes [90]. In subsequent years, Cosserat models have seen extensive use in describing foams and other porous media (see works

by Diebels [31, 33, 34, 32]) and human bones (Fatemi et al. [41]).

As pointed out by Pabst [110], the application of micropolar theory to solids with periodic microstructure has been more extensive and successful compared to those with random microstructure, natural or man-made. For example, the micropolar elastic moduli of KNO_3 crystals were determined experimentally by Askar [7, 6], with further improvements in modeling made by Fischer-Hjalmars [43, 42]. Pouget et al. [121] applied the micropolar theory to elastic ferroelectric crystals. In 2013, Beveridge et al. [12, 155] tested two kinds of heterogeneous specimens consisting of regular periodic arrays of circular voids – made as aluminum bars and rings from acrylic sheets – and in both cases found that sample stiffness depended on sample size, with stiffness increasing as size reduced. In terms of a micropolar theory, they also note that the characteristic length values obtained reflect the intrinsic length scales of the material given by the void size and spacing.

Engineering applications such as the modeling of micro or nano-scaled structures, carbon nanotubes and graphene sheets, analysis of MEMS (MicroElectroMechanical Systems), ultra-thin films, etc., have also seen widespread use of micropolar theories recently. Chong et al. [19] experimentally observed a size effect in the torsion and bending of micron-scaled structures present in MEMS devices and concluded that a strain-gradient analysis was necessary to determine the elastoplastic behavior in the micron scale. McFarland and Colton [99] studied polypropylene microcantilevers with a non-homogeneous microstructure and report a measurable increase in flexural rigidity at micron-order thicknesses, suggesting relevance in future MEMS applications. Guo and Zhao [59] investigated the size dependance of elastic properties of nanofilms with surface effects.

From this literature search on experimental evidence of length-scale dependent behavior, we can see that initial efforts to identify size effects have been inconclusive

where more recent models appear to be successful, especially when applied to porous media like foams, bone and ceramics. This inconsistency was pointed out and, in part, explained in the theoretical work by Bigoni and Drugan [13], who presented an analytical derivation of Cosserat elastic moduli via homogenization of heterogeneous elastic materials. Their analytical results explain published experimental findings that for a heterogeneous material to exhibit micropolar behavior the inclusions must be less stiff than the surrounding matrix and relatively dilute. On the other hand, for rigid or even relatively stiff inclusions, they showed that Cosserat effects can be neglected.

In conclusion, Cosserat elasticity seems well suited to model either macroscopically heterogeneous structures with voids or relatively compliant inclusions, or micron-scaled structures where specimen dimensions are comparable to the microstructure of the material.

1.3 Previous Work on the Construction of Plate Models

Traditionally, the problem of constructing reduced-dimensional models of beams, plates and shells, either starting from a classical or a Cosserat theory of elasticity, has been approached in one of two ways: the degenerate solid approach and the direct approach. A brief description and analysis of each approach will now be given, mentioning significant contributions from the scientific community to date in the development of plate models starting from a Cosserat or micropolar continuum. This will, then, lead us to a discussion of the principal methodology used in this dissertation.

1.3.1 Degenerate Solid Approaches

These approaches start from the equations of three-dimensional (3-D) continuum mechanics and transition to a 2-D surface problem by means of a dimensional reduction. Largely, this is done in one of two ways. The first method invokes certain

ad hoc assumptions regarding the through-thickness variation of the displacement and stress quantities expressed in terms of 2-D quantities defined on a chosen reference surface. These assumptions are mainly based on engineering intuition. Then, the thickness coordinate is eliminated by integration through the plate (shell) thickness, thereby yielding a 2-D boundary value problem. The Kirchhoff-Love type and Reissner-Mindlin type theories are plate models derived this way, albeit starting from classical elasticity. Likewise, there have been numerous plate theories derived starting from a higher-order elasticity theory.

The first attempt was Eringen's theory of micropolar plates [39] which assumes that the displacements u_1, u_2 vary linearly along x_3, while u_3 and the independent rotations ϕ_1, ϕ_2, ϕ_3 are constant (x_3 taken along the thickness of the plate). Moreover, the normal or "peeling" stress σ_{33} is assumed to be zero. This theory is based on eight unknowns: three averaged displacements, two averaged macrorotations of the cross-sections and three averaged microrotations.

Many others have since adopted and discussed Eringen's approach: Ariman [5] looked at laterally loaded circular micropolar plates. Constanda [23, 24] developed complex variable treatment of bending of micropolar plates with identical assumptions and added the effects of distributed and surface loads, while existence and uniqueness theorems were provided by Schiavone [131, 132], Schiavone and Constanda [133]. A general representation for solutions of Eringen's micropolar plate equations was provided by Wang [154]. Other theories with slightly varying assumptions (such as polynomial representations of through-thickness variations) include those by Steinberg [142, 143], Kvasov and Steinberg [88], Gevorkyan [50], Ambartsumian [4], Gao et al. [45], etc., of which the latter assumes a cubic variation of the in-plane displacements through the thickness (instead of linear) to develop a third-order shear deformation plate model using the (indeterminate) couple-stress theory. Some of the more recent works concerning the analysis of Kirchhoff and Reissner-Mindlin plates

based on couple-stress theory include Tsiatas [151], Kong et al. [82], Yin et al. [160], Jomehzadeh et al. [78], Ma et al. [98], Roque et al. [128] etc., to name a few.

The main drawback of this approach is that there is no justification provided for the ad hoc assumptions made. Also, there are various cases where such assumptions simply will not work (for example, peeling stresses are important while considering composite plates and cannot be assumed to be zero).

A second method of constructing 2-D plate models is by a formal asymptotic method, which takes advantage of the smallness of the thickness of the plate relative to the wavelength of its deformation. The field variables and their governing differential equations are expanded in an asymptotic series to deduce a series of 2-D problems corresponding to different kinds of deformation like membrane, bending and boundary effects. For example, Green and Naghdi [53] derived a set of micropolar plate equations this way which showed complete agreement to those they derived previously by a direct approach [54]. Unlike Eringen's theory, the theory of Green and Naghdi assumes the in-plane displacement components to be independent of the transverse coordinate for a first approximation. Erbay [36] presented an asymptotic theory of thin micropolar plates without a priori assumptions on the exact form of the field variables. Instead, the relative orders of the field variables (displacements, microrotations, stresses, couple stresses) are assumed, scaled in terms of a thickness parameter. It is also shown that Eringen's plate equations coincide with the zeroth-order approximation (with slight differences).

Although these theories are mathematically more rigorous and elegant than those based on ad hoc assumptions, they are still not free of assumptions which are best avoided whenever possible. It will be shown that the approach chosen in this work using the VAM does not need a priori assumptions as other formal asymptotic methods, making it best suited for an engineering approach to plate modeling.

1.3.2 Direct Approaches

These approaches construct what are known as Cosserat surface models: 2-D director plate theories that are not directly derived from a 3-D theory of elasticity. One of the earliest works to construct a reduced-dimensional Cosserat-type model was by Ericksen and Truesdell [37] who developed an exact theory of rods and shells. They introduced the notion of a "directed" curve and surface with deformable directors attached at every point. However, a treatment of the constitutive relations was lacking.

Later, Green et al. [54] formulated a theory of a restricted Cosserat surface (with one deformable director) that is exact, complete and fully consistent with the dynamical and thermodynamical principles of continuum mechanics. Using these results, Green and Naghdi also formulated a linear theory of plates [52], [55] and shells [56]. Cohen and DeSilva [22], DeSilva and Tsai [30] published a nonlinear theory for oriented surfaces undergoing isothermal or non-isothermal deformations, but with three deformable directors. Reissner [125] developed a nonlinear theory of shells allowing for arbitrarily large deformations and strains with equilibrium equations that are geometrically-exact. Other notable efforts in the development of plate (or shell) models are by Altenbach and Eremeyev [2], Pietraszkiewicz and Eremeyev [118], Chróścielewski and Witkowski [20], Pietraszkiewicz and Konopińska [119], where linear and nonlinear models using natural strain measures and exact kinematics are discussed.

All of these models mention, if at all, constitutive equations that are not directly related to the 3-D world. Specific constitutive laws are often developed for these formulations, as described by Naghdi [104]. The elastic constants of the 2-D Cosserat surface (eight in number if isotropic) could be connected to the 3-D elastic constants by comparing the strain energy expressions, as was done by Naghdi and Rubin [105], in [2], [20], among others. Alternately, as suggested by Reissner [125], one would

have to devise suitable experiments for a 2-D continuum to establish a constitutive law. Although relevant constitutive laws could be obtained from such a set of specific experiments, it would be much more expeditious to make use of the comparatively rich experimental data readily available for 3-D continua. A further alternative would be to deduce constitutive equations of a 2-D continuum as an asymptotic consequence of a given system of constitutive equations of a 3-D continuum.

Comparing the two approaches discussed so far, the exact surface kinematics that are available only in a direct approach are crucial to accurately simulate large deformations of a plate structure. If a rational and systematic way to obtain a 2-D constitute law can be established, Cosserat surface models could be very promising for the next generation of shell theories. As will be argued, the approach proposed herein using the VAM seems to be the ideal vehicle to eliminate the need for guessing of constitutive laws: it can be used to obtain asymptotically correct 2-D constitutive relationships from those of 3-D continuum mechanics, supplementing a plate formulation that is geometrically-exact and free from ad hoc assumptions like in [125].

1.4 Proposed Approach

To remedy the inadequacies of existing Cosserat plate theories, a theory is proposed with constitutive relations constructed from a 3-D Cosserat theory of elasticity without invoking any a priori assumptions. Also, exact two-dimensional kinematics of a Cosserat surface will be used as it is the best available model for plates.

The mathematical foundation of this approach is the Variational-Asymptotic Method or VAM. Originally proposed by Berdichevsky [10], the VAM is a powerful mathematical method to construct asymptotically correct models of dimensionally reducible structures. In order to reduce the original 3-D problem to an asymptotically correct 2-D plate problem, one must attempt to reproduce the energy stored in the three-dimensional structure in the 2-D formulation. VAM is used to rigorously split a

general 3-D nonlinear elasticity problem into a 1-D linear through-the-thickness analysis and a 2-D nonlinear plate analysis. This operation results in the replacement of a three-dimensional model with a reduced-order model in terms of an asymptotic series of certain small parameters inherent to the structure, such as the thickness of the plate relative to the wavelength of its deformation. Thus, the solution of the original problem can be approximated asymptotically by sequentially dropping small terms in the energy functional and solving a series of much simpler variational statements.

The proposed approach has been successfully applied by Hodges et al. [65] to construct classical plate models, and by Yu et al. [166, 167, 162] to construct Reissner-Mindlin type models for composite laminated plates. These models, implemented in the computer code VAPAS (Variational-Asymptotic Plate And Shell), have been shown by Demasi and Yu [29] to be as accurate as layer-wise models despite being as simple as equivalent single-layer first-order shear deformation theories. For a detailed description of how VAM can be used to construct reduced-dimensional models, the reader is referred to the book by Hodges [70].

A Cosserat plate theory constructed using the VAM will have the following highly desirable features:

- The theory is geometrically-exact, meaning that the displacement of the reference surface and the rotation of the normal line element are represented exactly. No restrictions such as small deflections or rotations are imposed, making it suitable to be directly incorporated into multi-body dynamics codes.

- No a priori assumptions regarding through-thickness variations of the field quantities are made. Instead, it will be shown that the dimensional reduction procedure using the VAM automatically determines their through-thickness behavior in an asymptotically correct manner.

- All nine components of the stress and couple-stress tensors (and their work-conjugate strain measures) can be recovered through the thickness from standard plate finite element solutions, essentially reproducing 3-D finite element results but with significantly reduced computational effort. This asymptotically-accurate recovery is only possible if one starts with 3-D continuum mechanics.

A Note on Degrees of Freedom and the Drilling Stiffness

Central to this work is the determination of the constitutive equations for micropolar plates. In addition to providing membrane and bending stiffnesses of a Cosserat elastic plate, first-order effects such as the shear stiffness (like in a Reissner-Mindlin theory) and the *drilling stiffness* will also be determined. It is worth noting that the in-plane curvatures, and hence the drilling degree of freedom (rotation about the normal to the plate), do not show up in any plate theory that is based on classical 3-D elasticity.

Indeed, Hodges et al. [64] showed that for a Reissner-type plate theory developed from classical elasticity only 5 independent measures of displacement and rotation are necessary, and the rotation about the normal can be expressed in terms of these 5 variables. Consequently, only 5 equilibrium equations (for statics) or equations of motion (EOM, for dynamics) are derived. A sixth equation used to express moment balance about the normal is expectedly absent due to the reciprocity of the in-plane shear forces (which has been inferred from moment equilibrium conditions in the first place). In all, an intrinsic formulation of a Reissner-Mindlin theory contains 5 equilibrium equations/EOM, 6 compatibility equations and 8 constitutive equations (relating 3 in-plane forces, 3 bending and twisting moments and 2 transverse shear resultants to their work-conjugate 2-D strain measures).

On the other hand, in a 3-D Cosserat theory of elasticity the rotation about the normal is taken to be independent of the other 5 displacement and rotation

measures. Also, the stress tensor is no longer required to be symmetric due to the presence of couple-stresses. Therefore, an intrinsic formulation of a plate theory will be derived containing 6 equilibrium equations/EOM, 6 compatibility equations and 12 constitutive equations (relating 4 in-plane forces, 4 bending and twisting moments, 2 transverse shear resultants and 2 drilling moments to their work-conjugate 2-D strain measures) – a total of 24 equations in as many unknowns.

In the context of a plate (or shell) finite element analysis an independent drilling degree of freedom has always been viewed as advantageous, especially where a plate bending element intersects with, say, a beam element or a membrane element (for example in [71], [137], [44], [72]). This is because the last two elements have six degrees of freedom per node while a plate element based on classical elasticity has five. A common workaround has been to incorporate a drill-rotation and introduce an artificial drilling stiffness which is not inherent to the theory at all. For example, this technique is used in commercial FEA packages like Nastran and Abaqus. It is clear that a nonclassical elasticity theory will result in an additional degree of freedom per node in a theoretical development of plate finite elements and the drilling stiffness is a natural outcome of the theory.

1.5 Specific Objectives of Present Work

The overall objective of this work is the formulation and implementation of a theory of elastic plates with microstructure. The construction of such a theory can be broken up into the following sub-tasks:

- **Plate through-the-thickness analysis**:

  In the context of Cosserat elasticity, this involves reworking most theoretical aspects of the plate formulation (compared to [64], [166], etc.), such as

  (i) plate kinematics, modified to accommodate a rotational field that is independent of the displacement field. Here, we treat the local rotation field to

be an independent 'rotational analogue' to the warping field. (Previously, the latter, along with the 2-D generalized strain measures, completely determined the former).

(ii) the three-dimensional formulation, which relates the 3-D force strain field and, now additionally, the 3-D moment strain field to a set of 2-D generalized plate strain measures. This 3-D moment strain tensor, also referred to as the wryness tensor, is introduced as work-conjugate to the couple-stress tensor which is unique to a Cosserat continuum.

(iii) the dimensional reduction, where we attempt to reproduce the potential energy of the 3-D problem on a 2-D Cosserat surface in an asymptotically-exact manner using the VAM. In this step, we obtain expressions for the zeroth-order and first-order warping and local rotation fields which minimize, respectively, the zeroth-order and second-order total potential energy functionals.

(iv) an energy transformation, to eliminate derivatives containing the 2-D generalized strain measures and package the strain energy expression in a more usable form. In previous efforts using classical elasticity, this yielded a Reissner-like plate model which added contributions of transverse shear measures to those by classical strain measures of a Kirchhoff-Love theory. In the present work, this exercise will yield a model that now adds the contribution of in-plane curvatures to the aforementioned strain measures. As before, partial derivatives of the resulting energy with respect to the 2-D strain measures determines the constitutive equations. Specifically, we pick up for the first time the drilling stiffnesses of the plate, by taking a partial derivative of the energy expression with respect to the in-plane curvatures. Although the drilling stiffness is mentioned a few times in the literature, this is the first attempt to the authors knowledge of determining

it without, say, invoking plane stress assumptions and with a basis in 3-D continuum mechanics.

This through-the-thickness analysis provides (a) a 2-D plate constitutive law, and (b) a set of recovery relations which help recover 3-D stress, strain and displacement data through the thickness from 2-D plate variables (estimated by a separate analysis) in an asymptotic sense. For practical reasons mentioned previously we note that the emphasis here is primarily on isotropic Cosserat elastic materials, although such restrictions are unnecessary from a theoretical standpoint. So, while the formulation has been developed to include orthotropic materials, from a validation standpoint a discussion focused on isotropic materials is deemed sufficient and even preferable.

- **Development of a geometrically-exact analysis of Cosserat plates using Galerkin's method**:

  Having dealt with the through-the-thickness analysis, the next objective is the modeling of a 2-D Cosserat continuum with appropriate kinematics, compatibility conditions, constitutive equations and the equations of motion. As was demonstrated for beams by Hodges [70], starting from Hamilton's extended principle three formulations are possible – a fully intrinsic formulation, a displacement formulation and a mixed formulation. Of these, the present work will reject a complete displacement based formulation due to inherent weaknesses – equations get very long and complicated for general nonlinear analysis and the formulation is tied to a chosen set of displacement/finite rotation variables.

  A fully intrinsic formulation is one which is independent of any displacement or rotation variables. The advantages of an intrinsic theory are it being geometrically-exact, with quadratic being the maximum nonlinearities present and the spatial and time derivatives being a maximum of first order. Also,

unless specifically requested, the equations can be solved without displacement or rotation variables for cases where applied loads are independent of deformation. A mixed variational formulation is also possible combining generalized strains, forces and moments, linear and angular momenta, motion variables along with displacements and rotations into a single formulation. As discussed in [70], it is certainly preferable over a complete displacement based formulation when these variables are necessary. While the fully intrinsic formulation has its advantanges, it is not suitable for dealing nonlinear statics of statically indeterminate structures. Plate problems, being inherently hyperstatic, cannot be dealt with adequately without being augmented with additional kinematical equations involving displacements and rotations. This can be remedied with the use of an incremental method, similar to that developed by Sotoudeh and Hodges [139]. Equations for an incremental method for plates will be developed that can handle both nonlinear statics and nonlinear steady-state calculations.

Hodges et al. [66] presented an intrinsic theory of plates for statics and dynamics starting with classical elasticity. They also discuss potential solution strategies for the resulting intrinsic equations. The main objective of this sub-task is two-fold:

(i) Extend the previous intrinsic theory to Cosserat elastic plates. The intrinsic formulation presented will be applicable to nonlinear statics and dynamics. Among other things, modifications include a sixth equation of motion, updated kinematical and constitutive relations and extra boundary conditions.

(ii) Develop a Galerkin-based implementation of the fully intrinsic variational formulations. Although a fully-intrinsic formulation has been developed for beams by Patil and Althoff [114], Patil and Hodges [115] and a mixed

formulation, called GEBT (Geometrically-Exact Beam Theory), has been developed by Yu and Blair [164] for beams, to the best of the author's knowledge, a 2-D solver implementing the intrinsic theory of plates has not been developed yet (based either on classical or Cosserat elasticity). This solver would take constitutive relations (and inertial properties) from the through-the-thickness analysis as input to predict the global behavior of a Cosserat elastic plate.

The rest of the thesis is organized as follows:

Chapter 2 starts off with a verification of the VAM itself. As explained earlier, VAM is applicable to dimensionally-reducible structures such as beams, plates and shells. This chapter looks at problems involving beams that are prismatic, initially curved and/or twisted beams and provides verification against known 3-D classical elasticity solutions and 3-D finite element analyses. This chapter is mostly adopted from Kovvali and Hodges [83], with the authors' permission. Since this chapter deals with the verification of the VAM as applied to beams, readers who wish to concentrate only on the development of a plate theory may skip this chapter without any consequence.

Chapter 3 will focus solely on the through-the-thickness analysis of Cosserat elastic plates and the development of the plate constitutive law. A discussion on the effect of micropolar elastic constants on the stiffness properties will be presented. As mentioned previously, it will be demonstrated that the drilling stiffness of a plate can be determined in a way that connects 2-D and 3-D continua, and a comparative study against other available results in the literature will be made.

Chapter 4 will detail the development of a geometrically-exact fully-intrinsic set of equations for Cosserat elastic plates. It will also be shown how the equations developed can be made "backwards-compatible" with classical theory of elasticity to work with more traditional Reissner-Mindlin or Kirchhoff-Love models. This will

tremendously broaden the usefulness of the solver, delivering a unified implementation of a theory of plates with or without observable Cosserat effects. In the latter case, the solver will be able to handle all types of plate constructions from isotropic to composite laminates providing a geometrically-exact analysis.

Chapter 5 will detail an energy-consistent Galerkin approach to solving the previously developed equations. After some commentary on the choice of shape functions, various example problems will be solved using the developed 2-D solver highlighting the advantages of a fully intrinsic or mixed variational formulation over traditional displacement based approaches and simplified plate theories, namely a simplification in treatment while being capable of carrying out a high-fidelity analysis. Solutions to linearized free vibration problems for a variety of boundary conditions will be provided to serve as a form of model validation and demonstrate the impact of micropolar effects on the system eigenvalues. This is followed by a discussion on linear statics and the applicability of a Galerkin's method to different boundary conditions (strictly speaking, using a mixed-method). Finally, analysis techniques for nonlinear static and steady-state analysis of plates are discussed using an incremental approach.

CHAPTER II

VERIFICATION OF THE VAM FOR PRISMATIC, INITIALLY CURVED AND TWISTED BEAMS

2.1 Introduction

Beams come under the category of dimensionally reducible structures, with one dimension (wavelength of deformation and radius of curvature/twist) much larger than the cross-sectional dimensions. Typical examples in the aircraft industry include high aspect-ratio wings and helicopter rotor blades. Because of the complexity of the interior region of such beam-like structures, their analysis and design may be thought to be best carried out using 3-D finite-element analyses (FEA) given that such analyses provide for high-fidelity modeling of complex geometries and accurate, reliable results. However, there are some obvious drawbacks: invariably all FEA tools are computationally expensive when compared to beam modeling tools, often by two to three orders of magnitude. Another aspect often overlooked is how labor-intensive even the modeling process can become, especially for complex layups and geometries. An obvious and popular alternative has been conventional beam modeling techniques. Although they are computationally less expensive, the results are seldom satisfactory, especially for composite structures, which are frequently the cases of interest. An ideal methodology would combine the relatively inexpensive nature of beam modeling tools with the ability to achieve high-fidelity in modeling procedures á la finite-element analyses, resulting in an efficient, reliable analysis tool with no ad hoc kinematic assumptions typically associated with standard beam modeling tools.

Such an asymptotically exact methodology, called the Variational Asymptotic Beam Section Analysis (VABS), has been developed over the last two decades with

the objective to model realistic rotor blades, creating the best possible set of elastic constants for an equivalent beam analysis from a detailed representation of the cross-sectional plane. Additionally, it can also recover detailed stress and strain fields based on inputs from a one-dimensional (1-D) global analysis. It uses the Variational Asymptotic Method (VAM) as its mathematical basis. The VAM is used to split a general 3-D nonlinear elasticity problem for a beam-like structure into a two-dimensional (2-D) linear cross-sectional analysis and a 1-D nonlinear beam analysis by taking advantage of certain small parameters inherent to the structure (typically a/l and a/R, where a is a characteristic cross-sectional dimension, l is the wavelength of deformation and R is the radius of curvature/twist). VAM applies an asymptotic expansion in terms of these small parameters of the energy functional instead of the system of differential equations [93, 14, 15, 80], thereby making the modeling procedure more compact, less cumbersome and variationally consistent. (The term "variationally consistent" is used here to mean that all unknown variables follow naturally from an appropriate minimization problem, based in turn on a variational principle.) The development of VABS was first given by Hodges et al. [63]. The cross-sectional modeling capability was later extended to include refinements such as transverse shear and effects of initial curvature and twist [17, 18, 120, 168].

Verification studies for prismatic, isotropic beams have been carried out in sufficient detail [170, 163], but rigorous verification studies for initially twisted and curved beams do not seem to exist. Even for orthotropic prismatic beams, there has been extensive numerical verification but none against solutions from theory of elasticity. The present effort presents verification against elasticity solutions for orthotropic prismatic beams. A recently updated energy transformation to the generalized Timoshenko form by VABS [61] was shown to affect certain cases of prismatic beams and, almost always, all beams with initial curvature and twist. The present effort seeks to verify these capabilities of VABS, viz., the correct modeling of how initial curvature

and twist affect global behavior of beams. Several cases are presented, which are essential to demonstrate that VABS can produce results with an accuracy comparable to that of 3-D finite element codes (and theory of elasticity solutions, when available).

The purpose of this chapter is to present results from studies that seek to verify and validate VABS, and hence the VAM; therefore, no details regarding the theoretical foundation for initially twisted/curved beams are repeated here. Details of the formulation may, instead, be found in refs. [17, 168, 68, 70, 61]. See work cited by Hodges [70] for a more complete history of the development and verification of VABS up to 2006 as well as the corresponding 1-D theory of beams. However, fig. 1 gives an overview of the beam-modeling procedure. Note that in all the verification cases considered, the cross-sectional analysis tool VABS is used to construct a generalized Timoshenko model, represented by a 6×6 stiffness matrix which, along with the 6×6 cross-sectional mass matrix, is then input into the 1-D geometrically exact, nonlinear equations of equilibrium for beams [68]. Results from such a 1-D global analysis, such as 1-D displacements, cross-sectional stress resultants and generalized strains can then be fed back to VABS in order to perform a 3-D recovery analysis to calculate pointwise displacement, strain and stress fields from the global behavior of a 1-D global beam analysis.

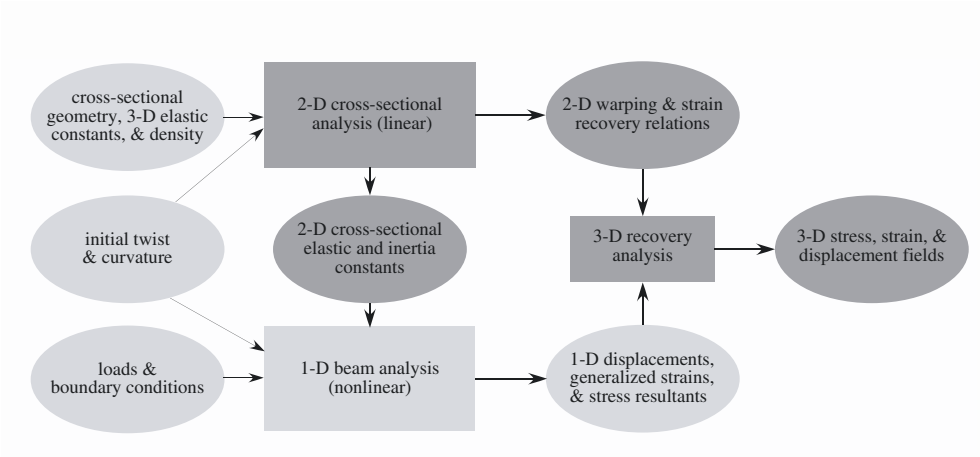

Figure 1: Beam analysis procedure

2.2 Bending and Torsion of an Orthotropic Cantilever

Verifications against solutions from the theory of elasticity are superior to verifications against numerical solutions, because numerical solutions such as 3-D FEA have issues such as locking that might be significant depending on the type of analysis and choice of elements. Analytical modeling of isotropic bars with elliptical and rectangular cross sections carried out by Yu and Hodges [163] showed that VABS results correlate well with those from theory of elasticity. Here, we consider the modeling of an orthotropic cantilevered strip beam subjected to, in turn, a unit tip force and a unit tip torque. Analytical solutions exist for such orthotropic beams (or a single-layer ply as the case may be), as derived by St. Venant and given by Lekhnitskii [96].

To this end, consider a cantilever with material properties and dimensions as shown in table 1. The beam is modeled as a single ply with 0° in VABS and is subjected to $F_3 = 1$ lb. (bending) and $M_1 = 1$ lb-in. (torsion). The structural and inertial properties as calculated by VABS for a generalized Timoshenko model [168] are provided in table 1. The beam's reference axis is along x_1, noting that specification of the length of the beam is not necessary as the solution is independent of the length (as long as it is sufficiently slender to be classified as a beam and the cross-section considered is not near the ends of the beam). To compare results from a series solution based on linear theory of elasticity given by Lekhnitskii [96] (Eqs. 49.10 and 31.16), we plot the recovered 3-D shear stress fields from VABS (σ_{12} and σ_{13}), resulting from the applied sectional loading, along the depth and the width of the said cross-section passing through the centroid.

When the beam is subjected to a tip force, we obtain, as expected, a parabolic variation of the shear stress σ_{13} through the thickness (along x_3) as indicated in fig. 2(a). However, since this beam is loaded along x_3 instead of along x_2, we also need to consider the variation of σ_{13} across the width (where there would be negligible variation for "in-plane" loading). As shown by fig. 2(b), VABS correctly captures this

Table 1: Material properties, dimensions and elastic constants

Material properties		VABS output	
E_{11} (psi)	1.873×10^7	S_{11} (lb)	3.746×10^6
E_{22} (psi)	1.364×10^6	S_{22} (lb)	1.247×10^5
G_{12} (psi)	0.7479×10^6	S_{33} (lb)	9.093×10^4
G_{13} (psi)	0.6242×10^6	S_{44} (lb-in^2)	4.819×10^2
ν_{12}	0.30	S_{55} (lb-in^2)	3.122×10^3
ν_{23}	0.30	S_{66} (lb-in^2)	1.249×10^6
ρ (lb-sec^2/in^4)	1.450×10^{-4}	μ (lb-sec^2/in^2)	2.956×10^{-5}
Width (in., along x_2)	2.0	i_2 (lb-sec^2)	2.464×10^{-8}
Thickness (in., along x_3)	0.1	i_3 (lb-sec^2)	9.856×10^{-6}

Note: The 6×6 stiffness matrix obtained from VABS has stiffness values $S_{ij}(i, j = 1, 2, \ldots, 6)$ arranged as 1 – extension; 2,3 – shear; 4 – torsion; 5,6 – bending; Inertia properties: μ – mass per unit length; i_2, i_3 – cross-sectional mass moments of inertia

variation too – it stays nearly constant across the width but shoots up significantly at the ends (while maintaining a parabolic variation along x_3 at every station along x_2). It is also worthy to note that the σ_{12} distribution along the width of the cross section is quite significant and cannot be neglected, as shown in fig. 2(c) for $x_3 = 0.05$ in. This trend is also anti-symmetric about the x_2 axis to satisfy a zero net-force condition along x_2.

The beam is now subjected to a tip torque, and again the distributions of the shear stresses throughout the cross section are compared. In particular, we look at variations of σ_{12} and σ_{13}. As expected, fig. 3(a) shows that σ_{12} varies linearly through the thickness even for an orthotropic beam, at least at points away from the ends. However, this is not the only stress quantity that is significant. It turns out that the σ_{13} distribution is also very significant at the faces where $x_2 = \pm 1$ in., which is shown in fig. 3(b). Again, the correlation between VABS and the analytical solution is quite satisfactory.

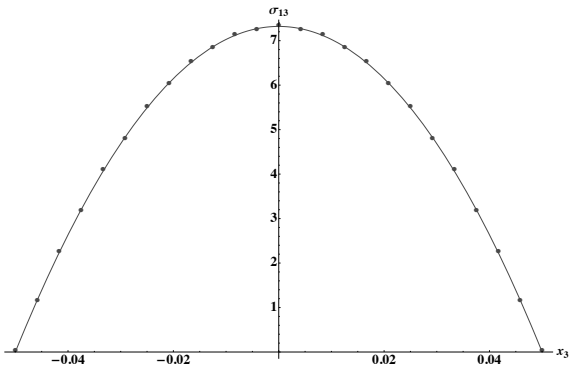

(a) σ_{13} vs. x_3; $x_2 = 0$ in.

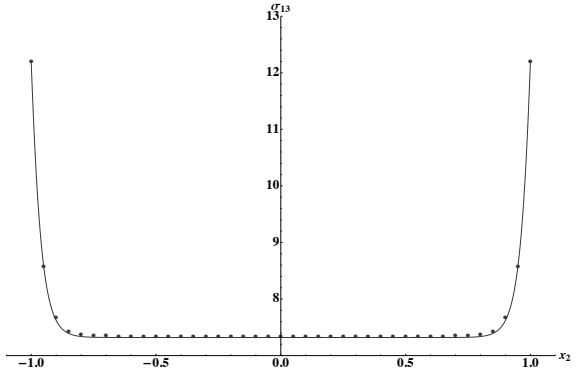

(b) σ_{13} vs. x_2; $x_3 = 0$ in.

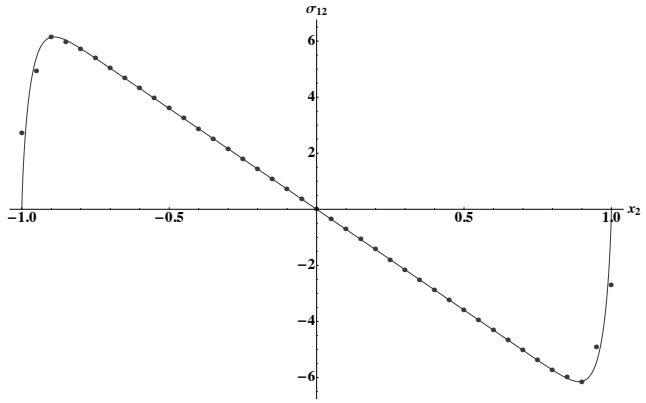

(c) σ_{12} vs. x_2; $x_3 = 0.05$ in.

Figure 2: Comparison of 3-D stresses σ_{12} and σ_{13} for bending, VABS vs. theory of elasticity

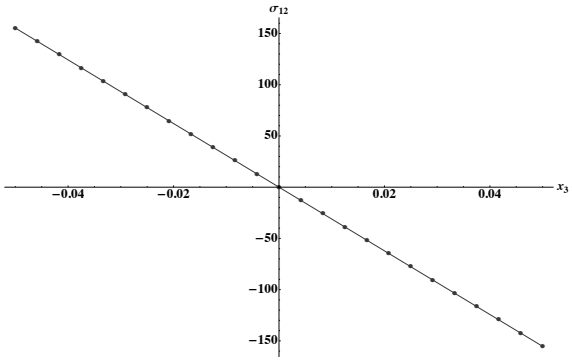

(a) σ_{12} vs. x_3; $x_2 = 0$ in.

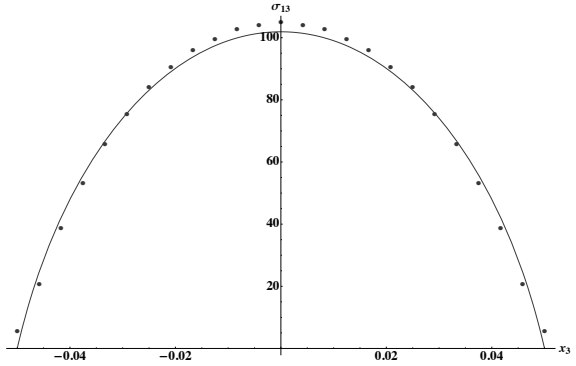

(b) σ_{13} vs. x_3; $x_3 = 1$ in.

Figure 3: Comparison of 3-D stresses σ_{12} and σ_{13} for torsion, VABS vs. theory of elasticity

2.3 Verification for Beams with Initial Curvature and Twist: Approach 1

The methodology for verification proposed in this section is applicable to beams with both initial twist and curvature, albeit, with minor differences; in either case, however, the method of analysis is strongly dependent on the choice of coordinates used. In particular, we analyze the beam once using a curvilinear coordinate system and once using a Cartesian coordinate system, making sure the two analyses are consistent. Care must be taken, however, to understand the meaning and implications of selecting one system over the other, which is explained briefly below.

For initially twisted beams, analysis using curvilinear coordinates involves choosing a coordinate system such that the local cross-sectional coordinates follow the twist, thereby continuously rotating along the length of the beam. For this set of test cases we assume that the beam is uniform along the span, and the twist is small (such that $|ak_1| << 1$). Such a choice of coordinates requires a single cross-sectional analysis for the stiffness constants and the initial twist measure k_1 enters both the 1-D global analysis and the 2-D cross-sectional analysis, as shown in chapters 4 and 5 of [70].

On the other hand, use of Cartesian coordinates implies that the cross-sectional coordinates are along fixed directions in space and thus do not follow the twist of the beam. Therefore, since the cross-sectional geometry varies along the length of the beam, one needs to carry out numerous sectional analyses along the beam to account for varying sectional properties (due to varying orientation) as seen from this fixed Cartesian system. The entire beam is discretized into a number of segments, and the sectional properties are only evaluated at the ends of each segment and interpolated linearly within it. As evident, in both the 1-D global analysis and the 2-D cross-sectional analysis, k_1 is set to zero.

For initially curved beams, analysis using curvilinear coordinates requires choosing

a coordinate system wherein the local cross-sectional coordinates continuously rotate with the beam reference line (but do not rotate when viewed from a plane normal to the beam reference line). This approach, again, requires only a single cross-sectional analysis for the stiffness constants, and the initial curvature measure(s) k_2 and/or k_3 enter both the 1-D global analysis and the 2-D cross-sectional analysis [70]. Unlike for beams with initial twist, an analysis using piecewise-Cartesian coordinates also requires just one cross-sectional analysis, but with k_2 and k_3 set to zero since we model the entire curved geometry as being piecewise linear and hence, locally prismatic. There is also a difference in the 1-D global analysis procedure: Instead of modeling it as a single beam, the beam is thought to be made up of numerous prismatic beams joined to each other to make up a curved beam. Therefore, again $k_2 = k_3 = 0$. The piecewise-Cartesian approach entails more approximations than the curvilinear approach, but increasing the number of elements (beams) produces very similar results for a wide variety of cases irrespective of the choice of coordinate system. For instance, if the mode of deformation considered is primarily bending, then Approach 1 is a practical form of verification, whereas a case with predominantly torsional deformation will render this approach invalid for verification purposes, although it does bring out certain important aspects pertaining to these methodologies. The exact nature of these additional approximations and their implications for predictive capability are discussed in a later section.

The crux of this methodology is as follows: In cases of both initial twist and curvature, whereas the curvilinear coordinates approach requires that the curvature measure numbers k_1, k_2 and k_3 enter the analysis, a modeling procedure using Cartesian/piecewise-Cartesian coordinates does not use them. Therefore, invariance in the 1-D global analyses results, such as static deflections under load and beam natural frequencies, can be taken as an indication that initial curvature and twist effects have been modeled accurately in the 2-D cross-sectional analysis as well as in

the 1-D global analysis.

2.4 Verification for Beams with Initial Curvature and Twist: Approach 2

The second and a more rigorous form of verification would be to compare results from VABS (in tandem with a geometrically-exact 1-D beam analysis code such as NATASHA [113] (Nonlinear Aeroelastic Trim And Stability of HALE Aircraft) with 1-D information extracted from a 3-D finite-element analysis (such as Abaqus). For example, to compare the static tip deflection under a dead load, the 1-D displacement variable from NATASHA is compared with the average cross-sectional tip-deflection from Abaqus. Comparing the beam natural frequencies against Abaqus can be viewed as a verification of both the static and dynamic behavior modeling capabilities of a beam approach using cross-sectional properties from VABS. It should be emphasized that the 1-D global analysis is geometrically exact; hence, the accuracy of the results would then solely depend on the accuracy of the stiffness constants provided to the beam analysis tool by VABS. Hence, good correlation between 1-D global results and 3-D finite-element results would automatically imply accurate 2-D cross-sectional modeling.

2.5 Results and Discussion

Several verification cases are now taken up following both the approaches described, and comparisons between the 1-D and 3-D analyses are conducted systematically. In this section, results are obtained and discussed for the following cases: (Case 1) initially twisted isotropic beams, (Case 2) initially curved isotropic beams, (Case 3) initially twisted anisotropic beams, (Case 4) initially curved anisotropic beams, and (Case 5) a helical spring.

2.5.1 Case 1: Initially Twisted Isotropic Beams

Results given by Ho et al. [61] showed the prediction of natural frequencies of an initially twisted isotropic rectangular section and verified by Approach 1. However, no static deflection results were shown and hence, supplementing results from Ref. [61] with results from the current section completes the discussion. An example of a statically-loaded, isotropic, initially-twisted beam is now shown, verified by Approach 1. Here, we consider an isotropic square cross section of side 0.5 in. The length of the beam is 10 in. and has an initial twist of $k_1 = 0.1$ rad/in. The Young's Modulus is $E = 2.6 \times 10^7$ lb/in^2, Poisson's ratio is $\nu = 0.3$ and the mass density $\rho = 7.3 \times 10^{-4}$ lb-sec^2/in^4. The beam is cantilevered and subjected to exaggerated gravitational loading of 500 times its normal value. Figure 4 shows vertical and lateral deflections of the beam by analyses using curvilinear and Cartesian coordinates. As can be seen, the curves show excellent agreement.

2.5.2 Case 2: Initially Curved Isotropic Beams

An initially curved, cantilevered, isotropic beam is chosen with the same material properties as in Case 1. However, the cross section is rectangular measuring 2 in.$\times$1 in. The length of the beam is now 20 in. and has an initial curvature of $k_2 = 0.05$ rad/in. Again, verification is carried out by Approach 1, where a set of curvilinear coordinates and piecewise-Cartesian coordinates are chosen to carry out a static and a dynamic analysis on the beam and the results compared. First, the beam is subjected to a uniform exaggerated gravitational loading 500 times its normal value. The beam undergoes axial and transverse displacements as shown in fig. 5. Again, clearly, both analyses show excellent agreement with one another.

Natural frequencies for the same beam were then calculated with a small modification: the clamp at the end is removed and the beam is made free-free. Results

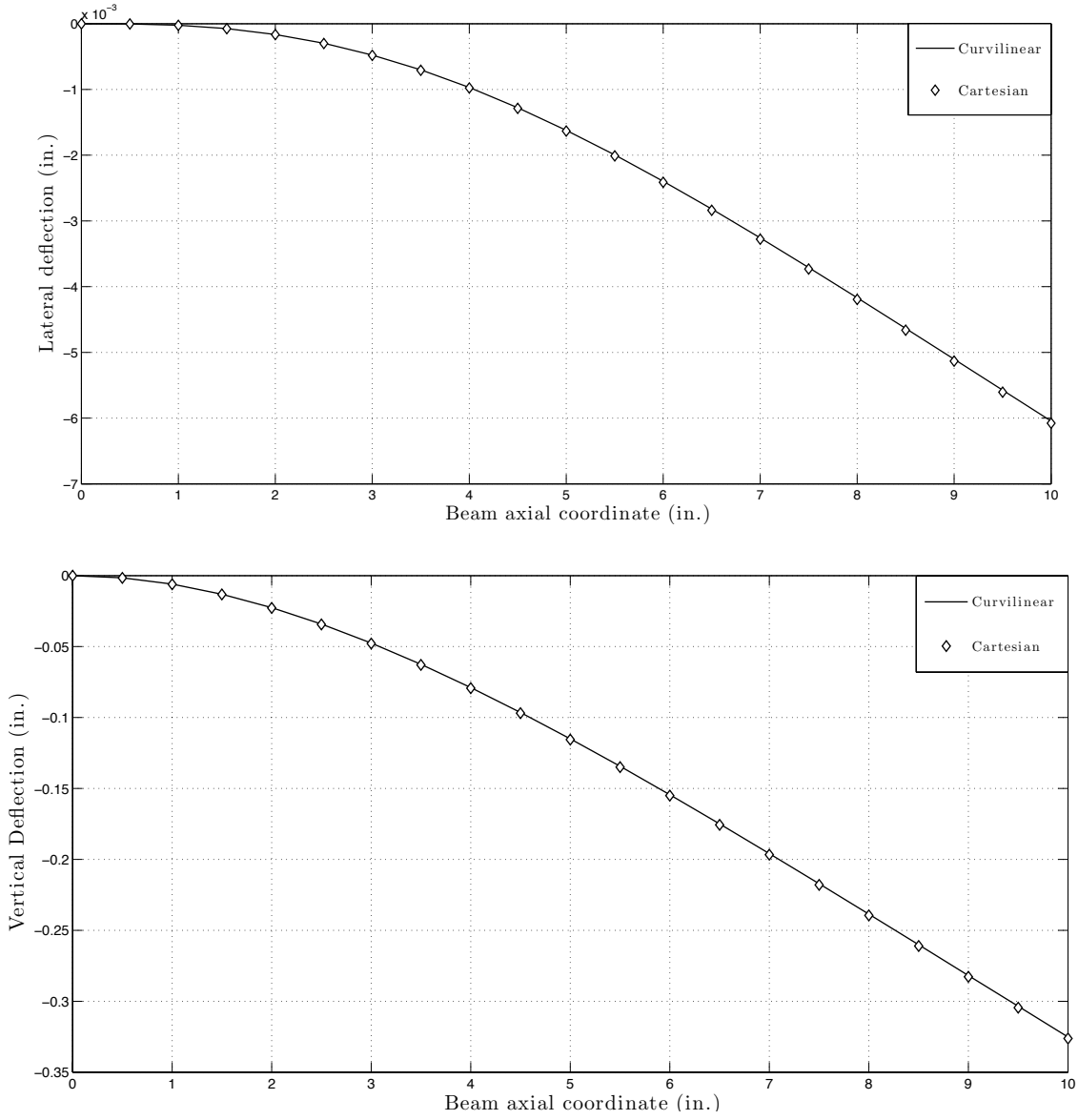

Figure 4: Static deflections of an isotropic initially twisted beam; $k_1 = 0.1$, $L = 10$ in., $a = 0.5$ in.

are plotted as a function of k_2 varying from -0.05 rad/in. to +0.05 rad/in. As expected, the curves are symmetric about $k_2 = 0$ due to material isotropy and overall symmetry. With the understanding that correct prediction of natural frequencies can be interpreted as an accurate representation of the elastic and dynamic behavior of the beam as influenced by initial curvature, fig. 6 clearly indicates the accuracy of modeling initial curvature effects in VABS.

2.5.3 Case 3: Initially Twisted Anisotropic Beams

The case considered is a structurally coupled composite beam with rectangular cross section manufactured from AS4/3501-6 graphite epoxy. The material properties and outer dimensions of the beam are provided in table 2. A prismatic cantilevered beam of this configuration has been experimentally tested by Minguet and Dugundji [102, 103]. Note that a prismatic beam with the given configuration will result in bending-twist coupling. In the present case, we consider an initial twist $k_1 = 0.05$ rad/in, which further introduces extension-torsion and shear-bending couplings (along with weak shear-torsion and extension-bending couplings). The beam is free on either end, and a free-vibration analysis is carried out. The decision to model the beam with free-free boundary conditions stems from the fact that results may vary considerably depending on how a boundary condition is applied in a finite element analysis, as discussed by Yu [165]. For example, there is an infinitely large variety of ways to model a clamped end in a 3-D finite-element analysis, none of them necessarily being "correct." The way a boundary is modeled does not affect long beams as much it does short ones, with short strip beams affected more than short regular beams. Therefore, choosing free-free boundary conditions eliminates the possibility that boundary conditions can contribute to differences, especially for higher frequencies.

Unlike the previous cases examined, we now verify VABS using Approach 2. The beam is modeled using curvilinear coordinates in VABS and NATASHA and compared

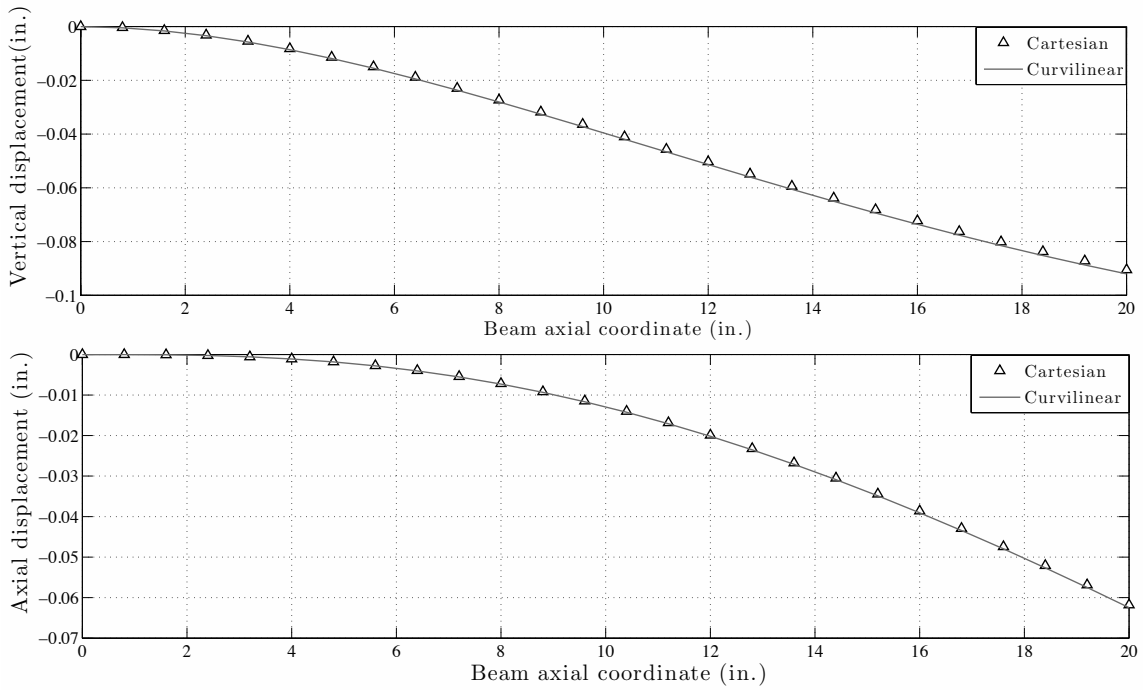

Figure 5: Static deflections of an initially curved isotropic beam; $k_2 = 0.05$, $L = 20$ in., $a = 2$ in.

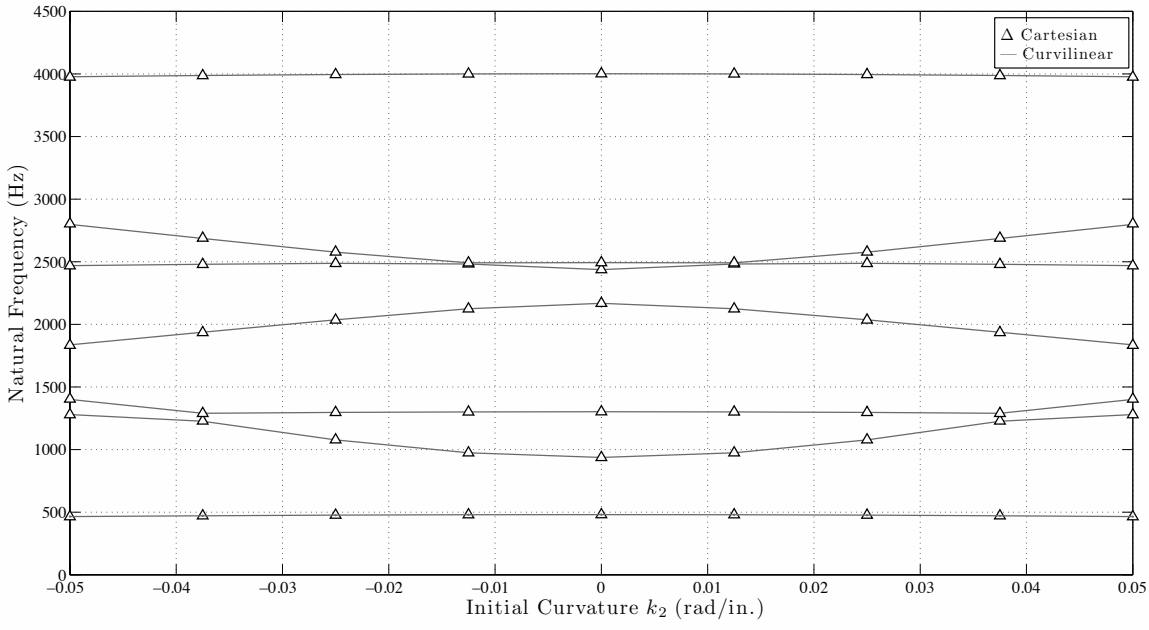

Figure 6: Natural frequencies of an initially curved free-free isotropic beam; $L = 20$ in., $a = 2$ in.

Table 2: Material properties and dimensions

Material	properties	Outer dimensions	
E_{11}	2.059×10^7 psi	Width	1.1820 in.
E_{22}, E_{33}	1.42×10^6 psi	Thickness	0.0579 in.
G_{12}, G_{13}	8.70×10^5 psi	Length	22.047 in.
G_{23}	6.96×10^5 psi	Layup	$[45°/0°]_{3s}$
ν_{12}, ν_{13}	0.30	k_1	$0 - 0.05$ rad/in.
ν_{23}	0.34	k_2	$0 - 0.05$ rad/in
ρ	1.4784×10^{-4} lb-sec^2/in.^{4}		

with finite-element results generated using Abaqus. Figure 7 compares the natural frequencies calculated for various values of k_1 ranging from 0 to 0.05 rad/in. The solid lines are results produced by VABS and the symbols denote results from Abaqus. Note that due to a symmetric layup and the nature of the boundary conditions, results would be identical for positive or negative values of initial twist, and varying k_1 starting at zero will suffice. The first ten modes shown are in the order of first, second and third flap-wise bending (F1, F2, F3), first torsion (T1), fourth and fifth flap-wise bending (F4, F5), second torsion (T2), sixth flap-wise bending (F6), first lead-lag bending (L1) and third torsion (T3). As should be the case, initial twist most strongly affects the torsional frequencies. While one may not be interested in so many modes of vibration, it is worth noting that even the sixth flap-wise bending mode differs from FEA results only by about 1.5%. This is in spite of the parameter a/l (which we assumed to be small) not being negligibly small compared to unity because l would approximately be one-sixth of the beam length. The rest of the frequencies are all within 0.5% for all values of k_1. With the correlation being this excellent, it is also relevant to consider the relative costs of these methods of analysis. The Abaqus model was meshed with 4,500 twenty-noded brick elements, and the code took roughly 180 seconds to run. On the other hand, VABS takes roughly 0.1 seconds to perform the cross-sectional analysis while NATASHA takes roughly 3 seconds to obtain converged results even when using a very large number of elements (roughly

200 along the length). Further, taking into account the relative ease of both pre- and post-processing of results in VABS/NATASHA, the gains of using a 2-D/1-D methodology become apparent. It should be noted that NATASHA is a MATLAB-based code and is therefore not optimized for speed, so actual gains in efficiency when using a compiled program for the beam analysis would be much greater than reported here.

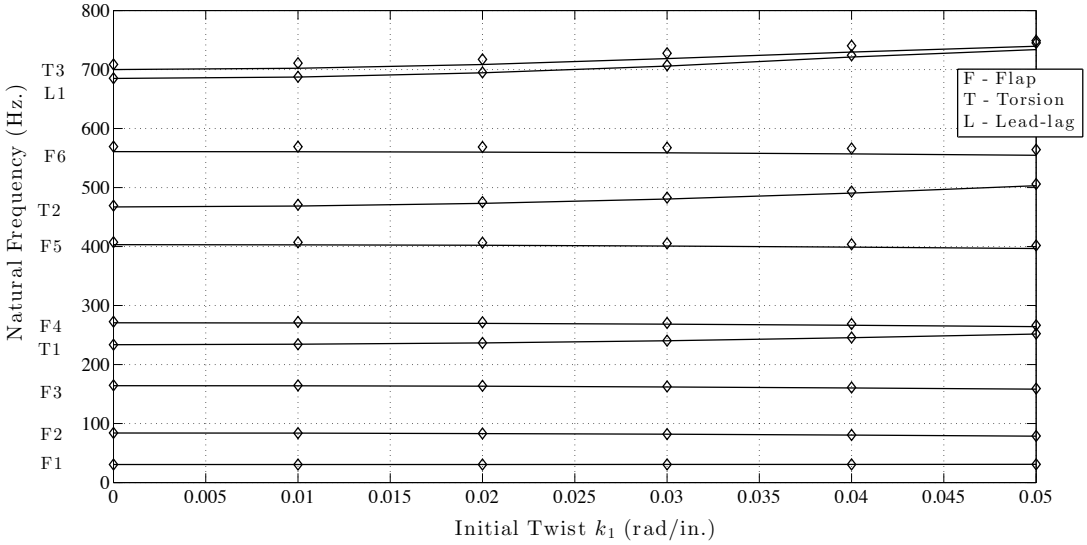

Figure 7: Natural frequencies of an initially twisted free-free anisotropic beam; VABS vs. Abaqus; $L = 22.047$ in., $a = 1.182$ in.

2.5.4 Case 4: Initially Curved Anisotropic Beams

The geometry and the material properties for this case remain exactly the same as in the previous case with the difference being that the beam is now initially curved rather than initially twisted. This modifies the stiffness matrix by introducing shear-twist and extension-bending couplings (along with weak extension-twist and shear-bending couplings). The beam has a strip-like geometry with curvature k_2 out of its plane, i.e., along the soft-bending direction. One of the reasons this case was chosen is because for strip-like beams k_2 affects the results more than k_3. A more important reason is that there exist elasticity solutions for isotropic strip-beams with in-plane

curvature [49] against which VABS has been verified [122]. However, no analytical solutions exist for anisotropic strip-beams curved out-of-plane. Thus, one has to resort to 3-D finite-element procedures, against which the present case is intended to be verified. Unlike the previous case, however, both approaches mentioned previously will be applied to this example. Figure 8 compares natural frequencies calculated by VABS/NATASHA (solid lines) against finite-element results generated using Abaqus (symbols). Most of the characteristics described for Case 3 hold true including the relative costs of the two analyses and the ordering of modes shown.

Figure 9 compares natural frequencies obtained via analyzing with curvilinear and piecewise-Cartesian coordinates using VABS and NATASHA (represented by solid lines and symbols, respectively). As one increases the number of elements one can observe that both analyses yield nearly identical results, thus verifying the capabilities of VABS. Just as in Case 3, of all the modes of vibration, the torsional frequencies are most strongly affected because of the initial curvature. While the presence of initial curvature does modify the equations governing the 1-D global beam analysis (and hence, the natural frequencies), it can also be shown that it is equally important to take into account how this curvature measure affects the 2-D cross-sectional analysis (and hence modifies the sectional stiffness properties that appear in the 1-D global analysis) in order to predict this variation with curvature completely and correctly. For example, table 3 shows the predicted torsional frequencies by Abaqus and VABS/NATASHA for an initial curvature measure $k_2 = 0.05$. In the last column are results from a 1-D global analysis with stiffness constants based on a prismatic beam cross-sectional analysis. In other words, the curvature measure(s) were neglected in VABS and the natural frequencies calculated. As can be seen, there is a considerable difference in results; and the prediction based on prismatic stiffness constants may lead to gross inaccuracies in certain cases.

One can observe that predictions of the torsional modes between the curvilinear and piecewise-Cartesian-coordinates methodologies slowly diverge as k_2 increases. This would be a manifestation of the fact that the piecewise-Cartesian coordinates approach entails more approximations than the curvilinear approach, viz., that initial curvatures (and twist) affect the cross-sectional modeling. For a very large number of elements, the Cartesian approach would tend to a procedure equivalent to just neglecting the curvature measures in VABS. This is evident by looking at the fourth column of table 3. It is important to understand this limitation of the methodology. For simple static load cases, this methodology works very well as the effect of k_2 on flap-wise deformation is not as significant. A detailed study of the importance of including curvature measures in the cross-sectional modeling has been given by Cesnik and Hodges [17], where it is shown that corrections to the stiffness model due to initial twist and curvature are vital for proper representation of anisotropic beams.

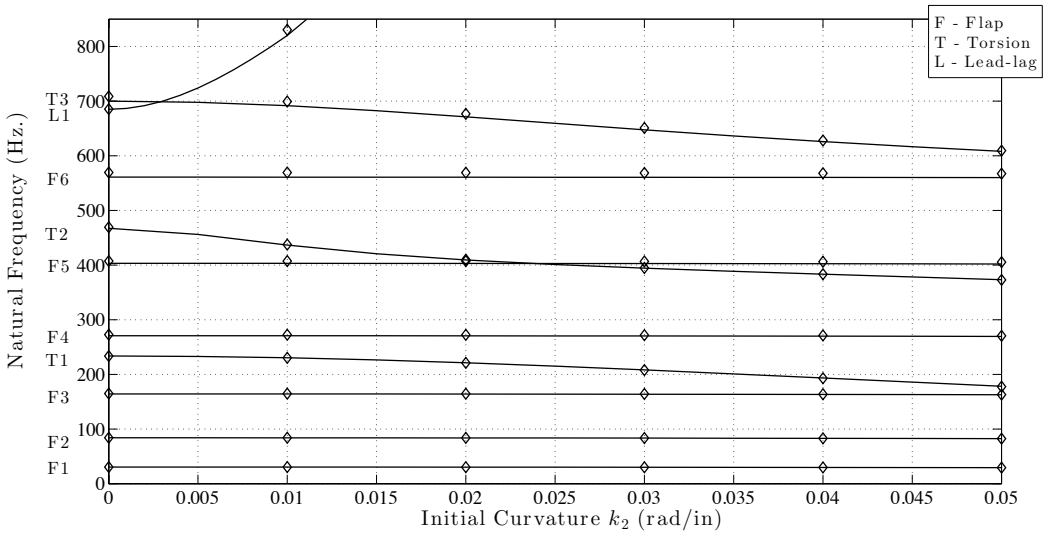

Figure 8: Natural frequencies of an initially curved free-free anisotropic beam; VABS vs. Abaqus; $L = 22.047$ in., $a = 1.182$ in.

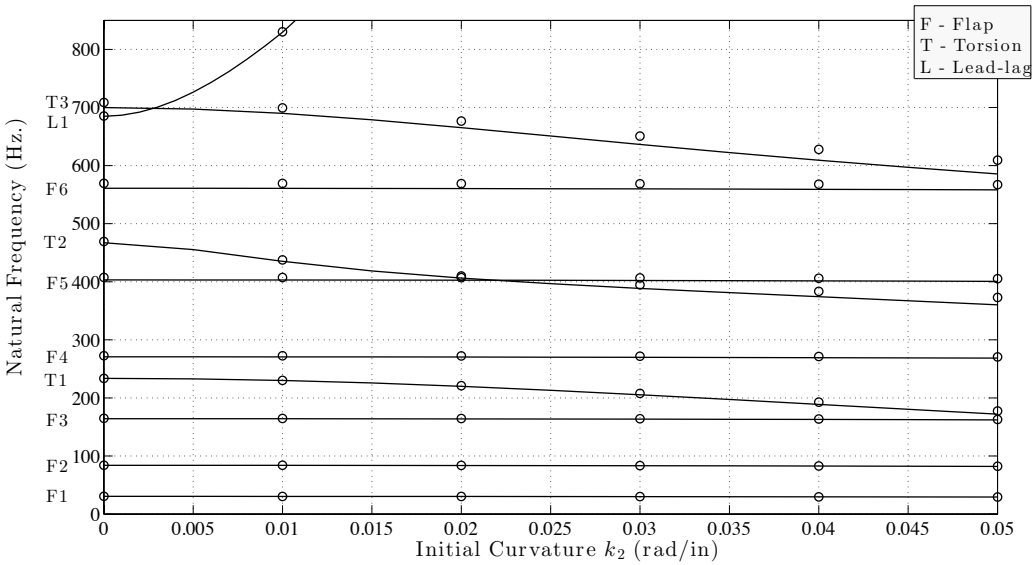

Figure 9: Natural frequencies of an initially curved free-free anisotropic beam: curvilinear vs. piecewise-Cartesian coordinates approaches; $L = 22.047$ in., $a = 1.182$ in.

Table 3: Effect of including curvature measures in VABS on torsional natural frequencies (in Hz.)

Mode	Abaqus	VABS	$\text{VABS}_{\text{prismatic}}$	VABS_{pc}
Torsion 1	177.60	178.31	172.14	171.78
Torsion 2	373.00	373.26	360.34	360.01
Torsion 3	609.46	608.10	585.72	585.17

2.5.5 Case 5: A Helical Spring

We now consider the case of a beam that is simultaneously initially twisted and curved. Imagining a really long beam with these two curvature measures results in what looks like a helical spring, shown in fig. 10 below. Such a "beam" is modeled in Abaqus and VABS with an isotropic circular cross section with $k_1 \neq 0$ and either $k_2 \neq 0$ or $k_3 \neq 0$. The geometric and material properties of the helix are shown in table 4. Using these specifications and the Frenet-Serret formulae for continuous, differentiable space curves, one can compute the initial curvature measures as $k_1 = 0.749$ rad/in.$^{-1}$ and $k_2 = 4.967$ rad/in.$^{-1}$. (Note that k_3 could have been used instead

of k_2 – the choices are equivalent. Also, no initial strains are assumed.)

Figure 11 compares the natural frequencies of a hanging helical spring (clamped-free boundary conditions) obtained from the 1-D/2-D methodology to a 3-D finite-element analysis in Abaqus. The lowest modes are predicted the most accurate, the accuracy declining with increasing mode number. However, all the frequencies shown in the bar graph predicted by VABS are within 1% of the results from Abaqus, yet at a far less computational cost. For example, the Abaqus model was meshed with 11,872 twenty-noded hexahedral elements, and the analysis took just under 180 seconds to complete (on a Core 2 Duo processor). On the other hand, VABS and NATASHA obtained results within 1% of the Abaqus result using far fewer degrees of freedom and much less computing time – in this case, 13 sec. Hence, this serves as another verified case for VABS with regard to initial twist and curvature, further demonstrating that VABS provides a far less costly alternative to 3-D FEA tools without significant loss of accuracy.

Table 4: Material and geometric properties of helix

Material	properties	Geometry	
E	2.9877×10^6 psi	Helical Radius	1.9685×10^{-1} in
ν	0.30	Wire Radius	1.9865×10^{-2} in
ρ	7.3921×10^{-4} lb-sec^2/in^4	Helical Angle	8.5744°
		Turns	7.6

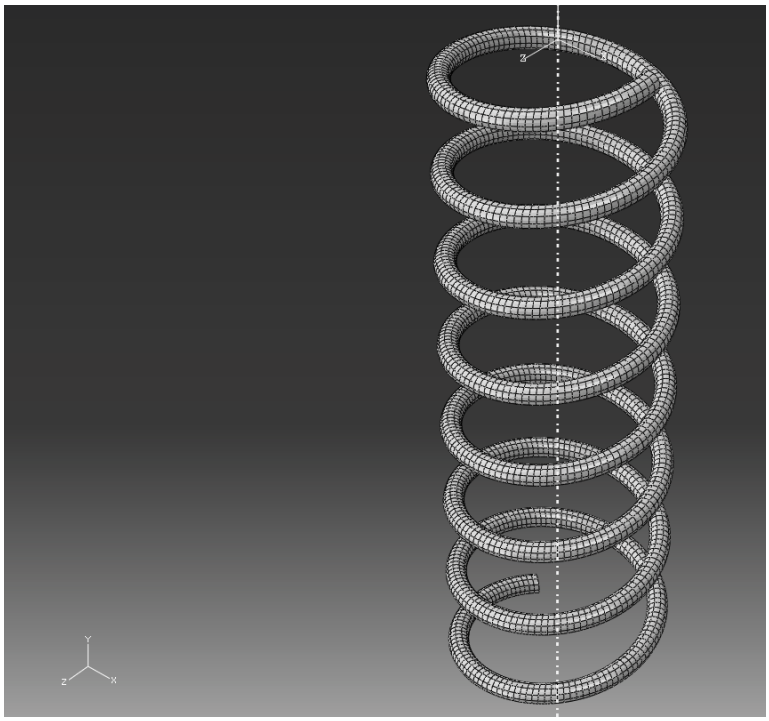

Figure 10: Abaqus model for the helical spring

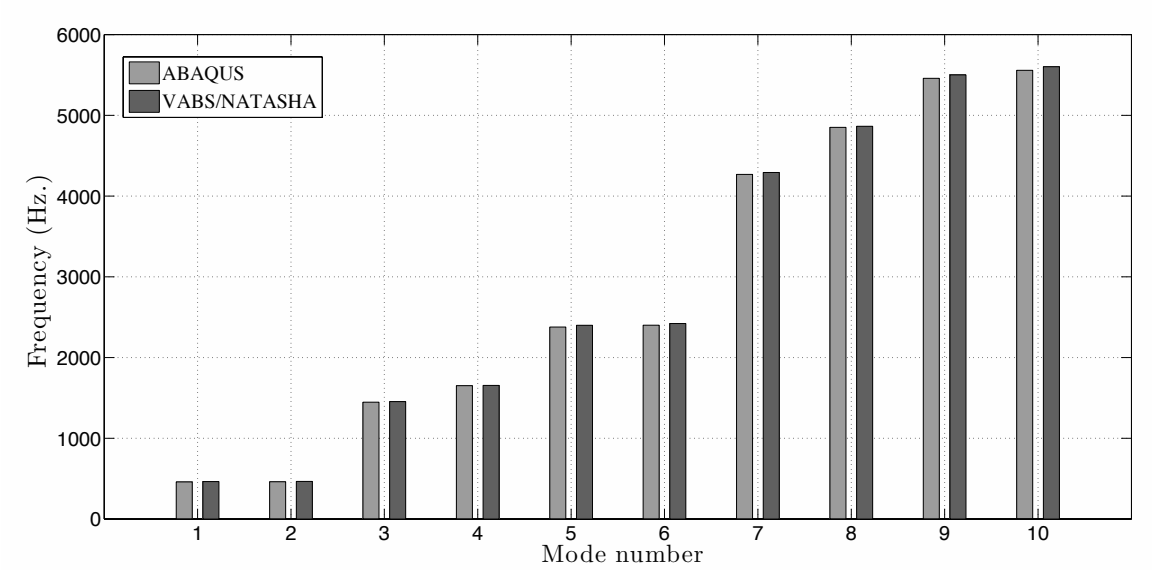

Figure 11: Natural frequencies of helical spring: VABS/NATASHA vs. Abaqus

CHAPTER III

VARIATIONAL ASYMPTOTIC MODELING OF COSSERAT PLATES

3.1 Plate Kinematics

Having satisfactorily verified the capabilities of the variational asymptotic method at dealing with dimensionally reducible structures, we can now proceed to the modeling of Cosserat plates.

Consider a Cosserat elastic plate in which matter is distributed about a planar surface so that one dimension is significantly smaller than the other two. Let us introduce Cartesian coordinates x_i such that x_α denotes lengths along orthogonal straight lines in the mid-surface of the undeformed plate, and x_3 is the distance of an arbitrary point to the mid-surface in the undeformed plate with $-h/2 \leq x_3 \leq h/2$. Let $\mathbf{b}_i$ denote an orthogonal reference triad along the undeformed coordinate lines. Covariant and contravariant undeformed base vectors ($\mathbf{g}_i$ and $\mathbf{g}^i$, respectively) both reduce to $\mathbf{b}_i$ since the coordinate system chosen is Cartesian.

The position vector from a fixed point O to an arbitrary point is (see fig. 12)

$$\hat{\mathbf{r}}(x_1, x_2, x_3) = \mathbf{r}(x_1, x_2) + x_3\mathbf{b}_3 \tag{2}$$

The position vector to the mid-surface is also the average position of points along the normal line, at a particular value of (x_1, x_2) so that

$$\mathbf{r}(x_1, x_2) = \int_{-h/2}^{h/2} \hat{\mathbf{r}} \mathrm{d}x_3 = \langle \hat{\mathbf{r}} \rangle \tag{3}$$

where the angle brackets $\langle\ \rangle$ are used throughout to denote integration through the thickness (assumed a constant).

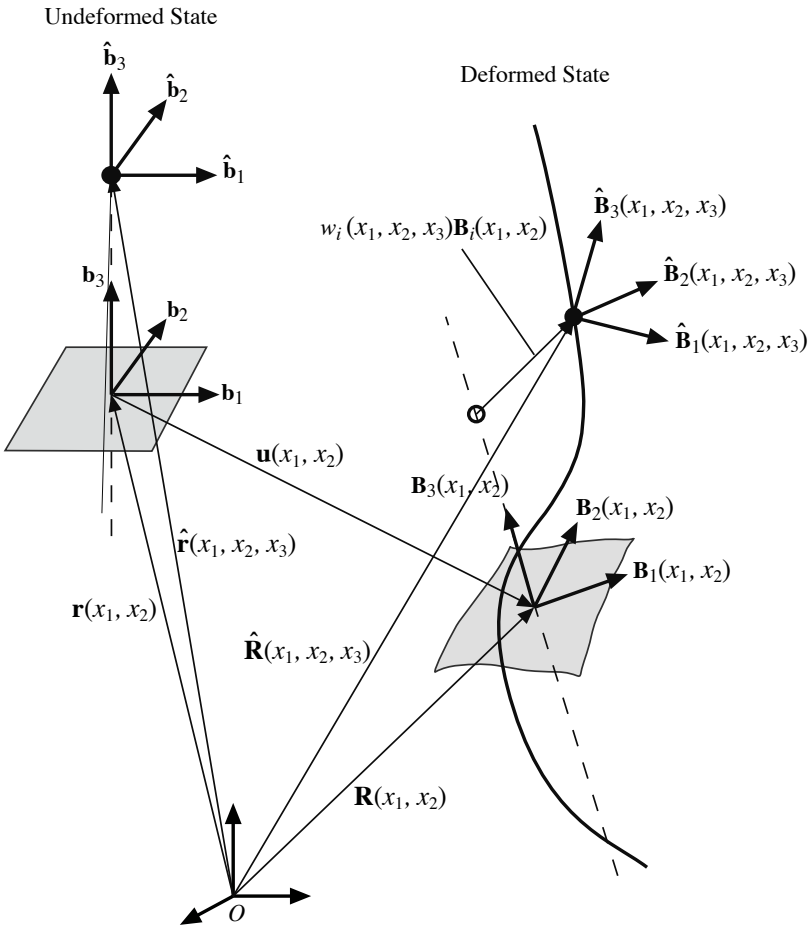

Figure 12: Schematic of plate deformation

A Cosserat continuum also incorporates a local rotation of each material point in addition to the translation assumed in classical elasticity. One can introduce the notion of a triad of vectors also called directors attached to each point and talk about an *independent* local rotation (or microrotation, as referred to by some authors) in addition to the macrorotation of the medium. For simplicity, we pick the three orthonormal directors needed for each 3-D material point in the undeformed state to be the same as the triad $\mathbf{b}_i$ of the undeformed reference surface. Therefore,

$$\hat{\mathbf{b}}_i(x_1, x_2, x_3) = \mathbf{b}_i(x_1, x_2) \tag{4}$$

Consider the deformed state configuration. The particle which had position vector $\hat{\mathbf{r}}(x_1, x_2, x_3)$ in the undeformed state now has the position vector $\hat{\mathbf{R}}(x_1, x_2, x_3)$. We

can write the position vector from O to any point in the deformed state as

$$\hat{\mathbf{R}}(x_1, x_2, x_3) = \mathbf{R}(x_1, x_2) + x_3\mathbf{B}_3(x_1, x_2) + w_i(x_1, x_2, x_3)\mathbf{B}_i(x_1, x_2) \tag{5}$$

$$= \mathbf{r}(x_1, x_2) + \mathbf{u}(x_1, x_2) + x_3\mathbf{B}_3(x_1, x_2) + w_i(x_1, x_2, x_3)\mathbf{B}_i(x_1, x_2) \tag{6}$$

where $w_i(x_1, x_2, x_3)$ is the three-dimensional (3-D) warping displacement field.

Similarly, the directors associated with each particle $\hat{\mathbf{b}}_i(x_1, x_2, x_3)$ in the undeformed state now are the orthonormal directors $\hat{\mathbf{B}}_i(x_1, x_2, x_3)$. The orientation of $\hat{\mathbf{B}}_i$ is coincident with $\hat{\mathbf{b}}_i$ when the plate is undeformed and must be defined in terms of the plate deformation; the rotation from $\hat{\mathbf{b}}_i$ to $\hat{\mathbf{B}}_i$ is described in terms of the rotation tensor $\underline{\boldsymbol{C}}(x_1, x_2, x_3)$.

$$\hat{\mathbf{B}}_i = \underline{\boldsymbol{C}} \cdot \hat{\mathbf{b}}_i \tag{7}$$

We can decompose the total rotation $\underline{\boldsymbol{C}}(x_1, x_2, x_3)$ into a *local* rotation (small) and a *global* rotation (potentially large) as

$$\underline{\boldsymbol{C}}(x_1, x_2, x_3) = \underline{\boldsymbol{C}}^{Bb}(x_1, x_2) \cdot \exp(\underline{\widetilde{\boldsymbol{\phi}}})(x_1, x_2, x_3) \tag{8}$$

where $\exp(\underline{\widetilde{\boldsymbol{\phi}}})$ is the local rotation tensor appropriate for small local rotations (Sedov 1966). The rotation tensor $\underline{\mathbf{C}}^{Bb}(x_1, x_2)$ describes the rotation from $\mathbf{b}_i$ to $\mathbf{B}_i$. Naturally, the orientation of $\mathbf{B}_i$ is coincident with $\mathbf{b}_i$ when the plate is undeformed. We have

$$\mathbf{B}_i = \underline{\boldsymbol{C}}^{Bb} \cdot \mathbf{b}_i \tag{9}$$

The axial vector $\boldsymbol{\phi}$ associated with the antisymmetric tensor $\underline{\widetilde{\boldsymbol{\phi}}}$, called the local rotation vector, can be expressed in the $\mathbf{b}_i$ basis:

$$\boldsymbol{\phi} = \phi_i(x_1, x_2, x_3)\mathbf{b}_i \tag{10}$$

The position $\mathbf{R}$ and the triad $\mathbf{B}_i$ must be well-defined in order to make eqs. (5) and (8) describe unique 3-D fields. Thus, it is necessary to identify six dependency relations

to ensure one-to-one maps. First, in order for eq. (5) to be analogous to eq. (2), $\mathbf{R}$ is defined as the average position of points parallel to the vector $\mathbf{B}_3$ corresponding to particular values of (x_1, x_2) in the plate. In order for this definition to hold, the warping must satisfy these three equations

$$\langle w_i(x_1, x_2, x_3) \rangle = 0 \tag{11}$$

In an analogous fashion, one can pick $\underline{\boldsymbol{C}}^{Bb}$ to be defined as the average rotation tensor of points parallel to the vector $\mathbf{B}_3$, giving

$$\langle \phi_i(x_1, x_2, x_3) \rangle = 0 \tag{12}$$

In order to express the 3-D strain measures in terms of intrinsic 2-D variables, the following generalized (two-dimensional) strain measures are introduced similar to those in [64]

$$\mathbf{R}_{,\alpha} = \mathbf{B}_\alpha + \epsilon_{\alpha\beta}\mathbf{B}_\beta + 2\gamma_{\alpha 3}\mathbf{B}_3 \tag{13}$$

and the components of the curvature vectors such that

$$\mathbf{B}_{i,\alpha} = (-K_{\alpha\beta}\mathbf{B}_\beta \times \mathbf{B}_3 + K_{\alpha 3}\mathbf{B}_3) \times \mathbf{B}_i \tag{14}$$

At this point, it is useful to note a few deviations from [64], [166], [167], [162] regarding the six constraints. Unlike before, having constraints as defined by eq. (12) does *not* allow one to pick $\epsilon_{12} = \epsilon_{21}$. Moreover, since $\mathbf{B}_3$ is not defined to be perpendicular to $\mathbf{R}_{,1} \times \mathbf{R}_{,2}$, we cannot set $2\gamma_{\alpha 3} = 0$ at this stage either, and must instead retain them as separate two-dimensional strain measures.

3.2 Three-Dimensional Formulation

A Cosserat elastic solid is distinguished from an elastic solid by the fact that it can support body and surface couples. Hence, two types of stresses are generated – force stresses and couple stresses – to equilibrate the applied loads. This leads to two sets of

constitutive equations, one relating the force stress tensor to a typical "force strain" or stretch tensor, and another relating the couple-stress tensor to an "angular/moment strain tensor", commonly referred to as the wryness tensor. We now need to develop expressions for these three-dimensional strain measures in terms of the generalized two-dimensional strain measures, the warping field and the local rotation field. For brevity, only the expressions are presented here with a detailed derivation provided in appendix A.

For the purpose of restricting ourselves to small strain, we will measure stretching and shear deformation by the Jaumann-Biot-Cauchy strain tensor (Γ), whose measure numbers are given by

$$\Gamma = \begin{pmatrix} \epsilon_{11} + x_3 K_{11} + \underline{w_{1,1}} & \epsilon_{21} + \phi_3 + x_3 K_{21} + \underline{w_{1,2}} & w_{1,3} - \phi_2 \\ \epsilon_{12} - \phi_3 + x_3 K_{12} + \underline{w_{2,1}} & \epsilon_{22} + x_3 K_{22} + \underline{w_{2,2}} & w_{2,3} + \phi_1 \\ \phi_2 + \underline{w_{3,1} + 2\gamma_{13}} & -\phi_1 + \underline{w_{3,2} + 2\gamma_{23}} & w_{3,3} \end{pmatrix} \tag{15}$$

where the non-underlined terms are $\mathcal{O}(\hat{\varepsilon})$ and the single-underlined terms are $\mathcal{O}(h\hat{\epsilon}/l)$[1]. Only the former are used to develop a "classical" theory of Cosserat elastic plates, while the latter are included in the development of a refined theory. Terms of $\mathcal{O}(\hat{\epsilon}^2)$ under the assumption of small strain ($\hat{\epsilon} \ll 1$) have been discarded for the sake of developing a linear constitutive model.

Work-conjugate to the couple-stress tensor, an additional strain measure unique to Cosserat elastic bodies, called the wryness tensor, can be defined similar to Reissner [127], Pietraszkiewicz and Eremeyev [118], Kafadar and Eringen [79], among others. Physically, we can explain this in the same manner as how we define a stretching strain as, loosely speaking, a measure of the gradient of a displacement field; the wryness tensor is, again loosely speaking, a measure of the gradient of a proper orthogonal

[1]Estimation of asymptotic order of derivatives is dependent on characteristic length of the domains – derivatives with respect to the in-plane coordinates evolve slower than those with respect to the thickness coordinate.

rotation tensor

$$X = \begin{pmatrix} -K_{12} - \underline{\phi_{1,1}} & K_{11} - \underline{\phi_{2,1}} & K_{13} - \phi_{3,1} \\ -K_{22} - \phi_{1,2} & K_{21} - \phi_{2,2} & K_{23} - \phi_{3,2} \\ -\phi_{1,3} & -\phi_{2,3} & -\phi_{3,3} \end{pmatrix} \tag{16}$$

where X is a nonsymmetric 3×3 matrix of the three-dimensional "moment" strain measures X_{ij}.

3.2.1 Strain Energy of an Isotropic Cosserat Elastic Material

The total elastically stored energy integrated through the thickness are the addition of two separate contributions:

$$2\,\mathcal{U} = \langle \boldsymbol{\sigma} : \boldsymbol{\Gamma} \rangle + \langle \boldsymbol{\mu} : \boldsymbol{X} \rangle \tag{17}$$

For an isotropic Cosserat elastic material, the constitutive laws are given by eq. (1), repeated here for convenience

$$\sigma_{ij} = \lambda \Gamma_{kk} \delta_{ij} + (\mu + \kappa)\Gamma_{ij} + \mu \Gamma_{ji}$$

$$\mu_{ij} = \alpha X_{kk} \delta_{ij} + \beta X_{ji} + \gamma X_{ij}$$

3.2.2 Virtual Work of the Applied Loads

Consider a plate with an applied body force distribution $\boldsymbol{\varphi}_f$ $(= \varphi_{f_i} \mathbf{B}_i)$, a body couple distribution $\boldsymbol{\varphi}_m$ $(= \varphi_{m_i} \mathbf{B}_i)$, a surface force distribution $\boldsymbol{\tau}_f$ $(= \tau_{f_i} \mathbf{B}_i)$ and a surface couple distribution $\boldsymbol{\tau}_m$ $(= \tau_{m_i} \mathbf{B}_i)$. As detailed in appendix C, the virtual work done *through the thickness* by the applied loads $\boldsymbol{\tau}_f^+$, $\boldsymbol{\tau}_m^+$ at the top surface, $\boldsymbol{\tau}_f^-$, $\boldsymbol{\tau}_m^-$ at the bottom surface, the body force $\boldsymbol{\varphi}_f$ and the body couple $\boldsymbol{\varphi}_m$ is

$$\begin{aligned} \overline{\delta \mathcal{W}} =& \langle \boldsymbol{\varphi}_f \cdot \delta \hat{\mathbf{R}} \rangle + \boldsymbol{\tau}_f^+ \cdot \delta \hat{\mathbf{R}}|_{h/2} + \boldsymbol{\tau}_f^- \cdot \delta \hat{\mathbf{R}}|_{-h/2} \\ &+ \langle \boldsymbol{\varphi}_m \cdot \overline{\delta \boldsymbol{\psi}}^{\hat{B}b} \rangle + \boldsymbol{\tau}_m^+ \cdot \overline{\delta \boldsymbol{\psi}}^{\hat{B}b}|_{h/2} + \boldsymbol{\tau}_m^- \cdot \overline{\delta \boldsymbol{\psi}}^{\hat{B}b}|_{-h/2} \end{aligned} \tag{18}$$

Following the steps and definitions detailed in appendix C, this becomes

$$\begin{aligned} \overline{\delta \mathcal{W}} =& \overline{\delta q}^{\mathrm{T}} f + \overline{\delta \psi}^{\mathrm{T}} m + \delta \left(\tau_f^{+\mathrm{T}} w^+ + \tau_f^{-\mathrm{T}} w^- + \langle \varphi_f^{\mathrm{T}} w \rangle \right) \\ &+ \delta \left(\tau_m^{+\mathrm{T}} \phi^+ + \tau_m^{-\mathrm{T}} \phi^- + \langle \varphi_m^{\mathrm{T}} \phi \rangle \right) \end{aligned} \tag{19}$$

where the generalized applied forces and moments distributed over the plate reference surface can be defined as

$$f = \tau_f^+ + \tau_f^- + \langle \varphi_f \rangle \tag{20}$$

$$m = \begin{Bmatrix} \tau_{m_1}^+ + \tau_{m_1}^- + \frac{h}{2}(\tau_{f_1}^+ - \tau_{f_1}^-) + \langle \varphi_{m_1} + x_3 \varphi_{f_1} \rangle \\ \tau_{m_2}^+ + \tau_{m_2}^- + \frac{h}{2}(\tau_{f_2}^+ - \tau_{f_2}^-) + \langle \varphi_{m_2} + x_3 \varphi_{f_2} \rangle \\ \tau_{m_3}^+ + \tau_{m_3}^- + \langle \varphi_{m_3} \rangle \end{Bmatrix} \tag{21}$$

3.3 Compatibility Equations

It is well known that the 12 quantities $\epsilon_{\alpha\beta}$, $2\gamma_{\alpha 3}$, $K_{\alpha\beta}$, $K_{\alpha 3}$ are not independent. It is clear that that the kinematics of the plate reference surface can be expressed in at most six independent quantities: three measures of displacement and three measures of rotation. Expressing the displacement vector $\mathbf{u}$ and rotation tensor $\boldsymbol{C^{Bb}}$ in matrix form as u and C^{Bb}, it can easily be shown that the following kinematical relations hold

$$\begin{aligned} \gamma_\alpha &= C^{Bb}(e_\alpha + u_{,\alpha}) - e_\alpha \\ \widetilde{K_\alpha} &= -C^{Bb}_{,\alpha} C^{bB} \end{aligned} \tag{22}$$

where $\widetilde{(\ )}_{ij} = -e_{ijk}(\ )_k$, and we have defined

$$\gamma_\alpha = \begin{Bmatrix} \epsilon_{\alpha 1} \\ \epsilon_{\alpha 2} \\ 2\gamma_{\alpha 3} \end{Bmatrix}, \qquad K_\alpha = \begin{Bmatrix} -K_{\alpha 2} \\ K_{\alpha 1} \\ K_{\alpha 3} \end{Bmatrix}, \qquad e_1 = \begin{Bmatrix} 1 \\ 0 \\ 0 \end{Bmatrix}, \qquad e_2 = \begin{Bmatrix} 0 \\ 1 \\ 0 \end{Bmatrix} \tag{23}$$

The appropriate compatibility equations can be derived following Simmonds and Danielson [136] or Reissner [125], and are similar in form to those reported by Hodges et al. [64] had we chosen $\epsilon_{12} = \epsilon_{21}$.

$$\begin{aligned} &\gamma_{1,2} - \gamma_{2,1} - \widetilde{K_1}(\gamma_2 + e_2) + \widetilde{K_2}(\gamma_1 + e_1) = 0 \\ &K_{1,2} - K_{2,1} - \widetilde{K_1} K_2 = 0 \end{aligned} \tag{24}$$

For the reader's convenience, these relations are expanded out and presented in appendix B.

Since we are restricting ourselves to small strains, such that $\hat{\varepsilon} = \max(|\epsilon_{\alpha\beta}|, h|K_{\alpha\beta}|)$, there are several inferences one can draw from these compatibility equations regarding the relative orders of some of these terms.

- $K_{\alpha 3}$ are higher order in an asymptotic sense, i.e., $\mathcal{O}(\hat{\varepsilon}/l)$. This implies that for the zeroth-order approximation of the total energy leading to a "classical" theory (where the energy is $\mathcal{O}(\bar{\mu}\hat{\varepsilon}^2)$), these strain measures do not appear. They will, however, appear in a refined theory where the strain energy has terms of $\mathcal{O}(\bar{\mu}h^2\hat{\varepsilon}^2/l^2)$.

- The transverse shear strains $2\gamma_{\alpha 3}$ are taken to be $\mathcal{O}(h\hat{\varepsilon}/l)$. This will also, like $K_{\alpha 3}$, result in these strain measures not appearing in a classical theory, but instead in a refined one.

- The difference $K_{12} - K_{21}$ is $\mathcal{O}(h\hat{\varepsilon}/l^2)$, involving the derivatives of the shear strain measures with respect to the in-plane coordinates. It is then natural to replace K_{12} and K_{21} with two other measures, $\kappa_{12} \equiv (K_{12} + K_{21})/2$ and $\Omega_\kappa \equiv (K_{12} - K_{21})/2$. As we shall see later, doing so makes Ω_κ vanish from both a classical theory and a second-order refined theory. It would only show up if terms of $\mathcal{O}(\mu h^4\hat{\varepsilon}^2/l^4)$ were considered for the strain energy.

- A similar change of variables with ϵ_{12} and ϵ_{21} can be done, with them replaced by $\varepsilon_{12} \equiv (\epsilon_{12} + \epsilon_{21})/2$ and $\Omega_\varepsilon \equiv (\epsilon_{12} - \epsilon_{21})/2$. However, none of the compatibility equations allow us to comment on the relative orders of these two strain measures and will have to be retained, even in a classical theory. But as will be shown later, the equilibrium equations enable us to conclude that Ω_ε is also $\mathcal{O}(h^2\hat{\varepsilon}/l^2)$.

3.4 Dimensional Reduction

Up to this point, we have simply stated an alternative formulation of the original 3-D Cosserat elasticity problem. If we attempt to solve this problem directly, we will meet the same difficulty as solving any full 3-D elasticity problem. Fortunately, as shown below, the VAM can be used to calculate the 3-D warping functions asymptotically. In order to reduce the original 3-D problem to an asymptotically correct 2-D plate problem, one must attempt to reproduce the energy stored in the 3-D structure in the 2-D formulation. This dimensional reduction can only be done in an approximate manner, by taking advantage of the certain small parameters inherent to the problem. For plates, this would be h/l, where l is the wavelength of deformation.

Central to this method is the assessment of the asymptotic orders of various quantities and their derivatives in the formulation. In the previous section, we have reported on the relative orders of the various generalized 2-D strain measures. Additionally, we need the orders of the distributed force and moment terms, f_i and m_i. Following Sutyrin [145], we will state for now that these terms do not contribute to a zeroth-order approximation. Later, when we develop a refined model, will prove that these terms need to be included.

The complete statement of the problem can now be presented in terms of the principle of virtual work, such that

$$\delta\mathcal{U} - \overline{\delta\mathcal{W}} = 0 \tag{25}$$

The VAM requires one to find the leading terms of the energy functional according to different orders (expanded in a series in the small parameter h/l). The total potential energy consists of terms involving the 2-D generalized strains and the generalized warping (w_i and ϕ_i). One can pose the problem that governs the warping as the minimization of a total potential functional Π in which only the generalized warping

functions w_i, ϕ_i are varied subject to constraints.

$$\begin{aligned} &\delta\Pi = 0 \quad \text{with} \\ &\Pi = \mathcal{U} - \tau_f^{+\mathrm{T}} w^+ - \tau_f^{-\mathrm{T}} w^- - \langle \varphi_f^{\mathrm{T}} w \rangle - \tau_m^{+\mathrm{T}} \phi^+ - \tau_m^{-\mathrm{T}} \phi^- - \langle \varphi_m^{\mathrm{T}} \phi \rangle \end{aligned} \tag{26}$$

3.4.1 Zeroth-Order Approximation

For the zeroth-order approximation, the generalized warping field that minimizes the total potential energy, subject to the constraints given by eqs. (11) and (12) is found using the usual calculus of variations (see appendix E for closed form expressions). Substituting the solution back into the total energy and integrating through-the-thickness (since the expression is now an explicit function of x_3), one can obtain a quadratic form of the total potential energy in the two-dimensional strain measures, asymptotically correct through $\mathcal{O}(\bar{\mu} h \hat{\varepsilon}^2)$ as

$$2\Pi_0 = \mathcal{E}^T A \mathcal{E} \tag{27}$$

where

$$\mathcal{E} = [\epsilon_{11}\ 2\varepsilon_{12}\ 2\Omega_\varepsilon\ \epsilon_{22}\ K_{11}\ 2\kappa_{12}\ K_{22}]^T \tag{28}$$

and $\bar{\mu}$ is the order of a typical material constant (such as E). It is worth noting that ϵ_{12} and ϵ_{21} appear as two separate strain measures (via ε_{12} and Ω_ε) due to the choice of constraints on the local rotation in eq. (12). On the other hand, only the sum $(K_{12} + K_{21})$ appears while the difference $(K_{12} - K_{21})$ is absent as previously expected. So, in all, we have 7 generalized strain measures appearing in a zeroth-order approximation.

Since Π_0 is a quadratic form, one can express the plate elastic law in a form where the conjugate stress resultants denoted by N_{11}, $\mathscr{N}_{12}$, $\mathscr{N}_\varepsilon$, N_{22}, M_{11}, $\mathscr{M}_{12}$ and M_{22} are *linear* functions of the aforementioned list of two-dimensional strain measures. The "classical" plate constitutive law is then obtained as follows

$$N_{11} = \frac{\partial \Pi_0}{\partial \epsilon_{11}} = \frac{Eh}{1-\nu^2}(\epsilon_{11} + \nu\epsilon_{22}) \tag{29a}$$

$$N_{22} = \frac{\partial \Pi_0}{\partial \epsilon_{22}} = \frac{Eh}{1-\nu^2}(\nu\epsilon_{11} + \epsilon_{22}) \tag{29b}$$

$$\mathscr{N}_{12} = \frac{\partial \Pi_0}{\partial (2\varepsilon_{12})} = \frac{Eh}{1-\nu^2}\frac{(1-\nu)}{2} 2\varepsilon_{12} \tag{29c}$$

$$\mathscr{N}_{\varepsilon} = \frac{\partial \Pi_0}{\partial (2\Omega_{\varepsilon})} = \frac{h\kappa}{2}(2\Omega_{\epsilon}) \tag{29d}$$

$$M_{11} = \frac{\partial \Pi_0}{\partial K_{11}} = \left[\frac{Eh^3}{12(1-\nu^2)} + \gamma h\right] K_{11} + \left[\frac{E\nu h^3}{12(1-\nu^2)} - \beta h\right] K_{22} \tag{29e}$$

$$\mathscr{M}_{12} = \frac{\partial \Pi_0}{\partial (2\kappa_{12})} = \left[\frac{Eh^3}{12(1-\nu^2)}\frac{1-\nu}{2} + \frac{(\beta+\gamma)h}{2}\right] 2\kappa_{12} \tag{29f}$$

$$M_{22} = \frac{\partial \Pi_0}{\partial K_{22}} = \left[\frac{E\nu h^3}{12(1-\nu^2)} - \beta h\right] K_{11} + \left[\frac{Eh^3}{12(1-\nu^2)} + \gamma h\right] K_{22} \tag{29g}$$

where

$$\begin{aligned} E &= \frac{(2\mu+\kappa)(3\lambda+2\mu+\kappa)}{2\lambda+2\mu+\kappa} \\ \nu &= \frac{\lambda}{2\lambda+2\mu+\kappa} \end{aligned} \tag{30}$$

There are a few important observations to be made here.

- The bending and torsional stiffnesses have contributions from the nonclassical elastic constants β and γ. Also, these additional terms are linear in h in contrast to the classical flexural rigidity which is cubic in h. This leads one to conclude that an increase in the flexural rigidity due to micropolar effects will become important only for very thin plates.

- Figures 13 and 14 show the increase in the cylindrical bending stiffness of a plate made of dense polyurethane and polystyrene, respectively as the plate thickness decreases. Figures 15 and 16 show a similar dependence of the torsional stiffness on the thickness of a plate made of the same materials. The stiffnesses have been normalized with their classical values. The constants l_b, l_t that appear in the plots are characteristic lengths associated with bending and torsion, defined

as $l_b^2 = \gamma/2(2\mu + \kappa)$ and $l_t^2 = (\beta + \gamma)/(2\mu + \kappa)$. All the necessary micropolar constants are presented in table 5 and have been taken from experimental data provided by Lakes [90].

- These expressions for the membrane and bending stiffnesses coincide with those published by Gauthier and Jahsman [47], Ellis and Smith [35], Altenbach and Eremeyev [2], etc. However, no a priori assumptions have been made regarding the deformation. For example, Ellis and Smith use standard Kirchhoff-Love-type assumptions regarding the deformation – normal lines remain straight and normal after deformation, vanishing of the normal stress, etc. Gauthier and Jahsman treat the problem as plane stress, which automatically implies a loss of through-the-thickness information. Altenbach and Eremeyev's linear plate theory also contains assumptions regarding the through-thickness variation of the displacements and stresses, not unlike those by Eringen [39]. Clearly, such assumptions are neither necessary nor are they correct.

- It is worth mentioning that expressions such as this modified plate constitutive law are what have been traditionally used to design experiments measuring the constants β, γ, etc. For example, one can consider plate specimens of different thicknesses and experimentally measure their flexural rigidity as a function of h in a cylindrical bending test, thereby determining a length scale parameter associate with bending (and hence determining γ).

3.4.2 Second-Order approximation

We note that the zeroth-order warping is $\mathcal{O}(\hat{\varepsilon})$. According to the VAM, to obtain a refined total energy (of $\mathcal{O}(\bar{\mu}h^2\hat{\varepsilon}^2/l^2)$), one needs to find the higher-order contribution in the asymptotic sense to the warping. To obtain the first-order approximations of

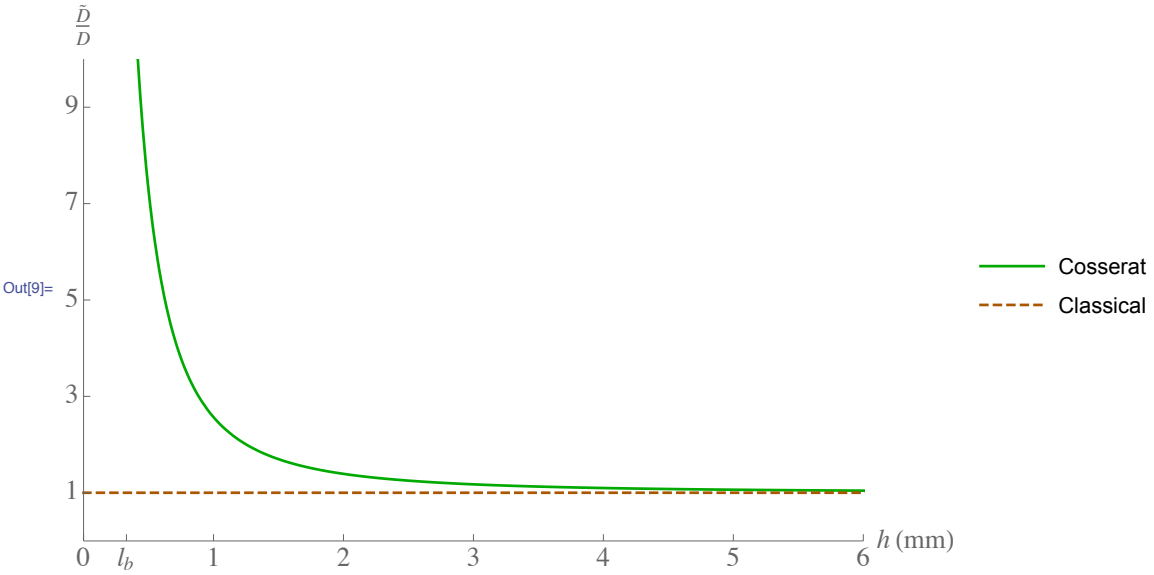

Figure 13: Dependence on thickness of cylindrical bending stiffness in plates made of dense Polyurethane

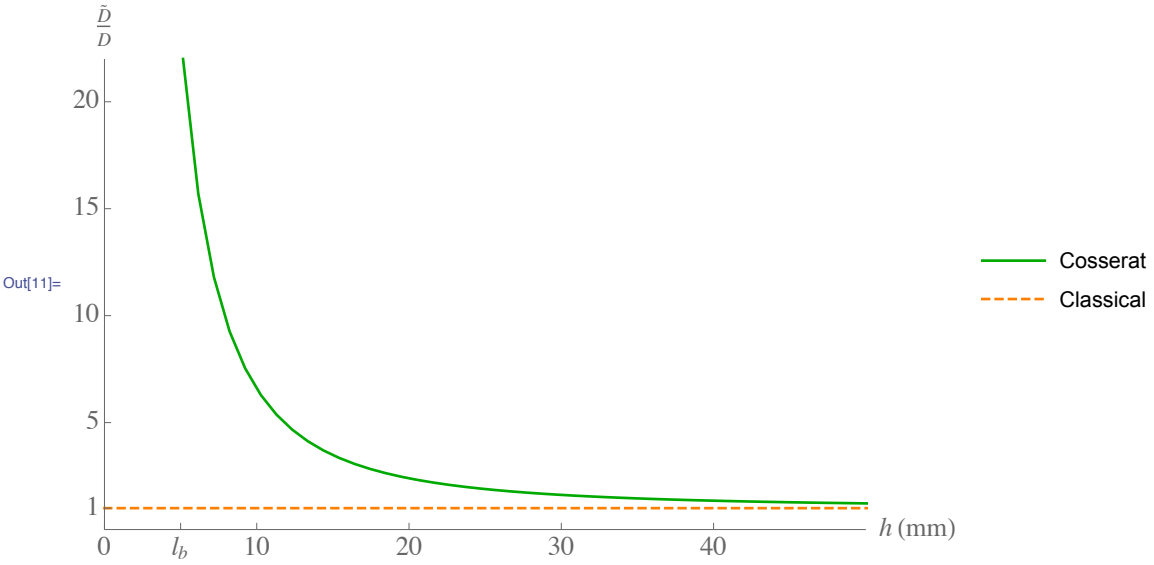

Figure 14: Dependence on thickness of cylindrical bending stiffness in plates made of Polystyrene

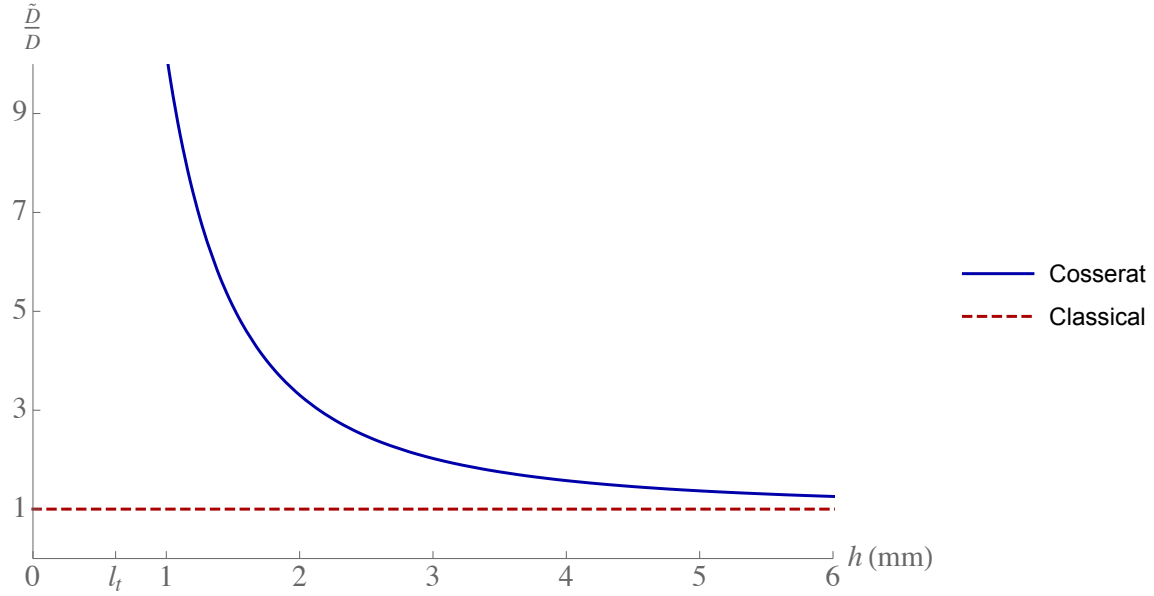

Figure 15: Dependence on thickness of twisting stiffness in plates made of dense Polyurethane

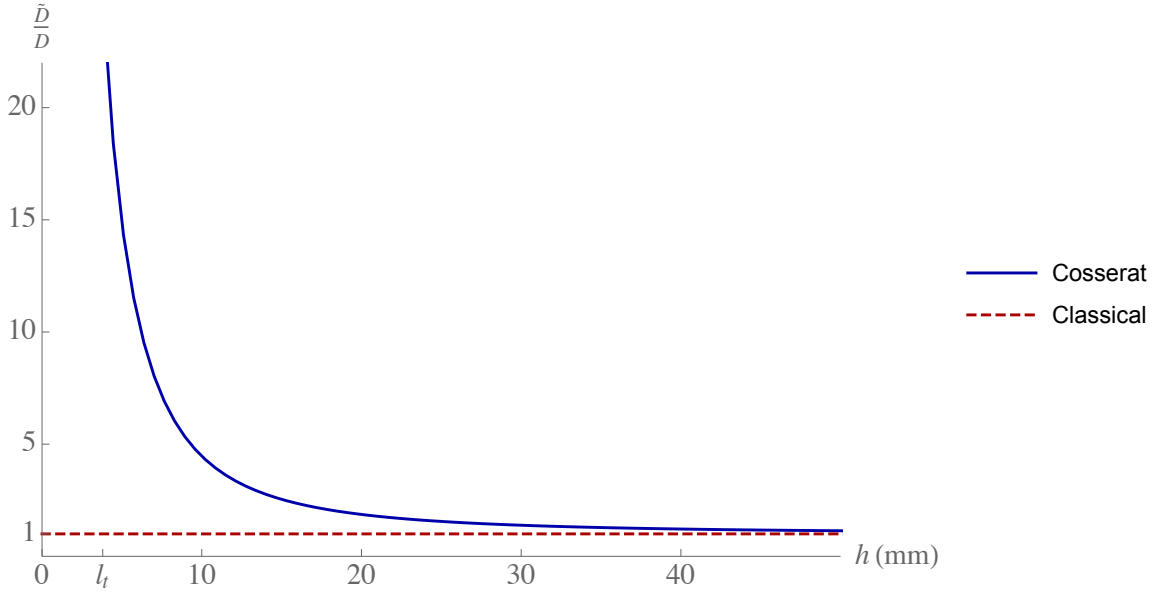

Figure 16: Dependence on thickness of twisting stiffness in plates made of Polystyrene

Table 5: Material properties of some foams showing length-scale dependent behavior

	Polyurethane (dense)	Polystyrene
E	2.995×10^8 N/m^2	1.300×10^6 N/m^2
ν	0.44	0.07
κ	8.666×10^6 N/m^2	5.062×10^4 N/m^2
β	3.547×10^1 N	-4.320×10^1 N
γ	4.448×10^1 N	6.075×10^1 N
l_0	1.635×10^{-3} m	1.666×10^{-2} m
ρ	3.40×10^2 kg/m^3	3.674×10^1 kg/m^3

the generalized warping functions, we simply perturb the zeroth-order results like so

$$\begin{aligned} w_\alpha &= < \text{zeroth-order in-plane warping} > + v_\alpha \\ w_3 &= < \text{zeroth-order out-of-plane warping} > + v_3 \\ \phi_\alpha &= < \text{zeroth-order in-plane local rotation} > + \varphi_\alpha \\ \phi_3 &= < \text{zeroth-order out-of-plane local rotation} > + \varphi_3 \end{aligned} \tag{31}$$

Substituting this back into eqs. (15) and (16), one can obtain the leading terms of the total energy that is asymptotically correct through the second order. Doing so will result in an expression involving, among other terms, derivatives of v_i, φ_i with respect to the in-plane coordinates. One can eliminate these terms using integration by parts, since the goal is to obtain an interior solution for the plate without considering edge effects. Then, a straightforward application of the calculus of variations again will get us expressions for the generalized warping fields. Closed form expressions for the same are presented in appendix E for the case of constant body-forces through the thickness of the plate[2]. Substituting the solution back into the total energy and integrating through-the-thickness, one can obtain the following form of the total potential energy in the two-dimensional strain measures and the externally applied

[2]Such restrictions are unnecessary although it does simplify calculations considerably.

loads, asymptotically correct through $\mathcal{O}(\bar{\mu}h^3/l^2\hat{\varepsilon}^2)$:

$$\begin{aligned} 2\Pi_1 =& \mathcal{E}^T A\mathcal{E} + \mathcal{E}_{,1}^T B\mathcal{E}_{,1} + 2\mathcal{E}_{,1}^T C\mathcal{E}_{,2} + \mathcal{E}_{,2}^T D\mathcal{E}_{,2} \\ &+ \mathcal{G}^T G\mathcal{G} + \mathcal{E}_{,1}^T G_1\mathcal{G} + \mathcal{E}_{,2}^T G_2\mathcal{G} + \mathcal{K}^T H\mathcal{K} + \mathcal{E}_{,1}^T H_1\mathcal{K} + \mathcal{E}_{,2}^T H_2\mathcal{K} + \mathcal{E}^T F \end{aligned} \tag{32}$$

where $\mathcal{G} = [2\gamma_{13}\ 2\gamma_{23}]^T$, $\mathcal{K} = [K_{13}\ K_{23}]^T$. Due to their lengthy nature, expressions for the matrices above are not provided.

The form of the strain energy in eq. (32) contains derivatives of the 2-D generalized strains which is unsuitable for practical use. If possible, we wish to eliminate these terms and repackage the energy expression in the following form:

$$2\Pi_c = \mathcal{E}^T \bar{A}\mathcal{E} + \mathcal{G}^T \bar{G}\mathcal{G} + \mathcal{K}^T \bar{H}\mathcal{K} + \mathcal{E}^T F_{\mathcal{E}} + \mathcal{G}^T F_{\mathcal{G}} + \mathcal{K}^T F_{\mathcal{K}} \tag{33}$$

This is possible with a careful use of the equilibrium equations (which are presented in the next section) and the compatibility equations. It can be shown that, for isotropic materials, this repackaging can be done in an asymptotically exact manner (i.e., terms discarded in the process are $\mathcal{O}(\bar{\mu}h^4\hat{\varepsilon}^2/l^3)$). On the other hand, for orthotropic or even generally anisotropic materials this can only be done in an approximate manner via an optimization technique similar to the one presented by Yu et al. [166].

At this stage, we will concentrate mainly on obtaining the $\bar{A}, \bar{G}, \bar{H}$ matrices for isotropic materials although the load-related terms can be easily determined as well. It can be shown that $\bar{A} = A$. This means that the constitutive relations provided by eq. (29) remain valid for a second-order accurate energy model. This leaves us with the determination of the shear stiffness matrix $\bar{G}$ and the drilling stiffness matrix $\bar{H}$. We will now comment on the solutions obtained for these quantities:

Shear Stiffness It can be shown that the shear stiffness $\bar{g}$ of the plate is the solution of the following quadratic equation

$$\frac{b}{(D+\gamma h)^2}\bar{g}^2 + \left[2\left(\frac{D}{D+\gamma h}\right)\left(\frac{\mu}{\mu+\kappa}\right) - 1\right]\bar{g} + \frac{2\mu+\kappa}{\mu+\kappa}h\kappa = 0 \tag{34}$$

where $D = Eh^3/12(1-\nu^2)$ and b is a complicated function of the 3-D material constants. To verify the correctness of the derived result, one can set all the micropolar constants to zero and check for the shear stiffness obtained. For a classical material, the expression for b reduces to $-Eh^5(6-\nu)/[360(1+\nu)(1-\nu)^2]$. Solving for $\bar{g}$, we obtain

$$\bar{g} = \frac{5Gh}{6-\nu} \tag{35}$$

One can compare this expression to the one that can be derived following the equations given by Yu et al. [166], where an optimization technique is used in the transformation procedure to construct a generalized Reissner-Mindlin model. This is plotted as a function of the Poisson's ratio in fig. 17 below. Note that for positive values of ν, the difference between two curves is negligible: for example, at $\nu = 0.3$, the present work results in $\bar{g} = 0.877Gh$ while the previous work gives $\bar{g} = 0.879Gh$, a difference of 0.22 %. We note that modifying the way the warping constraints in eqs. (11) and (12) are specified, as done by Yu [162], we will obtain a more conventional result of $5/6Gh$ for the shear stiffness. However, both approaches result in the same second-order strain energy expression and there is no benefit in doing so and, hence, such an approach is not pursued here. Most recently, Lee and Hodges [94] introduced a new hybrid transformational approach that does not require an optimization procedure or relaxation of warping constraints and gives the same shear stiffness as eq. (35).

In fact, there is a profusion of literature suggesting that the shear correction factor (defined here as simply the shear stiffness normalized by Gh) for plates ought to, and indeed does, depend on Poisson's ratio. While there is near universal agreement that the correct factor ought to be 5/6 for zero Poisson's ratio, there is a wide disagreement on the functional form of the dependence on ν.

For example, Timoshenko [147] obtained a value of $(5+5\nu)/(6+5\nu)$ by comparing a beam solution with a 2-D solution of the bending problem. Cowper [26] derived

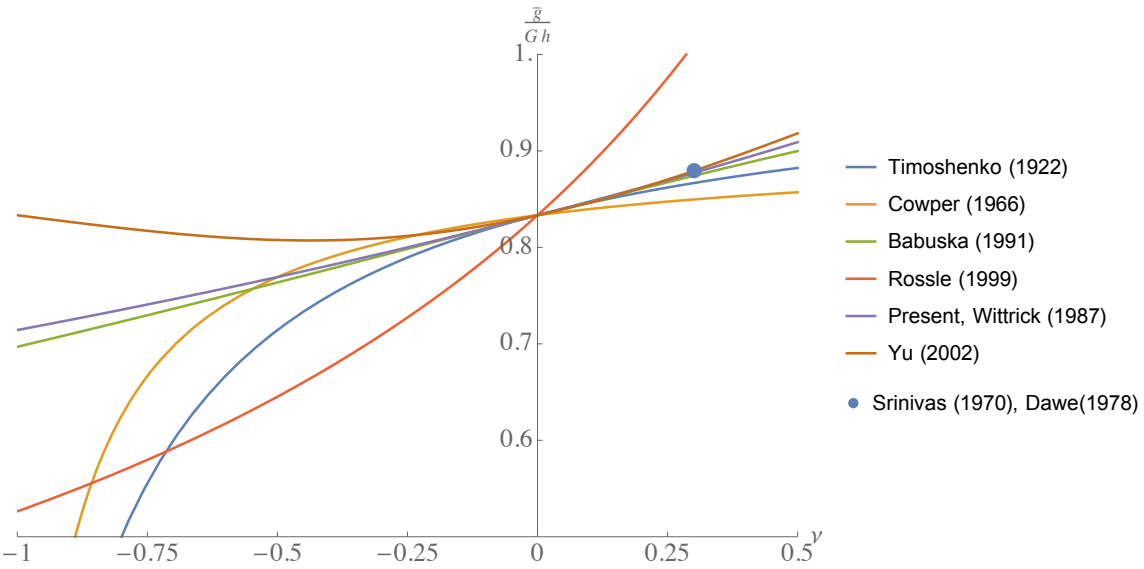

Figure 17: Variation of shear stiffness with Poisson's ratio

a very similar expression of $(10+10\nu)/(12+11\nu)$. Srinivas [141] and Dawe [27, 28] recommended a value of 0.88 to match the first eigenvalue of a Reissner-Mindin plate analysis to an exact 3-D (linear) elasticity solution, that is very close to a value of 0.877 obtained from the present work. Wittrick [156] arrived at the same shear correction factor of $5/(6-\nu)$ as ours based on an analytical vibration solution of a 3-D simply supported plate. Babuška [8] suggested a range of expressions dependent on ν, depending on the goal of the plate modeling. Rössle [129] compared asymptotic expansions of 3-D displacements from Reissner-Mindlin theory and 3-D elasticity for periodic boundary conditions and came up with a correction factor of $10/(12-7\nu)$. A visual comparison of all these different shear correction factors is shown in fig. 17.

Drilling Stiffness By taking a partial derivative of the drilling energy with respect to the in-plane curvatures, we obtain

$$\begin{aligned} M_{13} = \frac{\partial \Pi_c}{\partial K_{13}} = &\left[\frac{\gamma^2-\beta^2}{\gamma} + \frac{(\beta+\nu\gamma)^2}{\gamma}\left(1-\frac{\tanh\left(h/2l_0\right)}{h/2l_0}\right)\right] hK_{13} \\ &+(\beta+\nu\gamma)\left(\frac{\nu}{1-\nu}\right)\left(1-\frac{\tanh\left(h/2l_0\right)}{h/2l_0}\right)\frac{(1-\nu^2)}{E} f_2 \end{aligned} \tag{36}$$

$$M_{23} = \frac{\partial \Pi_c}{\partial K_{23}} = \left[\frac{\gamma^2 - \beta^2}{\gamma} + \frac{(\beta + \nu\gamma)^2}{\gamma} \left(1 - \frac{\tanh\left(h/2l_0\right)}{h/2l_0} \right) \right] hK_{23} \\ -(\beta + \nu\gamma) \left(\frac{\nu}{1-\nu} \right) \left(1 - \frac{\tanh\left(h/2l_0\right)}{h/2l_0} \right) \frac{(1-\nu^2)}{E} f_1 \tag{37}$$

where l_0 is a length-scale parameter defined as

$$l_0 = \sqrt{\frac{\gamma(\mu + \kappa)}{\kappa(2\mu + \kappa)}} \tag{38}$$

This same length-scale parameter shows up in several analyses involving micropolar elasticity in the literature and was first identified by Eringen [38]. A few observations can be made regarding the expressions for the drilling stiffness:

- For very thin plates (but $h \neq 0$), the expression for the drilling stiffness reduces to $(\gamma^2 - \beta^2)h/\gamma$. This is the same expression one would obtain with plane stress assumptions (i.e., taking $\mu_{31} = 0$). Indeed, several authors have derived this same expression for the drilling stiffness using various techniques (see Green and Naghdi [53], Steinberg [142, 144]). Such an approximation is only valid for cases where the plate thickness is of the order of the length-scale parameter l_0. To demonstrate, let us consider again the experimental data of two foams provided by Lakes [90] - dense Polyurethane and Polystyrene - whose material constants are given in table 5. Figures 18 and 19 show the variation of the drilling stiffness expression, normalized by $(\gamma^2 - \beta^2)h/\gamma$, with plate thickness. Clearly, this plane-stress expression is valid when $h \approx l_0$ but differs significantly for larger h.

- The assumption of plane stress also dictates that the location rotation vary linearly through the thickness. From the expression derived in this work (see appendix E), one can see that such an approximation does not accurately capture the through-the-thickness behavior.

- Other authors report a drilling stiffness of γh, which is consistent with an assumption of plane strain (see Altenbach and Eremeyev [2]). Clearly, this does

not capture all the terms needed and, by the authors' own admission, is possibly in error.

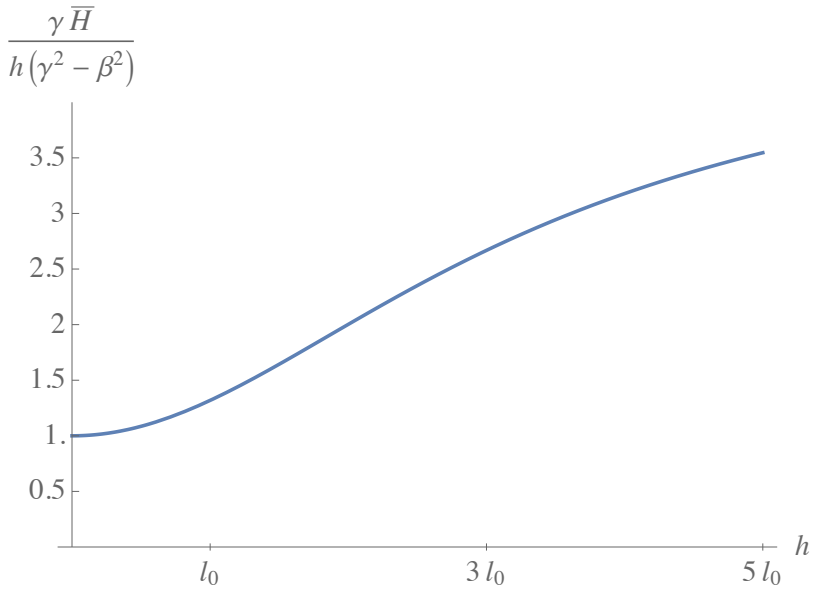

Figure 18: Drilling stiffness of plates made of dense Polyurethane, with $l_0 = 1.635$mm

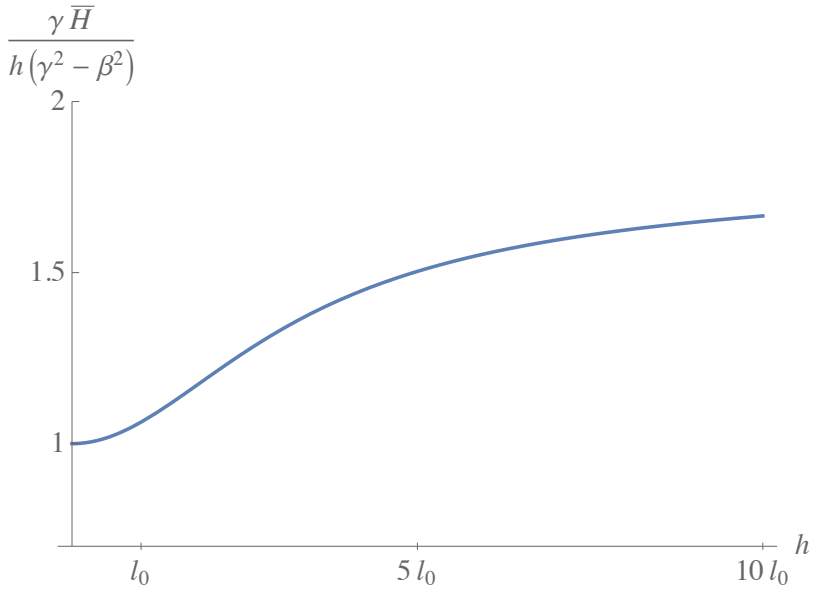

Figure 19: Drilling stiffness of plates made of Polystyrene, with $l_0 = 16.66$mm

CHAPTER IV

FULLY INTRINSIC TWO-DIMENSIONAL THEORY OF COSSERAT PLATES

Following the dimensional reduction of the original three-dimensional representation, we will now develop a geometrically-exact intrinsic formulation for the dynamics of a moving plate. A theory is said to be *intrinsic* when it is independent of any specific choice of displacement or rotation variables (see [64] for a detailed discussion). The formulation will instead result in a system of algebraic-differential equations in terms of the generalized strains and stress resultants, velocities, angular velocities, linear momenta and angular momenta, with spatial and time derivatives of the unknowns no higher than the first, and nonlinearities no higher than quadratic. This has several benefits over formulations based on displacement and rotation variables, including computational efficiency and avoidance of singularities associated with rotation variables.

A formulation of this nature was developed by Hodges [69] for the dynamics of curved and twisted composite beams. More recently, this methodology was applied to the dynamics of composite plates [66]. In the current effort, this will be extended to plates that can be modeled as polar media. It is to be noted that the theory is equally applicable to anisotropic and isotropic plates. The difficulty associated with anisotropy is dealt with in the through-the-thickness analysis, allowing the 2-D plate analysis to be formulated exactly as a Cosserat surface and confines all approximations to the through-the-thickness analysis, whose accuracy is guaranteed to be the best by VAM.

4.1 Intrinsic Equations from Hamilton's Principle

We begin with Hamilton's extended principle for a surface

$$\int_{t_1}^{t_2}\int_{\mathcal{S}}[\delta(\mathcal{K}-\mathcal{U})+\overline{\delta\mathcal{W}}]dsdt=\overline{\delta\mathcal{A}} \tag{39}$$

At this point, the constitutive law is assumed to be known (either determined by VAM or another suitable through-the-thickness analysis) and can be written for a general anisotropic micropolar material in stiffness form as

$$\begin{aligned} N_\alpha &= \mathbb{A}_{\alpha\beta}\gamma_\beta + \mathbb{B}_{\alpha\beta}K_\beta \\ M_\alpha &= \mathbb{B}_{\beta\alpha}\gamma_\beta + \mathbb{D}_{\alpha\beta}K_\beta \end{aligned} \tag{40}$$

or in flexibility form as

$$\begin{aligned} \gamma_\alpha &= \mathbb{R}_{\alpha\beta}N_\beta + \mathbb{S}_{\alpha\beta}M_\beta \\ K_\alpha &= \mathbb{S}_{\beta\alpha}N_\beta + \mathbb{T}_{\alpha\beta}M_\beta \end{aligned} \tag{41}$$

We can therefore write the variation of the two-dimensional strain energy as

$$\delta\mathcal{U}=\delta\gamma_\alpha^T N_\alpha+\delta K_\alpha^T M_\alpha \tag{42}$$

where summation is implied over repeated indices, and we define

$$N_\alpha=\begin{Bmatrix} N_{\alpha1} \\ N_{\alpha2} \\ Q_\alpha \end{Bmatrix} \qquad M_\alpha=\begin{Bmatrix} -M_{\alpha2} \\ M_{\alpha1} \\ M_{\alpha3} \end{Bmatrix} \tag{43}$$

However, the variations of the twelve generalized strains are not independent and can be expressed in terms of six independent virtual displacements and virtual rotations

$$\begin{aligned} \delta\epsilon_{\alpha\beta} &= e_\beta^T\left[\overline{\delta q}_{,\alpha}+\widetilde{K_\alpha}\overline{\delta q}+(\widetilde{e}_\alpha+\widetilde{\gamma}_\alpha)\overline{\delta\psi}\right] \\ \delta(2\gamma_{\alpha3}) &= \overline{\delta q}_{3,\alpha}+\overline{\delta\psi}_\alpha+\epsilon_{\alpha\beta}\overline{\delta\psi}_\beta-K_{\alpha\beta}\overline{\delta q}_\beta \\ \delta K_\alpha &= \overline{\delta\psi}_{,\alpha}+\widetilde{K_\alpha}\overline{\delta\psi} \end{aligned} \tag{44}$$

For the virtual work of applied loads per unit area, $\overline{\delta\mathcal{W}}$, we can use the expression given eq. (19) minus the influence of warping, which is negligible for present purposes. The next step is to express the variation of the kinetic energy per unit area in intrinsic form. By definition,

$$\mathcal{K} = \frac{1}{2}\langle \rho \mathbf{v}^{MI} \cdot \mathbf{v}^{MI} \rangle + \frac{1}{2}\langle j\boldsymbol{\omega}^{MI} \cdot \boldsymbol{\omega}^{MI} \rangle \tag{45}$$

where $\mathbf{v}^{MI}$ and $\boldsymbol{\omega}^{MI}$ are the inertial velocity and angular velocity of any material point in the moving plate. Note that the rotary inertia j is a consequence of micropolar elasticity. For low frequency dynamics we can ignore the warping and local rotation in the kinetic energy. Then, it can be shown that the column matrix of measure numbers of the velocity and angular velocity, expressed in the basis $\mathbf{B}_i$ can be written as

$$\mathrm{v}^{MI} = V + \widetilde{\Omega}\xi \tag{46}$$

$$\omega^{MI} = \Omega \tag{47}$$

where $\xi = \begin{bmatrix} 0 & 0 & x_3 \end{bmatrix}^T$ with x_3 as the normal coordinate, V and Ω are the column matrices of measure numbers of the inertial velocity and angular velocity of any material point on the plate reference surface, both expressed in the basis $\mathbf{B}_i$. Denoting the inertial velocity and angular velocity vectors on the undeformed reference plane, expressed in the basis $\mathbf{b}_i$, by column matrices v, ω we can easily derive the following *generalized velocity-displacement equations*:

$$V = C(v + \dot{u} + \widetilde{\omega}u) \tag{48}$$

$$\widetilde{\Omega} = -\dot{C}C^T + C\widetilde{\omega}C^T \tag{49}$$

The expression for the kinetic energy per unit area of the plate now becomes

$$\mathcal{K} = \frac{1}{2}\langle \rho((V_1 + x_3\Omega_1)^2 + (V_2 + x_3\Omega_2)^2 + V_3^2) \rangle + \frac{1}{2}\langle j(\Omega_1^2 + \Omega_2^2 + \Omega_3^2) \rangle \tag{50}$$

and its variation can be written as

$$\delta\mathcal{K} = \delta V^T P + \delta\Omega^T H \tag{51}$$

with P and H as the linear and angular momenta, respectively, given by

$$\begin{Bmatrix} P \\ H \end{Bmatrix} = \begin{bmatrix} \mu\Delta & -\mu\widetilde{\overline{\xi}} \\ \mu\widetilde{\overline{\xi}} & I \end{bmatrix} \begin{Bmatrix} V \\ \Omega \end{Bmatrix} \tag{52}$$

Here, we define inertial constants commonly used in plate dynamics

$$\begin{aligned} \mu &= \langle\rho\rangle \qquad & \mu\overline{\xi} &= [0\ 0\ \langle x_3\rho\rangle]^T \\ J &= \langle j\rangle \qquad & \mu r^2 &= \langle x_3^2\rho\rangle \\ I &= \begin{bmatrix} \mu r^2 + J & 0 & 0 \\ 0 & \mu r^2 + J & 0 \\ 0 & 0 & J \end{bmatrix} \end{aligned} \tag{53}$$

To derive the intrinsic equations of motion, the variations $\delta V, \delta\Omega$ need to be expressed in terms of $\overline{\delta q}$ and $\overline{\delta\psi}$. To do so, recall the following definitions:

$$\begin{aligned} \overline{\delta q} &= C\delta u \\ \widetilde{\overline{\delta\psi}} &= \delta C C^T \end{aligned} \tag{54}$$

Then, using the generalized velocity-displacement relations from eq. (48), we can obtain:

$$\begin{aligned} \delta V &= \dot{\overline{\delta q}} + \widetilde{\Omega}\overline{\delta q} + \widetilde{V}\overline{\delta\psi} \\ \delta\Omega &= \dot{\overline{\delta\psi}} + \widetilde{\Omega}\overline{\delta\psi} \end{aligned} \tag{55}$$

At this point, we note that it is possible to relate the generalized strains γ_α, K_α and the generalized velocities V, Ω by eliminating u, C from the eqs. (22) and (48) to obtain the following *intrinsic kinematical partial differential equations* similar to Hodges et al. [66]

$$\begin{aligned} V_{,\alpha} &= \dot{\gamma}_\alpha + \widetilde{V}K_\alpha + \widetilde{\Omega}(e_\alpha + \gamma_\alpha) \\ \Omega_{,\alpha} &= \dot{K}_\alpha + \widetilde{\Omega}K_\alpha \end{aligned} \tag{56}$$

Finally, we also need to express the virtual action $\overline{\delta\mathcal{A}}$ along the boundary of plate and at the ends of the time interval in terms of virtual displacements and virtual rotations. Along the boundary one can specify appropriate combinations of displacements, rotations (geometrical boundary conditions), and running forces and moments (natural boundary conditions) along the boundary around the reference plane. Consider a boundary region $\mathit{\Gamma}$ where force resultants $\hat{N}$ and moment resultants $\hat{M}$ are specified, such that

$$\hat{N} = \begin{bmatrix} N_{\nu\nu} & N_{\nu\tau} & N_{\nu 3} \end{bmatrix}^T, \qquad \hat{M} = \begin{bmatrix} M_{\nu\nu} & M_{\nu\tau} & M_{\nu 3} \end{bmatrix}^T \tag{57}$$

where ν, τ are, respectively, along the outward normal of and tangent to the boundary curve. Also, we assume that at the ends of the time interval, we have virtual actions $(\overline{\delta q}^T \hat{P} + \overline{\delta\psi}^T \hat{H})$ entering and leaving the system. Then, $\overline{\delta\mathcal{A}}$ can be expressed as:

$$\overline{\delta\mathcal{A}} = \int_{\mathcal{S}} (\overline{\delta q}^T \hat{P} + \overline{\delta\psi}^T \hat{H})\big|_{t_1}^{t_2} \mathrm{d}s - \int_{t_1}^{t_2} \int_{\mathit{\Gamma}} (\overline{\delta q}^T \hat{N} + \overline{\delta\psi}^T \hat{M}) \mathrm{d}\Gamma \mathrm{d}t \tag{58}$$

Using eqs. (19), (44), (55), (F.3), (F.4) and (F.6), it is now possible to write the exact intrinsic equations of a Cosserat elastic plate as

$$\begin{aligned} &N_{\alpha,\alpha} + \widetilde{K}_\alpha N_\alpha + f = \dot{P} + \widetilde{\Omega} P \\ &M_{\alpha,\alpha} + \widetilde{K}_\alpha M_\alpha + (\widetilde{e}_\alpha + \widetilde{\gamma}_\alpha) N_\alpha + m = \dot{H} + \widetilde{\Omega} H + \widetilde{V} P \end{aligned} \tag{59}$$

The associated natural boundary conditions on $\mathit{\Gamma}$ are

$$\begin{aligned} N_{\nu\nu} &= n_1^2 N_{11} + n_1 n_2 (N_{12} + N_{21}) + n_2^2 N_{22} \\ N_{\nu\tau} &= n_1 n_2 (N_{22} - N_{11}) + n_1^2 N_{12} - n_2^2 N_{21} \\ N_{\nu 3} &= n_1 Q_1 + n_2 Q_2 \\ M_{\nu\nu} &= n_1^2 M_{11} + n_1 n_2 (M_{12} + M_{21}) + n_2^2 M_{22} \\ M_{\nu\tau} &= n_1 n_2 (M_{22} - M_{11}) + n_1^2 M_{12} - n_2^2 M_{21} \\ M_{\nu 3} &= n_1 M_{13} + n_2 M_{23} \end{aligned} \tag{60}$$

where $n_1 = \cos\phi, n_2 = \sin\phi$ and ϕ is the angle between the outward normal of the boundary and the x_1 direction. Finally, for the conditions at the ends of time intervals, one can either prescribe the 2-D displacement field, so that the 2-D generalized strains are known, or corresponding momenta such that

$$\begin{aligned} P(t_1) &= \hat{P}(t_1) \qquad & H(t_1) &= \hat{H}(t_1) \\ P(t_2) &= \hat{P}(t_2) \qquad & H(t_2) &= \hat{H}(t_2) \end{aligned} \tag{61}$$

It can be seen that the six equations of motion given by eq. (59), when specialized to static problems, are identical to the nonlinear equations derived by Reissner [125]. A linear theory can also be derived from these equations for purposes like order analysis and validation against 3-D linear Cosserat elasticity solutions. It can be verified that they coincide with those derived by Eringen [39], Altenbach et al. [2], and several others.

$$\begin{aligned} N_{11,1} + N_{21,2} + f_1 &= \dot{P}_1 \\ N_{12,1} + N_{22,2} + f_2 &= \dot{P}_2 \\ Q_{1,1} + Q_{2,2} + f_3 &= \dot{P}_3 \\ M_{11,1} + M_{21,2} - Q_1 + m_1 &= \dot{H}_1 \\ M_{12,1} + M_{22,2} - Q_2 + m_2 &= \dot{H}_2 \\ M_{13,1} + M_{23,2} + N_{12} - N_{21} + m_3 &= \dot{H}_3 \end{aligned} \tag{62}$$

4.2 A Note on Stress Resultants

Before we progress to discuss solution techniques of these 2-D plate equations, it may be beneficial to see if the stress resultants we defined have any physical significance. According to the present approach, N_α, M_α are merely quantities that are work conjugate to the 2-D generalized strains γ_α, K_α. It is however interesting to see if they can be related to the 3-D stress and couple stress measures in a more direct manner.

First, let us digress a little and recall that the 3-D generalized warping functions have been determined only through first order, i.e., $\mathcal{O}(h\hat{\varepsilon}/l)$, which helped us

construct a strain energy expression correct through second order $\mathcal{O}(\bar{\mu}h^2\hat{\varepsilon}/l^2)$. This means that the plate constitutive law is second-order accurate while the recovery analysis (retrieval of 3-D displacements, stresses, etc., from a 2-D analysis) is second-order accurate for $\Gamma_{\alpha\beta}, X_{\alpha\beta}$, but only first-order accurate for $\Gamma_{i3}, \Gamma_{3i}, X_{i3}, X_{3,i}$. For example, as shown by Yu et al. [166, 167] for Reissner-Mindlin plates, this causes the normal stress to be (inaccurately) predicted as being nonexistent. The same happens with Cosserat plates as well, only with the added inaccuracy in prediction of the normal couple stress. To amend this and to have a uniform second-order accuracy in the recovery relations too along with the total energy, one must go one step further in the asymptotic analysis and determine the second-order generalized warping solution. For the isotropic micropolar case, this has been done to arrive at second order corrections to w_3 and ϕ_3, while corrections to the rest of the warping variables come out to be zero. It turns out that these corrections are mostly functions of in-plane derivatives of the applied distributed loads and surface tractions. Therefore, with the help of these warping solutions, we can compute all the 3-D stresses and couple stresses in terms of the 2-D strains up to $\mathcal{O}(\mu h^2\hat{\varepsilon}/l^2)$.

Keeping this in mind, using eqs. (1), (15) and (16) and results listed in appendix E, one can show that the following relations hold

$$\begin{aligned} \langle \sigma_{\alpha\beta} \rangle &= e_\beta^T N_\alpha^* + \mathcal{O}(\mu h^2/l^2\hat{\epsilon}) \\ \langle \mu_{\alpha\beta} \rangle + e_3^T \langle \sigma_{x_3\alpha\beta} \rangle &= e_\beta^T M_\alpha^* + \mathcal{O}(\mu h^2/l^2\hat{\epsilon}) \end{aligned} \tag{63}$$

The asterisk over N_α, M_α serves to remind that these resultants have been computed using the first-order warping solutions whereas the 3-D stresses are accurate to second-order, letting us use eqs. (29), (34), (36) and (37) to come up with a simple relation such as this. In fact, if one were to use a plate theory with Kirchhoff-Love type assumptions, it is quite easy to derive eq. (63). For example, such a relation is implied by [2]. This is because $\sigma_{\alpha\beta}, \mu_{\alpha\beta}$ all have zeroth-order terms (plus second-order terms that we did not explicitly write out). On the other hand, it is not so

straightforward with either the shear forces or the drilling moments, because they are made up entirely out of first-order warping solutions and tend to include terms from the applied distributed and surface loads. So, for an isotropic material, we can write

$$\begin{aligned}\langle\sigma_{\alpha 3}\rangle &= \frac{D}{D+\gamma h}Q^*_\alpha + \text{terms of } \mathcal{O}(h\hat{\varepsilon}/l) \text{ from applied loads} \\ \langle\sigma_{3\alpha}\rangle &= \left[\frac{\mu}{\mu+\kappa}\frac{D}{D+\gamma h} + \frac{\gamma h}{\bar{g}l_0^2}\right] Q^*_\alpha + \text{terms of } \mathcal{O}(h\hat{\varepsilon}/l) \text{ from applied loads}\end{aligned} \tag{64}$$

and we can see why a direct connection is hard to establish. In the absence of micropolar effects, it may be tempting to think that the leading term of the integral of shear stresses are Q_α, but it has to be remembered that any externally applied loads contribute terms of the same order. Finally, we have

$$\begin{aligned}\langle\mu_{13}\rangle = \frac{\gamma^2-\beta^2}{\gamma}hK_{13} + \frac{\beta(\beta-\nu\gamma)}{\gamma}\left(1-\frac{\tanh\left(h/2l_0\right)}{h/2l_0}\right)hK_{13} \\ + \text{terms of } \mathcal{O}(h\hat{\varepsilon}/l) \text{ from applied loads}\end{aligned} \tag{65}$$

Comparing this equation with eqs. (36) and (37), we can see that only for $l_0 \ll h$ and in the absence of external loading, $\langle\sigma_{13}\rangle \approx M_{13}$.

Despite this, a most interesting result presents itself through eq. (65): *A drilling moment resultant cannot be generated by Cauchy stressses alone.* Unlike all the other stress resultants, $M_{\alpha 3}$ are the only quantities that can exist only if the medium supports of couple stresses. This observation also sets us up nicely to discuss another important topic of what happens in the limiting case when a Cosserat elastic medium becomes Cauchy elastic.

4.3 Reduction to a generalized Reissner-Mindlin theory

As described in the introduction, higher-order elasticity theories were originally proposed as generalizations of the classical theory of elasticity. Indeed, setting $\alpha = \beta = \gamma = \kappa = 0$ in eq. (1) recovers the familiar 3-D constitutive law. Similarly, it is useful to see if the fully intrinsic equations for a Cosserat plate reduce to a set of equations applicable to a Cauchy elastic plate, and preferably so by setting a group of constants

and/or variables to their limiting values. Here, the term reduction refers to a decrease in the number of degrees of freedom present in the model.

Let us begin by explicitly writing out eq. (59) in scalar form

$$N_{11,1} + N_{21,2} - N_{12}K_{13} - N_{22}K_{23} + Q_1K_{11} + Q_2K_{21} + f_1 = \dot{P}_1 + \Omega_1P_3 - \Omega_3P_2 \tag{66a}$$

$$N_{12,1} + N_{22,2} + N_{11}K_{13} + N_{21}K_{23} + Q_1K_{12} + Q_2K_{22} + f_2 = \dot{P}_2 + \Omega_3P_1 + \Omega_2P_3 \tag{66b}$$

$$Q_{1,1} + Q_{2,2} - N_{11}K_{11} - N_{12}K_{12} - N_{21}K_{21} - N_{22}K_{22} + f_3 = \dot{P}_3 - \Omega_2P_2 - \Omega_1P_1 \tag{66c}$$

$$\begin{aligned} M_{11,1} + M_{21,2} - M_{12}K_{13} - M_{22}K_{23} + M_{13}K_{12} + M_{23}K_{22} + N_{11}2\gamma_{13} + N_{21}2\gamma_{23} \\ -Q_1(1+\epsilon_{11}) - Q_2\epsilon_{21} + m_1 = \dot{H}_1 + \Omega_2H_3 - \Omega_3H_2 - V_1P_3 + V_3P_1 \end{aligned} \tag{67a}$$

$$\begin{aligned} M_{12,1} + M_{22,2} + M_{11}K_{13} + M_{21}K_{23} - M_{13}K_{11} - M_{23}K_{21} + N_{12}2\gamma_{13} + N_{22}2\gamma_{23} \\ -Q_1\epsilon_{12} - Q_2(1+\epsilon_{22}) + m_2 = \dot{H}_2 + \Omega_3H_1 - \Omega_1H_3 - V_2P_3 + V_3P_2 \end{aligned} \tag{67b}$$

$$\begin{aligned} M_{13,1} + M_{23,2} - M_{11}K_{12} + M_{12}K_{11} - M_{21}K_{22} + M_{22}K_{21} - N_{11}\epsilon_{12} + N_{22}\epsilon_{21} \\ +N_{12}(1+\epsilon_{11}) - N_{21}(1+\epsilon_{22}) + m_3 = \dot{H}_3 + \Omega_1H_2 - \Omega_2H_1 + V_1P_2 - V_2P_1 \end{aligned} \tag{67c}$$

The following remarks can now be made in the reduction to a classical elastic plate:

- As discussed in the preceding section, M_{13}, M_{23} only appear in presence of couple stresses. Therefore, one can set these variables to zero in eq. (67c).

- The polar moment of inertia (also referred to as *microinertia [39]*) of a through-thickness plate element in classical elasticity is zero. From eq. (53), this amounts to setting $J = 0$, which implies $H_3 = 0$.

- Since individual material points are no longer allowed to undergo independent rotations, ϕ_i need not be primary warping variables and we do not have eq. (12) to restrict us from picking $\epsilon_{12} = \epsilon_{21}$. While it is not compulsory to set them equal to each other, it does result in certain mathematical simplifications.

- We argued in section 3.3 that $K_{12} - K_{21}$ does not show up in the first-order refined theory that we developed. Despite this, in the development of the present

theory in section 4.1, we have always expressed M_{12} and M_{21}, and therefore K_{12} and K_{21}, as separate variables, even though we have implied their usage to be interchangeable while only introducing an error of $\mathcal{O}(h\hat{\epsilon}/l^2)$. This was done mainly to maintain a certain mathematical elegance. Now, based on eq. (29), we can simply pick the one curvature, $(K_{12} + K_{21})/2$ and the corresponding generalized force $\mathcal{M}_{12}$ since it is only the sum of the curvatures that appears in the strain energy.

Having "lost" the only terms that were being differentiated upon, eq. (67c) is now purely an algebraic equation that can be thought of as a constraint equation. For reasons that will become clear momentarily, let us switch from using the variables N_{12}, N_{21} to their sum-and-difference forms as they were presented in eq. (29). This gives us a constraint equation of the form

$$\begin{aligned}(2 + \epsilon_{11} + \epsilon_{22})\mathcal{N}_\epsilon = M_{11}K_{12} - M_{22}K_{21} - \mathcal{M}_{12}(K_{11} - K_{22}) + (N_{11} - N_{22})\epsilon_{12} \\ -\mathcal{N}_{12}(\epsilon_{11} - \epsilon_{22}) + m_3 + \Omega_1 H_2 - \Omega_2 H_1 + V_1 P_2 - V_2 P_1 \end{aligned} \quad (68)$$

One can see that eq. (68) is exactly the same as eq. (28) derived in [66] if one sets $\mathcal{N}_{12} = N_{12}$ and $\mathcal{N}_\epsilon = -\mathcal{N}$. It is easy to show that using the remarks above along with eq. (68) in eqs. (66a) to (66c), (67a) and (67b) also reproduces the fully intrinsic equations of motion of a generalized Reissner-Mindlin plate as given by eqs. (27) in [66]. Next, the kinematical equations (56) can also be easily modified to give their counterparts (eqs. (19) from [66]). Finally, we need to come up with a way of reducing the constitutive equations to their classical forms.

- The drilling stiffness needs to vanish in order to have $M_{\alpha 3} = 0$. Looking at eqs. (36) and (37), we see that setting $\beta = \gamma = 0$ not only is consistent with a reduction to classical elasticity, it also results in zero drilling resultants.

- An expression for the shear stiffness has already been presented in eq. (35), which has been derived from eq. (34) by setting $\kappa = \gamma = \beta = 0$.

- The in-plane and bending stiffnesses from eq. (29) can also be reduced to their classical counterparts by simply setting $\gamma = \beta = \kappa = 0$.

Therefore, we have shown that it is almost trivial to reduce the present Cosserat elasticity based plate theory to a classical one, resulting in equations coincident with a generalized Reissner-Mindlin theory. However, the discussion is not complete unless we also address the situation of the curvatures $K_{\alpha 3}$. In eq. (36), we have a situation where the the drilling stiffness and resultants are zero but the in-plane curvatures are not. The solution, then, is to find a way of expressing $K_{\alpha 3}$ in terms of the other strain measures. This procedure is best described with the help of the following comparison.

A Kirchhoff-Love theory is obtained from a Reissner-Mindlin theory by setting the shear strains to zero. The shear forces, still present but now not arising from a shear strain, are instead expressed in terms of the bending moments via the equilibrium equations. Similarly, a Reissner-Mindlin theory is obtained from a Cosserat theory by setting the drilling resultants to zero. The in-plane curvatures, still present but now not arising from a drilling moment, are instead expressed in terms of the in-plane stretching strains via the strain compatibility equations (eqs. (B.3b) and (B.3c)).

CHAPTER V

ENERGY-CONSISTENT GALERKIN APPROACH

The fully intrinsic nonlinear equations for Cosserat plates presented in the preceding chapter cannot, in general, be solved analytically except for a few special cases. For arbitrary loading and boundary conditions, one has to resort to approximate techniques. This chapter presents a Galerkin approach for the solution of these nonlinear equations. Morever, the specific weighting of all the equations will be shown to be energy-consistent. In some ways, this portion of the theoretical development can be thought of as a 2-D analogue to the work done by Patil and Althoff [114], Patil and Hodges [115] for the nonlinear analysis of beams.

Typically, approximate solution techniques fall into three different categories. The first is to perform a finite element analysis using the weakest possible shape functions. This is also known as the h-version of the finite element method. The second is to completely avoid domain discretization and instead use a very high polynomial degree in the interpolation and weighting functions to achieve convergence. Examples of such techniques are the Galerkin method or the Rayleigh-Ritz method (for conservative systems) and are also referred to as p-versions of the FEM. A third technique, introduced by Babuška [9] and known as the hp-method, involves a combination of mesh refinement and increase in polynomial order. By now, it has been widely demonstrated and accepted that p-refinements almost always lead to a faster convergence than corresponding h-refinements, with the hp-method being the most optimal of the three providing exponential convergence.

The present work explores several different solution techniques, each suitable for

a different type of analysis (static vs. dynamic, linear vs. nonlinear, effect of boundary conditions). This is, for instance, unlike the case of beam analysis in [115]. To make keeping track of the various methods and their differences easier, all the example problems chosen feature plates with simple rectangular geometries and uniform loading conditions, and are prime candidates for a p-method analysis. Therefore, all the theoretical development focuses mainly by using the Galerkin method, i.e., a p-version. The method will, however, be developed in a way that makes it easy to extend it to a finite element analysis.

5.1 Energy-Consistent Weighting

The complete set of equations (the equations of motion from (59), the kinematical equations from (56) and the constitutive relations from (40) or (41)) involves three sets of field variables: the stress resultants N_α, M_α, the generalized strains γ_α, K_α and the motion variables V, Ω. However, of the three sets of equations, if we stipulate that the constitutive laws are known exactly, we can eliminate either the generalized strains in terms of the stress resultants or vice-versa. This leaves us with only two sets of field variables. Appropriately, an approximate method can be described with the construction of a two-field principle of the Hellinger-Reissner type. Consider the following weighting of the equations of motion, the kinematical equations and appropriate boundary conditions on a rectangular domain ($x_1 : 0 \to \mathbb{L}_1, x_2 \to \mathbb{L}_2$).

$$\int_0^{\mathbb{L}_1}\int_0^{\mathbb{L}_2}\Big\{V^T\Big[\dot{P}+\widetilde{\Omega}P-f-N_{\alpha,\alpha}-\widetilde{K}_\alpha N_\alpha\Big]+\Omega^T\Big[\dot{H}+\widetilde{\Omega}H+\widetilde{V}P-m-M_{\alpha,\alpha}-\widetilde{K}_\alpha M_\alpha$$
$$-(\widetilde{e_\alpha}+\widetilde{\gamma_\alpha})N_\alpha\Big]+N_\alpha^T\Big[\dot{\gamma_\alpha}-V_{,\alpha}-\widetilde{K}_\alpha V-(\widetilde{e_\alpha}+\widetilde{\gamma_\alpha})\Omega\Big]+M_\alpha^T\Big[\dot{K}_\alpha-\Omega_{,\alpha}-\widetilde{K}_\alpha\Omega\Big]\Big\}\mathrm{d}x_1\mathrm{d}x_2$$
$$-\ (1-\tau_1^{(f)})\int_0^{\mathbb{L}_1}N_2^T\Big[V-\mathbb{V}^{(1)}\Big]\mathrm{d}x_1\Big|_{x_2=-\frac{\mathbb{L}_2}{2}}-\ (1-\tau_1^{(m)})\int_0^{\mathbb{L}_1}M_2^T\Big[\Omega-\mathbb{\Omega}^{(1)}\Big]\mathrm{d}x_1\Big|_{x_2=-\frac{\mathbb{L}_2}{2}}$$

$$
\begin{aligned}
&- \tau_1^{(f)} \int_0^{\mathbb{L}_1} V^T \Big[N_2 - \mathbb{N}_2{}^{(1)} \Big] \mathrm{d}x_1 \Big|_{x_2=-\frac{\mathbb{L}_2}{2}} - \tau_1^{(m)} \int_0^{\mathbb{L}_1} \Omega^T \Big[M_2 - \mathbb{M}_2{}^{(1)} \Big] \mathrm{d}x_1 \Big|_{x_2=-\frac{\mathbb{L}_2}{2}} \\
&+ (1-\tau_2^{(f)}) \int_0^{\mathbb{L}_2} N_1^T \Big[V - \mathbb{V}^{(2)} \Big] \mathrm{d}x_2 \Big|_{x_1=\frac{\mathbb{L}_1}{2}} + (1-\tau_2^{(m)}) \int_0^{\mathbb{L}_2} M_1^T \Big[\Omega - \mathbb{\Omega}^{(2)} \Big] \mathrm{d} \Big|_{x_1=\frac{\mathbb{L}_1}{2}} \\
&+ \tau_2^{(f)} \int_0^{\mathbb{L}_2} V^T \Big[N_1 - \mathbb{N}_1{}^{(2)} \Big] \mathrm{d}x_2 \Big|_{x_1=\frac{\mathbb{L}_1}{2}} + \tau_2^{(m)} \int_0^{\mathbb{L}_2} \Omega^T \Big[M_1 - \mathbb{M}_1{}^{(2)} \Big] \mathrm{d}x_2 \Big|_{x_1=\frac{\mathbb{L}_1}{2}} \\
&+ (1-\tau_3^{(f)}) \int_0^{\mathbb{L}_1} N_2^T \Big[V - \mathbb{V}^{(3)} \Big] \mathrm{d}x_1 \Big|_{x_2=\frac{\mathbb{L}_2}{2}} + (1-\tau_3^{(f)}) \int_0^{\mathbb{L}_1} M_2^T \Big[\Omega - \mathbb{\Omega}^{(3)} \Big] \mathrm{d}x_1 \Big|_{x_2=\frac{\mathbb{L}_2}{2}} \\
&+ \tau_3^{(f)} \int_0^{\mathbb{L}_1} V^T \Big[N_2 - \mathbb{N}_2{}^{(3)} \Big] \mathrm{d}x_1 \Big|_{x_2=\frac{\mathbb{L}_2}{2}} + \tau_3^{(m)} \int_0^{\mathbb{L}_1} \Omega^T \Big[M_2 - \mathbb{M}_2{}^{(3)} \Big] \mathrm{d}x_1 \Big|_{x_2=\frac{\mathbb{L}_2}{2}} \\
&- (1-\tau_4^{(f)}) \int_0^{\mathbb{L}_2} N_1^T \Big[V - \mathbb{V}^{(4)} \Big] \mathrm{d}x_2 \Big|_{x_1=-\frac{\mathbb{L}_1}{2}} - (1-\tau_4^{(m)}) \int_0^{\mathbb{L}_2} M_1^T \Big[\Omega - \mathbb{\Omega}^{(4)} \Big] \mathrm{d}x_2 \Big|_{x_1=-\frac{\mathbb{L}_1}{2}} \\
&- \tau_4^{(f)} \int_0^{\mathbb{L}_2} V^T \Big[N_1 - \mathbb{N}_1{}^{(4)} \Big] \mathrm{d}x_2 \Big|_{x_1=-\frac{\mathbb{L}_1}{2}} - \tau_4^{(m)} \int_0^{\mathbb{L}_2} \Omega^T \Big[M_1 - \mathbb{M}_1{}^{(4)} \Big] \mathrm{d}x_2 \Big|_{x_1=-\frac{\mathbb{L}_1}{2}} = 0 \quad (69)
\end{aligned}
$$

where $\hat{\mathbb{V}}^{(i)}, \hat{\mathbb{\Omega}}^{(i)}, \hat{\mathbb{N}}_1^{(i)}, \hat{\mathbb{M}}_1^{(i)} (i = 2, 4)$ are possible prescribled boundary conditions on $x_1 = \pm\frac{\mathbb{L}_1}{2}$, $\hat{\mathbb{V}}^{(i)}, \hat{\mathbb{\Omega}}^{(i)}, \hat{\mathbb{N}}_2^{(i)}, \hat{\mathbb{M}}_2^{(i)} (i = 1, 3)$ are possible prescribed boundary conditions on $x_2 = \pm\frac{\mathbb{L}_2}{2}$, and $\tau_i^{(f)}, \tau_i^{(m)}$ are 3×1 column matrices of flags (zero or one) denoting a prescription of of either geometric or natural boundary conditions, respectively.

This weighted-residual integral can be shown to be an energy balance equation. To demonstrate this, let us consider, without loss of generality, the example of a plate that is free along edges (1) and (2), and fully clamped along edges (3) and (4). A

simple integration-by-parts on eq. (69) results in

$$\int_0^{\mathbb{L}_1}\int_0^{\mathbb{L}_2}\Big[V^T\dot{P}+\Omega^T\dot{H}\Big]\mathrm{d}\xi\mathrm{d}\eta+\int_0^{\mathbb{L}_1}\int_0^{\mathbb{L}_2}\Big[N_\alpha^T\dot{\gamma}_\alpha+M_\alpha^T\dot{K}_\alpha\Big]\mathrm{d}\xi\mathrm{d}\eta=\int_0^{\mathbb{L}_1}\int_0^{\mathbb{L}_2}\Big[V^Tf+\Omega^Tm\Big]\mathrm{d}\xi\mathrm{d}\eta$$
$$-\int_0^{\mathbb{L}_1}\Big[V^T\mathbb{N}_2{}^{(1)}+\Omega^T\mathbb{M}_2{}^{(1)}\Big]\mathrm{d}x_1\Big|_{x_2=-\frac{\mathbb{L}_2}{2}}+\int_0^{\mathbb{L}_2}\Big[V^T\mathbb{N}_1{}^{(2)}+\Omega^T\mathbb{M}_1{}^{(2)}\Big]\mathrm{d}x_2\Big|_{x_1=\frac{\mathbb{L}_1}{2}}$$
$$+\int_0^{\mathbb{L}_1}\Big[N_2^T\mathbb{V}^{(3)}+M_2^T\mathbb{\Omega}^{(3)}\Big]\mathrm{d}x_1\Big|_{x_2=\frac{\mathbb{L}_2}{2}}-\int_0^{\mathbb{L}_2}\Big[N_1^T\mathbb{V}^{(4)}+M_1^T\mathbb{\Omega}^{(4)}\Big]\mathrm{d}x_2\Big|_{x_1=-\frac{\mathbb{L}_1}{2}} \tag{70}$$

The first two area integrals represent the rate of change of kinetic and potential energy, respectively, while the rest of the terms represent the rate of work done by the applied distributed loads on the plate surface and at the boundaries. This is clearly an energy balance equation with the rate of work done on the plate equal to the rate of change of its total energy.

5.2 Shape Functions and the Galerkin approximation

To derive a Galerkin approach based on eq. (69), a suitable family of shape functions must be chosen. First, it is important to see that both geometric and natural boundary conditions have been included in the weighted-residual integral and, hence, only satisfied weakly. This lets us choose shape functions that do not have to be admissible functions, let alone comparison functions. A set of hierarchic shape functions (or bubble functions) are best suited for the present analysis since additional degrees of freedom can be added to the model without having to generate a new geometry. Since the goal is to eventually extend this Galerkin method to a variable-order finite element analysis, working with hierarchic functions simplifies the process considerably.

Let us now shift to working on a mapped domain described by fig. 20. The family of shape functions chosen, inspired by the set of orthogonal polynomials proposed by

Hodges [62] for one-dimensional structures, are

$$\begin{aligned} \phi^1_\xi &= \frac{1-\xi}{2} & \phi^1_\eta &= \frac{1-\eta}{2} \\ \phi^2_\xi &= \frac{1+\xi}{2} & \phi^2_\eta &= \frac{1+\eta}{2} \\ \phi^n_\xi &= \frac{1-\xi^2}{4} P_n^{(2,2)}(\xi) & \phi^n_\eta &= \frac{1-\eta^2}{4} P_n^{(2,2)}(\eta), \qquad n \geq 3 \end{aligned} \tag{71}$$

where $P_n^{(2,2)}(x)$ are Jacobi polynomials orthogonal with respect to the weight $(1+x)^2(1-x)^2$ on the interval $[-1,1]$. For $n \geq 3$, this choice of shape functions ensures that each ϕ^n vanishes at the boundaries and remains orthogonal with the others.

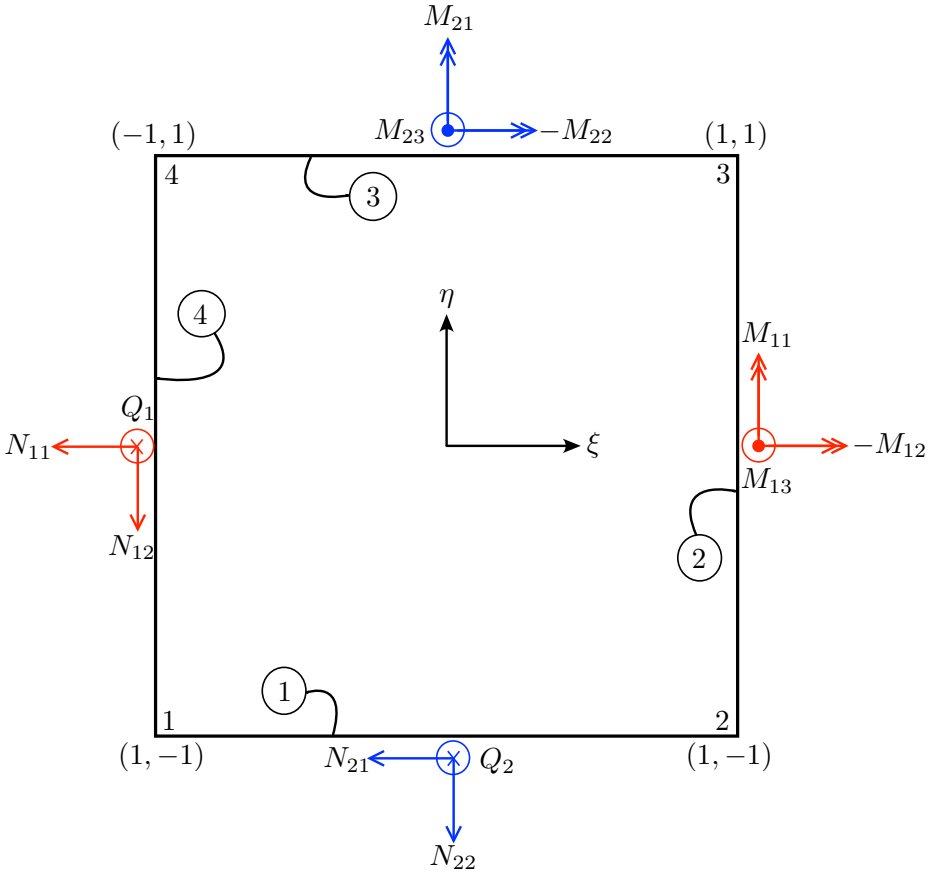

Figure 20: Schematic of a typical plate element. Variables in red are defined on all edges normal to ξ, those in blue are defined on all edges normal to η.

The two-dimensional interpolation functions for a chosen polynomial degree p are

now expressed as

$$\Phi^k(\xi,\eta) = \begin{bmatrix} \phi^i_\xi \phi^j_\eta & 0 & 0 \\ 0 & \phi^i_\xi \phi^j_\eta & 0 \\ 0 & 0 & \phi^i_\xi \phi^j_\eta \end{bmatrix} \tag{72}$$

$$i,j = 1,2,\ldots,p;\ i+j = 1,2,\ldots,p;\ k = 1,2,\ldots,N_e$$

Note that p here represents the total degree of the polynomial over the entire plate element and not along the individual directions. So, the total number of shape functions, and hence the degrees of freedom per variable, is $N_e = \frac{(p+1)(p+2)}{2}$.

It is also worth comparing the present construction of shape functions to those recommended by Szabó and Babuška [146]. The space of monomials used to construct the present family of shape functions is given by $\xi^i\eta^j (i,j = 0,1,,\ldots,p; i+j = 0,1,\ldots,p)$. The shape functions recommended in [146] supplement this space of monomials with $\xi^p\eta$ and $\xi\eta^p$ (for $p \geq 2$). While this makes an elegant categorization of the shape functions into nodal, side and internal modes possible, it has been found that, at least for a purely p-method of analysis, the addition of these two monomials hurts the monotony of the convergence process and even gives erroneous results. This will be demonstrated shortly.

Representing the field variables in terms of independent generalized coordinates, we have a Galerkin approximation of the form

$$V(\xi,\eta,t) = \sum_{k=1}^{N_e} \Phi^k(\xi,\eta) v^k(t) \tag{73a}$$

$$\Omega(\xi,\eta,t) = \sum_{k=1}^{N_e} \Phi^k(\xi,\eta) \omega^k(t) \tag{73b}$$

$$N_\alpha(\xi,\eta,t) = \sum_{k=1}^{N_e} \Phi^k(\xi,\eta) n^k_\alpha(t) \tag{73c}$$

$$M_\alpha(\xi,\eta,t) = \sum_{k=1}^{N_e} \Phi^k(\xi,\eta) m^k_\alpha(t) \tag{73d}$$

where

$$v^k = \begin{Bmatrix} v_1^k \\ v_2^k \\ v_3^k \end{Bmatrix} \qquad \omega^k = \begin{Bmatrix} -\omega_2^k \\ \omega_1^k \\ \omega_3^k \end{Bmatrix} \qquad n_\alpha^k = \begin{Bmatrix} n_{\alpha 1}^k \\ n_{\alpha 2}^k \\ q_\alpha^k \end{Bmatrix} \qquad m_\alpha^k = \begin{Bmatrix} -m_{\alpha 2}^k \\ m_{\alpha 1}^k \\ m_{\alpha 3}^k \end{Bmatrix} \tag{74}$$

Using the constitutive law to eliminate the generalized strains, the six sets of Galerkin equations can be derived as

$$\begin{aligned}
&\mathbb{L}_1\mathbb{L}_2 \int_{-1}^{1}\int_{-1}^{1} \Phi^j \Big[(\mathbb{C}\Phi^i \dot{v}^i + \mathbb{K}\Phi^i \dot{\omega}^i) + \widetilde{\Phi^k \omega^k}(\mathbb{C}\Phi^i v^i + \mathbb{K}\Phi^i \omega^i) - (\mathbb{S}_{\beta\alpha}\widetilde{\Phi^k} n_\beta^k + \mathbb{T}_{\alpha\beta}\widetilde{\Phi^k} m_\beta^k)\Phi^i n_\alpha^i \\
&- \frac{1}{\mathbb{L}_\alpha}\Phi^i_{,\alpha} n_\alpha^i - f \Big] \mathrm{d}\xi \mathrm{d}\eta - \tau_1^{(f)}\mathbb{L}_1 \int_{-1}^{1} \Phi^j \Big[\Phi^i n_2^i - \mathbb{N}_2^{(1)} \Big] \mathrm{d}\xi \Big|_{\eta=-1} + \tau_2^{(f)}\mathbb{L}_2 \int_{-1}^{1} \Phi^j \Big[\Phi^i n_1^i - \mathbb{N}_1^{(2)} \Big] \mathrm{d}\eta \Big|_{\xi=1} \\
&+ \tau_3^{(f)}\mathbb{L}_1 \int_{-1}^{1} \Phi^j \Big[\Phi^i n_2^i - \mathbb{N}_2^{(3)} \Big] \mathrm{d}\xi \Big|_{\eta=1} - \tau_4^{(f)}\mathbb{L}_2 \int_{-1}^{1} \Phi^j \Big[\Phi^i n_1^i - \mathbb{N}_1^{(4)} \Big] \mathrm{d}\eta \Big|_{\xi=-1} = 0
\end{aligned} \tag{75a}$$

$$\begin{aligned}
&\mathbb{L}_1\mathbb{L}_2 \int_{-1}^{1}\int_{-1}^{1} \Phi^j \Big[(\mathbb{K}^T\Phi^i \dot{v}^i + \mathbb{I}\Phi^i \dot{\omega}^i) + \widetilde{\Phi^k \omega^k}(\mathbb{K}^T\Phi^i v^i + \mathbb{I}\Phi^i \omega^i) + \widetilde{\Phi^k v^k}(\mathbb{C}\Phi^i v^i + \mathbb{K}\Phi^i \omega^i) - \frac{1}{\mathbb{L}_\alpha}\Phi^i_{,\alpha} m_\alpha^i \\
&- (\mathbb{S}_{\beta\alpha}\widetilde{\Phi^k} n_\beta^k + \mathbb{T}_{\alpha\beta}\widetilde{\Phi^k} m_\beta^k)\Phi^i m_\alpha^i - (\tilde{e}_\alpha + \mathbb{R}_{\alpha\beta}\widetilde{\Phi^k} n_\beta^k + \mathbb{S}_{\alpha\beta}\widetilde{\Phi^k} m_\beta^k)\Phi^i n_\alpha^i - m \Big] \mathrm{d}\xi \mathrm{d}\eta \\
&- \tau_1^{(m)}\mathbb{L}_1 \int_{-1}^{1} \Phi^j \Big[\Phi^i m_2^i - \mathbb{M}_2^{(1)} \Big] \mathrm{d}\xi \Big|_{\eta=-1} + \tau_2^{(m)}\mathbb{L}_2 \int_{-1}^{1} \Phi^j \Big[\Phi^i m_1^i - \mathbb{M}_1^{(2)} \Big] \mathrm{d}\eta \Big|_{\xi=1} \\
&+ \tau_3^{(m)}\mathbb{L}_1 \int_{-1}^{1} \Phi^j \Big[\Phi^i m_2^i - \mathbb{M}_2^{(3)} \Big] \mathrm{d}\xi \Big|_{\eta=1} - \tau_4^{(m)}\mathbb{L}_2 \int_{-1}^{1} \Phi^j \Big[\Phi^i m_1^i - \mathbb{M}_1^{(4)} \Big] \mathrm{d}\eta \Big|_{\xi=-1} = 0
\end{aligned} \tag{75b}$$

$$\begin{aligned}
&\mathbb{L}_1\mathbb{L}_2 \int_{-1}^{1}\int_{-1}^{1} \Phi^j \Big[\mathbb{R}_{1\beta}\Phi^i \dot{n}_\beta^i + \mathbb{S}_{1\beta}\Phi^i \dot{m}_\beta^i - \frac{1}{\mathbb{L}_1}\Phi^i_{,1} v^i - \Big(\widetilde{\mathbb{S}_{\beta 1}\Phi^k} n_\beta^k + \widetilde{\mathbb{T}_{1\beta}\Phi^k} m_\beta^k \Big)\Phi^i v^i - \Big(\widetilde{e}_1 \\
&+ \widetilde{\mathbb{R}_{1\beta}\Phi^k} n_\beta^k + \widetilde{\mathbb{S}_{1\beta}\Phi^k} m_\beta^k \Big)\Phi^i \omega^i \Big] \mathrm{d}\xi \mathrm{d}\eta + (1 - \tau_2^{(f)})\mathbb{L}_2 \int_{-1}^{1} \Phi^j \Big[\Phi^i v^i - \mathbb{V}^{(2)} \Big] \mathrm{d}\eta \Big|_{\xi=1} \\
&- (1 - \tau_4^{(f)})\mathbb{L}_2 \int_{-1}^{1} \Phi^j \Big[\Phi^i v^i - \mathbb{V}^{(4)} \Big] \mathrm{d}\eta \Big|_{\xi=-1} = 0
\end{aligned} \tag{75c}$$

$$\mathbb{L}_1\mathbb{L}_2 \int_{-1}^{1}\int_{-1}^{1} \Phi^j \Big[\mathbb{R}_{2\beta}\Phi^i \dot{n}_\beta^i + \mathbb{S}_{2\beta}\Phi^i \dot{m}_\beta^i - \frac{1}{\mathbb{L}_2}\Phi^i_{,2} v^i - \Big(\widetilde{\mathbb{S}_{\beta 2}\Phi^k} n_\beta^k + \widetilde{\mathbb{T}_{2\beta}\Phi^k} m_\beta^k \Big)\Phi^i v^i - \Big(\widetilde{e}_2$$

$$+\mathbb{R}_{2\beta}\widetilde{\Phi^k n^k_\beta}+\mathbb{S}_{2\beta}\widetilde{\Phi^k m^k_\beta}\Big)\Phi^i\omega^i\Big]\mathrm{d}\xi\mathrm{d}\eta-(1-\tau_1)^{(f)}\mathbb{L}_1\int_{-1}^{1}\Phi^j\Big[\Phi^i v^i-\mathbb{V}^{(1)}\Big]\mathrm{d}\xi\Big|_{\eta=-1}$$

$$+(1-\tau_3^{(f)})\mathbb{L}_1\int_{-1}^{1}\Phi^j\Big[\Phi^i v^i-\mathbb{V}^{(3)}\Big]\mathrm{d}\xi\Big|_{\eta=1}=0 \tag{75d}$$

$$\mathbb{L}_1\mathbb{L}_2\int_{-1}^{1}\int_{-1}^{1}\Phi^j\Big[\mathbb{S}_{\beta 1}\Phi^i\dot{n}^i_\beta+\mathbb{T}_{1\beta}\Phi^i\dot{m}^i_\beta-\frac{1}{\mathbb{L}_1}\Phi^i_{,1}\omega^i-\Big(\mathbb{S}_{\beta 1}\widetilde{\Phi^k n^k_\beta}+\mathbb{T}_{1\beta}\widetilde{\Phi^k m^k_\beta}\Big)\Phi^i\omega^i\Big]\mathrm{d}\xi\mathrm{d}\eta$$

$$+(1-\tau_2^{(m)})\mathbb{L}_2\int_{-1}^{1}\Phi^j\Big[\Phi^i\omega^i-\mathbb{\Omega}^{(2)}\Big]\mathrm{d}\eta\Big|_{\xi=1}-(1-\tau_4^{(m)})\mathbb{L}_2\int_{-1}^{1}\Phi^j\Big[\Phi^i\omega^i-\mathbb{\Omega}^{(4)}\Big]\mathrm{d}\eta\Big|_{\xi=-1}=0 \tag{75e}$$

$$\mathbb{L}_1\mathbb{L}_2\int_{-1}^{1}\int_{-1}^{1}\Phi^j\Big[\mathbb{S}_{\beta 2}\Phi^i\dot{n}^i_\beta+\mathbb{T}_{2\beta}\Phi^i\dot{m}^i_\beta-\frac{1}{\mathbb{L}_2}\Phi^i_{,2}\omega^i-\Big(\mathbb{S}_{\beta 2}\widetilde{\Phi^k n^k_\beta}+\mathbb{T}_{2\beta}\widetilde{\Phi^k m^k_\beta}\Big)\Phi^i\omega^i\Big]\mathrm{d}\xi\mathrm{d}\eta$$

$$-(1-\tau_1^{(m)})\mathbb{L}_1\int_{-1}^{1}\Phi^j\Big[\Phi^i\omega^i-\mathbb{\Omega}^{(1)}\Big]\mathrm{d}\xi\Big|_{\eta=-1}+(1-\tau_3^{(m)})\mathbb{L}_1\int_{-1}^{1}\Phi^j\Big[\Phi^i\omega^i-\mathbb{\Omega}^{(3)}\Big]\mathrm{d}\xi\Big|_{\eta=1}=0 \tag{75f}$$

5.3 Special Case: Uniform Plates

For the purpose of demonstration, let us look at plates with constant stiffness and inertia properties. In the context of a finite element implementation, assuming such constancy certainly makes sense. One can then replace all the integrals above in terms of the following

$$\mathcal{A}^{ji}=\mathbb{L}_1\mathbb{L}_2\int_{-1}^{1}\int_{-1}^{1}\Phi^j(\xi,\eta)\Phi^i(\xi,\eta)\mathrm{d}\xi\mathrm{d}\eta \qquad \mathcal{B}^{ji}_\alpha=\frac{\mathbb{L}_1\mathbb{L}_2}{\mathbb{L}_\alpha}\int_{-1}^{1}\int_{-1}^{1}\Phi^j(\xi,\eta)\Phi^i_{,\alpha}(\xi,\eta)\mathrm{d}\xi\mathrm{d}\eta$$

$$\mathcal{E}^{ji}_{(1)}=\mathbb{L}_1\int_{-1}^{1}\Phi^j(\xi,-1)\Phi^i(\xi,-1)\mathrm{d}\xi \qquad \mathcal{E}^{ji}_{(2)}=\mathbb{L}_2\int_{-1}^{1}\Phi^j(1,\eta)\Phi^i(1,\eta)\mathrm{d}\eta$$

$$\mathcal{E}^{ji}_{(3)}=\mathbb{L}_1\int_{-1}^{1}\Phi^j(\xi,1)\Phi^i(\xi,1)\mathrm{d}\xi \qquad \mathcal{E}^{ji}_{(4)}=\mathbb{L}_2\int_{-1}^{1}\Phi^j(-1,\eta)\Phi^i(-1,\eta)\mathrm{d}\eta$$

$$\mathcal{C}^{jik} = \mathbb{L}_1\mathbb{L}_2 \int_{-1}^{1}\int_{-1}^{1} \Phi^j(\xi,\eta)\Phi^i(\xi,\eta)\Phi^k(\xi,\eta)\mathrm{d}\xi\mathrm{d}\eta \tag{76}$$

We can rewrite the Galerkin equations above as

$$\begin{aligned}
&\mathcal{A}^{ji}(\mathbb{G}\dot{v}^i + \mathbb{K}\dot{\omega}^i) + \mathcal{C}^{jik}\widetilde{\omega^k}(\mathbb{G}v^i + \mathbb{K}\omega^i) - \mathcal{B}_1^{ji}n_1^i - \mathcal{B}_2^{ji}n_2^i \\
&- \mathcal{C}^{jik}(\widetilde{\mathbb{S}_{\beta\alpha}n_\beta^k} + \widetilde{\mathbb{T}_{\alpha\beta}m_\beta^k})n_\alpha^i - \mathbb{L}_1\mathbb{L}_2\int_{-1}^{1}\int_{-1}^{1}\Phi^j f\ \mathrm{d}\xi\mathrm{d}\eta \\
&- \tau_1^{(f)}\left[\mathcal{E}_{(1)}^{ji}n_2^i - \mathbb{L}_1\int_{-1}^{1}\Phi^j\mathbb{N}_2^{(1)}\mathrm{d}\xi\Big|_{\eta=-1}\right] + \tau_2^{(f)}\left[\mathcal{E}_{(2)}^{ji}n_1^i - \mathbb{L}_2\int_{-1}^{1}\Phi^j\mathbb{N}_1^{(2)}\mathrm{d}\eta\Big|_{\xi=1}\right] \\
&+ \tau_3^{(f)}\left[\mathcal{E}_{(3)}^{ji}n_2^i - \mathbb{L}_1\int_{-1}^{1}\Phi^j\mathbb{N}_2^{(3)}\mathrm{d}\xi\Big|_{\eta=1}\right] - \tau_4^{(f)}\left[\mathcal{E}_{(4)}^{ji}n_1^i - \mathbb{L}_2\int_{-1}^{1}\Phi^j\mathbb{N}_1^{(4)}\mathrm{d}\eta\Big|_{\xi=-1}\right] = 0
\end{aligned} \tag{77a}$$

$$\begin{aligned}
&\mathcal{A}^{ji}(\mathbb{K}^T\dot{v^i} + \mathbb{I}\dot{\omega}^i) + \mathcal{C}^{jik}\widetilde{\omega^k}(\mathbb{K}^Tv^i + \mathbb{I}\omega^i) + \mathcal{C}^{jik}\widetilde{v^k}(\mathbb{G}v^i + \mathbb{K}\omega^i) - \mathcal{B}_1^{ji}m_1^i - \mathcal{B}_2^{ji}m_2^i \\
&- \mathcal{C}^{jik}(\widetilde{\mathbb{S}_{\beta\alpha}n_\beta^k} + \widetilde{\mathbb{T}_{\alpha\beta}m_\beta^k})m_\alpha^i - \left(\mathcal{A}^{ji}\widetilde{e}_\alpha + \mathcal{C}^{jik}(\widetilde{\mathbb{R}_{\alpha\beta}n_\beta^k} + \widetilde{\mathbb{S}_{\alpha\beta}m_\beta^k})\right)n_\alpha^i - \mathbb{L}_1\mathbb{L}_2\int_{-1}^{1}\int_{-1}^{1}\Phi^j m\ \mathrm{d}\xi\mathrm{d}\eta \\
&- \tau_1^{(m)}\left[\mathcal{E}_{(1)}^{ji}m_2^i - \mathbb{L}_1\int_{-1}^{1}\Phi^j\mathbb{M}_2^{(1)}\mathrm{d}\xi\Big|_{\eta=-1}\right] + \tau_2^{(m)}\left[\mathcal{E}_{(2)}^{ji}m_1^i - \mathbb{L}_2\int_{-1}^{1}\Phi^j\mathbb{M}_1^{(2)}\mathrm{d}\eta\Big|_{\xi=1}\right] \\
&+ \tau_3^{(m)}\left[\mathcal{E}_{(3)}^{ji}m_2^i - \mathbb{L}_1\int_{-1}^{1}\Phi^j\mathbb{M}_2^{(3)}\mathrm{d}\xi\Big|_{\eta=1}\right] - \tau_4^{(m)}\left[\mathcal{E}_{(4)}^{ji}m_1^i - \mathbb{L}_2\int_{-1}^{1}\Phi^j\mathbb{M}_1^{(4)}\mathrm{d}\eta\Big|_{\xi=-1}\right] = 0
\end{aligned} \tag{77b}$$

$$\begin{aligned}
&\mathcal{A}^{ji}(\mathbb{R}_{1\beta}\dot{n}_\beta^i + \mathbb{S}_{1\beta}\dot{m}_\beta^i) - \mathcal{B}_1^{ji}v^i - \mathcal{C}^{jik}(\widetilde{\mathbb{S}_{\beta1}n_\beta^k} + \widetilde{\mathbb{T}_{1\beta}m_\beta^k})v^i - \left(\mathcal{A}^{ji}\widetilde{e}_1 + \mathcal{C}^{jik}(\widetilde{\mathbb{R}_{1\beta}n_\beta^k} + \widetilde{\mathbb{S}_{1\beta}m_\beta^k})\right)\omega^i \\
&+ (1-\tau_2^{(f)})\left[\mathcal{E}_{(2)}^{ji}v^i - \mathbb{L}_2\int_{-1}^{1}\Phi^j\mathbb{V}^{(2)}\mathrm{d}\eta\Big|_{\xi=1}\right] - (1-\tau_4^{(f)})\left[\mathcal{E}_{(4)}^{ji}v^i - \mathbb{L}_2\int_{-1}^{1}\Phi^j\mathbb{V}^{(4)}\mathrm{d}\eta\Big|_{\xi=-1}\right] = 0
\end{aligned} \tag{77c}$$

$$\begin{aligned}
&\mathcal{A}^{ji}(\mathbb{R}_{2\beta}\dot{n}_\beta^i + \mathbb{S}_{2\beta}\dot{m}_\beta^i) - \mathcal{B}_2^{ji}v^i - \mathcal{C}^{jik}(\widetilde{\mathbb{S}_{\beta2}n_\beta^k} + \widetilde{\mathbb{T}_{2\beta}m_\beta^k})v^i - \left(\mathcal{A}^{ji}\widetilde{e}_2 + \mathcal{C}^{jik}(\widetilde{\mathbb{R}_{2\beta}n_\beta^k} + \widetilde{\mathbb{S}_{2\beta}m_\beta^k})\right)\omega^i \\
&- (1-\tau_1^{(f)})\left[\mathcal{E}_{(1)}^{ji}v^i - \mathbb{L}_1\int_{-1}^{1}\Phi^j\mathbb{V}^{(1)}\mathrm{d}\xi\Big|_{\eta=-1}\right] + (1-\tau_3^{(f)})\left[\mathcal{E}_{(3)}^{ji}v^i - \mathbb{L}_1\int_{-1}^{1}\Phi^j\mathbb{V}^{(3)}\mathrm{d}\xi\Big|_{\eta=1}\right] = 0
\end{aligned} \tag{77d}$$

$$\mathcal{A}^{ji}(\mathbb{S}_{\beta 1}\dot{n}^i_\beta + \mathbb{T}_{1\beta}\dot{m}^i_\beta) - \mathcal{B}^{ji}_1\omega^i - \mathcal{C}^{jik}(\widetilde{\mathbb{S}_{\beta 1}n^k_\beta} + \widetilde{\mathbb{T}_{1\beta}m^k_\beta})\omega^i$$
$$+ (1-\tau^{(m)}_2)\left[\mathcal{E}^{ji}_{(2)}\omega^i - \mathbb{L}_2\int_{-1}^{1}\Phi^j\mathbb{\Omega}^{(2)}\mathrm{d}\eta\Big|_{\xi=1}\right] - (1-\tau^{(m)}_4)\left[\mathcal{E}^{ji}_{(4)}\omega^i - \mathbb{L}_2\int_{-1}^{1}\Phi^j\mathbb{\Omega}^{(4)}\mathrm{d}\eta\Big|_{\xi=-1}\right] = 0 \tag{77e}$$

$$\mathcal{A}^{ji}(\mathbb{S}_{\beta 2}\dot{n}^i_\beta + \mathbb{T}_{2\beta}\dot{m}^i_\beta) - \mathcal{B}^{ji}_2\omega^i - \mathcal{C}^{jik}(\widetilde{\mathbb{S}_{\beta 2}n^k_\beta} + \widetilde{\mathbb{T}_{2\beta}m^k_\beta})\omega^i$$
$$- (1-\tau^{(m)}_1)\left[\mathcal{E}^{ji}_{(1)}\omega^i - \mathbb{L}_1\int_{-1}^{1}\Phi^j\mathbb{\Omega}^{(1)}\mathrm{d}\xi\Big|_{\eta=-1}\right] + (1-\tau^{(m)}_3)\left[\mathcal{E}^{ji}_{(3)}\omega^i - \mathbb{L}_1\int_{-1}^{1}\Phi^j\mathbb{\Omega}^{(3)}\mathrm{d}\xi\Big|_{\eta=1}\right] = 0 \tag{77f}$$

The above set of equations can be written compactly as

$$A_{ji}\dot{z}_i + B_{ji}z_i + C_{jik}z_iz_k + D_j = 0 \tag{78}$$

where the generalized coordinates are represented in a $18N_e \times 1$ column matrix:

$$z = \begin{bmatrix} v^1(t) & \dots & v^{N_e}(t) & \omega^1(t) & \dots & \omega^{N_e}(t) & n^1_1(t) & \dots & \dots & m^{N_e}_2(t)\end{bmatrix}^T \tag{79}$$

5.4 Linear Free Vibration Analysis

In this section, let us further specialize eqs. (77) to the case of a free vibration analysis, resulting in an eigenvalue problem. All the nonlinear terms as well as terms coming from the applied loads are set to zero leaving us with a considerably simplified set of equations of the form:

$$\mathcal{A}^{ji}(\mathbb{G}\dot{v}^i + \mathbb{K}\dot{\omega}^i) - \left[\mathcal{B}^{ji}_1 - \tau^{(f)}_2\mathcal{E}^{ji}_{(2)} + \tau^{(f)}_4\mathcal{E}^{ji}_{(4)}\right]n^i_1 - \left[\mathcal{B}^{ji}_2 + \tau^{(f)}_1\mathcal{E}^{ji}_{(1)} - \tau^{(f)}_3\mathcal{E}^{ji}_{(3)}\right]n^i_2 = 0 \tag{80a}$$

$$\mathcal{A}^{ji}(\mathbb{K}^T\dot{v}^i + \mathbb{I}\dot{\omega}^i) - \left[\mathcal{B}^{ji}_1 - \tau^{(m)}_2\mathcal{E}^{ji}_{(2)} + \tau^{(m)}_4\mathcal{E}^{ji}_{(4)}\right]m^i_1 - \left[\mathcal{B}^{ji}_2 + \tau^{(m)}_1\mathcal{E}^{ji}_{(1)} - \tau^{(m)}_3\mathcal{E}^{ji}_{(3)}\right]m^i_2$$
$$-\mathcal{A}^{ji}\widetilde{e}_\alpha n^i_\alpha = 0 \tag{80b}$$

$$\mathcal{A}^{ji}(\mathbb{R}_{1\beta}\dot{n}^i_\beta + \mathbb{S}_{1\beta}\dot{m}^i_\beta) - \left[\mathcal{B}^{ji}_1 - (1-\tau^{(f)}_2)\mathcal{E}^{ji}_{(2)} + (1-\tau^{(f)}_4)\mathcal{E}^{ji}_{(4)}\right]v^i - \mathcal{A}^{ji}\widetilde{e}_1\omega^i = 0 \tag{80c}$$

$$\mathcal{A}^{ji}(\mathbb{R}_{2\beta}\dot{n}^i_\beta + \mathbb{S}_{2\beta}\dot{m}^i_\beta) - \left[\mathcal{B}^{ji}_2 + (1-\tau^{(f)}_1)\mathcal{E}^{ji}_{(1)} - (1-\tau^{(f)}_3)\mathcal{E}^{ji}_{(3)}\right]v^i - \mathcal{A}^{ji}\widetilde{e}_2\omega^i = 0 \tag{80d}$$

$$\mathcal{A}^{ji}(\mathbb{S}_{\beta 1}\dot{n}^i_\beta + \mathbb{T}_{1\beta}\dot{m}^i_\beta) - \left[\mathcal{B}^{ji}_1 - (1-\tau^{(m)}_2)\mathcal{E}^{ji}_{(2)} + (1-\tau^{(m)}_4)\mathcal{E}^{ji}_{(4)}\right]\omega^i = 0 \tag{80e}$$

$$\mathcal{A}^{ji}(\mathbb{S}_{\beta 2}\dot{n}^i_\beta + \mathbb{T}_{2\beta}\dot{m}^i_\beta) - \left[\mathcal{B}^{ji}_2 + (1-\tau^{(m)}_1)\mathcal{E}^{ji}_{(1)} - (1-\tau^{(m)}_3)\mathcal{E}^{ji}_{(3)}\right]\omega^i = 0 \tag{80f}$$

Equation (80) can be assembled into the form

$$A\dot{z} + Bz = 0 \tag{81}$$

It is interesting to note that due to our choice of stress resultants and velocity variables as the primary unknowns, all the information regarding the material and inertial properties of the plate is contained solely in the matrix A and all the information regarding the boundary conditions is contained solely in the matrix B. This observation will be useful in a later section. It is now easy to cast eq. (81) into a generalized eigenvalue problem. Results from a free vibration analysis for a variety of boundary conditions will now be presented along with appropriate validation.

5.4.1 Natural frequencies of simply supported (S-S-S-S) plates

Due to the simplicity of its validation, we can first look at the case of a plate that is simply supported (either hard or soft) on all four edges. This case has a simple analytical solution for the natural frequencies when analyzed using a Kirchhoff-Love theory, of the form

$$\omega_{mn} = (m^2 + n^2)\pi^2 \tag{82}$$

where ω_{mn} is the mn^{th} nondimensional frequency, related to the dimensional natural frequency λ_{mn} as

$$\omega_{mn} = \lambda_{mn}\sqrt{\frac{\mu \mathbb{L}^4}{D}} \tag{83}$$

Reducing eq. (80) to represent a generalized Kirchhoff-Love theory as shown in section 4.3 and looking at only the decoupled bending problem, we can obtain the nondimensional frequencies and compare them with eq. (82), as given by table 6. These results have been obtained by using 276 assumed modes per variable ($p = 22$), although accuracy up to three significant digits can be obtained by using only 66 assumed modes per variable ($p = 10$). A plot showing the convergence of the Galerkin

Table 6: Comparison of frequency parameters of S-S-S-S square plate against analytical solution: Generalized Kirchhoff-Love theory

Mode	Analytical	Kirchhoff-Love
1-1	19.7392	19.7389
1-2,2-1	49.3480	49.3463
2-2	78.9568	78.9482
1-3,3,1	98.6960	98.6895
2-3,3-1	128.3049	128.2826
1-4,4,1	167.7833	167.7718
3-3	177.6529	177.5896

procedure to the analytical solution for the first two nondimensional frequencies is shown in fig. 21. As expected, a lower frequency will converge quicker than a higher one. For most practical purposes, agreement to four or five significant digits is considered excellent. One must also keep in mind that for a p-method, the problem size increases exponentially with p. Consequently, this increases computational time and needs to be weighed against the accuracy desired. Figure 22 shows the exponential increase in computational cost (run time) with increasing polynomial degree.

With a preliminary model validation giving satisfactory results, let us look now at the case of a plate that is fully clamped on all of its edges for further analysis

5.4.2 Natural frequencies of fully clamped (C-C-C-C) plates

Unlike the previous case of a simply supported plate, exact, closed form solutions were not known for plates that have all their edges clamped (or a mix of clamped and free edges). As such, the problem of determining the dynamic characteristics using approximate techniques has attracted a lot of attention since at least the 1930s. The reader is referred to Leissa [95] for a rigorous survey of the literature treating clamped plates in an approximate manner. More recently, however, Xing and Liu [157] presented an exact solution to the problem of thin, clamped plates for the first time. It might be a worthwhile exercise to validate the present Galerkin method

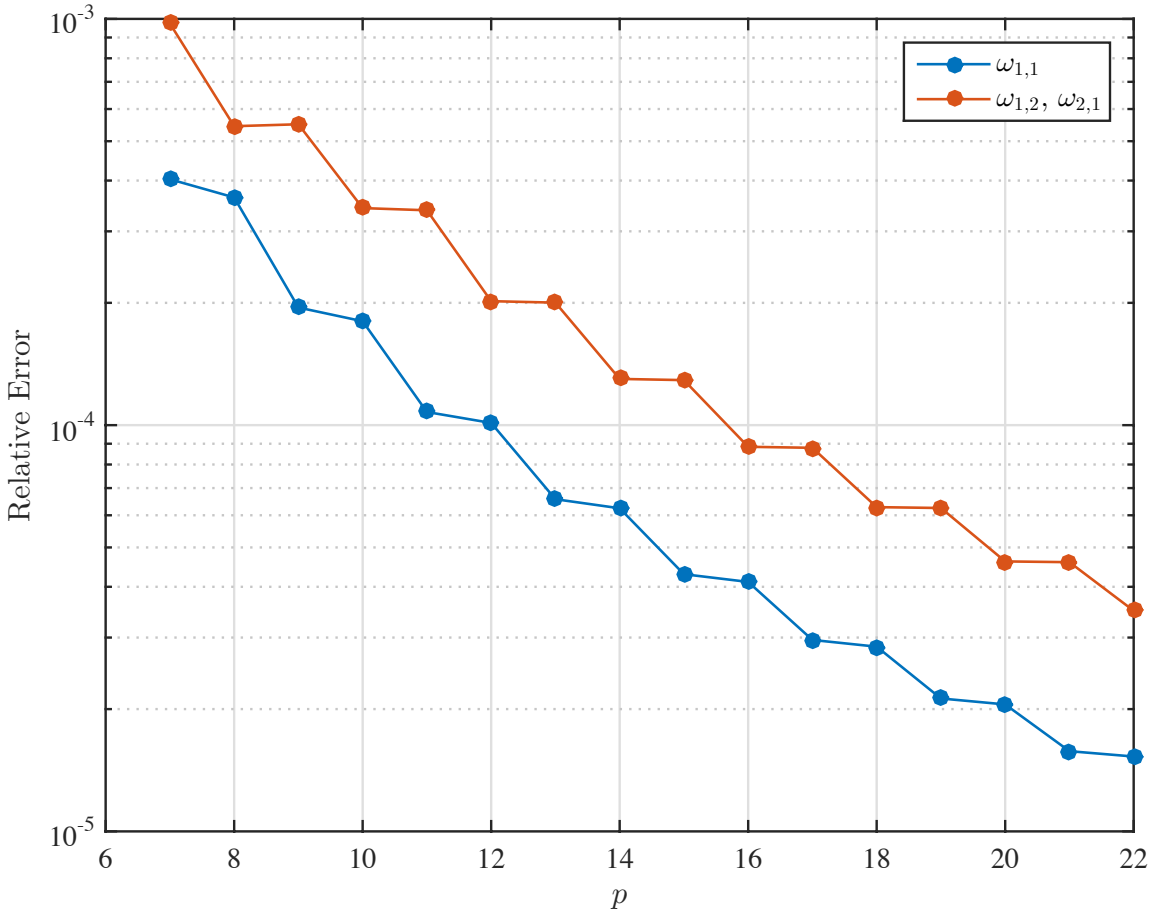

Figure 21: Relative error of the Galerkin method : Natural Frequencies of S-S-S-S Plates

against some of the results commonly accepted as accurate for the bending vibration of thin Kirchhoff-type plates along with the exact solutions from [157].

Table 7 compares the first twelve (nondimensional) natural frequencies with those derived by Young [161], Claassen and Thorne [21], Vijayakumar and Ramaiah [152], and Rajalingham et al. [123]. Most of these attempts only differ in their choice of shape functions: Young used products of beam shape functions (for C-C beams) in a Rayleigh-Ritz method. Vijayakumar and Ramaiah also used a Rayleigh-Ritz method, but used a superior set of shape functions derived from a modified Bolotin's method. Claassen and Thorne used a double Fourier sine series for the deflection. Vijayakumar

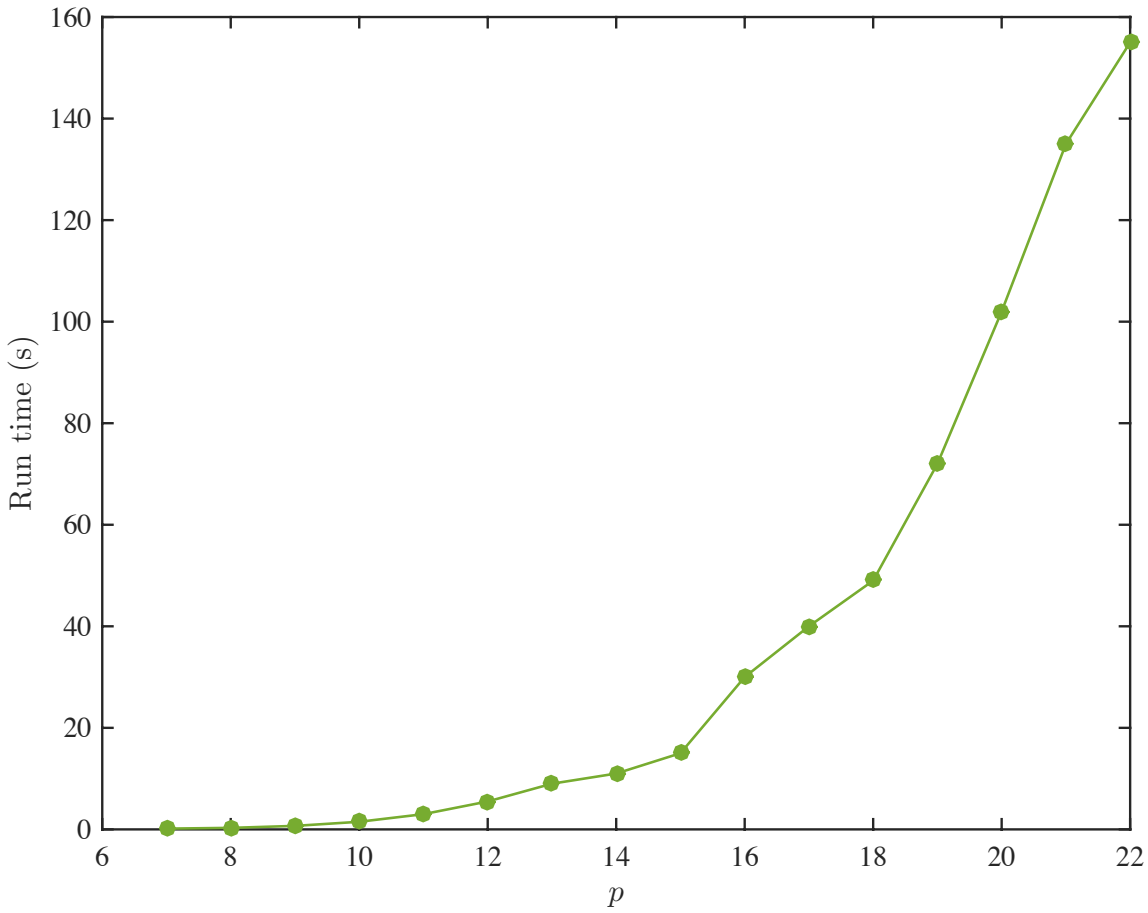

Figure 22: Increase in run time of linear free vibration analysis with polynomial degree p

and Ramaiah used what are known as "plate characteristic functions" derived from an extended Kantorovich-Krylov approach. Notably, all of these works, and numerous others, investigate only Kirchhoff plates using the displacement method.

Figures 23 and 24 show the percentage differences between the present Kirchhoff solution and the aforementioned references. It is clear from table 7 and figs. 23 and 24 that the present method yields results that are in excellent agreement with the aforementioned literature using approximate techniques, with a tenth of a percent being the maximum order of difference between other well known approximate solutions. It is worth remembering that the family of shape functions used here are made to satisfy the geometric boundary conditions only in a weak sense, thereby avoiding the

Table 7: Comparison of frequency parameters of a C-C-C-C square plate: Generalized Kirchhoff-Love theory

Mode	Present	Ref. [161]	Ref.[21]	Ref. [152]	Ref. [123]
1	35.9852	35.9904	35.9852	35.9853	35.9854
2, 3	73.3938	73.4106	73.3938	73.3942	73.3943
5	108.2165	108.2703	108.2165	108.2174	108.2178
5	131.5808	131.6389	131.5808	131.5808	131.5809
6	132.2048	132.2500	132.2048	132.2063	132.2067
7,8	165.0003	165.1508	165.0004	165.0026	165.0033
9,10	210.5218	—	210.5218	210.5229	210.5230
11	220.0325	—	—	220.0375	220.0389
12	242.1539	—	242.1539	242.1539	242.1542

Note: Ref. [161] – Young (1950); Ref. [21] – Claassen and Thorne (1961); Ref. [152] – Vijayakumar and Ramaiah (1978); Ref. [123] – Rajalingham et al. (1996).

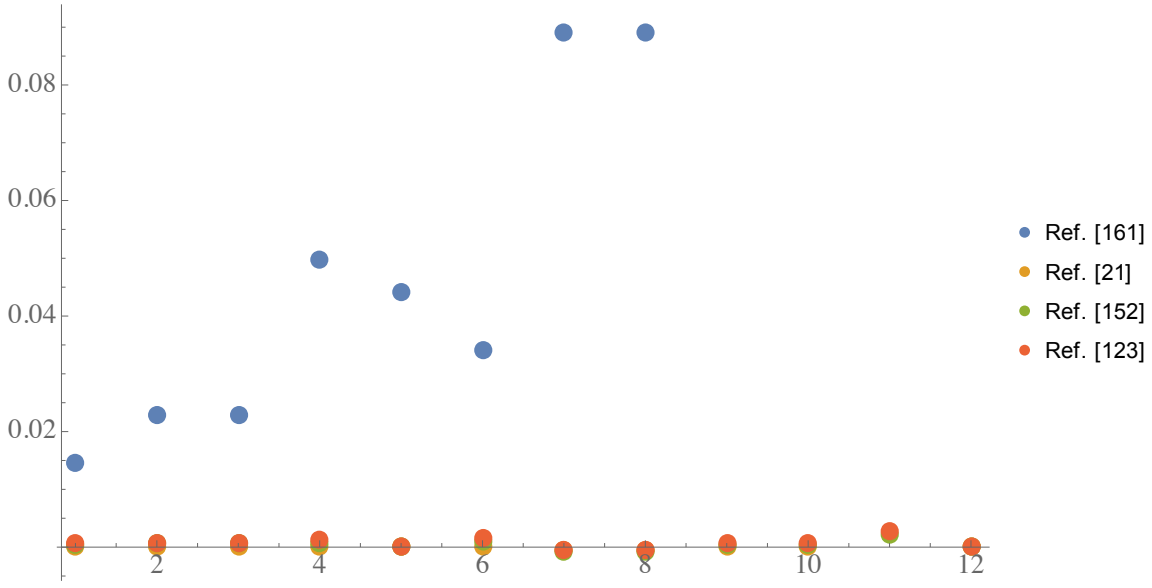

Figure 23: Percentage error of the frequency parameters against FEA

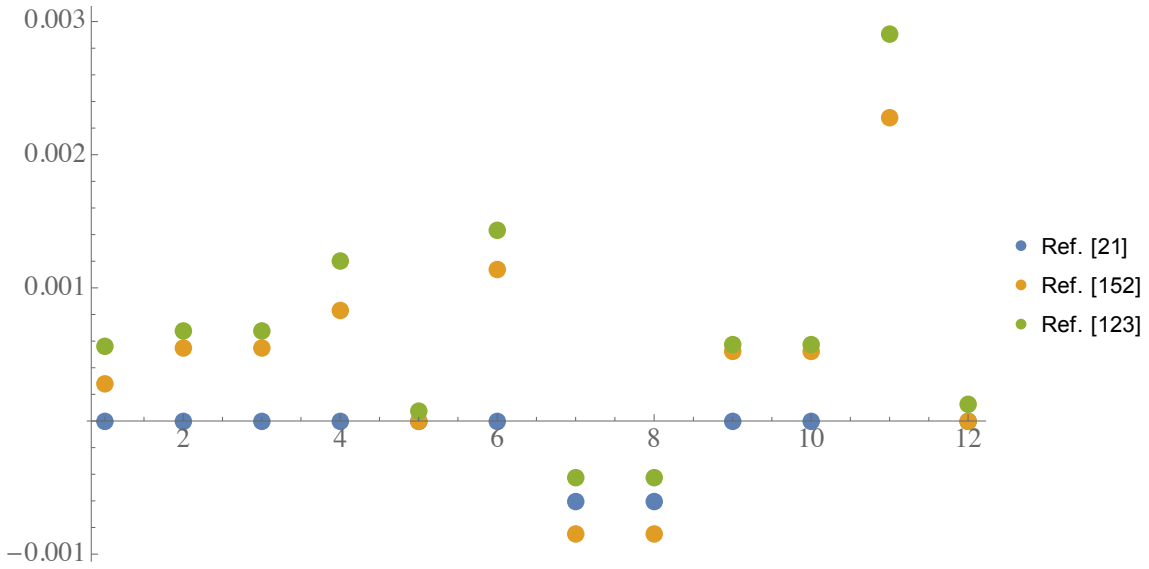

Figure 24: Percentage error of the frequency parameters against FEA: magnified

trouble of having to fabricate shape functions with agreeable characteristics.

The convergence behavior and computational time remain similar to the simply supported case before. Figures 25 to 28 show the convergence of the first, second (third), fourth and, to look at a higher mode, the twelfth frequencies to their final values given in table 7 with increasing polynomial degree p. Symbols have been used to differentiate between the converged results (up to six significant digits) from the rest. One can again see the expected behavior of lower frequencies converging earlier than the higher ones. That said, even the twelfth mode converges to six significant digits for only $p = 18$, where the first mode converges at $p = 14$.

More rigorous forms of verification are comparisons with exact solutions, 3-D FE solutions and experimental data. Xing and Liu [157] used a novel separation of variables to come up with an exact solution for thin, clamped plates for the first time. For example, Hazell and Mitchell [60] conducted experiments to measure eigenvalues of square clamped plates using holographic interferometry to measure mode shapes. Their results are compared with those from the present Galerkin approach (using $p = 20$) in table 8. The plate under consideration is a very thin one ($L/h \approx 166.55$), with

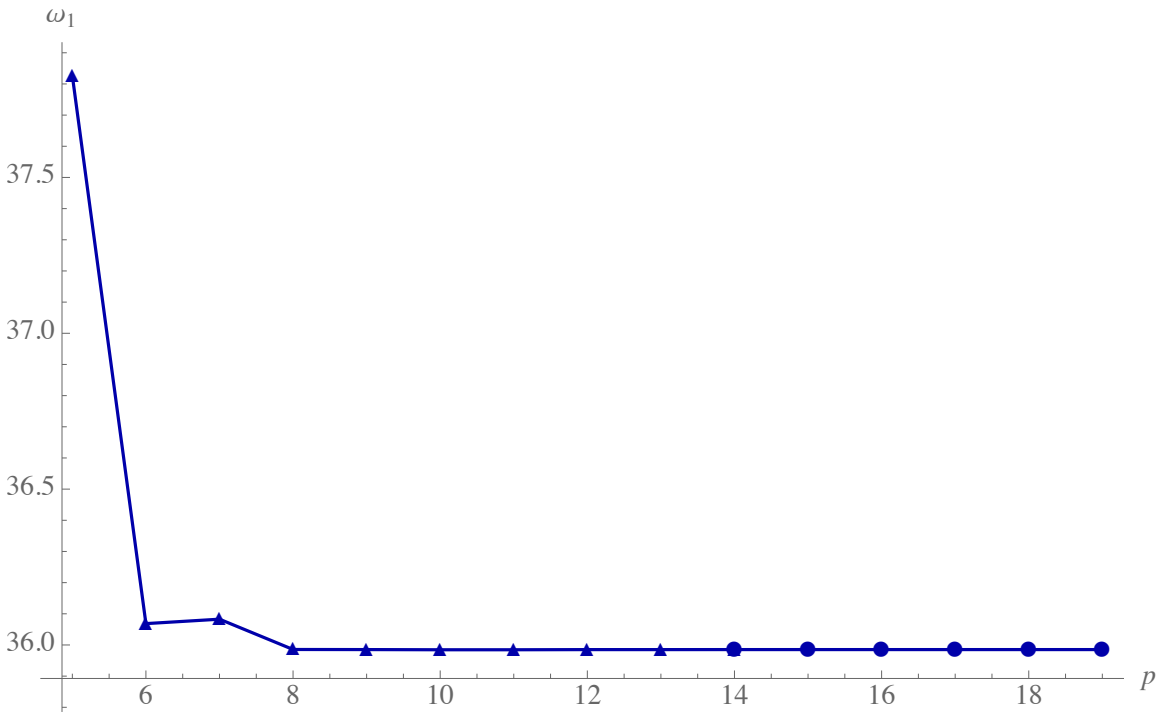

Figure 25: Convergence of the Galerkin method for C-C-C-C plates: ω_1 vs. p

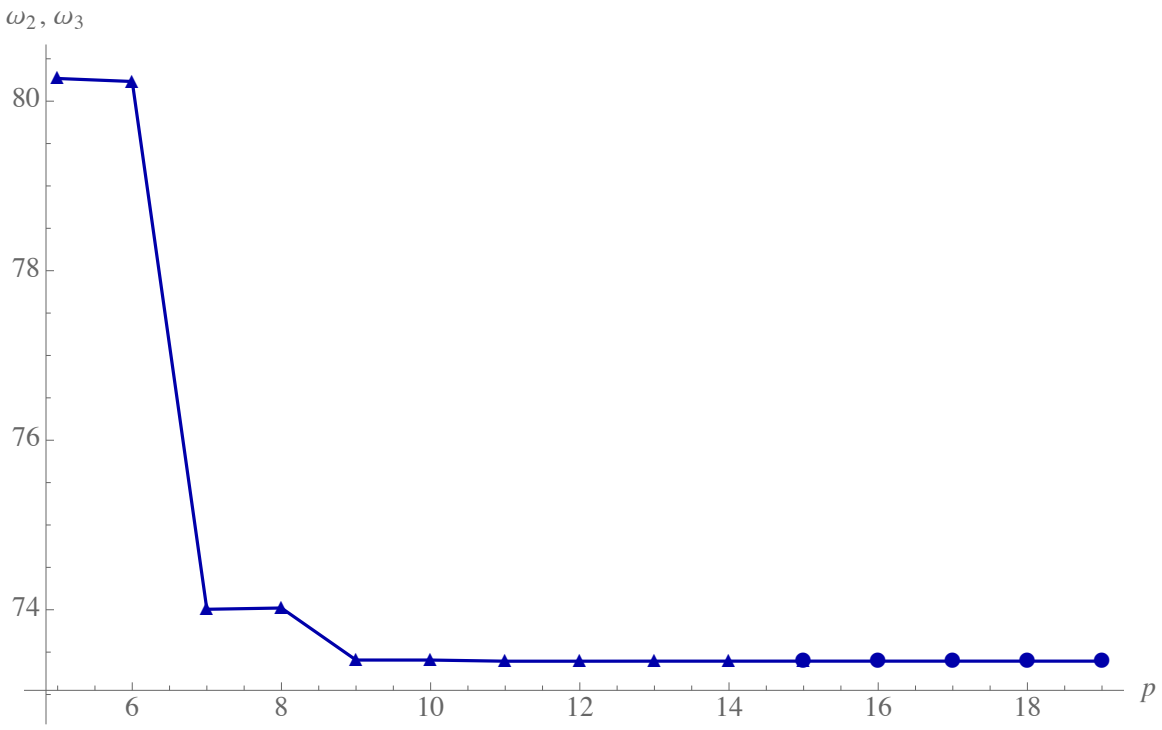

Figure 26: Convergence of the Galerkin method for C-C-C-C plates: ω_2, ω_3 vs. p

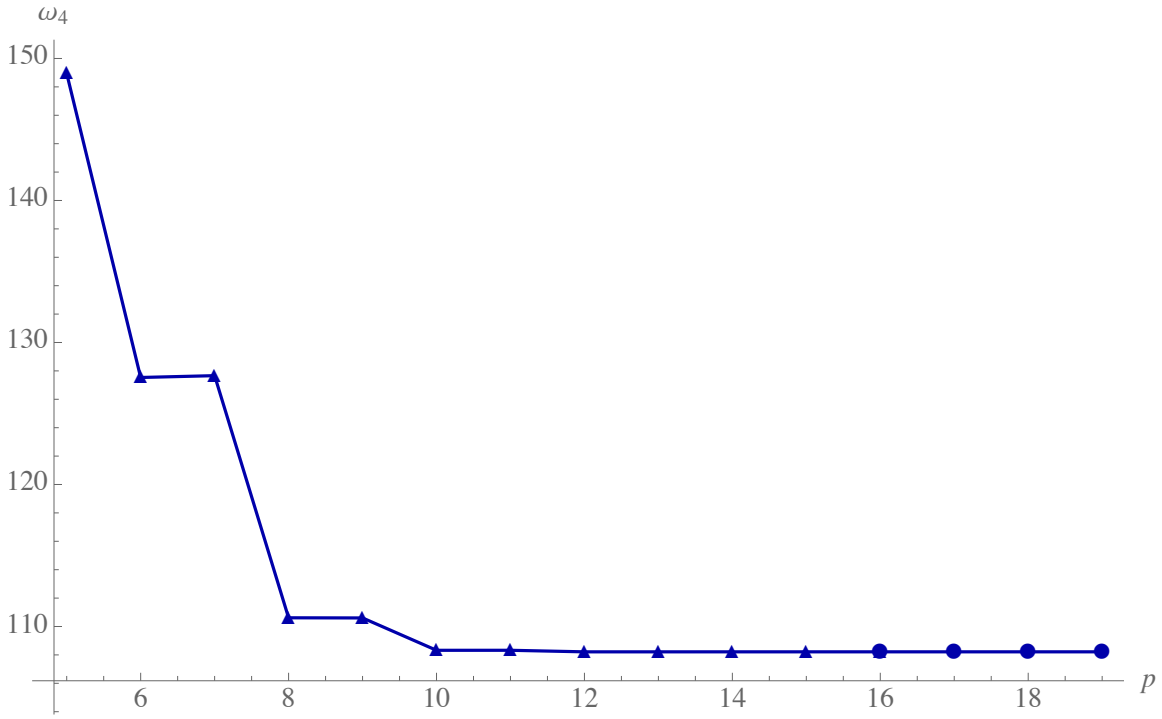

Figure 27: Convergence of the Galerkin method for C-C-C-C plates: ω_4 vs. p

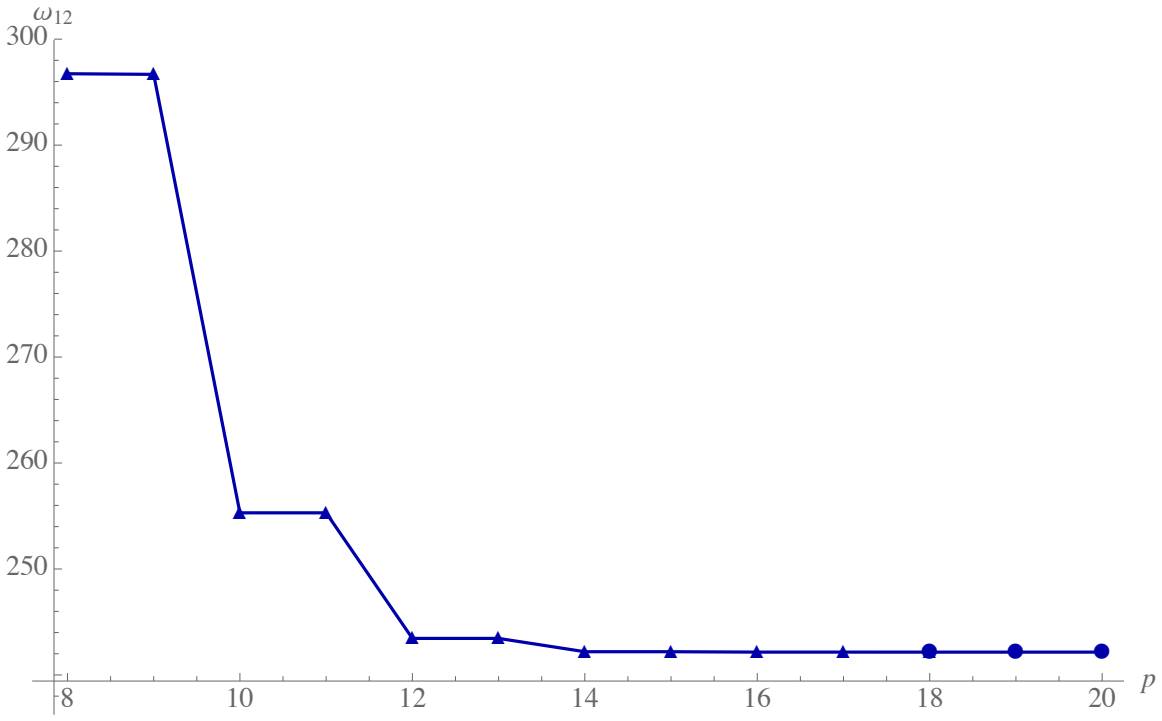

Figure 28: Convergence of the Galerkin method for C-C-C-C plates: ω_{12} vs. p

minimal transverse shear effects. Nevertheless, we now compare frequencies obtained from both a generalized Reissner-Mindlin theory and a Kirchhoff-Love theory to this experimental data. Additionally, a further comparison is made with 3-D finite element analysis, performed using 40,000 20-node brick elements in Abaqus.

Taking a closer look at the frequency parameters listed, it can be seen that a Kirchhoff model gives results that are slightly higher than those from 3-D FEM while a shear deformable model gives values that are both slightly higher and lower values. In either case, all the differences are with $\pm 0.05\%$. Owing to the smooth second-order convergence of FEM solution, it is conceivable that for an even greater number of brick elements, the FE solution will slowly approach the latter. On the other hand, the exact solution consistently provides frequencies lower in magnitude than any other approximate computational technique, showing that the latter are merely upper bounds. It is worth noting, however, that the fifth and sixth frequencies are predicted to be identical whereas all approximate plate solutions as well as 3-D FEM predict them to be close, but otherwise different. Indeed, a look at the corresponding mode shapes from 3-D FEM (not provided here) shows them to be as unmistakably distinct. This is a well known debate among mechanicians whether this source of discrepancy is physical or numerical and remains, to the authors knowledge, unresolved. Finally, experimental results, which are typically not known to the same precision, render the differences between these three solution sets insignificant. A plot showing the percentage error of the results presented in **??** with respect to 3-D finite element results (regarded as being a reliable representation of the 3-D elasticity solution) is given in fig. 29.

Further verification of classical elasticity based results for shear deformable beams in particular can be made by varying the length-to-thickness ratio and comparing to 3-D FE analysis. Figures 30 and 31 show the dependance of the first and the second (or third) frequency parameters, respectively, on L/h, which is varied from a value

Table 8: Validation of frequency parameters of a C-C-C-C square plate against experiment

Mode	Expt. [60]	Exact [157]	Reissner-Mindlin	Kirchhoff-Love	3-D FEM
1	35.986	35.1124	35.9717	35.9852	35.9955
2, 3	72.83 ±.98	72.8994	73.3465	73.3938	73.3920
4	108.0 ±1.4	107.4688	108.1182	108.2165	108.1798
5	132.2±1.7	131.6289	131.4462	131.5808	131.5170
6	132.2±1.7	131.6289	132.0725	132.2048	132.1438
7,8	166.2 ±2.1	164.3867	164.791	165.0003	164.8728
9,10	209.1 ±2.6	210.3617	210.2106	210.5218	210.3022
11	220.2 ±2.7	219.3245	219.6741	220.0325	219.7669
12	245.0 ±3.0	242.1969	241.7327	242.1539	241.8268

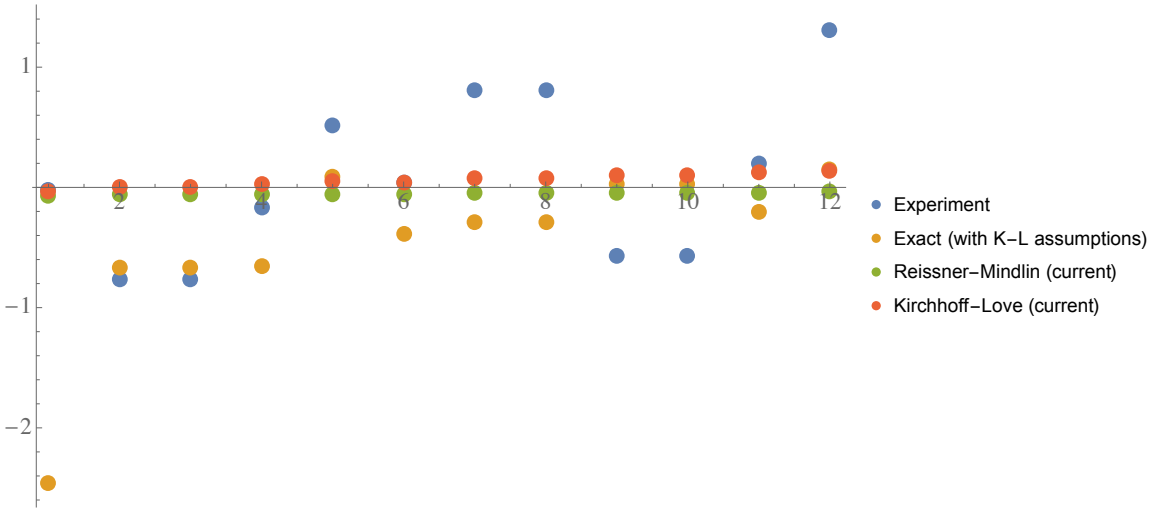

Figure 29: Percentage error of the frequency parameters against FEA

of 5 to 200. As the plate gets thicker, the two results start to deviate in increasingly greater amounts: for $L/h = 5$, we see a 2.73% difference in the first natural frequency and a 4.72% difference in the next two.

Having looked at basic model validation of Reissner-Mindlin and Kirchhoff-Love plates, both of which are based on classical elasticity, we can now investigate the effect micropolar elastic constants have on the (linear) dynamic behavior. Specifically, we can look at how varying the thickness of the plate relative to the internal length-scale parameters affects the predicted natural frequencies of the bending problem.

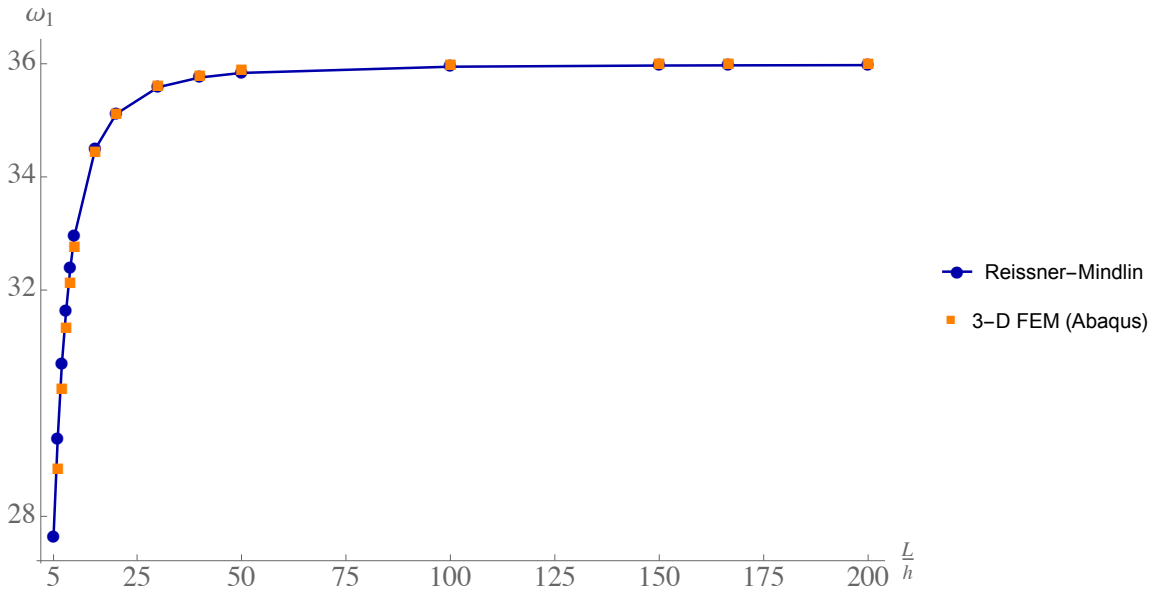

Figure 30: First nondimensional frequency of a C-C-C-C Plate for various L/h: 3-D FEM vs. Reissner-Mindlin

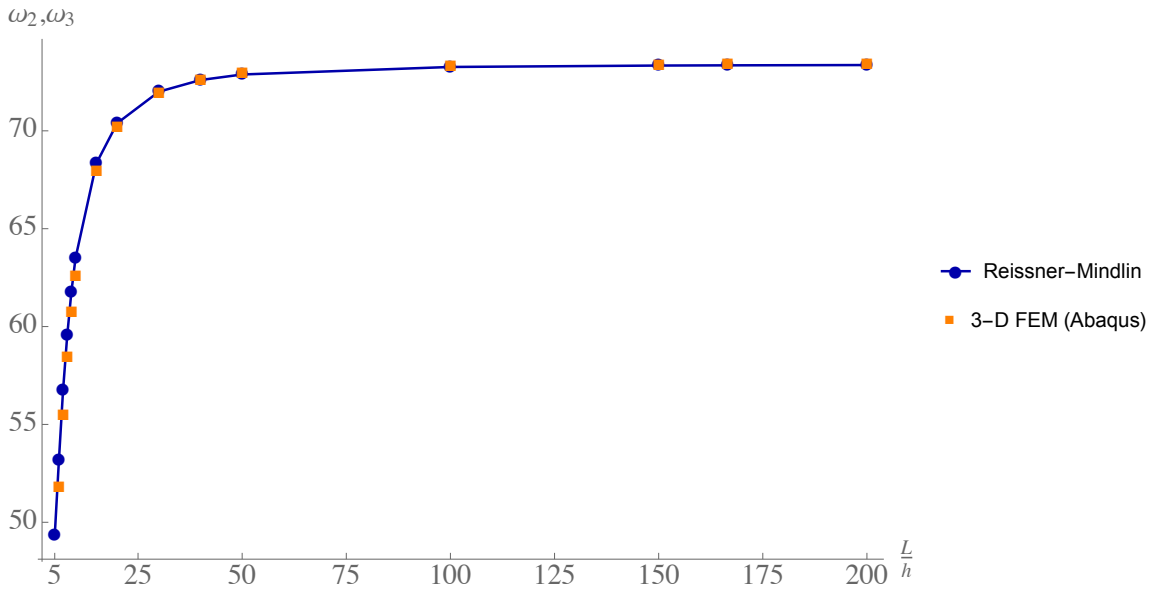

Figure 31: Second (and third) nondimensional frequency of a C-C-C-C Plate for various L/h: 3-D FEM vs. Reissner-Mindlin

Let us focus, without loss of generality, on the example of the Polystyrene foam mentioned in table 5. Since we wish to isolate the effect of varying h with respect to l_0, let us also maintain the ratio L/h a constant. A value of $L/h = 15$ was chosen so as to have sufficiently different results between a Kirchhoff-Love and a Reissner-Mindlin plate, both of which are limiting cases of a Cosserat elastic plate (as shown in section 4.3). The plate thickness is varied from l_0 to $30l_0$ and plotted against the first 10 nondimensional natural frequencies in figs. 32 to 37. For the sake of comparison, the classical results are also presented.

Looking at figs. 32 to 37, the following observations can be made:

- For plates where $h \sim l_0$, length-scale effects have a significant impact on the predicted natural frequencies. For the example at hand, all the natural frequencies are predicted to be $15\% - 20\%$ higher for a micropolar plate when $h = l_0$ (when compared to classical Reissner-Mindlin frequencies). Note that since it may be physically unreasonable to have a plate that is much thinner than the length-scale of the microstructure of the material, all the plots presented consider a minimum thickness of l_0 .

- For thicker plates ($h \gg l_0$), we see that the stiffening caused by the microstructure become increasingly unimportant and the predicted frequency parameters very close to those from a Reissner-Mindlin theory. The results will not, however, coincide exactly unless all the micropolar constants vanish. This difference arises due to the shear stiffness predicted by eq. (34) being different from eq. (35) for nonzero β, γ, κ.

- In the same manner that a Kirchhoff plate model yields stiffer results than a Reissner-Mindlin one for moderately thick classical elastic plates, a Kirchhoff-type micropolar or couple stress based plate theory will also yield unrealistic results unless $L \gg h$. Since the effect of including microstructure-dependent

length-scale effects is the same as suppressing shear deformation, i.e., both yield stiffer results, using a Kirchhoff based theory for even moderately thick micropolar plates will often result in a gross overestimation of the stiffening effect. The magnitude of this over-estimation depends on the particular frequency of interest: for the present case, the lowest frequency is predicted to be around 30% higher while the tenth frequency is, theoretically, greater by as much as 45% when compared to the classical Reissner-Mindlin frequencies. It is important to note that for higher frequencies, the wavelength of deformation is much smaller than L. Since the suitability of a plate theory for a dynamic analysis is dictated by the ratio of thickness to the wavelength of deformation (which is the appropriate small parameter of the problem, instead of h/L), one must be wary when looking at results for higher frequencies (for example, ω_9, ω_{10} and higher), making sure the parameter remains suitably 'small'.

Therefore, for the present example at least, the difference between results from a Cosserat plate theory and classical Reissner-Mindlin frequencies is of the same order as the difference between Kirchhoff-Love and Reissner-Mindlin frequencies and, as such, one must take care not to neglect shear flexibility while accounting for length-scale effects.

Having satisfactorily dealt with linear free vibration analysis, let us now shift our attention to dealing with linear static problems.

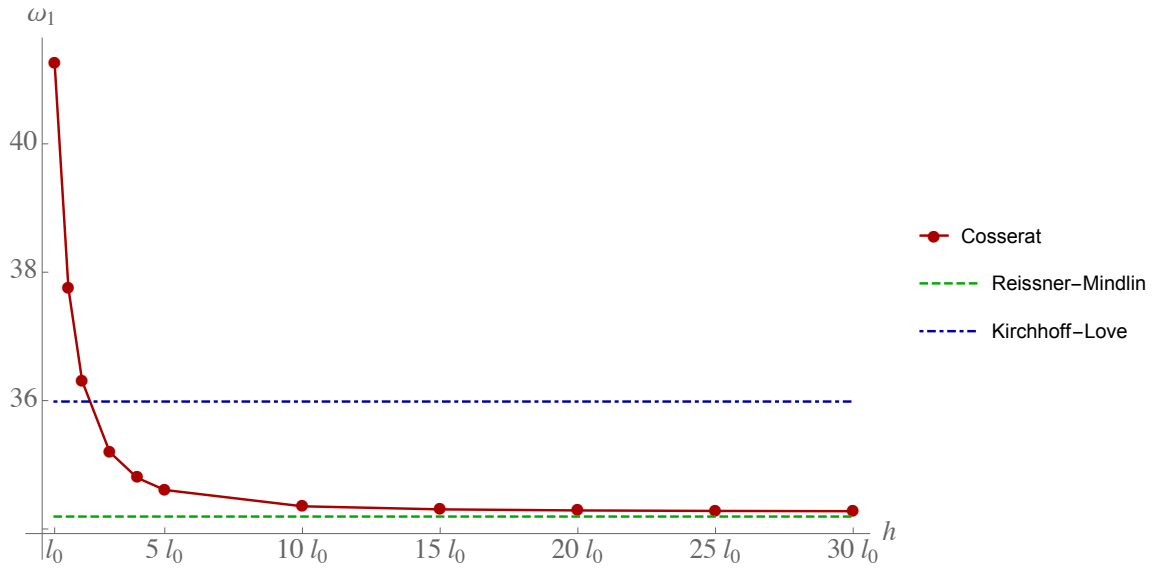

Figure 32: First nondimensional frequency of a C-C-C-C Cosserat Plate for various h/l_0; $L/h = 15$

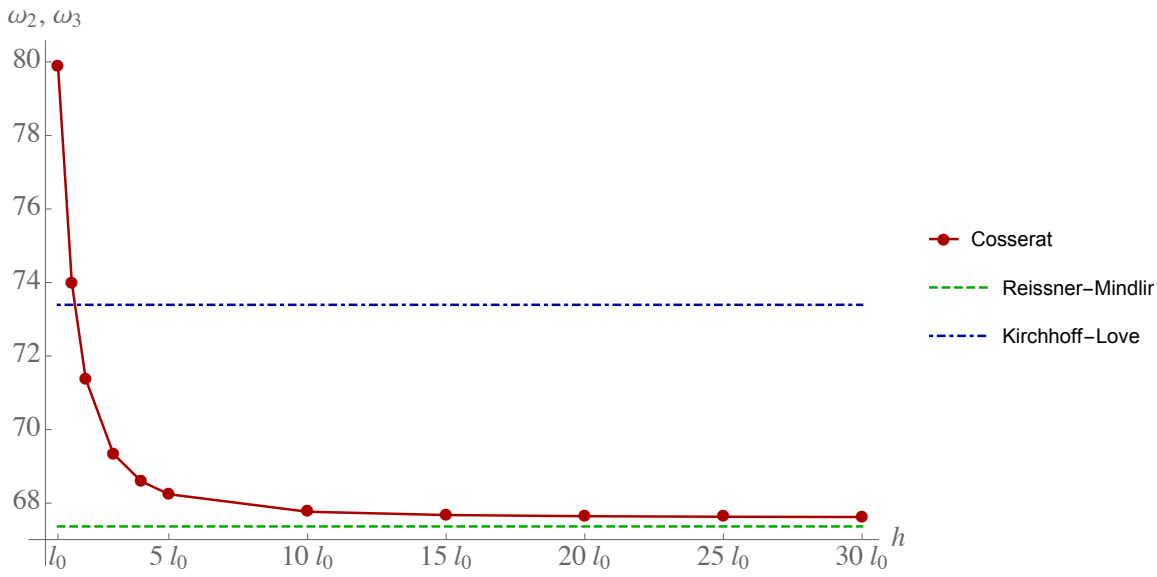

Figure 33: Second (third) nondimensional frequency of a C-C-C-C Cosserat Plate for various h/l_0; $L/h = 15$

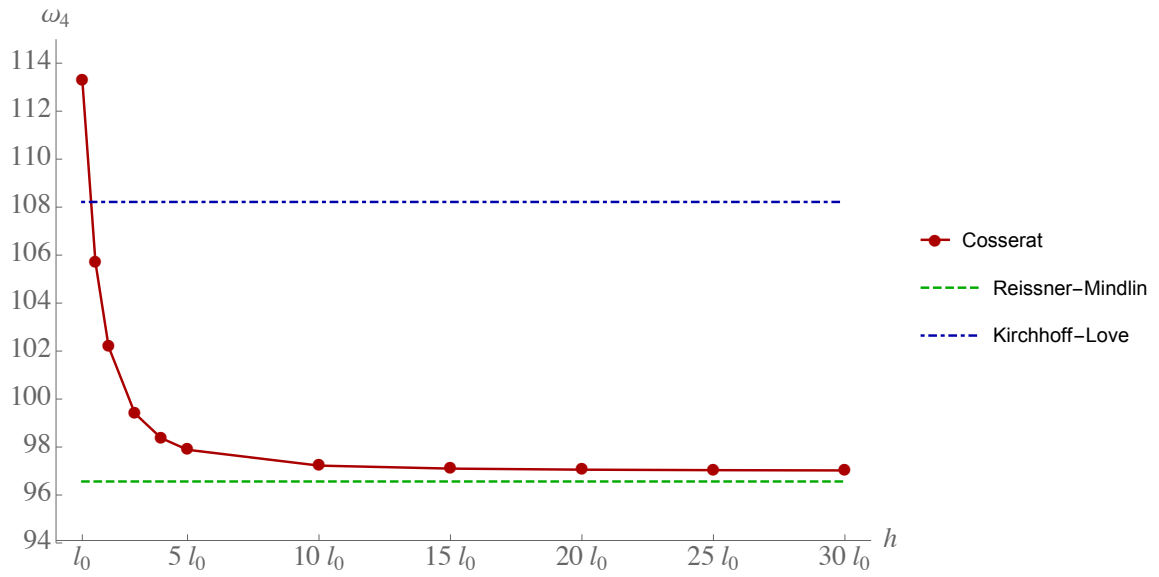

Figure 34: Fourth nondimensional frequency of a C-C-C-C Cosserat Plate for various h/l_0; $L/h = 15$

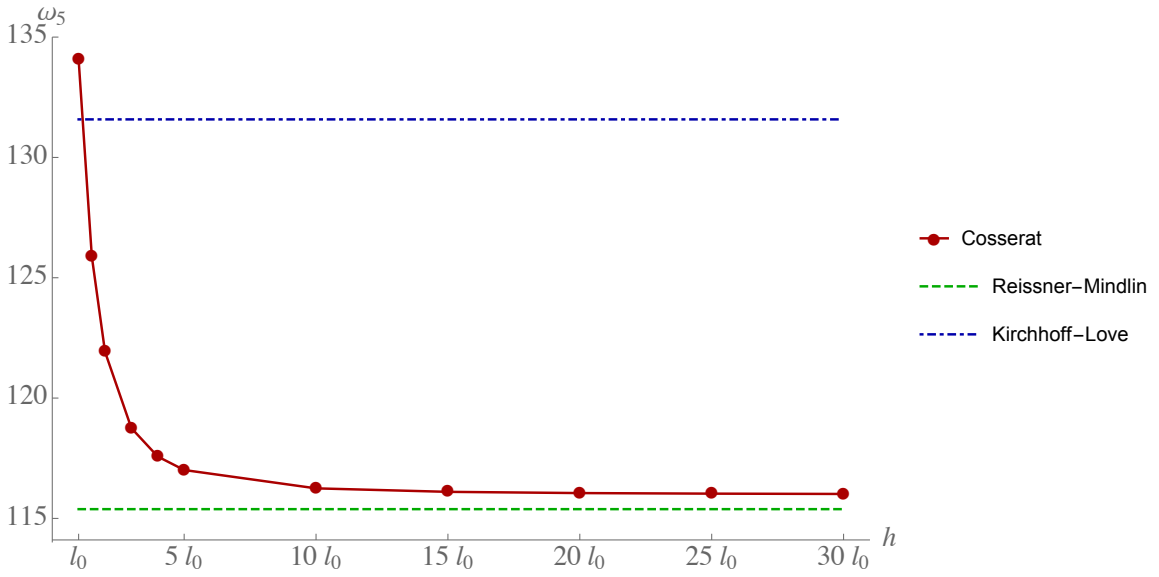

Figure 35: Fifth nondimensional frequency of a C-C-C-C Cosserat Plate for various h/l_0; $L/h = 15$

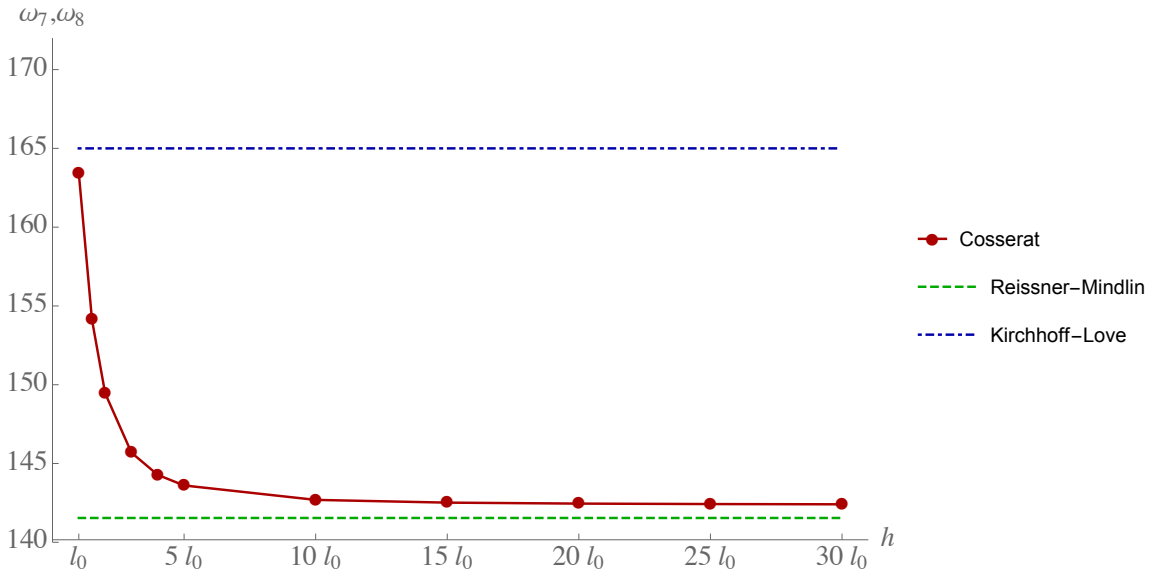

Figure 36: Seventh nondimensional frequency of a C-C-C-C Cosserat Plate for various h/l_0; $L/h = 15$

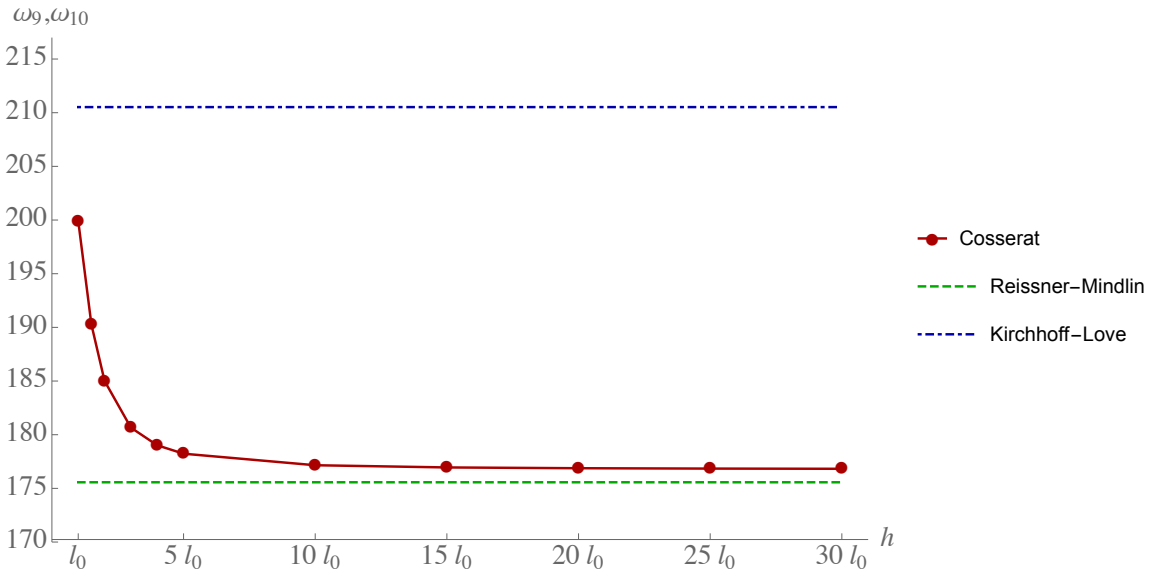

Figure 37: Ninth (tenth) nondimensional frequency of a C-C-C-C Cosserat Plate for various h/l_0; $L/h = 15$

5.5 Linear Static Analysis

The fully intrinsic equations are unsuitable for static analysis (linear or nonlinear) of stationary structures [139]. This is easily seen by noting that for non-moving plates, eqs. (56) are identically satisfied because $V = \Omega = 0$. This leaves us with the six equilibrium equations in 12 unknowns - a case of static indeterminacy that cannot be solved without some augmentation. We shall address linear statics in this section and defer the discussion on nonlinear static behavior to the next chapter.

Solving a linearized static problem is best done using a mixed formulation with displacement and rotation variables. Since these quantities would have to be small, they pose none of the problems associated with dealing with a direction cosine matrix of finite rotations such as infinite degree nonlinearities and singularities. However, for a linear analysis, the generalized strain-velocity relations are simply time derivatives of the generalized strain-displacement relations. So, the matrices A, B, D assembled in eq. (78) can be reused here if one removes the time derivatives on the generalized strains and set all inertia terms in the equilibrium equations to zero (the latter is easily implemented by simply setting the mass density to zero). This results in the following system of equations

$$(A_{ji}\big|_{\mu=0} + B_{ji})z_i + D_j = 0 \tag{84}$$

Strictly speaking, this formulation is now a mixed formulation involving infinitesimal displacements and rotations along with force and moment resultants. Nevertheless, it is worth pursuing such a mixed method as will be demonstrated in the next chapter. For illustrative purposes, we will now solve a few static problems. Additionally, for reasons that will be clear shortly, let us differentiate between two kinds of problems, with respect to boundary conditions: those plate problems where there is at least one direct boundary condition in terms of all the variables of the problem (force, moment, displacements and rotations), and those where no such requirements are

made. For example, cantilever plates fall into the former category while clamped or simply supported plates, having no boundary condition on the force resultants, belong to the latter. For the purpose of demonstration, it will suffice to look at simple cases of static deflections of classical elastic plates under a uniformly applied distributed dead load, p_3, normal to the plate reference surface. For Cosserat elastic plates, similar qualitative observations can be made as before (viz., they yield stiffer results for $h \sim l_0$). Since we are looking at linear statics, no distinction is made between the plate's undeformed and deformed configurations. Therefore, in the Galerkin equations given by eq. (84), we set $f = p_3 e_3$ and $m = 0$.

5.5.1 Linear statics of uniform F-F-C-C plates

Consider once again a uniform isotropic plate whose domain is described by fig. 20. Let edges 1, 2 be rigidly clamped while edges 3, 4 remain traction free. The distribution of the transverse displacement field u_3, nondimensionalized with $p_3\mathbb{L}^4/D$, under a uniform load p_3 is given by fig. 38. The solution converges to its final value up to four significant digits for only $p = 11$. A plot showing the convergence behavior for increasing p is given in fig. 39. Also provided in fig. 39 is a validation of the obtained solution against a 3-D finite element solution from Abaqus (using approximately 40k 20-node brick elements). Expectedly, there are significant gains to be had in computational time using a plate solver as opposed to full-blown 3-D finite elements: the present Galerkin approach, implemented in Fortran, took 0.05s to run (for $p = 11$), as opposed to over 4 minutes in Abaqus. Even if one wishes to use a much higher polynomial degree, say $p = 24$, the plate solver still only takes under 4 seconds. These cost savings do not come at the expense of accuracy: the difference in solutions shown by fig. 39 is, at best, only 0.04% (for $p \geq 10$). Also, as will be discussed in the following subsections, the problem size was reduced significantly from the original $18N_e$ variables to a much smaller set of $6N_e$, which immensely helps in

reducing the computational time with no (further) loss of accuracy.

5.5.2 Linear statics of uniform cantilever (C-C-C-F) plates

Next, consider the case of a cantilever plate. Referring to fig. 20, let us arbitrarily pick edge 4 to be rigidly clamped and leave the remaining edges traction-free. The plate is subjected to the same uniform loading as before. The distribution of the transverse displacement field u_3, nondimensionalized with $p_3\mathbb{L}^4/D$, is given by fig. 40. Let us take a look at the transverse deflection of the mid-point of edge 2 (opposite to the clamped edge). Figure 41 shows a rapid convergence of the solution, similar to previous case. The figure also shows this solution compared against that obtained from a 3-D finite element analysis. The gains in computational cost are, naturally, almost identical to the previous case. While it appears that the results do not match with Abaqus as well as the previous case, there is still only a 0.1% between the two solutions which, for all practical purposes, is excellent agreement.

Unlike cantilever beams, we also pick up variations in field quantities along both the in-plane directions for cantilever plates. For the present loading case, while a cursory glance at fig. 40 may lead one to think that the transverse displacement along edge 2 is a constant, there is a small, but non-negligible variation. Figure 42 shows this variation in u_3 and a comparison with the corresponding finite element solution. Again, these solutions are within 0.1% of each other.

5.5.3 Linear statics of uniform fully clamped (C-C-C-C) and simply supported (S-S-S-S) plates

The case of a fully clamped plate has only geometric boundary conditions specified on every edge (and importantly, has no edge with natural boundary conditions). On the other hand, the simply supported plate has no edge with rotations or forces specified. As noted by Sotoudeh and Hodges [140], because every single equation does not have a boundary condition that can be associated with it, these cases are

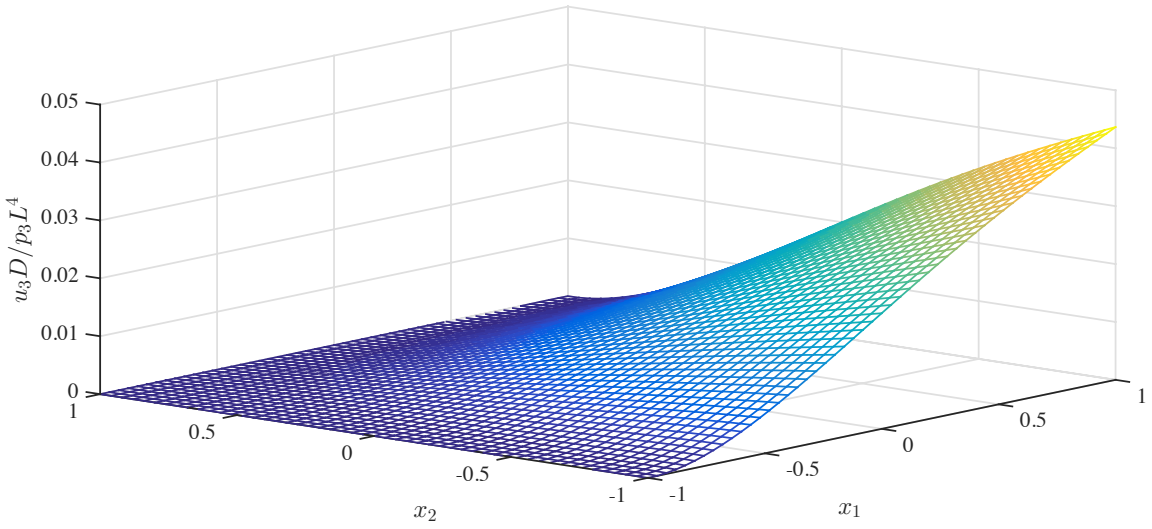

Figure 38: Static deflection of a F-F-C-C plate under uniform loading

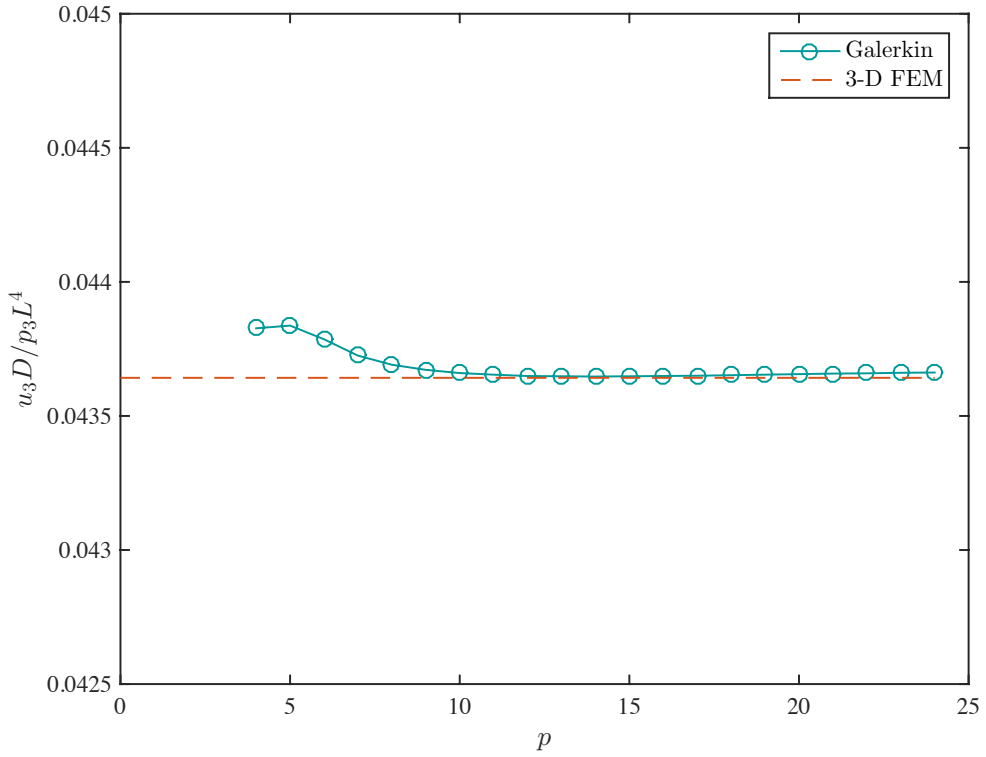

Figure 39: Convergence of transverse displacement at (1,-1) for F-F-C-C plate: $\frac{u_3}{p_3L^4/D}$ vs. p

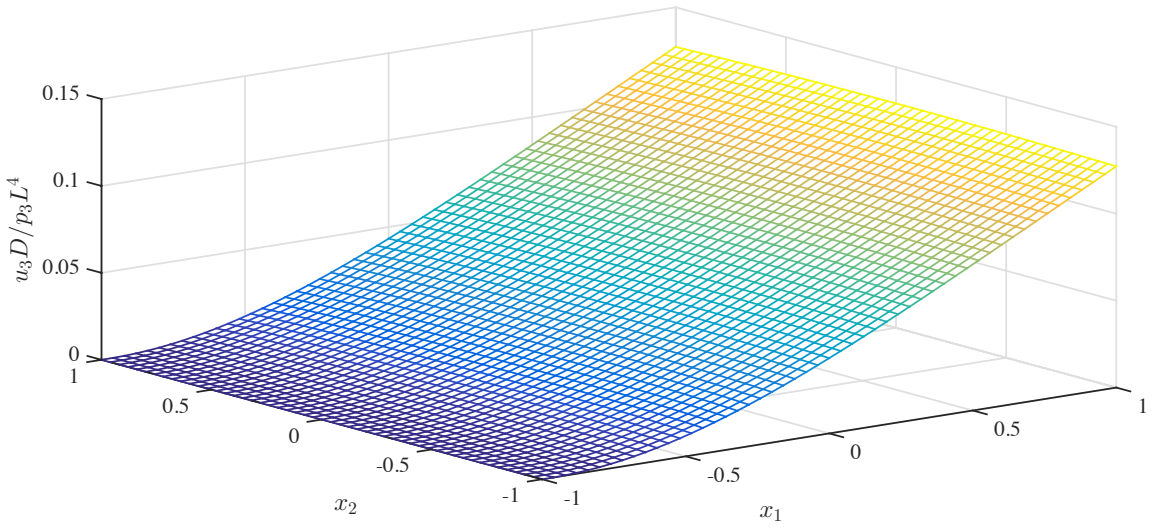

Figure 40: Static deflection of a cantilever plate under uniform loading

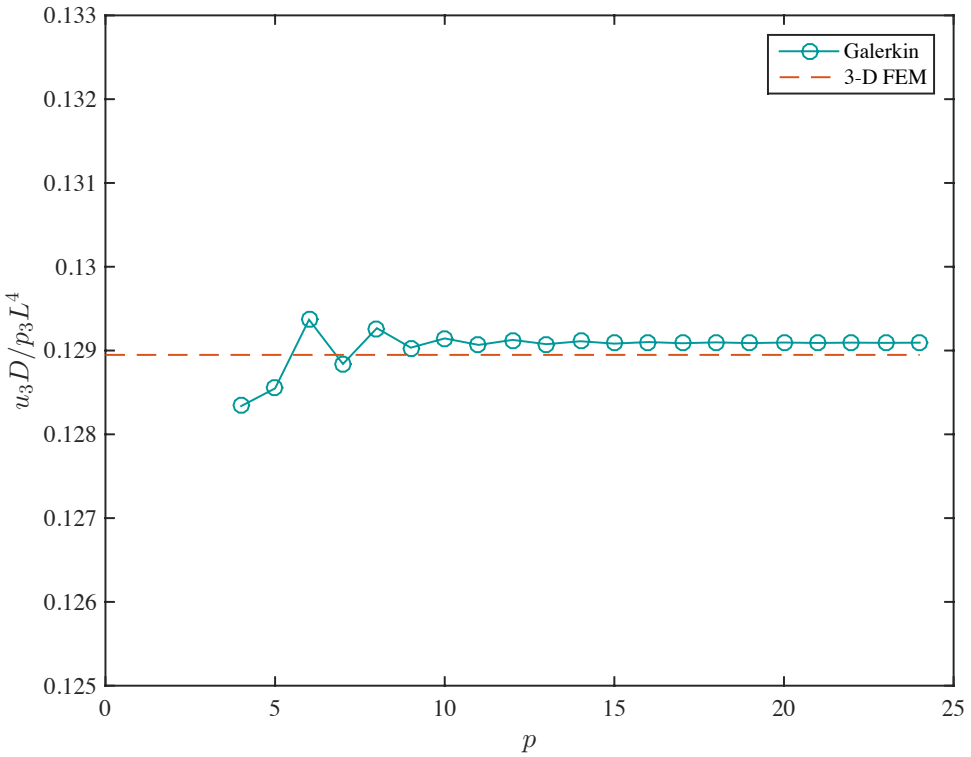

Figure 41: Convergence of transverse displacement at (1,0) for F-F-F-C plate: $\frac{u_3}{p_3L^4/D}$ vs. p

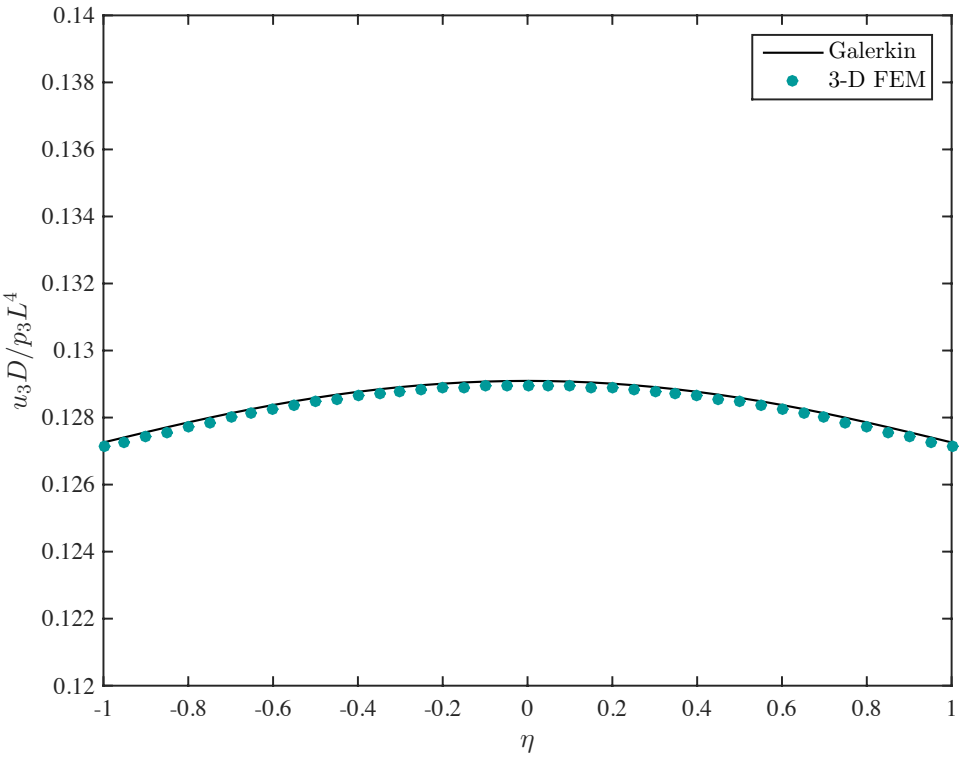

Figure 42: Comparison of transverse displacement for F-F-C-C plate at $\xi = 1$, Galerkin vs. 3-D FEM

not well posed. This is in contrast to the previous cases of clamped-free plates where we had one boundary condition in terms of every force, moment, displacement and rotation variable. It is most likely due to this reason that eq. (84), when applied to these problems, results in matrices that are severely ill-conditioned and provide no useable results.

It is worth noting that Sotoudeh [138] applied the same mixed formulation for linear statics successfully to simply supported plates. The key differences from the present approach lie in the manner in which variables are interpolated (an h-method vs. the current p-method), and a strict enforcement of boundary conditions at nodal points/edges (as opposed to a weak form of both the geometric and natural boundary conditions in eq. (69)).

Since it is important that problems with all types of boundary conditions be handled satisfactorily, a workaround has been developed that involves restructuring of the original Galerkin equations. This will be detailed now.

Let us first explicitly write out eq. (84) in the form of these six sets of equations:

$$\left[\mathcal{B}_1^{ji} - \tau_2^{(f)}\mathcal{E}_{(2)}^{ji} + \tau_4^{(f)}\mathcal{E}_{(4)}^{ji}\right]n_1^i + \left[\mathcal{B}_2^{ji} + \tau_1^{(f)}\mathcal{E}_{(1)}^{ji} - \tau_3^{(f)}\mathcal{E}_{(3)}^{ji}\right]n_2^i + \mathbb{L}_1\mathbb{L}_2\int_{-1}^{1}\int_{-1}^{1}\Phi^j f \,\mathrm{d}\xi\mathrm{d}\eta = 0 \tag{85a}$$

$$\left[\mathcal{B}_1^{ji} - \tau_2^{(m)}\mathcal{E}_{(2)}^{ji} + \tau_4^{(m)}\mathcal{E}_{(4)}^{ji}\right]m_1^i + \left[\mathcal{B}_2^{ji} + \tau_1^{(m)}\mathcal{E}_{(1)}^{ji} - \tau_3^{(m)}\mathcal{E}_{(3)}^{ji}\right]m_2^i + \mathcal{A}^{ji}\widetilde{e}_\alpha n_\alpha^i + \mathbb{L}_1\mathbb{L}_2\int_{-1}^{1}\int_{-1}^{1}\Phi^j m \,\mathrm{d}\xi\mathrm{d}\eta = 0 \tag{85b}$$

$$\mathcal{A}^{ji}\gamma_1^i = \left[\mathcal{B}_1^{ji} - (1-\tau_2^{(f)})\mathcal{E}_{(2)}^{ji} + (1-\tau_4^{(f)})\mathcal{E}_{(4)}^{ji}\right]v^i + \mathcal{A}^{ji}\widetilde{e}_1\psi^i \equiv \mathcal{B}_{1f}^{ji}q^i + \mathcal{A}^{ji}\widetilde{e}_1\psi^i \tag{85c}$$

$$\mathcal{A}^{ji}\gamma_2^i = \left[\mathcal{B}_2^{ji} + (1-\tau_1^{(f)})\mathcal{E}_{(1)}^{ji} - (1-\tau_3^{(f)})\mathcal{E}_{(3)}^{ji}\right]v^i + \mathcal{A}^{ji}\widetilde{e}_2\psi^i \equiv \mathcal{B}_{2f}^{ji}q^i + \mathcal{A}^{ji}\widetilde{e}_2\psi^i \tag{85d}$$

$$\mathcal{A}^{ji}K_1^i = \left[\mathcal{B}_1^{ji} - (1-\tau_2^{(m)})\mathcal{E}_{(2)}^{ji} + (1-\tau_4^{(m)})\mathcal{E}_{(4)}^{ji}\right]\psi^i \equiv \mathcal{B}_{1m}^{ji}\psi^i \tag{85e}$$

$$\mathcal{A}^{ji}K_2^i = \left[\mathcal{B}_2^{ji} + (1-\tau_1^{(m)})\mathcal{E}_{(1)}^{ji} - (1-\tau_3^{(m)})\mathcal{E}_{(3)}^{ji}\right]\psi^i \equiv \mathcal{B}_{2m}^{ji}\psi^i \tag{85f}$$

Using eqs. (85c) to (85f), it is now possible to express the generalized coordinates

of the 2-D strains solely in terms of those of the displacements and rotations in the form

$$\begin{aligned} \gamma_\alpha^i &= (\mathcal{A}^{ij})^{-1}\mathcal{B}_{\alpha f}^{jk} q^k + \widetilde{e_\alpha}\psi^i \\ K_\alpha^i &= (\mathcal{A}^{-1})^{ij}\mathcal{B}_{\alpha m}^{jk}\psi^k \end{aligned} \tag{86}$$

Using eq. (86) along with the appropriate constitutive laws, one can replace all the force and moment resultants in eqs. (85a) and (85b) in terms of the displacements and rotation variables. This will result in a system of $6N_e$ equations in $6N_e$ unknowns, a reduction from the original system of $18N_e$ equations in as many unknowns.

It is very important to note that this reduction of variables does not equal to the application of a purely displacement-based method. Since the Galerkin approximation is applied *prior* to the aforementioned substitution of variables, this remains a mixed-method. In fact, for the previous case of a cantilever plate, identical results are obtained for all the 18 variables with or without a reduction of variables. However, even though it is in unnecessary for this case, it is still beneficial to do so because of significant savings in computational cost.

Solving the reduced set of equations for the cases of uniform, isotropic, fully clamped and simply supported plates under uniformly distributed loads results in the transverse displacement fields shown by figs. 43 and 45. It is immediately obvious that the solution satisfies the geometric boundary conditions rather poorly in a point-wise sense. Plots showing the behavior of the central deflection for increasing p are given by figs. 44 and 46. While it may be said that the obtained solution is close to the expected value (obtained from 3-D finite elements for the clamped plate, Navier's solution for the simply supported plate), the convergence behavior is extremely erratic. For certain p, the solution obtained is often unacceptably far-removed from solutions of neighboring values of p and, in general, the overall quality of the solution is poor. It has been observed that small changes in, say, the values of the material constants cause large variations in these solutions obtained. This clearly indicates that, despite the

process mentioned above, the issue of ill-conditioning persists, albeit not identical in severity. As suggested previously, a stronger enforcement of the boundary conditions (i.e. , requiring the use of admissible functions) along with an h-refinement is expected to improve results. Indeed, the same set of equations have been solved successfully for a simply supported plate with solely an h-refinement by Sotoudeh [138].

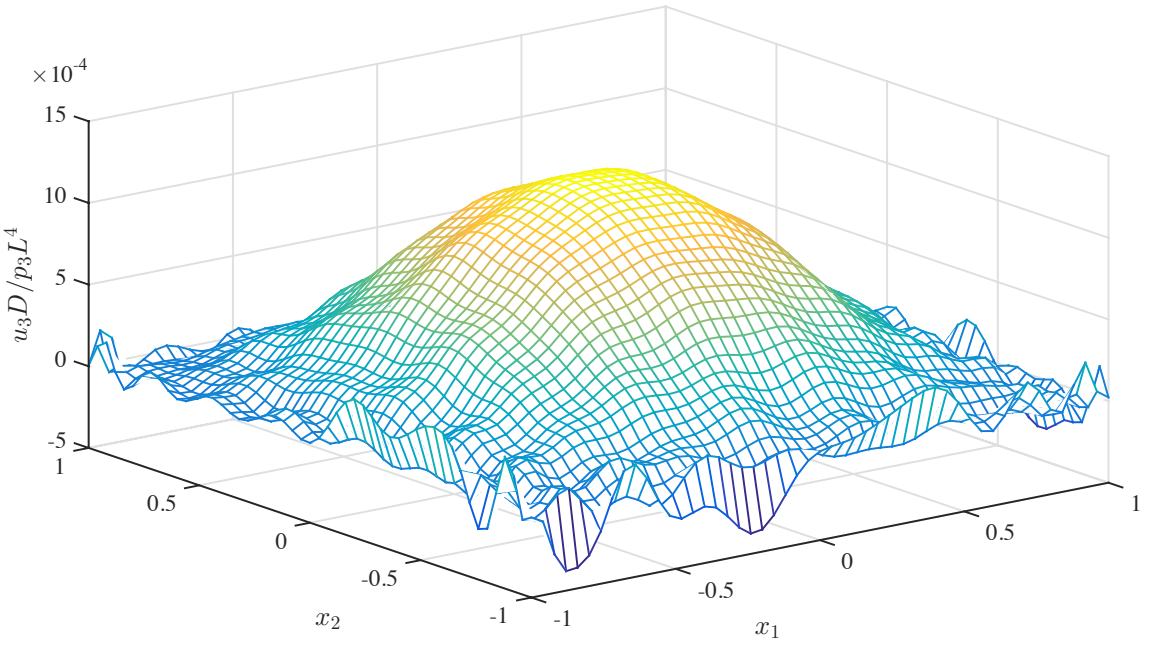

Figure 43: Static deflection of a fully clamped plate under uniform loading

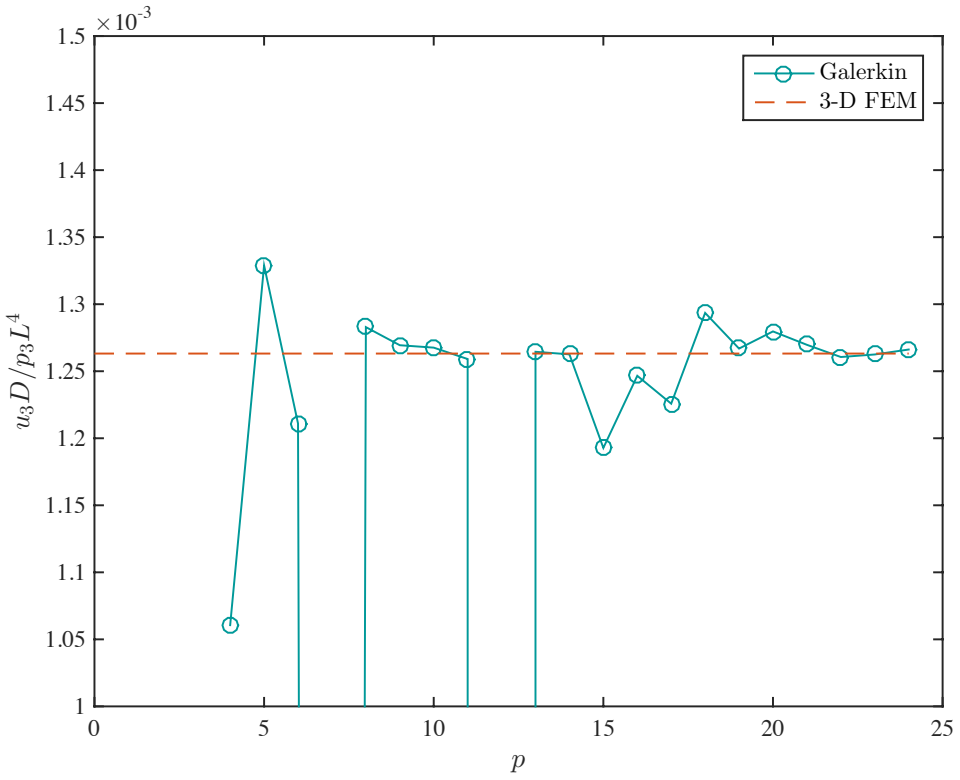

Figure 44: Convergence of transverse displacement at (0,0) for C-C-C-C plates: $\frac{u_3}{p_3L^4/D}$ vs. p

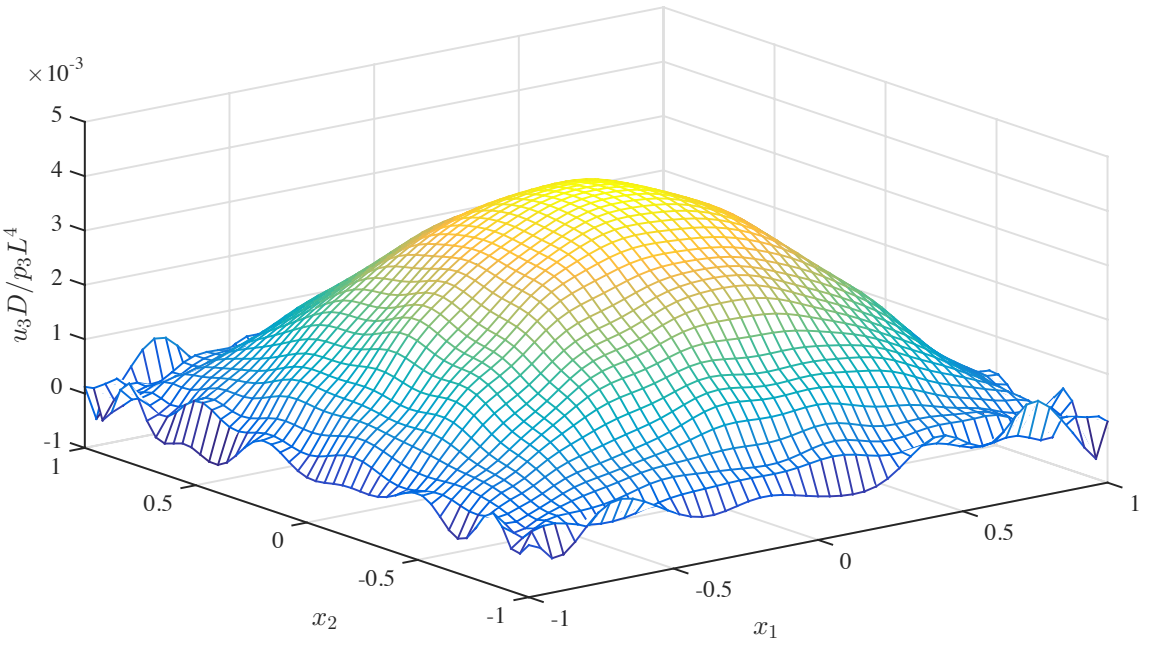

Figure 45: Static deflection of a simply supported plate under uniform loading

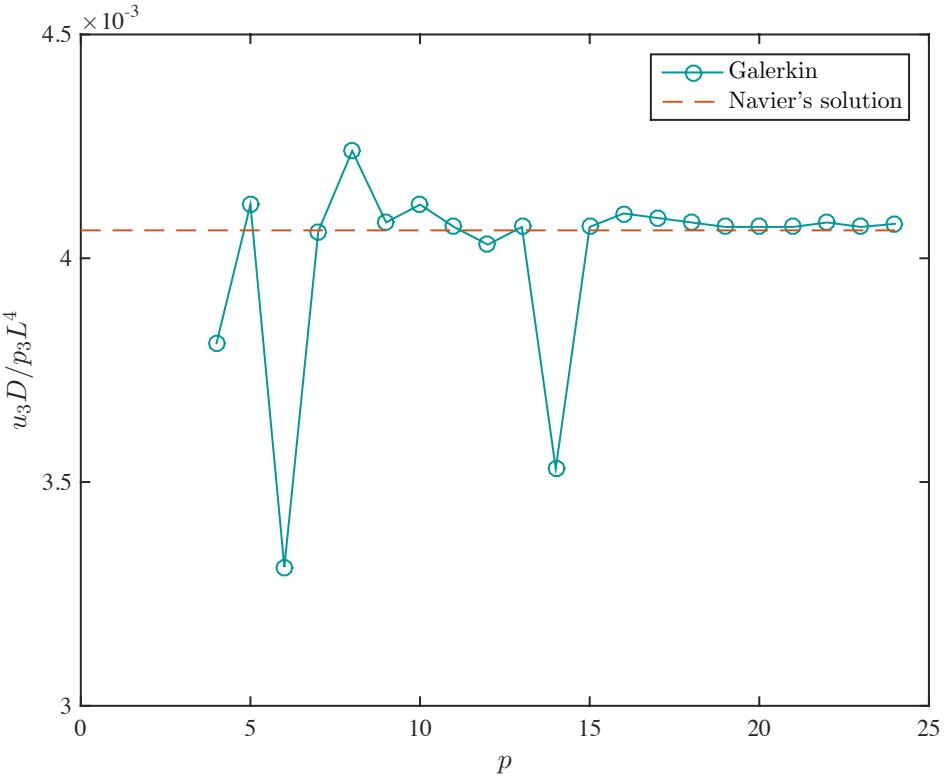

Figure 46: Convergence of transverse displacement at (0,0) for S-S-S-S plates: $\frac{u_3}{p_3 L^4/D}$ vs. p

CHAPTER VI

NONLINEAR ANALYSIS OF COSSERAT PLATES

As demonstrated in the previous chapter, a mixed formulation for linear statics worked well for certain boundary conditions but not for others. To be able to accommodate for a wider variety of boundary conditions, a method of modifying the solution procedure was presented that improved the results considerably. This modification, however, hinged on the fact that the generalized coordinates of the 2-D generalized strain measures could be simply expressed in terms of those for the displacements and rotations using eq. (86). Keeping this in mind, let us now discuss potential solution strategies for computing (a) a nonlinear static solution, and (b) a nonlinear steady-state solution. On paper, there are at least three ways of doing so. The advantages and drawbacks of each approach will now be discussed.

6.1 A Mixed Variational Formulation

The first approach is to simply use a mixed formulation as previously done in the linear case. This certainly has the advantage of being equipped to handle both static and dynamic problems well, and for all boundary conditions. In fact, a similar mixed formulation for the nonlinear analysis of beams was developed by Hodges [67] and successfully implemented by Yu and Blair [164] in the computer code GEBT. With the relevant derivation for a mixed variational statement for Cosserat plates is provided in appendix F, the variational statement representing the dynamics of a moving plate

is given by

$$\int_{\mathcal{S}} \Big\{ \overline{\delta q}_{,\alpha}^{T} N_\alpha + \overline{\delta q}^{T} \left[\dot{P} + \widetilde{\Omega} P - \widetilde{K}_\alpha N_\alpha - f \right] + \overline{\delta \psi}_{,\alpha}^{T} M_\alpha$$
$$+ \overline{\delta \psi}^{T} \left[\dot{H} + \widetilde{V} P + \widetilde{\Omega} H - \widetilde{K}_\alpha M_\alpha - (\widetilde{e}_\alpha + \widetilde{\gamma}_\alpha) N_\alpha - m \right] - \overline{\delta N}_{\alpha,\alpha}^{T} u$$
$$- \overline{\delta N}_{\alpha}^{T} \left[C^T (\gamma_\alpha + e_\alpha) - e_\alpha \right] - \overline{\delta M}_{\alpha,\alpha}^{T} \theta - \overline{\delta M}_{\alpha}^{T} \left(\Delta + \frac{1}{2}\widetilde{\theta} + \frac{1}{4}\theta\theta^T \right) K_\alpha \qquad (87)$$
$$- \overline{\delta P}^{T} \left[\dot{u} + v + \widetilde{\omega} u - C^T V \right] - \overline{\delta H}^{T} \left[\left(\Delta + \frac{1}{2}\widetilde{\theta} + \frac{1}{4}\theta\theta^T \right) (C\omega - \Omega) + \dot{\theta} \right] \Big\} \, \mathrm{d}s$$
$$= \int_{\Gamma} (\overline{\delta q}^{T} \hat{N} + \overline{\delta \psi}^{T} \hat{M} - \overline{\delta N_\alpha}^{T} u - \overline{\delta M_\alpha}^{T} \theta) \mathrm{d}\Gamma$$

where the direction cosine matrix C has been expressed in terms of Rodrigues parameters θ. For obtaining a steady-state solution, one simply sets the terms with time derivatives to zero. The fundamental unknowns of the mixed formulation are $u, \theta, N_\alpha, M_\alpha, P$ and H (24 variables). One can further specialize for the static case by simply setting P, H (and hence, V, Ω) to zero, leaving us with 18 variables.

This approach, while certainly viable, also comes with all the disadvantages traditionally associated with mixed or displacement based formulations - the presence of finite rotation variables gives rise to singularities and infinite-degree nonlinearities. On the other hand, fully intrinsic formulations, with the kinematics solely described by velocity and angular velocity variables, have a maximum degree of nonlinearity of two. Ideally, we would like to retain the advantages of a fully intrinsic formulation but also be able to deal with static equilibrium problems.

6.2 A Fully Intrinsic Formulation for Statics

For static problems, yet another approach that is possible is the one outlined by Hodges et al. [66]. Here, recognizing that the velocity and angular velocity measures are identically zero, we lose the 12 generalized strain-velocity equations since they are trivially satisfied. The remaining six equilibrium equations are now in terms of 12 variables and, owing to the statically indeterminate nature of plates, cannot be

solved. However, one can use the six strain compatibility equations and end up with a balanced set of 12 equations in 12 unknowns. For convenience, these equations are presented here again in matrix form

$$\begin{aligned} &N_{\alpha,\alpha} + \widetilde{K}_\alpha N_\alpha + f = 0 \\ &M_{\alpha,\alpha} + \widetilde{K}_\alpha M_\alpha + (\widetilde{e}_\alpha + \widetilde{\gamma}_\alpha) N_\alpha + m = 0 \\ &\gamma_{1,2} - \gamma_{2,1} - \widetilde{e_1} K_2 + \widetilde{e_2} K_1 = 0 \\ &K_{1,2} - K_{2,1} = 0 \end{aligned} \tag{88}$$

Despite the parity of equations and unknowns, there is now an issue with the specification of boundary conditions. While natural boundary conditions can be handled easily, those of the geometric type require a bit more thought. For example, as demonstrated by Sotoudeh [140], certain geometric boundary conditions can be expressed in terms of integrals of the strain measures. Besides, as was also observed in [140], finding a good initial guess for the Newton-Raphson procedure can be tricky. Later, a third and arguably superior way of solving for the nonlinear static equilibrium will be presented.

6.3 Nonlinear Steady-State Solution

The nonlinear algebraic equations resulting from applying Galerkin's method to the fully intrinsic formulation were derived in the previous chapter as given by eq. (81):

$$A_{ji}\dot{z}_i + B_{ji}z_i + C_{jik}z_j z_k + D_j = 0$$

One can observe that these equations are set up in the same way as those developed by Patil and Althoff [114] or Patil and Hodges [115] for beams. Given this set of equations, it was straightforward to solve the linear eigenvalue problem by simply ignoring the nonlinear terms. This, though, is equivalent to assuming that the steady-state about which the system was linearized is simply $\bar{z}_i = 0$. Except for cases where the external loading is absent and the plate is not in motion (such as a prescribed

rotation), this assumption that the free vibration analysis is unaffected by applied loading or prescribed motion is clearly invalid. Instead, the nonlinear steady-state solution has to be determined first, followed by a linearization of the system *about the steady-state*. One can expect this to be done by solving the following equations using a suitable iterative method.

$$B_{ji}\bar{z}_i + C_{jik}\bar{z}_j\bar{z}_k + \bar{D}_j = 0 \tag{89}$$

Moving plates are most amenable to be solved with the fully intrinsic nonlinear equations because of nonzero V and Ω distributions. Unlike static problems, this implies we now have the right number of equations and unknowns to solve for the nonlinear steady-state. To demonstrate, let us look at a very simple example.

6.3.1 Example: A Freely Spinning Plate

Consider a square (classical) isotropic plate of side L spinning about its center at a constant angular velocity ω_3. We wish to compute the steady-state deformation that the plate develops caused only by the spinning motion. There are no additional loads applied either on the surface or at the boundaries. A schematic of the plate is shown in fig. 47. For this problem, it is easy to see that the only nonzero variables are the in-plane generalized strains and velocities. The governing equations for this problem are

$$N_{11,1} + N_{21.2} - N_{12}K_{13} - N_{22}K_{23} = -\mu\Omega_3 V_2 \tag{90a}$$

$$N_{12,1} + N_{22.2} + N_{11}K_{13} + N_{21}K_{23} = \mu\Omega_3 V_1 \tag{90b}$$

$$M_{13,1} + M_{23,2} - N_{11}\epsilon_{12} + N_{12}(1+\epsilon_{11}) - N_{21}(1+\epsilon_{22}) + N_{22}\epsilon_{21} = 0 \tag{90c}$$

$$V_{1,1} + \Omega_3\epsilon_{12} = 0 \tag{91a}$$

$$V_{2,1} - \Omega_3(1+\epsilon_{11}) = 0 \tag{91b}$$

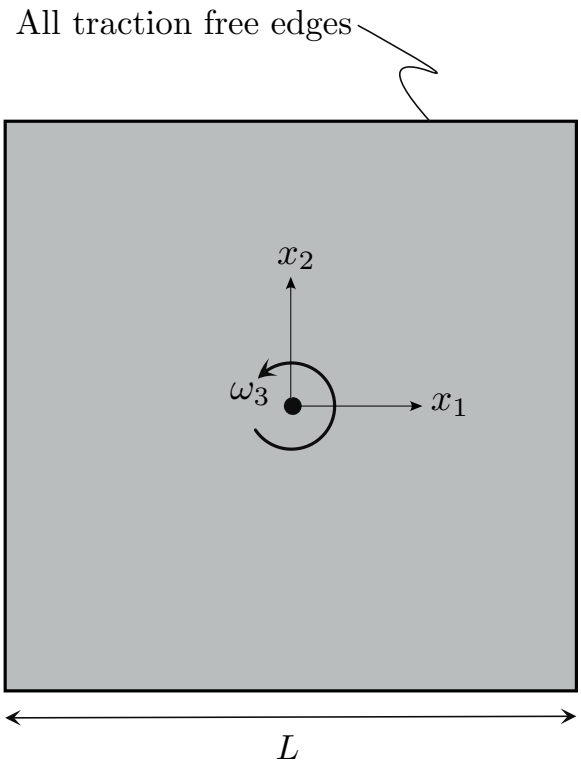

Figure 47: Schematic of free plate spinning at a constant angular velocity

$$V_{1,2} + \Omega_3(1 + \epsilon_{22}) = 0 \tag{91c}$$

$$V_{2,2} - \Omega_3\epsilon_{21} = 0 \tag{91d}$$

$$\Omega_{3,1} = 0 \tag{91e}$$

$$\Omega_{3,2} = 0 \tag{91f}$$

with the boundary conditions $\epsilon_{\alpha\beta} = 0$, $K_{\alpha 3} = 0$ on all four edges, and $\Omega_3 = \omega_3$ at the center.

First, we can immediately observe from eqs. (91e) and (91e) that $\Omega_3 = constant = \omega_3$. This greatly simplifies the solution procedure. Using this result in the eqs. (91a) to (91d) and then substituting into eqs. (B.3b) and (B.3c) in appendix B gives us $K_{13} = K_{23} = 0$. Using the standard constitutive law for the in-plane behavior of a classical elastic isotropic plate and noting that $\epsilon_{12} = \epsilon_{21}$, we can express eqs. (90a)

and (90b) as

$$\frac{Eh}{1-\nu^2}(\epsilon_{11,1}+\epsilon_{22,1}) = -\mu\omega_3 V2 \tag{92a}$$

$$\frac{Eh}{1-\nu^2}(\epsilon_{11,2}+\epsilon_{22,2}) = \mu\omega_3 V1 \tag{92b}$$

Differentiating eq. (92a) with respect to x_1, eq. (92b) with respect to x_2, adding the resulting equations and nondimensionalizing, we obtain

$$\nabla^2\varepsilon_s + \alpha^2\varepsilon_s = -\alpha^2 \tag{93}$$

where $\alpha^2 = \mu\omega_3^2 L^2(1-\nu^2)/Eh$. Here, we have taken advantage of the symmetry of the problem to set $\epsilon_{11} = \epsilon_{22} = \varepsilon_s$. Equation (93) resembles the two-dimensional Helmholtz equation. Indeed, many problems in physics related to steady-state oscillations lead to the Helmholtz equation. For a rectangular domain with prescribed boundary conditions, the solution of the above equation is well known (for example, see [16]) and can be expressed as an infinite series as

$$\varepsilon_s = \int_0^1\int_0^1 4\alpha^2 \sum_{n=1}^{\infty}\sum_{m=1}^{\infty} \frac{\sin(n\pi\bar{x}_1)\sin(m\pi\bar{x}_2)\sin(n\pi\xi)\sin(m\pi\eta)}{\pi^2(m^2+n^2)-\alpha^2}\mathrm{d}\xi\mathrm{d}\eta \tag{94}$$

After determining ϵ_{11} and ϵ_{22}, it is fairly straightforward to determine ϵ_{12}, V_1 and V_2 and is therefore not expounded here.

It is also worth noting that a linear analysis would have simply resulted in a trivial solution for the deformations while V_1, V_2 and Ω_3 would merely describe a rigid body rotation. It is the nonlinear terms in the generalized strain-velocity relations that provide the necessary coupling between the imposed motion and the deformations developed. By inspection of eq. (94), it can be seen that this depends on how large the magnitude of α, and hence, ω_3 can get. Notice that the denominator of α^2 has Eh, which is typically a very large value. Therefore, one must impart a very large angular velocity ω_3 to the plate to cause any noticeable deformation. Figure 48 shows the distribution of the non-dimensional velocity $\bar{V}_2(\equiv V_2/L\omega_3)$ at $x_2 = 0.5$ for all x_1.

In the case of a rigid plate, V_2 would vary linearly along x_1 going from -1/2 to 1/2. For lower (but more meaningful) values of α, this practically remains unchanged. For very large values of α, say of the order of unity, this changes to yield a significantly different velocity distribution. In fact, as can be seen from fig. 49, values of α just over unity start to violate the small strain assumption and the solution is likely to be incorrect anyway. To better illustrate the nature of the ϵ_{11} distribution, a value of $\alpha = 0.1$ has been picked to plot ϵ_{11} in fig. 50.

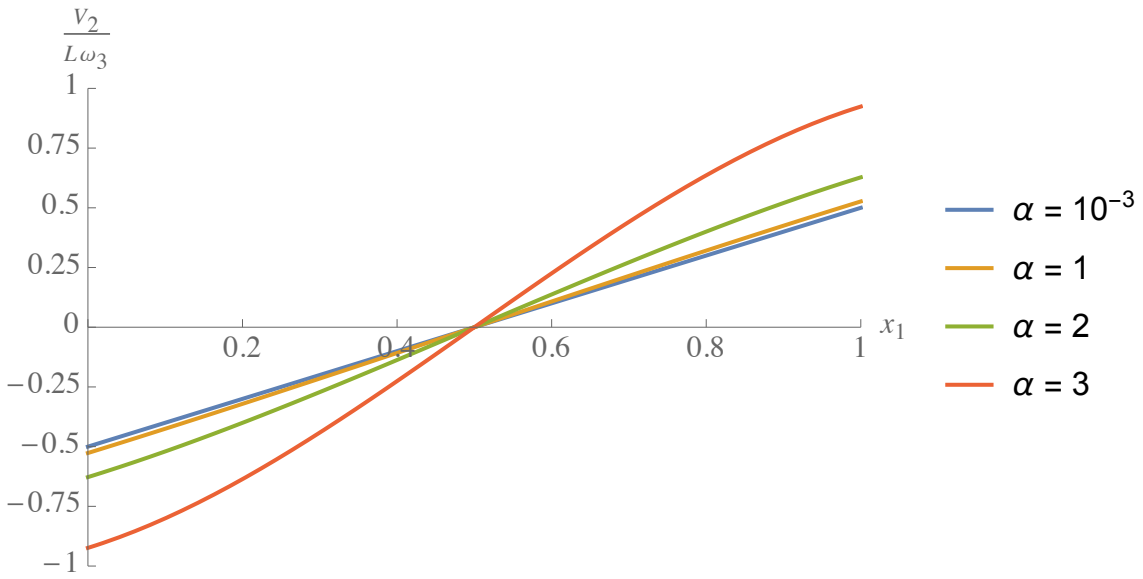

Figure 48: V_2 distribution along x_1, $x_2 = 0.5$ for $\alpha = 10^{-3}, 1, 2, 3$

This example is provided mainly to highlight the difference between dealing with static and moving plates using the fully intrinsic equations. To reiterate, while a static problem will not have the right balance between equations and unknowns, a moving plate problem can be solved due to nonzero V and Ω.

Finally, in the case of beams, Sotoudeh and Hodges [140] note that the fully intrinsic equations are easier to solve when at least one end is subjected to only natural boundary conditions, thereby giving at least one direct boundary condition in terms of forces and moments. Now, for plates, it has been found that a similar conclusion is applicable. So for example, plates with two edges clamped and two

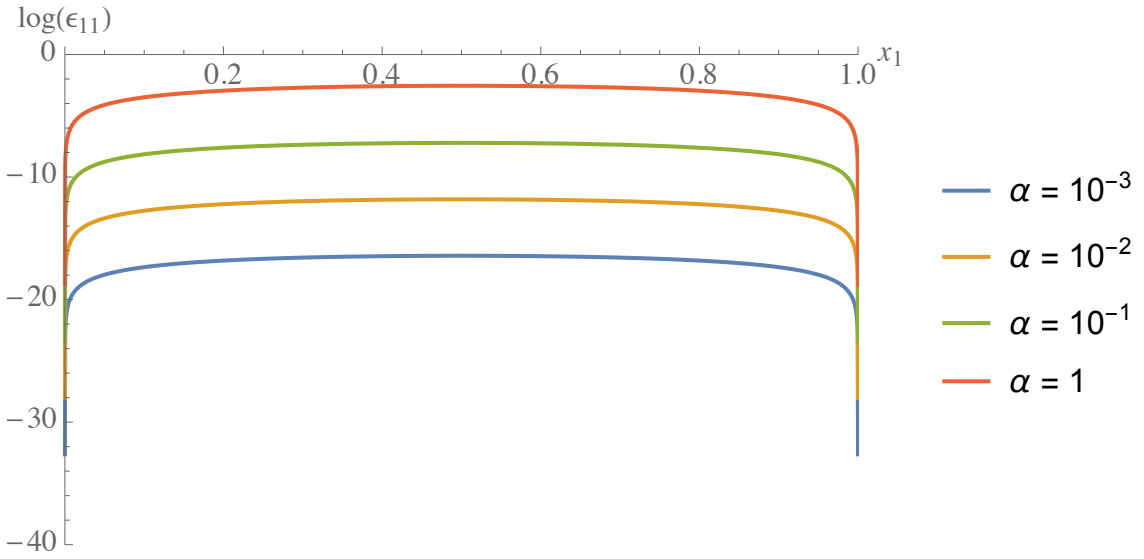

Figure 49: Log(ϵ_{11}) distribution along x_1, $x_2 = 0.5$ for $\alpha = 10^{-3}, 1, 2, 3$

edges free are easier to solve than, say, a plate with all edges clamped. Similar behavior has already been demonstrated while solving the linear static problem which, therefore, necessitated a workaround presented in section 5.5.3. Expectedly, this difficulty carries over to the nonlinear problem too, although it is easy to see that the same workaround cannot be applied because the generalized strain-velocity relations cannot be easily inverted to express the strain measures solely in terms of the velocity and angular velocity measures.

In fact, with a wide variety of boundary conditions, all efforts to apply a Newton-Raphson procedure to the complete set of fully intrinsic equations have been unfruitful in yielding a steady-state solution. So, while certain cases, such as the analytical example presented previously, work as expected, a large majority of problems seem unsuitable for analysis by this approach. On inspection of the Jacobian matrix needed to compute the solution iteratively, it may be safe to say that severe ill-conditioning is likely the culprit. This behavior has also observed in beam analyses using equations derived by Patil and Althoff [114], wherein only cantilever beams have been studied. However, application of the same equations to, say, a pinned-pinned beam with one

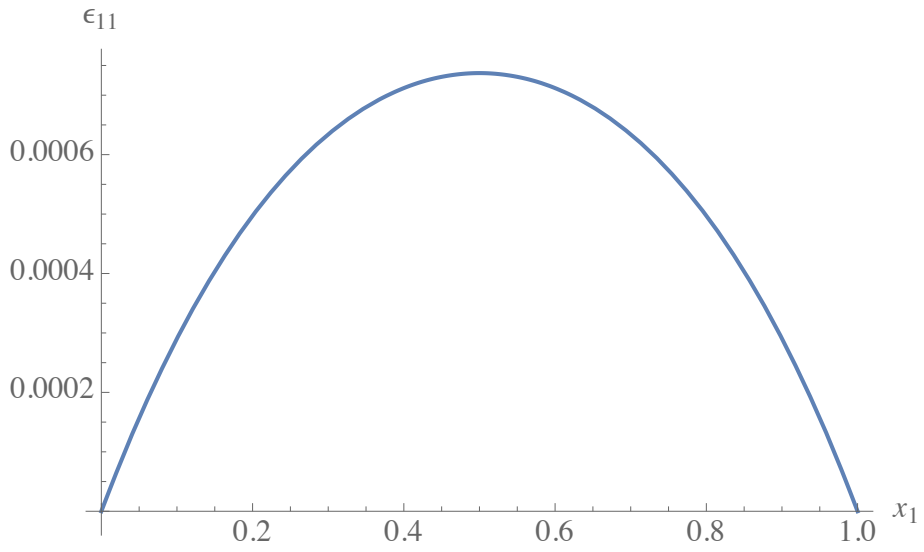

Figure 50: ϵ_{11} distribution along x_1, $x_2 = 0.5$ for $\alpha = 0.1$

moveable end (to avoid static indeterminacy) fails to compute the nonlinear steady-state solution whereas a linear eigenvalue analysis behaves as expected. It would be a worthwhile exercise to try and pin-point the exact reason for this behavior by examining the structure of the nonlinear algebraic equations for various boundary conditions.

6.4 Incremental Method for Nonlinear Plate Analysis

A way of circumventing similar problems that arise in the nonlinear analysis of statically indeterminate beams has been successfully developed by Sotoudeh and Hodges [139]. This approach, typically referred to as an incremental method, can be applied to plate analysis as well. The same method can be used to carry out either a nonlinear static analysis or to find the steady-state solution of a moving plate. For dynamic problems, once a steady-state solution has been found, the behavior of small motions about this state can be analyzed by a generalized eigenvalue problem.

The incremental method is based on applying loads in small increments and solving a linearized set of the fully intrinsic equations after each load increment. All time derivative terms are naturally set to zero. In addition to these equations, equations

that govern incremental displacements and rotations are also included which, because of the incremental nature of the quantities, are linear. Therefore, the disadvantage of a mixed method in introducing infinite-degree nonlinearities is not present here. Also, since only incremental rotations are used instead of a finite rotation tensor, no singularities are encountered. One has to remember that the incremental method is ultimately an approximate way of solving the nonlinear system of equations. However, with a suitable choice of loading increments, the method can yield excellent results. The derivation of the necessary equations is presented next.

Starting with the geometrically-exact intrinsic equations given by eq. (59) and setting all time derivatives to zero, they can be linearized as follows

$$\hat{N}_{\alpha,\alpha} + \tilde{\bar{K}}_\alpha \hat{N}_\alpha - \tilde{\bar{N}}_\alpha \hat{K}_\alpha + \hat{f} = \tilde{\bar{\Omega}}\hat{P} - \tilde{\bar{P}}\hat{\Omega} \tag{95a}$$

$$\hat{M}_{\alpha,\alpha} + \tilde{\bar{K}}_\alpha \hat{M}_\alpha - \widetilde{\bar{M}}_\alpha \hat{K}_\alpha + (\widetilde{\bar{e}_\alpha} + \widetilde{\bar{\gamma}_\alpha})\hat{N}_\alpha - \tilde{\bar{N}}_\alpha \hat{\gamma}_\alpha + \hat{m} = \tilde{\bar{\Omega}}\hat{H} - \tilde{\bar{H}}\hat{\Omega} + \tilde{\bar{V}}\hat{P} - \tilde{\bar{P}}\hat{V} \tag{95b}$$

Here, we have marked all quantities known from a previous loading step by $(\bar{})$ quantities and the unknowns at each step by the $(\hat{})$ quantities, the exceptions being $\hat{f}$ and $\hat{m}$, which are the incremental loads applied in the current step, and will be detailed momentarily. Since these quantities are all expressed in the $\mathbf{B}_i$ system, it is easy to update them after any given step as

$$\bar{X}_{new} = \bar{X}_{old} + \hat{X} \tag{96}$$

The generalized strain-velocity relations from eq. (56) can similarly be linearized as

$$\hat{V}_{,\alpha} + \tilde{\bar{K}}_\alpha \hat{V} - \tilde{\bar{V}}\hat{K}_\alpha + (e_\alpha + \bar{\gamma}_\alpha)\hat{\Omega} - \tilde{\bar{\Omega}}\hat{\gamma}_\alpha = 0 \tag{97a}$$

$$\hat{\Omega}_{,\alpha} + \tilde{\bar{K}}_\alpha \hat{\Omega} - \tilde{\bar{\Omega}}\hat{K}_\alpha = 0 \tag{97b}$$

In the incremental method, we also need to introduce incremental displacements and rotations, and derive equations relating them to increments in V, Ω, γ_α and K_α.

While a detailed derivation has been provided in appendix G, the necessary equations are simply listed here as

$$\hat{V} = \widetilde{\bar{\Omega}}\hat{q} + \widetilde{\bar{V}}\hat{\psi} \tag{98a}$$

$$\hat{\Omega} = \widetilde{\bar{\Omega}}\hat{\psi} \tag{98b}$$

$$\hat{\gamma}_\alpha = \hat{q}_{,\alpha} + \widetilde{\bar{K}}_\alpha\hat{q} + (\widetilde{e}_\alpha + \widetilde{\bar{\gamma}}_\alpha)\hat{\psi} \tag{98c}$$

$$\hat{K}_\alpha = \hat{\psi}_{,\alpha} + \widetilde{\bar{K}}_\alpha\hat{\psi} \tag{98d}$$

Applying the incremental method to a nonlinear static problem, one can simply use eqs. (95), (98c) and (98d) to solve for the equilibrium state. A nonlinear steady-state computation for moving plates requires the inclusion of $\hat{V}$ and $\hat{\Omega}$ that is easily done by using eqs. (98a) and (98b) to simply substitute for these variables in terms of $\hat{q}$ and $\hat{\psi}$ without increasing the size of the problem. Therefore, in both cases we have a system of 12 equations in 12 unknowns, while eq. (97a) is redundant.

6.4.1 Weighted–Integral Statement

To solve the static problem, consider the following weighting of eqs. (95), (98c) and (98d) on a domain given by fig. 20

$$\begin{aligned}
&\int_{-1}^{1}\int_{-1}^{1}\Big\{\hat{q}^T\Big[\hat{N}_{\alpha,\alpha} + \widetilde{\bar{K}}_\alpha\hat{N}_\alpha - \widetilde{\bar{N}}_\alpha\hat{K}_\alpha + \hat{f}\Big] + \hat{\psi}^T\Big[\hat{M}_{\alpha,\alpha} + \widetilde{\bar{K}}_\alpha\hat{M}_\alpha - \widetilde{\bar{M}}_\alpha\hat{K}_\alpha + (\widetilde{e}_\alpha + \widetilde{\bar{\gamma}}_\alpha)\hat{N}_\alpha \\
&\quad -\widetilde{\bar{N}}_\alpha\hat{\gamma}_\alpha + \hat{m}\Big] + \hat{N}_\alpha^T\Big[\hat{q}_{,\alpha} + \widetilde{\bar{K}}_\alpha\hat{q} + (\widetilde{e}_\alpha + \widetilde{\bar{\gamma}}_\alpha)\hat{\psi} - \hat{\gamma}_\alpha\Big] + \hat{M}_\alpha^T\Big[\hat{\psi}_{,\alpha} + \widetilde{\bar{K}}_\alpha\hat{\psi} - \hat{K}_\alpha\Big]\Big\}\mathrm{d}\xi\mathrm{d}\eta \\
&\quad +(1-\tau_1^{(f)})\int_{-1}^{1}\hat{N}_2^T\Big[\hat{q} - \hat{\mathfrak{q}}^{(1)}\Big]\mathrm{d}\xi\Big|_{\eta=-1} + (1-\tau_1^{(m)})\int_{-1}^{1}\hat{M}_2^T\Big[\hat{\psi} - \hat{\mathfrak{P}}^{(1)}\Big]\mathrm{d}\xi\Big|_{\eta=-1} \\
&\quad +\tau_1^{(f)}\int_{-1}^{1}\hat{q}^T\Big[\hat{N}_2 - \hat{\mathbb{N}}_2^{(1)}\Big]\mathrm{d}\xi\Big|_{\eta=-1} + \tau_1^{(m)}\int_{-1}^{1}\hat{\psi}^T\Big[\hat{M}_2 - \hat{\mathbb{M}}_2^{(1)}\Big]\mathrm{d}\xi\Big|_{\eta=-1} \\
&\quad -(1-\tau_2^{(f)})\int_{-1}^{1}\hat{N}_1^T\Big[\hat{q} - \hat{\mathfrak{q}}^{(2)}\Big]\mathrm{d}\eta\Big|_{\xi=1} - (1-\tau_2^{(m)})\int_{-1}^{1}\hat{M}_1^T\Big[\hat{\psi} - \hat{\mathfrak{P}}^{(2)}\Big]\mathrm{d}\eta\Big|_{\xi=1}
\end{aligned}$$

$$
\begin{aligned}
&-\tau_2^{(f)} \int_{-1}^{1} \hat{q}^T \left[\hat{N}_1 - \hat{\mathbb{N}}_1^{(2)}\right] \mathrm{d}\eta \Big|_{\xi=1} - \tau_2^{(m)} \int_{-1}^{1} \hat{\psi}^T \left[\hat{M}_1 - \hat{\mathbb{M}}_1^{(2)}\right] \mathrm{d}\eta \Big|_{\xi=1} \\
&-(1-\tau_3^{(f)}) \int_{-1}^{1} \hat{N}_2^T \left[\hat{q} - \hat{\mathfrak{q}}^{(3)}\right] \mathrm{d}\xi \Big|_{\eta=1} - (1-\tau_3^{(m)}) \int_{-1}^{1} \hat{M}_2^T \left[\hat{\psi} - \hat{\mathfrak{Y}}^{(3)}\right] \mathrm{d}\xi \Big|_{\eta=1} \\
&-\tau_3^{(f)} \int_{-1}^{1} \hat{q}^T \left[\hat{N}_2 - \hat{\mathbb{N}}_2^{(3)}\right] \mathrm{d}\xi \Big|_{\eta=1} - \tau_3^{(m)} \int_{-1}^{1} \hat{\psi}^T \left[\hat{M}_2 - \hat{\mathbb{M}}_2^{(3)}\right] \mathrm{d}\xi \Big|_{\eta=1} \\
&+(1-\tau_4^{(f)}) \int_{-1}^{1} \hat{N}_1^T \left[\hat{q} - \hat{\mathfrak{q}}^{(4)}\right] \mathrm{d}\eta \Big|_{\xi=-1} + (1-\tau_4^{(m)}) \int_{-1}^{1} \hat{M}_1^T \left[\hat{\psi} - \hat{\mathfrak{Y}}^{(4)}\right] \mathrm{d}\eta \Big|_{\xi=-1} \\
&+\tau_4^{(f)} \int_{-1}^{1} \hat{q}^T \left[\hat{N}_1 - \hat{\mathbb{N}}_1^{(4)}\right] \mathrm{d}\eta \Big|_{\xi=-1} + \tau_4^{(m)} \int_{-1}^{1} \hat{\psi}^T \left[\hat{M}_1 - \hat{\mathbb{M}}_1^{(4)}\right] \mathrm{d}\eta \Big|_{\xi=-1} = 0
\end{aligned} \tag{99}
$$

where $\hat{\mathfrak{q}}^{(i)}, \hat{\mathfrak{Y}}^{(i)}, \hat{\mathbb{N}}_1^{(i)}, \hat{\mathbb{M}}_1^{(i)} (i = 2, 4)$ are possible prescribled boundary conditions on edges 2 and 4, $\hat{\mathfrak{q}}^{(i)}, \hat{\mathfrak{Y}}^{(i)}, \hat{\mathbb{N}}_2^{(i)}, \hat{\mathbb{M}}_2^{(i)} (i = 1, 3)$ are possible prescribed boundary conditions on edges 1 and 3, and $\tau_i^{(f)}, \tau_i^{(m)}$ are 3×1 column matrices of flags (zero or one) denoting a prescription of of either geometric or natural boundary conditions, respectively.

Before we proceed, it is worthwhile to note this weighting of the equations is not energy-consistent, in that an integration by parts will not yield an energy balance equation as before due to the approximate nature of these linearized equations.

The incremental displacements and rotations are not updated as per eq. (96), but can instead be updated as

$$\bar{q}_{new} = \bar{q}_{old} + C^T \hat{q} \tag{100a}$$

$$\bar{C}_{new} = (\Delta - \widetilde{\hat{\psi}}) \bar{C}_{old} \tag{100b}$$

Since the final values of the displacements and direction cosine matrix may be computed from the generalized strains using eq. (22), it is not essential to keep track of either $\hat{q}$ or $\hat{\psi}$ after every load step and update q and C. However, doing so may prove useful in checking the accuracy of the solution obtained at every step - for instance, one may check the deviation of C from being a perfectly orthogonal matrix.

Also, it is worth making an important observation regarding the weighted-integral statement above. If one looks at only the linear terms, then the equations look exactly like eqs. (85a) to (85f) written for linear statics. This also means that, left unchanged, the problems of ill-conditioning encountered with certain boundary condition types will carry over here as well. To avoid this, it is recommended to shift entirely to using only the six incremental displacement and rotation variables. While this would not have been possible if one were dealing with the original nonlinear generalized strain-velocity relations, it can be done easily here in their incremental form.

Applying a Galerkin approximation to eqs. (98c) and (98d) along with the appropriate geometric boundary conditions, one can obtain the following equations expressed in terms of generalized coordinates:

$$\begin{aligned}&\mathcal{A}^{ji}\hat{\gamma}_1^i - \left[\mathcal{B}_1^{ji} - (1-\tau_2^f)\mathcal{E}_2^{ji} + (1-\tau_4^f)\mathcal{E}_4^{ji}\right]\hat{q}^i - \mathcal{C}^{jik}\widetilde{\bar{k}_1}^k\hat{q}^i - \mathcal{A}^{ji}\widetilde{e}_1\hat{\psi}^i \\ &- \mathcal{C}^{jik}\widetilde{\bar{\gamma}_1}^k\hat{\psi}^i = (1-\tau_2^{(f)})\int_{-1}^{1}\Phi^j\hat{\mathfrak{q}}^{(2)}\mathrm{d}\eta\Big|_{\xi=1} - (1-\tau_4^{(f)})\int_{-1}^{1}\Phi^j\hat{\mathfrak{q}}^{(4)}\mathrm{d}\eta\Big|_{\xi=-1}\end{aligned} \tag{101}$$

$$\begin{aligned}&\mathcal{A}^{ji}\hat{\gamma}_2^i - \left[\mathcal{B}_2^{ji} + (1-\tau_1^f)\mathcal{E}_1^{ji} - (1-\tau_3^f)\mathcal{E}_3^{ji}\right]\hat{q}^i - \mathcal{C}^{jik}\widetilde{\bar{k}_2}^k\hat{q}^i - \mathcal{A}^{ji}\widetilde{e}_2\hat{\psi}^i \\ &- \mathcal{C}^{jik}\widetilde{\bar{\gamma}_2}^k\hat{\psi}^i = -(1-\tau_1^{(f)})\int_{-1}^{1}\Phi^j\hat{\mathfrak{q}}^{(1)}\mathrm{d}\xi\Big|_{\eta=-1} + (1-\tau_3^{(f)})\int_{-1}^{1}\Phi^j\hat{\mathfrak{q}}^{(3)}\mathrm{d}\xi\Big|_{\eta=1}\end{aligned} \tag{102}$$

$$\begin{aligned}&\mathcal{A}^{ji}\hat{k}_1^i - \left[\mathcal{B}_1^{ji} - (1-\tau_2^m)\mathcal{E}_2^{ji} + (1-\tau_4^m)\mathcal{E}_4^{ji}\right]\hat{\psi}^i - \mathcal{C}^{jik}\widetilde{\bar{k}_1}^k\hat{\psi}^i \\ &= (1-\tau_2^{(m)})\int_{-1}^{1}\Phi^j\hat{\mathfrak{y}}^{(2)}\mathrm{d}\eta\Big|_{\xi=1} - (1-\tau_4^{(m)})\int_{-1}^{1}\Phi^j\hat{\mathfrak{y}}^{(4)}\mathrm{d}\eta\Big|_{\xi=-1}\end{aligned} \tag{103}$$

$$\begin{aligned}&\mathcal{A}^{ji}\hat{k}_2^i - \left[\mathcal{B}_2^{ji} + (1-\tau_1^m)\mathcal{E}_1^{ji} - (1-\tau_3^m)\mathcal{E}_3^{ji}\right]\hat{\psi}^i - \mathcal{C}^{jik}\widetilde{\bar{k}_2}^k\hat{\psi}^i \\ &= -(1-\tau_1^{(m)})\int_{-1}^{1}\Phi^j\hat{\mathfrak{y}}^{(1)}\mathrm{d}\xi\Big|_{\eta=-1} + (1-\tau_3^{(m)})\int_{-1}^{1}\Phi^j\hat{\mathfrak{y}}^{(3)}\mathrm{d}\xi\Big|_{\eta=1}\end{aligned} \tag{104}$$

where $\mathcal{A}, \mathcal{B}_1, \mathcal{B}_2, \mathcal{E}_1 \ldots \mathcal{E}_4$ are integrals of shape functions as defined in eq. (76).

These equations, linear in the unknowns, can now be easily inverted to yield

$$\hat{\gamma}_1^i = (\mathcal{A}^{ij})^{-1}\left[\mathcal{B}_1^{jk} - (1-\tau_2^f)\mathcal{E}_2^{jk} + (1-\tau_4^f)\mathcal{E}_4^{jk}\right]\hat{q}^k + (\mathcal{A}^{ji})^{-1}\mathcal{C}^{jik}\widetilde{\bar{k}_1}^k\hat{q}^i + \widetilde{e_1}\hat{\psi}^k$$
$$+ (\mathcal{A}^{ij})^{-1}\mathcal{C}^{jlk}\widetilde{\bar{\gamma}_1}^k\hat{\psi}^l + (\mathcal{A}^{ij})^{-1}\left[(1-\tau_2^{(f)})\int_{-1}^{1}\Phi^j\hat{\mathfrak{q}}^{(2)}\mathrm{d}\eta\Big|_{\xi=1} - (1-\tau_4^{(f)})\int_{-1}^{1}\Phi^j\hat{\mathfrak{q}}^{(4)}\mathrm{d}\eta\Big|_{\xi=-1}\right] \tag{105}$$

$$\hat{\gamma}_2^i = (\mathcal{A}^{ij})^{-1}\left[\mathcal{B}_2^{jk} + (1-\tau_1^f)\mathcal{E}_1^{jk} - (1-\tau_3^f)\mathcal{E}_3^{jk}\right]\hat{q}^k + (\mathcal{A}^{ij})^{-1}\mathcal{C}^{jlk}\widetilde{\bar{k}_2}^k\hat{q}^l + \widetilde{e_2}\hat{\psi}^k$$
$$+ (\mathcal{A}^{ij})^{-1}\mathcal{C}^{jlk}\widetilde{\bar{\gamma}_2}^k\hat{\psi}^l + (\mathcal{A}^{ij})^{-1}\left[-(1-\tau_1^{(f)})\int_{-1}^{1}\Phi^j\hat{\mathfrak{q}}^{(1)}\mathrm{d}\xi\Big|_{\eta=-1} + (1-\tau_3^{(f)})\int_{-1}^{1}\Phi^j\hat{\mathfrak{q}}^{(3)}\mathrm{d}\xi\Big|_{\eta=1}\right] \tag{106}$$

$$\hat{k}_1^i = (\mathcal{A}^{ij})^{-1}\left[\mathcal{B}_1^{jk} - (1-\tau_2^m)\mathcal{E}_2^{jk} + (1-\tau_4^m)\mathcal{E}_4^{jk}\right]\hat{\psi}^k + (\mathcal{A}^{ij})^{-1}\mathcal{C}^{jlk}\widetilde{\bar{k}_1}^k\hat{\psi}^l$$
$$+(\mathcal{A}^{ij})^{-1}\left[(1-\tau_2^{(m)})\int_{-1}^{1}\Phi^j\hat{\Psi}^{(2)}\mathrm{d}\eta\Big|_{\xi=1} - (1-\tau_4^{(m)})\int_{-1}^{1}\Phi^j\hat{\Psi}^{(4)}\mathrm{d}\eta\Big|_{\xi=-1}\right] \tag{107}$$

$$\hat{k}_2^i = (\mathcal{A}^{ij})^{-1}\left[\mathcal{B}_2^{jk} + (1-\tau_1^m)\mathcal{E}_1^{jk} - (1-\tau_3^m)\mathcal{E}_3^{jk}\right]\hat{\psi}^k + (\mathcal{A}^{ij})^{-1}\mathcal{C}^{jlk}\widetilde{\bar{k}_2}^k\hat{\psi}^l$$
$$+(\mathcal{A}^{ij})^{-1}\left[-(1-\tau_1^{(m)})\int_{-1}^{1}\Phi^j\hat{\Psi}^{(1)}\mathrm{d}\xi\Big|_{\eta=-1} + (1-\tau_3^{(m)})\int_{-1}^{1}\Phi^j\hat{\Psi}^{(3)}\mathrm{d}\xi\Big|_{\eta=1}\right] \tag{108}$$

The remaining Galerkin equations are given by

$$\left[\mathcal{B}_1^{ji} - \tau_2^f\mathcal{E}_2^{ji} + \tau_4^f\mathcal{E}_4^{ji}\right]\hat{n}_1^i + \left[\mathcal{B}_2^{ji} + \tau_1^f\mathcal{E}_1^{ji} - \tau_3^f\mathcal{E}_3^{ji}\right]\hat{n}_2^i + \mathcal{C}^{jik}\widetilde{\bar{k}_\alpha}^k\hat{n}_\alpha^i - \mathcal{C}^{jik}\widetilde{\bar{n}_\alpha}^k\hat{k}_\alpha^i$$
$$= -\int_{-1}^{1}\int_{-1}^{1}\Phi^j\hat{f}\mathrm{d}\xi\mathrm{d}\eta - \tau_2^{(f)}\int_{-1}^{1}\Phi^j\hat{\mathbb{N}}_1^{(2)}\mathrm{d}\eta\Big|_{\xi=1} + \tau_4^{(f)}\int_{-1}^{1}\Phi^j\hat{\mathbb{N}}_1^{(4)}\mathrm{d}\eta\Big|_{\xi=-1} \tag{109}$$
$$+ \tau_1^{(f)}\int_{-1}^{1}\Phi^j\hat{\mathbb{N}}_2^{(1)}\mathrm{d}\xi\Big|_{\eta=-1} - \tau_3^{(f)}\int_{-1}^{1}\Phi^j\hat{\mathbb{N}}_2^{(3)}\mathrm{d}\xi\Big|_{\eta=1}$$

$$
\begin{aligned}
&\left[\mathcal{B}_1^{ji} - \tau_2^m \mathcal{E}_2^{ji} + \tau_4^m \mathcal{E}_4^{ji}\right] \hat{m}_1^i + \left[\mathcal{B}_2^{ji} + \tau_1^m \mathcal{E}_1^{ji} - \tau_3^m \mathcal{E}_3^{ji}\right] \hat{m}_2^i + \mathcal{C}^{jik} \widetilde{\bar{k}_\alpha}^k \hat{m}_\alpha^i \\
&- \mathcal{C}^{jik} \widetilde{\bar{m}_\alpha}^k \hat{k}_\alpha^i + \mathcal{C}^{jik} \widetilde{\bar{\gamma}_\alpha}^k \hat{n}_\alpha^i - \mathcal{C}^{jik} \widetilde{\bar{n}_\alpha}^k \hat{\gamma}_\alpha^i + \mathcal{A}^{ji} \widetilde{e}_\alpha \hat{n}_\alpha^i = -\int_{-1}^{1}\int_{-1}^{1} \Phi^j \hat{m} \mathrm{d}\xi \mathrm{d}\eta \\
&- \tau_2^{(m)} \int_{-1}^{1} \Phi^j \hat{\mathbb{M}}_1^{(2)} \mathrm{d}\eta \Big|_{\xi=1} + \tau_4^{(m)} \int_{-1}^{1} \Phi^j \hat{\mathbb{M}}_1^{(4)} \mathrm{d}\eta \Big|_{\xi=-1} + \tau_1^{(m)} \int_{-1}^{1} \Phi^j \hat{\mathbb{M}}_2^{(1)} \mathrm{d}\xi \Big|_{\eta=-1} \\
&- \tau_3^{(m)} \int_{-1}^{1} \Phi^j \hat{\mathbb{M}}_2^{(3)} \mathrm{d}\xi \Big|_{\eta=1}
\end{aligned}
\tag{110}
$$

The generalized coordinates of the stress resultants can be expressed in terms of those of the strain measures via the plate stiffness matrix, as

$$\hat{n}_\alpha^i = \mathbb{A}_{\alpha\beta} \hat{\gamma}_\beta^i + \mathbb{B}_{\alpha\beta} \hat{k}_\beta^i \tag{111a}$$

$$\hat{m}_\alpha^i = \mathbb{B}_{\beta\alpha} \hat{\gamma}_\beta^i + \mathbb{D}_{\alpha\beta} \hat{k}_\beta^i \tag{111b}$$

Therefore, using eqs. (105) to (108) along with eqs. (111) to substitute for $\hat{n}_\alpha^i, \hat{m}_\alpha^i, \hat{\gamma}_\alpha^i, \hat{k}_\alpha^i$ in terms of $\hat{q}^i, \hat{\psi}^i$ into eqs. (109) and (110) gives us the final system of linear algebraic equations to be solved at every load step. Owing to the lengthy nature of the resulting equations, these are not explicitly written out. Finally, this development can be complete with a discussion on how to express increments in the applied distributed loads.

6.4.2 Modeling Distributed Loads

In the preceding development, very little was said about the expressions for increments in the applied distributed loads, $\hat{f}$ and $\hat{m}$. Conceptually, while they can be thought of as being a fraction of the total loads f, m applied at a given loading step, their exact expression depends on the behavior of the applied loads *during* the loading process. Here, a treatment will be provided for two cases - loads that "follow" the deformation, or *follower* loads, and loads that do not change in magnitude or direction during the loading process, or *dead* loads.

Modeling follower loads is extremely straightforward in the present formulation since f_i, m_i are already expressed in the $\mathbf{B}_i$ basis associated with the deformed plate reference surface. For example, consider a constant distributed force $p_i\mathbf{B}_i$ acting on the plate. We have

$$f_i(x_1, x_2) = (p_j\mathbf{B}_j) \cdot \mathbf{B}_i = p_i$$

Therefore, the incremental applied force is simply

$$\hat{f} = \hat{p} \tag{112}$$

where $\hat{p}$ are incremental values of the load in each step.

In the case of dead loads, one has to take into account the change in orientation of the $\mathbf{B}_i$ basis relative to the inertial basis in which the applied forces are specified. Considering a similar constant distributed force of $p_i\mathbf{i}_i$ on the plate, we have

$$\begin{aligned} f_i(x_1, x_2) &= (p_j\mathbf{i}_j) \cdot \mathbf{B}_i = C_{ij}p_j \\ \Rightarrow f &= Cp \end{aligned} \tag{113}$$

where the matrix of direction cosines is now necessary to correctly determine f_i. For this case, $\hat{f}$ can be found as

$$\begin{aligned} \bar{f} &= \bar{C}\bar{p} \\ \text{and } \bar{f} + \hat{f} &= Cp = (\Delta - \widetilde{\hat{\psi}})\bar{C}(\bar{p} + \hat{p}) \\ \Rightarrow \hat{f} &= \bar{C}\hat{p} - \widetilde{\hat{\psi}}\bar{C}\bar{p} = \bar{C}\hat{p} + \widetilde{\bar{f}}\hat{\psi} \end{aligned} \tag{114}$$

The first term, $\bar{C}\hat{p}$, is the inhomogeneous part with $\hat{p}$ being the incremental value at every step while the second, $\widetilde{\bar{f}}\hat{\psi}$, is a homogeneous term.

CHAPTER VII

CONCLUSIONS AND FUTURE WORK

7.1 Conclusions

The objective of the dissertation was to derive a nonlinear theory of Cosserat elastic plates using the VAM. Any plate theory requires the following sets of equations: kinematic relations, constitutive laws, compatibility equations and the equilibrium equations/equations of motion. A systematic derivation of each of these is presented. Using the VAM, the original three-dimensional problem was rigorously split into a through-the-thickness analysis that is asymptotically correct and a two-dimensional plate analysis that is geometrically-exact.

The zeroth-order approximation in the through-the-thickness analysis provided a two-dimensional constitutive law that matched well with published results, although no assumptions regarding the through-thickness variation of the displacements and stresses. Additionally, the analysis also provides a means to recover the 3-D stress, strain and displacement fields from plate variables. A second-order approximation of the total energy is then found using an energy transformation, which augments the previously determined constitutive law with the shear stiffness and the drilling stiffness. The additional drilling degree of freedom comes from the appearance of the in-plane curvature terms $K_{\alpha 3}$ in the strain energy of a micropolar plate. To the best of the authors' knowledge, this is the first time the drilling stiffness, interpreted as relating the internal drilling moments to the in-plane curvatures of a plate, has been determined in a mathematically rigorous manner. Several comparisons are made with expressions found in the literature for the drilling stiffness, highlighting potential errors in using such simplified forms.

Next, a fully intrinsic theory of Cosserat elastic plates is derived from Hamilton's extended principle. Since the rotation about the plate normal can be considered as independent, this results in six nonlinear equations of motion for the dynamics of a moving plate. In contrast to a Reissner-Mindlin-type theory, the moment equilibrium about the normal is not satisfied implicitly and is instead given in terms of the internal drilling moments. A systematic way of obtaining a Reissner-Mindlin theory from the more general Cosserat plate theory is also presented, delivering a unified implementation of a theory of plates with or without observable Cosserat effects.

This work also presents a Galerkin approach for solving the fully intrinsic equations of Cosserat plates. It is also shown that the weighted-integral statement is energy preserving. For linear free vibration problems, it was shown to yield very accurate results in comparison with 3-D finite element results. Next, a mixed-method for linear statics was presented and analyzed using a Galerkin method. It was found that the current approach gave excellent results provided there was at least one boundary condition each in terms of all the unknowns. This meant that cantilever plates fared well while fully clamped or simply supported plates gave extremely unsatisfactory results due to ill-conditioning. A method to restructure the Galerkin equations and eliminate a set of unknowns in favor of the rest was shown to improve results considerably, although not as accurate as a finite-element implementation with strong enforcement of boundary conditions.

Finally, methods to tackle nonlinear static and dynamic problems are discussed in the context of plates (both classical and Cosserat). It was shown with the help of an example that the fully intrinsic equations are ideally suited to solve problems involving moving plates. To avoid dealing with infinite degree nonlinearities associated with finite rotation tensors in a mixed method, but have the well-posedness of such a formulation, an incremental method was developed that is suitable for both moving and stationary plates. The method involves successive solving sets of linear algebraic

equations, thereby avoiding solution of sets of nonlinear algebraic equations using an iterative procedure, which was said to not work as expected for hyperstatic structures. Although inherently approximate, the incremental method is known to provide very good results in beam analyses and is expected to perform similarly for plates.

7.2 Future Work

The present work can be considered as providing the initial, yet crucial, developments towards the formulation of a unified theory of two-dimensional plate structures. It does, however, leave a lot of scope for further research and development.

- *Extensive validation of plate modeling.* As of today, there is an avalanche of work being done on the theoretical side of Cosserat plate modeling. However, there are only a precious few sources of dependable experimental data materials modeled as micropolar elastic. Over time, with further availability of test data, a more rigorous testing of the plate modeling effort needs to be done including anisotropic micropolar materials.

- *Computational determination of micropolar constants.* One of the challenges concerning the accurate determination of the additional length-scale dependent elastic constants by way of experiment is the extremely precise measurement techniques required. This is the reason why higher-order elasticity was dismissed in the 1960s ([134, 35]) as being insignificant or inadequate. However, with improved measurement techniques in the mid 1980s and after, interest in higher-order elasticity theories was rekindled and reliable, repeatable data started to appear. As just mentioned however, there is still far less data available than one might like. Recently, an alternate way of determining these elastic constants by computational techniques has gained traction. For instance, there has been a lot of interest in modeling single layer graphene sheets and carbon nanotubes as equivalent micropolar continua at the macro scale with the help of atomistic

simulations. Some notable examples include the works by Odegard et al. [108], Lu et al. [97], Scarpa et al. [130], Kumar et al. [85] and, recently, Selmi et al. [135]. Although explored only in concept, a micromechanics approach, such as the one presented by Yu and Tang [169], might also prove useful integrating the VAM to length-scale dependent behavior.

- *Implementation of variable-order finite elements.* Galerkin's method and the associated p-refinement provide a very desirable exponential rate of convergence as opposed to an h-refinement. However, the cases we have looked at were uniform plates subjected to uniform loading. If one wishes to solve plate problems that are (a) not rectangular in geometry but arbitrarily shaped, (b) subject to discontinuous loading and/or boundary conditions, it is computationally less expensive to have multiple elements rather than use an extraordinarily high polynomial degree to accurately capture sharp transitions. This extension from the Galerkin method is fairly straightforward, and is made easy with the present choice of hierarchical bubble functions.

- *Validation of the incremental method.* The incremental method developed in section 6.4 requires a thorough validation for both nonlinear static and dynamic problems. The implementation is no more complicated than that of the linear analysis presented earlier, with the addition of having to repeat the process over multiple loading steps. Using an h-method, this approach to solving nonlinear beam problems has been validated by Sotoudeh and Hodges [139]. Specifically, care has to be taken to ensure solution consistency after every load step, such as verifying the orthogonality of the direction cosine matrix. Additionally, an exploration into the development of a corrector method, to work in tandem with the predictor step, might be beneficial in reducing the number of load steps required or ensure convergence to the correct solution. It is worth

noting that the incremental method, in the form presented here, does not have a mathematical proof that guarantees convergence.

- *Extension to shell modeling.* While plenty of two-dimensional structures can be modeled as plate structures, it is certainly restrictive to require a zero initial curvature. An important step in the generalization of the current methodology is to extend the analysis to Cosserat elastic shells. This is viewed as being fundamentally similar to the generalization of a theory of classical elastic plates to classical elastic shells, which, in and of itself, is fairly involved, requiring a careful consideration of the orders of all the additional terms introduced in the asymptotic analysis. After the development of such a theory of shells, it is recommended to solve the resulting equations with variable-order finite elements instead of exclusively a p-refinement. Depending on the shell geometry, having a single element over the entire geometry might cause difficulties when using Galerkin method without no h-refinement. This is especially likely for shells whose curvatures are much smaller than their wavelengths of deformation, such as a half tube, where the local normal changes orientation significantly along the shell surface, making higher degree polynomial interpolations of variables ineffective in improving results.

- *Examples demonstrating the advantages of Cosserat elasticity in the context of drilling rotations.* A rigorous demonstration of the advantages of modeling stiffness about a plate normal is required. The simplest example is to consider an infinite plate subjected to a concentrated drilling moment. Classical plate models (of the Kirchhoff or Mindlin types) predict an infinite response at the point of application of the moment. Realistically, we know that the rotation at the point of application ought to be finite. Cosserat or micropolar elasticity has postulated, from the outset, the existence of independent microrotations and the

ability of the medium to support concentrated couples. Solving the aforementioned problem will help illustrate the advantages of using a more general theory of plates that is based on higher-order elasticity theories. The corresponding three dimensional problem of a concentrated couple in an infinite micropolar solid has been solved successfully by Eringen [40], where the expression for a nontrivial microrotation field is derived. The present problem can be thought of as the corresponding 2-D analogue of Eringen's problem and is, consequently, expected to yield a finite solution dependent on the material parameters. A partial attempt at solving this problem is presented in appendix H and needs to be completed in the future.

APPENDIX A

EXPRESSIONS FOR THE THREE-DIMENSIONAL STRAIN MEASURES

A.1 Force Strain

The Jaumann-Biot-Cauchy strain tensor Γ is defined as

$$\underline{\boldsymbol{\Gamma}} = \underline{\overline{\boldsymbol{U}}} - \underline{\boldsymbol{\Delta}} \tag{A.1}$$

Here, the Cosserat stretch tensor $\underline{\overline{\boldsymbol{U}}}$ is *not* symmetric and does not coincide with the symmetric right stretch tensor $\underline{\boldsymbol{U}}$ from the polar decomposition theorem. The deformation gradient tensor can be written as

$$\underline{\boldsymbol{\chi}} = \underline{\boldsymbol{C}} \cdot \underline{\overline{\boldsymbol{U}}} \tag{A.2}$$

Substituting for the $\underline{\overline{\mathbf{U}}}$ using eqs. (8) and (A.2), we have

$$\underline{\boldsymbol{\Gamma}} = \exp(-\underline{\widetilde{\boldsymbol{\phi}}}) \cdot \underline{\boldsymbol{C}}^{bB} \cdot \underline{\boldsymbol{\chi}} - \underline{\boldsymbol{\Delta}} \tag{A.3}$$

To make the formulation simpler, we can write these expressions in matrix form. Expressing $\underline{\Gamma}$ in the $\mathbf{b}_i$ triad and the deformation gradient in mixed bases,

$$\underline{\Gamma} = \boldsymbol{b}_i \Gamma_{ij} \boldsymbol{b}_j \tag{A.4}$$

$$\underline{\chi} = \boldsymbol{B}_i \chi_{ij} \boldsymbol{b}_j \tag{A.5}$$

Following a development similar to [70], we can express in matrix notation

$$\Gamma = \exp(-\widetilde{\phi})\chi - \Delta \tag{A.6}$$

where Γ is a nonsymmetric 3×3 matrix of the three-dimensional "force" strain measures Γ_{ij} and χ contains the measure numbers of the deformation gradient, as

defined by Ogden [109]. For the case of small strain and small local rotation $\widetilde{\phi}$, with $\varphi \equiv \max|\widetilde{\phi}_{ij}| = \mathcal{O}(\max|\Gamma_{ij}|) \equiv \mathcal{O}(\varepsilon)$, we can write

$$\Gamma = \chi - \widetilde{\phi} - \Delta + \mathcal{O}(\varphi^2, \varphi\varepsilon) \approx \chi - \widetilde{\phi} - \Delta \tag{A.7}$$

This definition holds as long as such that max $|\Gamma_{ij}| \equiv \hat{\varepsilon} \ll 1$. For a plate, the components of the matrix χ can be determined as

$$\begin{aligned} \chi_{ij} &= (\mathbf{B}_i \cdot \mathbf{G}_k)(\mathbf{g}^k \cdot \mathbf{b}_j) \\ &= \mathbf{B}_i \cdot \mathbf{G}_j \end{aligned} \tag{A.8}$$

where $\mathbf{G}_i$ are the covariant vase vectors tangent to the coordinate curves of the deformed plate:

$$\mathbf{G}_i(x_1, x_2, x_3) = \frac{\partial \hat{\mathbf{R}}}{\partial x_i} \tag{A.9}$$

This gives us the following expression for Γ in terms of the 2-D generalized strain variables:

$$\Gamma = \begin{pmatrix} \epsilon_{11} + x_3 K_{11} + \underline{w_{1,1}} & \epsilon_{21} + \phi_3 + x_3 K_{21} + \underline{w_{1,2}} & w_{1,3} - \phi_2 \\ \epsilon_{12} - \phi_3 + x_3 K_{12} + \underline{w_{2,1}} & \epsilon_{22} + x_3 K_{22} + \underline{w_{2,2}} & w_{2,3} + \phi_1 \\ \phi_2 + \underline{w_{3,1} + 2\gamma_{13}} & -\phi_1 + \underline{w_{3,2} + 2\gamma_{23}} & w_{3,3} \end{pmatrix} \tag{A.10}$$

A.2 Moment Strain/Wryness Tensor

Similar to the definitions in [127], [118], [79], etc., the wryness tensor is defined as

$$\underline{\boldsymbol{X}} = \mathbf{b}_i \, \boldsymbol{\kappa}_i^b \tag{A.11}$$

where we define the curvature vectors of the three-dimensional deformed Cosserat continuum $\boldsymbol{\kappa}_i^B$ expressed in the $\mathbf{B}_i$ basis (three-dimensional equivalents to $\boldsymbol{K}$ for beams and $\boldsymbol{K}_\alpha$ for plates/shells) as

$$\widetilde{\boldsymbol{\kappa}}_i^B = \underline{\boldsymbol{C}}_{,i} . \underline{\boldsymbol{C}}^T \tag{A.12}$$

where $(\ )_{,i}$ denotes the differentiation $\frac{\partial(\ )}{\partial x_i}$ $(i = 1, 2, 3)$. The quantities $\boldsymbol{\kappa}_i^b$ simply represent a pull-back of the vectors $\boldsymbol{\kappa}_i^B$. Using eq. (8) and writing separate relations for $i = \alpha$ and $i = 3$,

$$\begin{aligned}\widetilde{\boldsymbol{\kappa}}_\alpha^B &= (\underline{\boldsymbol{C}}^{Bb}.\exp(\underline{\widetilde{\boldsymbol{\phi}}}))_{,\alpha}.\exp(-\underline{\widetilde{\boldsymbol{\phi}}}).\underline{\boldsymbol{C}}^{bB} \\ &= \underline{\boldsymbol{C}}^{Bb}_{,\alpha}.\underline{\boldsymbol{C}}^{bB} + \underline{\boldsymbol{C}}^{Bb}.\exp(\underline{\widetilde{\boldsymbol{\phi}}})_{,\alpha}.\exp(-\underline{\widetilde{\boldsymbol{\phi}}}).\underline{\boldsymbol{C}}^{bB} \\ &= \widetilde{\boldsymbol{K}}_{,\alpha} + \underline{\boldsymbol{C}}^{Bb}.\exp(\underline{\widetilde{\boldsymbol{\phi}}})_{,\alpha}.\exp(-\underline{\widetilde{\boldsymbol{\phi}}}).\underline{\boldsymbol{C}}^{bB}\end{aligned} \tag{A.13}$$

$$\begin{aligned}\widetilde{\boldsymbol{\kappa}}_3^B &= (\underline{\boldsymbol{C}}^{Bb}.\exp(\underline{\widetilde{\boldsymbol{\phi}}}))_{,3}.\exp(-\underline{\widetilde{\boldsymbol{\phi}}}).\underline{\boldsymbol{C}}^{bB} \\ &= \underline{\boldsymbol{C}}^{Bb}.\exp(\underline{\widetilde{\boldsymbol{\phi}}})_{,3}.\exp(-\underline{\widetilde{\boldsymbol{\phi}}}).\underline{\boldsymbol{C}}^{bB}\end{aligned} \tag{A.14}$$

Switching to writing these expressions in matrix form, it can be simplified to

$$\widetilde{\kappa}_\alpha^B = \widetilde{K}_\alpha - \exp(\widetilde{\phi})\widetilde{\phi}_{,\alpha}\exp(-\widetilde{\phi}) \tag{A.15}$$

$$\widetilde{\kappa}_3^B = -\exp(\widetilde{\phi})\widetilde{\phi}_{,3}\exp(-\widetilde{\phi}) \tag{A.16}$$

For small local rotations, we can approximate $\exp(\widetilde{\phi}) \approx \Delta + \widetilde{\phi}$, giving

$$\kappa_\alpha^B = K_\alpha - \phi_{,\alpha} + \mathcal{O}(\varphi^2) \approx K_\alpha - \phi_{,\alpha} \tag{A.17}$$

$$\kappa_3^B \approx -\phi_{,3} \tag{A.18}$$

Here it is noted that the negative signs in these relations stem from a sign convention stipulated while relating the matrix and tensor forms of $\underline{\boldsymbol{C}}^{Bb}$ that is different from those for $\exp(\underline{\widetilde{\boldsymbol{\phi}}})$. Using these relations, we can write

$$\boldsymbol{X} = \mathbf{b}_i\ \boldsymbol{\kappa}_i^b\ = \mathbf{B}_i\ \boldsymbol{\kappa}_i^B \tag{A.19}$$

$$\Rightarrow X_{ij} = e_j^T \kappa_i^B \tag{A.20}$$

Expanded out In matrix form,

$$X = \begin{pmatrix} -K_{12} - \phi_{1,1} & K_{11} - \phi_{2,1} & K_{13} - \phi_{3,1} \\ -K_{22} - \phi_{1,2} & K_{21} - \phi_{2,2} & K_{23} - \phi_{3,2} \\ -\phi_{1,3} & -\phi_{2,3} & -\phi_{3,3} \end{pmatrix} \tag{A.21}$$

APPENDIX B

COMPATIBILITY EQUATIONS FOR PLATES

Following [136], we can enforce the following equalities regarding the kinematic variables of a plate

$$\mathbf{R}_{,12} = \mathbf{R}_{,21} \tag{B.1}$$

$$\mathbf{B}_{i,12} = \mathbf{B}_{i,21} \tag{B.2}$$

These four vector equations lead to only six independent compatibility equations similar to those reported by Hodges et al. [64] when $\epsilon_{12} \neq \epsilon_{21}$. These equations are

$$(1+\epsilon_{22})K_{12} - (1+\epsilon_{11})K_{21} = 2\gamma_{23,1} - 2\gamma_{13,2} + \epsilon_{12}K_{22} - \epsilon_{21}K_{11} \tag{B.3a}$$

$$(1+\epsilon_{22})K_{13} - \epsilon_{12}K_{23} = \epsilon_{21,1} - \epsilon_{11,2} - 2\gamma_{13}K_{21} + 2\gamma_{23}K_{11} \tag{B.3b}$$

$$(1+\epsilon_{11})K_{23} + \epsilon_{21}K_{13} = \epsilon_{22,1} - \epsilon_{12,2} - 2\gamma_{13}K_{22} + 2\gamma_{23}K_{12} \tag{B.3c}$$

$$K_{11,2} - K_{21,1} + K_{13}K_{22} - K_{12}K_{23} = 0 \tag{B.3d}$$

$$K_{22,1} - K_{12,2} + K_{23}K_{11} - K_{21}K_{13} = 0 \tag{B.3e}$$

$$K_{23,1} - K_{13,2} + K_{11}K_{22} - K_{12}K_{21} = 0 \tag{B.3f}$$

APPENDIX C

EXPRESSION FOR VIRTUAL WORK OF THE APPLIED LOADS

For any point in the deformed configuration,

$$\delta\hat{\mathbf{R}} = \delta\mathbf{R} + x_3\delta\mathbf{B}_3 + \delta w_i\mathbf{B}_i + w_i\delta\mathbf{B}_i \tag{C.1}$$

The virtual displacement and rotation of the reference surface and the virtual rotation at any 3-D material point are defined as

$$\overline{\delta q}_{Bi} = \delta\mathbf{u}\cdot\mathbf{B}_i = \delta\mathbf{R}\cdot\mathbf{B}_i \tag{C.2}$$

$$\delta\mathbf{B}_i = \overline{\delta\boldsymbol{\psi}}^{Bb}\times\mathbf{B}_i = (-\overline{\delta\psi}^{Bb}_{B\beta}\mathbf{B}_\beta\times\mathbf{B}_3 + \overline{\delta\psi}^{Bb}_{B3}\mathbf{B}_3)\times\mathbf{B}_i \tag{C.3}$$

$$\delta\hat{\mathbf{B}}_i = \overline{\delta\boldsymbol{\psi}}^{\hat{B}B}\times\hat{\mathbf{B}}_i = (-\overline{\delta\psi}^{\hat{B}B}_{\hat{B}\beta}\hat{\mathbf{B}}_\beta\times\hat{\mathbf{B}}_3 + \overline{\delta\psi}^{\hat{B}B}_{\hat{B}3}\hat{\mathbf{B}}_3)\times\hat{\mathbf{B}}_i \tag{C.4}$$

Therefore, eq. (C.1) becomes (after neglecting products of warping and virtual rotations)

$$\delta\hat{\mathbf{R}} = \overline{\delta q}_{Bi}\mathbf{B}_i + x_3(\overline{\delta\psi}_1\mathbf{B}_1 + \overline{\delta\psi}_2\mathbf{B}_2) + \delta w_i\mathbf{B}_i \tag{C.5}$$

where we simply denote $\overline{\delta\psi}^{Bb}_{Bi}$ by $\overline{\delta\psi}_{Bi}$.

Next, we need to write $\overline{\delta\boldsymbol{\psi}}^{\hat{B}B}$ in terms of $\mathbf{B}_i$ and $\delta\phi_i$. Consider

$$\underline{\boldsymbol{C}} = \underline{\boldsymbol{C}}^{Bb}.\exp(\underline{\widetilde{\boldsymbol{\phi}}})$$

$$\Rightarrow\hat{\mathbf{B}}_i = \underline{\boldsymbol{C}}.\mathbf{b}_i = (\mathbf{B}_j\mathbf{b}_j.\mathbf{b}_k\exp(\widetilde{\phi})_{kl}\mathbf{b}_l).\mathbf{b}_i$$

$$= \mathbf{B}_j\exp(\widetilde{\phi})_{ji} = \exp(-\widetilde{\phi})_{ij}\mathbf{B}_j$$

$$\Rightarrow\mathbf{B}_i = \exp(\widetilde{\phi})_{ij}\hat{\mathbf{B}}_j$$

Taking the variation of the equation above and ignoring products of local rotation and virtual rotations,

$$\begin{aligned}\delta\hat{\mathbf{B}}_i &= \exp\left(-\delta\widetilde{\phi}\right)_{ij}\mathbf{B}_j + \exp\left(-\widetilde{\phi}\right)_{ij}\delta\mathbf{B}_j \\ &\approx \exp\left(-\delta\widetilde{\phi}\right)_{ij}\exp\left(\widetilde{\phi}\right)_{jk}\hat{\mathbf{B}}_k\end{aligned} \tag{C.6}$$

Comparing eq. (C.4) with eq. (C.6) we can conclude that

$$\overline{\delta\psi}^{\hat{B}B}_{\hat{B}} \equiv \begin{Bmatrix} -\overline{\delta\psi}^{\hat{B}B}_{\hat{B}2} \\ \overline{\delta\psi}^{\hat{B}B}_{\hat{B}1} \\ \overline{\delta\psi}^{\hat{B}B}_{\hat{B}3} \end{Bmatrix} = \begin{Bmatrix} \delta\phi_1 \\ \delta\phi_2 \\ \delta\phi_3 \end{Bmatrix} \tag{C.7}$$

Neglecting products of local rotation times the virtual rotations again, we have the virtual rotations in the $\mathbf{B}_i$ system as

$$\overline{\delta\psi}^{\hat{B}B}_{B} \equiv \begin{Bmatrix} -\overline{\delta\psi}^{\hat{B}B}_{B2} \\ \overline{\delta\psi}^{\hat{B}B}_{B1} \\ \overline{\delta\psi}^{\hat{B}B}_{B3} \end{Bmatrix} = \begin{Bmatrix} \delta\phi_1 \\ \delta\phi_2 \\ \delta\phi_3 \end{Bmatrix} \tag{C.8}$$

Making use of the addition theorem, we can write

$$\overline{\delta\boldsymbol{\psi}}^{\hat{B}b} = \overline{\delta\boldsymbol{\psi}}^{\hat{B}B} + \overline{\delta\boldsymbol{\psi}}^{Bb} \tag{C.9}$$

or, in matrix notation,

$$\begin{aligned}\overline{\delta\psi}^{\hat{B}b}_{B} &= \overline{\delta\psi}^{\hat{B}B}_{B} + \overline{\delta\psi}^{Bb}_{B} \\ &= \begin{Bmatrix} -\overline{\delta\psi}_{B2} \\ \overline{\delta\psi}_{B1} \\ \overline{\delta\psi}_{B3} \end{Bmatrix} + \begin{Bmatrix} \delta\phi_1 \\ \delta\phi_2 \\ \delta\phi_3 \end{Bmatrix}\end{aligned} \tag{C.10}$$

$$\begin{aligned}\overline{\delta\mathcal{W}} = \Bigg(&\langle\boldsymbol{\varphi}_f\cdot\delta\hat{\mathbf{R}}\rangle + \langle\boldsymbol{\varphi}_m\cdot\overline{\delta\boldsymbol{\psi}}^{\hat{B}b}\rangle + \boldsymbol{\tau}_f^{+}\cdot\delta\hat{\mathbf{R}}|_{h/2} + \boldsymbol{\tau}_f^{-}\cdot\delta\hat{\mathbf{R}}|_{-h/2} \\ &+\boldsymbol{\tau}_m^{+}\cdot\overline{\delta\boldsymbol{\psi}}^{\hat{B}b}|_{h/2} + \boldsymbol{\tau}_m^{-}\cdot\overline{\delta\boldsymbol{\psi}}^{\hat{B}b}|_{-h/2}\Bigg)\end{aligned} \tag{C.11}$$

Using results from eqs. (C.1) and (C.10), we can express this as

$$\begin{aligned}
\overline{\delta\mathcal{W}} &= \overline{\delta\mathcal{W}}_{1D} + \overline{\delta\mathcal{W}}^{*} \\
\overline{\delta\mathcal{W}}_{1D} &= \Bigg(\left(\tau_{f_i}^{+} + \tau_{f_i}^{-} + \langle\varphi_{f_i}\rangle\right) \overline{\delta q}_{Bi} + \left[\frac{h}{2}(\tau_{f_\alpha}^{+} - \tau_{f_\alpha}^{-}) + \langle x_3 \varphi_{f_\alpha}\rangle\right] \overline{\delta\psi}_{\alpha} \\
&\qquad + (\tau_{m_i}^{+} + \tau_{m_i}^{-} + \langle\varphi_{m_i}\rangle)\overline{\delta\psi}_{i} \Bigg) \\
\overline{\delta\mathcal{W}}^{*} &= \delta\left[\tau_{f_i}^{+} w_i^{+} + \tau_{f_i}^{-} w_i^{-} + \langle\varphi_{f_i} w_i\rangle\right] + \delta\left[\tau_{m_i}^{+}\phi_i^{+} + \tau_{m_i}^{-}\phi_i^{-} + \langle\varphi_{m_i}\phi_i\rangle\right]
\end{aligned}$$

By introducing column matrices $\overline{\delta q}$, $\overline{\delta\psi}$, τ_f, τ_m, φ_f and φ_m, which are formed by stacking the three elements associated with indexed symbols of the same names, one may write the virtual work in matrix form:

$$\begin{aligned}
\overline{\delta\mathcal{W}} = &\left(\overline{\delta q}^{\mathrm{T}} f + \overline{\delta\psi}^{\mathrm{T}} m\right) + \delta\left(\tau_f^{+\mathrm{T}} w^{+} + \tau_f^{-\mathrm{T}} w^{-} + \langle\varphi_f^{\mathrm{T}} w\rangle\right) \\
&+ \delta\left(\tau_m^{+\mathrm{T}}\phi^{+} + \tau_m^{-\mathrm{T}}\phi^{-} + \langle\varphi_m^{\mathrm{T}}\phi\rangle\right)
\end{aligned} \tag{C.12}$$

APPENDIX D

ESTIMATING ORDERS OF THE APPLIED LOADS

Previously, we stipulated that $\epsilon_{\alpha\beta}, hK_{\alpha\beta} \sim \mathcal{O}(\hat{\varepsilon})$, $2\gamma_{\alpha 3}, hK_{\alpha 3} \sim \mathcal{O}(h\hat{\varepsilon}/l)$, and $\bar{\mu}$ is the order of the material constants (all of which are assumed to be of the same order here). Therefore, we know the order of the $N_{\alpha\beta}$, $M_{\alpha\beta}$, Q_α and $M_{\alpha 3}$ from the plate constitutive law as

$$N_{\alpha\beta} \sim \bar{\mu}h\hat{\varepsilon} \qquad M_{\alpha\beta} \sim \bar{\mu}h^3\frac{\hat{\varepsilon}}{h} \tag{D.1}$$

$$Q_\alpha \sim \bar{\mu}h\frac{h}{l}\hat{\varepsilon} \qquad M_{\alpha 3} \sim \bar{\mu}h^3\frac{h}{l}\frac{\hat{\varepsilon}}{h} \tag{D.2}$$

Using the linearized equilibrium equations, we can find the order of the forces and moments distributed over the plate reference surface as

$$f_\alpha \sim \bar{\mu}(\frac{h}{l})\hat{\varepsilon} \tag{D.3}$$

$$f_3 \sim \bar{\mu}(\frac{h}{l})^2\hat{\varepsilon} \tag{D.4}$$

$$m_\alpha \sim \bar{\mu}h(\frac{h}{l})\hat{\varepsilon} \tag{D.5}$$

$$m_3 \sim \bar{\mu}h(\frac{h}{l})^2\hat{\varepsilon} \tag{D.6}$$

The orders of these distributed forces and moments coincides with the orders assumed by Erbay [36].

We also can see that the influence of warping on the virtual work contributes to terms that are $\mathcal{O}(\bar{\mu}h^2\hat{\varepsilon}^2/l^2)$. This justifies our earlier statement that in a refined theory one must take into account the effect of surface tractions and body forces while evaluating the expressions for the warping.

Additionally, as mentioned before, the sixth equilibrium equation (from eq. (62)) in tells us about the order of the 2-D strain measure Ω_ε. Consider, for the sake

of order analysis, a case where $m_3 = 0$. In that case, $N_{12} - N_{21} \equiv 2\mathcal{N}_\epsilon$ is of the same order as $M_{13,1}$ and $M_{23,2}$. From the plate constitutive law we just derived, it follows that Ω_ε is $\mathcal{O}(h^2\hat{\varepsilon}/l^2)$. This observation simplifies the analysis somewhat while deriving a refined theory of plates.

APPENDIX E

EXPRESSIONS FOR THE GENERALIZED WARPING FUNCTIONS

The expressions for the zeroth-order warping and local rotation fields:

$$
\begin{aligned}
w_\alpha &= 0 \\
w_3 &= \frac{\lambda}{\lambda+2\mu+\kappa}\left[-x_3(\epsilon_{11}+\epsilon_{22}) + \left(\frac{h^2}{24}-\frac{x_3^2}{2}\right)(K_{11}+K_{22})\right] \\
\phi_\alpha &= 0 \\
\phi_3 &= 0
\end{aligned}
\tag{E.1}
$$

The expressions for the first-order warping and local rotation fields:

$$
\begin{aligned}
v_1 =& \frac{\lambda}{\lambda+2\mu+\kappa}(\epsilon_{11,1}+\epsilon_{22,1})\left[\frac{x_3^2}{2}-\frac{h^2}{24}-\frac{\gamma}{2\mu+\kappa}\left(\frac{\cosh x_3/l_0}{\cosh h/2l_0}-\frac{\tanh h/2l_0}{h/2l_0}\right)\right] \\
&+\frac{\lambda}{\lambda+2\mu+\kappa}(K_{11,1}+K_{22,1})\left[\frac{h^2x_3}{8}-\frac{x_3^3}{6}+\frac{\mu}{\mu+\kappa}\frac{h^2x_3}{12}\right] \\
&+(K_{11,1}+\kappa_{12,2})\left[\frac{x_3^3}{3}-\frac{(3\mu+2\kappa)h^2x_3}{(\kappa+\mu)12}+\frac{\gamma}{2\mu+\kappa}\left(x_3-\frac{\sinh(x_3/l_0)}{\sinh(h/2l_0)}\frac{h}{2}\right)\right] \\
&+\frac{\tau_{f1}+\beta_{f1}}{(2\mu+\kappa)h}\left[x_3^2-\frac{h^2}{12}-\frac{\gamma}{2\mu+\kappa}\left(\frac{\cosh x_3/l_0}{\cosh h/2l_0}-\frac{\tanh h/2l_0}{h/2l_0}\right)\right] \\
&+\frac{\tau_{f1}-\beta_{f1}-2\mu(2\gamma_{13})}{2(\mu+\kappa)}x_3-\frac{\tau_{m2}+\beta_{m_2}}{(2\mu+\kappa)h}\left(x_3-\frac{\sinh x_3/l_0}{\sinh h/2l_0}\frac{h}{2}\right) \\
&+\frac{\tau_{m2}-\beta_{m2}+2\beta K_{23}}{2(2\mu+\kappa)}\left(\frac{\cosh x_3/l_0}{\cosh h/2l_0}-\frac{\tanh h/2l_0}{h/2l_0}\right)
\end{aligned}
\tag{E.2}
$$

$$
\begin{aligned}
v_2 =& \frac{\lambda}{\lambda+2\mu+\kappa}\left(\epsilon_{11,2}+\epsilon_{22,2}\right)\left[\frac{x_3^2}{2}-\frac{h^2}{24}-\frac{\gamma}{2\mu+\kappa}\left(\frac{\cosh\left(x_3/l_0\right)}{\cosh\left(h/2l_0\right)}-\frac{\tanh\left(h/2l_0\right)}{h/2l_0}\right)\right] \\
&+\frac{\lambda}{\lambda+2\mu+\kappa}\left(K_{11,2}+K_{22,2}\right)\left[\frac{h^2x_3}{8}-\frac{x_3^3}{6}+\frac{\mu}{\mu+\kappa}\frac{h^2x_3}{12}\right] \\
&+\left(K_{22,2}+\kappa_{12,1}\right)\left[\frac{x_3^3}{3}-\frac{(3\mu+2\kappa)h^2x_3}{(\kappa+\mu)12}+\frac{\gamma}{2\mu+\kappa}\left(x_3-\frac{\sinh\left(x_3/l_0\right)}{\sinh\left(h/2l_0\right)}\frac{h}{2}\right)\right] \\
&+\frac{\tau_{f2}+\beta_{f2}}{(2\mu+\kappa)h}\left[x_3^2-\frac{h^2}{12}-\frac{\gamma}{2\mu+\kappa}\left(\frac{\cosh x_3/l_0}{\cosh h/2l_0}-\frac{\tanh\left(h/2l_0\right)}{h/2l_0}\right)\right] \\
&+\frac{\tau_{f2}-\beta_{f2}-2\mu(2\gamma_{23})}{2(\mu+\kappa)}x_3+\frac{\tau_{m1}+\beta_{m_1}}{(2\mu+\kappa)h}\left(x_3-\frac{\sinh\left(x_3/l_0\right)}{\sinh\left(h/2l_0\right)}\frac{h}{2}\right) \\
&-\frac{\tau_{m1}-\beta_{m1}+2\beta K_{23}}{2(2\mu+\kappa)}\left(\frac{\cosh\left(x_3/l_0\right)}{\cosh\left(h/2l_0\right)}-\frac{\tanh\left(h/2l_0\right)}{h/2l_0}\right)
\end{aligned}
\tag{E.3}
$$

$$
v_3 = 0 \tag{E.4}
$$

$$
\begin{aligned}
\varphi_1 =& -\left(\frac{\lambda}{\lambda+2\mu+\kappa}\left(\epsilon_{11,2}+\epsilon_{22,2}\right)+\frac{\tau_{f2}+\beta_{f2}}{(2\mu+\kappa)h}\right)\left[x_3-\frac{\sinh\left(x_3/l_0\right)}{\sinh\left(h/2l_0\right)}\frac{h}{2}\right] \\
&-\left(K_{22,2}+\kappa_{12,1}\right)\left[\frac{x_3^2}{2}-\frac{h^2}{24}+l_0^2-\frac{\cosh\left(x_3/l_0\right)}{\sinh\left(h/2l_0\right)}\frac{hl}{2}\right] \\
&-\tau_{m1}\frac{l_0}{2\gamma}\left[\frac{\cosh\left(x_3/l_0\right)}{\sinh\left(h/2l_0\right)}+\frac{\sinh\left(x_3/l_0\right)}{\cosh\left(h/2l_0\right)}-\frac{2l_0}{h}\right]-\beta_{m1}\frac{l_0}{2\gamma}\left[\frac{\cosh\left(x_3/l_0\right)}{\sinh\left(h/2l_0\right)}-\frac{\sinh\left(x_3/l_0\right)}{\cosh\left(h/2l_0\right)}-\frac{2l_0}{h}\right] \\
&-\frac{\sinh\left(x_3/l_0\right)}{\cosh\left(h/2l_0\right)}\frac{l_0}{\gamma}\beta K_{13}
\end{aligned}
\tag{E.5}
$$

$$
\begin{aligned}
\varphi_2 =& \left(\frac{\lambda}{\lambda+2\mu+\kappa}\left(\epsilon_{11,1}+\epsilon_{22,1}\right)+\frac{\tau_{f1}+\beta_{f1}}{(2\mu+\kappa)h}\right)\left[x_3-\frac{\sinh\left(x_3/l_0\right)}{\sinh\left(h/2l_0\right)}\frac{h}{2}\right] \\
&-\left(K_{11,1}+\kappa_{12,2}\right)\left[\frac{x_3^2}{2}-\frac{h^2}{24}+l_0^2-\frac{\cosh\left(x_3/l_0\right)}{\sinh\left(h/2l_0\right)}\frac{hl}{2}\right] \\
&+\tau_{m2}\frac{l_0}{2\gamma}\left[\frac{\cosh\left(x_3/l_0\right)}{\sinh\left(h/2l_0\right)}+\frac{\sinh\left(x_3/l_0\right)}{\cosh\left(h/2l_0\right)}-\frac{2l_0}{h}\right]\beta_{m2}\frac{l_0}{2\gamma}\left[\frac{\cosh\left(x_3/l_0\right)}{\sinh\left(h/2l_0\right)}-\frac{\sinh\left(x_3/l_0\right)}{\cosh\left(h/2l_0\right)}-\frac{2l_0}{h}\right] \\
&+\frac{\sinh\left(x_3/l_0\right)}{\cosh\left(h/2l_0\right)}\frac{l_0}{\gamma}\beta K_{23}
\end{aligned}
\tag{E.6}
$$

$$
\varphi_3 = 0 \tag{E.7}
$$

APPENDIX F

MIXED VARIATIONAL STATEMENT FOR COSSERAT PLATES

A mixed formulation is obtained by adjoining the appropriate kinematical relations to Hamilton's weak principle with Lagrange multipliers and identifying the Lagrange multipliers. The rotation variables chosen are the Rodrigues parameters

$$\theta = \begin{Bmatrix} \theta_1 \\ \theta_2 \\ \theta_3 \end{Bmatrix}$$

and the direction cosine matrix C^{Bb}, henceforth denoted simply by C, can be expressed as

$$C = \frac{[(1-(1/4)\theta^T\theta)\Delta - \widetilde{\theta} + (1/2)\theta\theta^T]}{1+(1/4)\theta^T\theta} \tag{F.1}$$

It is useful to obtain the inverse kinematical relations before proceeding further. We have

$$\begin{aligned} u_{,\alpha} &= C^T(e_\alpha + \gamma_\alpha) - e_\alpha \\ \dot{u} &= C^T V - v - \widetilde{\omega} u \\ \theta_{,\alpha} &= \left(\Delta + \frac{1}{2}\widetilde{\theta} + \frac{1}{4}\theta\theta^T\right) K_\alpha \\ \dot{\theta} &= \left(\Delta + \frac{1}{2}\widetilde{\theta} + \frac{1}{4}\theta\theta^T\right)(\Omega - C\omega) \end{aligned}$$

Hamilton's extended principle

$$\int_{t_1}^{t_2} \int_{\mathcal{S}} [\delta(\mathcal{K} - \mathcal{U}) + \overline{\delta W}]\, \mathrm{d}s\mathrm{d}t = \overline{\delta \mathcal{A}} \tag{F.2}$$

After following the procedure for obtaining the Lagrange multipliers outlined by Hodges [70], we can write the variations in potential and kinetic energy as

$$\begin{aligned}\delta\mathcal{U} = &\delta\gamma_\alpha^T\left[A_{\alpha\beta}\gamma_\beta - N_\alpha\right] + \overline{\delta N}_\alpha^T\left[u_{,\alpha} + e_\alpha - C^T(\gamma_\alpha + e_\alpha)\right] \\ &+ \left[\overline{\delta q}_{,\alpha}^T - \overline{\delta q}^T\widetilde{K}_\alpha - \overline{\delta\psi}^T(\widetilde{e}_\alpha + \widetilde{\gamma}_\alpha)\right]N_\alpha + \delta K_\alpha^T\left[D_{\alpha\beta}K_\beta - M_\alpha\right] \\ &+ \overline{\delta M}_\alpha^T\left[\theta_{,\alpha} - \left(\Delta + \frac{1}{2}\widetilde{\theta} + \frac{1}{4}\theta\theta^T\right)K_\alpha\right] + \left[\overline{\delta\psi}_{,\alpha}^T - \overline{\delta\psi}^T\widetilde{K}_\alpha\right]M_\alpha\end{aligned} \tag{F.3}$$

where

$$\begin{aligned}\overline{\delta N}_\alpha &= C^T\delta N_\alpha \\ \overline{\delta M}_\alpha &= \frac{\Delta + \frac{1}{2}\widetilde{\theta}}{1 + \frac{1}{4}\theta^T\theta}\delta M_\alpha\end{aligned}$$

$$\begin{aligned}\delta\mathcal{K} = &\delta V^T\left[\mu(V - \widetilde{\bar{\xi}}\Omega) - P\right] + \overline{\delta P}^T\left[\dot{u} + v + \widetilde{\omega}u - C^TV\right] \\ &+ \left[\dot{\overline{\delta q}}^T - \overline{\delta q}^T\widetilde{\Omega} - \overline{\delta\psi}^T\widetilde{V}\right]P + \delta\Omega^T\left[\mu\widetilde{\bar{\xi}V} + i\Omega - H\right] \\ &+ \overline{\delta H}^T\left[\left(\Delta + \frac{1}{2}\widetilde{\theta} + \frac{1}{4}\theta\theta^T\right)(C\omega - \Omega) + \dot{\theta}\right] + \left[\dot{\overline{\delta\psi}}^T - \overline{\delta\psi}^T\widetilde{\Omega}\right]H\end{aligned} \tag{F.4}$$

where

$$\begin{aligned}\overline{\delta P} &= C^T\delta P \\ \overline{\delta H} &= \frac{\Delta + \frac{1}{2}\widetilde{\theta}}{1 + \frac{1}{4}\theta^T\theta}\delta H\end{aligned}$$

Ignoring the effect of warping (acceptable unless we are interested in high-frequency dynamics),

$$\overline{\delta\mathcal{W}} = \overline{\delta q}^T f + \overline{\delta\psi}^T m \tag{F.5}$$

Finally, the virtual action can be written as

$$\overline{\delta\mathcal{A}} = \int_{\mathcal{S}}(\overline{\delta q}^T\hat{P} + \overline{\delta\psi}^T\hat{H})\big|_{t_1}^{t_2}\mathrm{d}s - \int_{t_1}^{t_2}\int_{\Gamma}(\overline{\delta q}^T\hat{N} + \overline{\delta\psi}^T\hat{M})\mathrm{d}\Gamma\mathrm{d}t \tag{F.6}$$

Using eqs. (F.3) to (F.6) in eq. (F.2),

$$
\begin{aligned}
&\int_{t_1}^{t_2}\int_{\mathcal{S}}\Bigg\{\delta\gamma_\alpha^T\left[\left(\frac{\partial\mathcal{U}}{\partial\gamma_\alpha}\right)^T-N_\alpha\right]+\delta K_\alpha^T\left[\left(\frac{\partial\mathcal{U}}{\partial K_\alpha}\right)^T-M_\alpha\right]-\delta V^T\left[\mu(V-\widetilde{\bar{\xi}}\Omega)-P\right]\\
&\quad-\delta\Omega^T\left[\mu\widetilde{\bar{\xi}}V+i\Omega-H\right]+\left[\overline{\delta q}_{,\alpha}^T-\overline{\delta q}^T\widetilde{K}_\alpha-\overline{\delta\psi}^T(\widetilde{e}_\alpha+\widetilde{\gamma}_\alpha)\right]N_\alpha+\left[\overline{\delta\psi}_{,\alpha}^T-\overline{\delta\psi}^T\widetilde{K}_\alpha\right]M_\alpha\\
&\quad-\left[\dot{\overline{\delta q}}^T-\overline{\delta q}^T\widetilde{\Omega}-\overline{\delta\psi}^T\widetilde{V}\right]P-\left[\dot{\overline{\delta\psi}}^T-\overline{\delta\psi}^T\widetilde{\Omega}\right]H+\overline{\delta N}_\alpha^T\left[u_{,\alpha}+e_\alpha-C^T(\gamma_\alpha+e_\alpha)\right]\\
&\quad+\overline{\delta M}_\alpha^T\left[\theta_{,\alpha}-\left(\Delta+\frac{1}{2}\widetilde{\theta}+\frac{1}{4}\theta\theta^T\right)K_\alpha\right]-\overline{\delta P}^T\left[\dot{u}+v+\widetilde{\omega}u-C^TV\right]\\
&\quad-\overline{\delta H}^T\left[\left(\Delta+\frac{1}{2}\widetilde{\theta}+\frac{1}{4}\theta\theta^T\right)(C\omega-\Omega)+\dot{\theta}\right]-\overline{\delta q}^Tf-\overline{\delta\psi}^Tm\Bigg\}\,\mathrm{d}s\mathrm{d}t\\
&=-\int_{\mathcal{S}}(\overline{\delta q}^T\hat{P}+\overline{\delta\psi}^T\hat{H})\big|_{t_1}^{t_2}\mathrm{d}s+\int_{t_1}^{t_2}\int_{\Gamma}(\overline{\delta q}^T\hat{N}+\overline{\delta\psi}^T\hat{M})\mathrm{d}\Gamma\mathrm{d}t
\end{aligned}
\tag{F.7}
$$

Performing an integration by parts to remove the time derivatives of virtual quantities, we get

$$
\begin{aligned}
&\int_{t_1}^{t_2}\int_{\mathcal{S}}\Bigg\{\delta\gamma_\alpha^T\left[\left(\frac{\partial\mathcal{U}}{\partial\gamma_\alpha}\right)^T-N_\alpha\right]+\delta K_\alpha^T\left[\left(\frac{\partial\mathcal{U}}{\partial K_\alpha}\right)^T-M_\alpha\right]-\delta V^T\left[\mu(V-\widetilde{\bar{\xi}}\Omega)-P\right]\\
&\quad-\delta\Omega^T\left[\mu\widetilde{\bar{\xi}V}+i\Omega-H\right]+\overline{\delta q}_{,\alpha}^TN_\alpha+\overline{\delta q}^T\left[\dot{P}+\widetilde{\Omega}P-\widetilde{K}_\alpha N_\alpha-f\right]+\overline{\delta\psi}_{,\alpha}^TM_\alpha\\
&\quad+\overline{\delta\psi}^T\left[\dot{H}+\widetilde{V}P+\widetilde{\Omega}H-\widetilde{K}_\alpha M_\alpha-(\widetilde{e}_\alpha+\widetilde{\gamma}_\alpha)N_\alpha-m\right]\\
&\quad+\overline{\delta N}_\alpha^T\left[u_{,\alpha}+e_\alpha-C^T(\gamma_\alpha+e_\alpha)\right]+\overline{\delta M}_\alpha^T\left[\theta_{,\alpha}-\left(\Delta+\frac{1}{2}\widetilde{\theta}+\frac{1}{4}\theta\theta^T\right)K_\alpha\right]\\
&\quad-\overline{\delta P}^T\left[\dot{u}+v+\widetilde{\omega}u-C^TV\right]-\overline{\delta H}^T\left[\left(\Delta+\frac{1}{2}\widetilde{\theta}+\frac{1}{4}\theta\theta^T\right)(C\omega-\Omega)+\dot{\theta}\right]\Bigg\}\,\mathrm{d}s\mathrm{d}t\\
&=-\int_{\mathcal{S}}\left(\overline{\delta q}^T(\hat{P}-P)+\overline{\delta\psi}^T(\hat{H}-H)\right)\big|_{t_1}^{t_2}\mathrm{d}s+\int_{t_1}^{t_2}\int_{\Gamma}(\overline{\delta q}^T\hat{N}+\overline{\delta\psi}^T\hat{M})\mathrm{d}\Gamma\mathrm{d}t
\end{aligned}
\tag{F.8}
$$

Next, to obtain the weakest possible form, we need to remove the (spatial) derivatives

of all the unknowns. Performing another integration by parts,

$$\begin{aligned}
&\int_{t_1}^{t_2}\int_{\mathcal{S}}\Bigg\{\delta\gamma_\alpha^T\left[\left(\frac{\partial\mathcal{U}}{\partial\gamma_\alpha}\right)^T-N_\alpha\right]+\delta K_\alpha^T\left[\left(\frac{\partial\mathcal{U}}{\partial K_\alpha}\right)^T-M_\alpha\right]-\delta V^T\left[\mu(V-\widetilde{\bar{\xi}}\Omega)-P\right]\\
&\quad-\delta\Omega^T\left[\mu\widetilde{\bar{\xi}V}+i\Omega-H\right]+\overline{\delta q}_{,\alpha}^T N_\alpha+\overline{\delta q}^T\left[\dot{P}+\widetilde{\Omega}P-\widetilde{K}_\alpha N_\alpha-f\right]+\overline{\delta\psi}_{,\alpha}^T M_\alpha\\
&\quad+\overline{\delta\psi}^T\left[\dot{H}+\widetilde{V}P+\widetilde{\Omega}H-\widetilde{K}_\alpha M_\alpha-(\widetilde{e}_\alpha+\widetilde{\gamma}_\alpha)N_\alpha-m\right]\\
&\quad-\overline{\delta N}_{\alpha,\alpha}^T u-\overline{\delta N}_\alpha^T\left[C^T(\gamma_\alpha+e_\alpha)-e_\alpha\right]-\overline{\delta M}_{\alpha,\alpha}^T\theta-\overline{\delta M}_\alpha^T\left(\Delta+\frac{1}{2}\widetilde{\theta}+\frac{1}{4}\theta\theta^T\right)K_\alpha\\
&\quad-\overline{\delta P}^T\left[\dot{u}+v+\widetilde{\omega}u-C^TV\right]-\overline{\delta H}^T\left[\left(\Delta+\frac{1}{2}\widetilde{\theta}+\frac{1}{4}\theta\theta^T\right)(C\omega-\Omega)+\dot{\theta}\right]\Bigg\}\mathrm{d}s\mathrm{d}t\\
&=-\int_{\mathcal{S}}\left(\overline{\delta q}^T(\hat{P}-P)+\overline{\delta\psi}^T(\hat{H}-H)\right)\Big|_{t_1}^{t_2}\mathrm{d}s+\int_{t_1}^{t_2}\int_{\Gamma}(\overline{\delta q}^T\hat{N}+\overline{\delta\psi}^T\hat{M}-\overline{\delta N_\alpha}^T u-\overline{\delta M_\alpha}^T\theta)\mathrm{d}\Gamma\mathrm{d}t
\end{aligned}\tag{F.9}$$

The first four terms are determined by the through-the-thickness analysis using VAM and can be taken as a given. Also, assuming $P=\hat{P}, H=\hat{H}$ at t_1, t_2, we can drop the time integral. This leaves us with the following mixed variational statement:

$$\begin{aligned}
&\int_{\mathcal{S}}\Bigg\{\overline{\delta q}_{,\alpha}^T N_\alpha+\overline{\delta q}^T\left[\dot{P}+\widetilde{\Omega}P-\widetilde{K}_\alpha N_\alpha-f\right]+\overline{\delta\psi}_{,\alpha}^T M_\alpha\\
&\quad+\overline{\delta\psi}^T\left[\dot{H}+\widetilde{V}P+\widetilde{\Omega}H-\widetilde{K}_\alpha M_\alpha-(\widetilde{e}_\alpha+\widetilde{\gamma}_\alpha)N_\alpha-m\right]-\overline{\delta N}_{\alpha,\alpha}^T u\\
&\quad-\overline{\delta N}_\alpha^T\left[C^T(\gamma_\alpha+e_\alpha)-e_\alpha\right]-\overline{\delta M}_{\alpha,\alpha}^T\theta-\overline{\delta M}_\alpha^T\left(\Delta+\frac{1}{2}\widetilde{\theta}+\frac{1}{4}\theta\theta^T\right)K_\alpha\\
&\quad-\overline{\delta P}^T\left[\dot{u}+v+\widetilde{\omega}u-C^TV\right]-\overline{\delta H}^T\left[\left(\Delta+\frac{1}{2}\widetilde{\theta}+\frac{1}{4}\theta\theta^T\right)(C\omega-\Omega)+\dot{\theta}\right]\Bigg\}\mathrm{d}s\\
&=\int_{\Gamma}(\overline{\delta q}^T\hat{N}+\overline{\delta\psi}^T\hat{M}-\overline{\delta N_\alpha}^T u-\overline{\delta M_\alpha}^T\theta)\mathrm{d}\Gamma
\end{aligned}\tag{F.10}$$

The primary variables of our mixed formulation are $u, \psi, N_\alpha, M_\alpha, P$ and H.

APPENDIX G

RELATING INCREMENTAL QUANTITIES IN THE KINEMATICAL EQUATIONS

A detailed derivation of eqs. (98) is provided here for interested readers. Too often, equations such as these are simply used without showing how one could obtain them and this appendix, along with some of the prior ones, try to rectify that.

From the generalized velocity-displacement equations presented in eq. (48),

$$V = C(v + \dot{u} + \widetilde{\omega} u)$$

Now, if u and C have small perturbations from a "steady-state" value, i.e.,

$$\begin{aligned} u &= \overline{u} + \hat{u} \\ C &= (\Delta - \widetilde{\hat{\psi}})\overline{C} \end{aligned} \tag{G.1}$$

we need to find expressions for corresponding incrementals in the quantities V, Ω, γ_α and K_α. Let us start with V:

$$\begin{aligned} & V = C(v + \dot{u} + \widetilde{\omega} u) \\ \Rightarrow\ & \overline{V} = \overline{C}(v + \dot{\overline{u}} + \widetilde{\omega}\overline{u}), \\ & \overline{V} + \hat{V} = (\Delta - \widetilde{\hat{\psi}})\overline{C}\left[v + \dot{\overline{u}} + \dot{\hat{u}} + \widetilde{\omega}(\overline{u} + \hat{u})\right] \\ \Rightarrow & \overline{V} + \hat{V} = \overline{C}(v + \dot{\overline{u}} + \widetilde{\omega}\overline{u}) + \overline{C}(\dot{\hat{u}} + \widetilde{\omega}\hat{u}) - \widetilde{\hat{\psi}}\overline{C}(v + \dot{\overline{u}} + \widetilde{\omega}\overline{u}) \\ \Rightarrow & \hat{V} = \overline{C}(\dot{\hat{u}} + \widetilde{\omega}\hat{u}) - \widetilde{\hat{\psi}}\overline{V} = \overline{C}(\dot{\hat{u}} + \widetilde{\omega}\hat{u}) + \widetilde{\overline{V}}\hat{\psi} \end{aligned}$$

Defining $\hat{q} = \overline{C}\hat{u}$, we have $\dot{\hat{q}} = \dot{\overline{C}}\hat{u} + \overline{C}\dot{\hat{u}} = \dot{\overline{C}}\overline{C}^T\hat{q} + \overline{C}\dot{\hat{u}}$. Therefore,

$$\begin{aligned} \hat{V} &= \overline{C}\dot{\hat{u}} + \overline{C}\widetilde{\omega}\overline{C}^T\hat{q} + \widetilde{\overline{V}}\hat{\psi} \\ &= \dot{\hat{q}} - \dot{\overline{C}}\overline{C}^T\hat{q} + \overline{C}\widetilde{\omega}\overline{C}^T\hat{q} + \widetilde{\overline{V}}\hat{\psi} \\ &= \dot{\hat{q}} + \widetilde{\overline{\Omega}}\hat{q} + \widetilde{\overline{V}}\hat{\psi} \end{aligned}$$

We have our expression for an increment in V as

$$\hat{V} = \dot{\hat{q}} + \widetilde{\overline{\Omega}}\hat{q} + \widetilde{\overline{V}}\hat{\psi} \tag{G.2}$$

Next, let us find an expression for an increment in Ω. From eq. (49), we have

$$\begin{aligned}
&\widetilde{\Omega} = -\dot{C}C^T + C\widetilde{\omega}C^T \\
\Rightarrow\ &\widetilde{\overline{\Omega}} = -\dot{\overline{C}}\overline{C}^T + \overline{C}\widetilde{\omega}\overline{C}^T, \\
&\widetilde{\overline{\Omega}} + \widetilde{\hat{\Omega}} = -\left[(\Delta - \widetilde{\hat{\psi}})\dot{\overline{C}} - \dot{\widetilde{\hat{\psi}}}\overline{C}\right]\overline{C}^T(\Delta + \widetilde{\hat{\psi}}) + (\Delta - \widetilde{\hat{\psi}})\overline{C}\widetilde{\omega}\overline{C}^T(\Delta + \widetilde{\hat{\psi}}) \\
\Rightarrow\ &\widetilde{\hat{\Omega}} = \dot{\widetilde{\hat{\psi}}} + \widetilde{\overline{\Omega}}\widetilde{\hat{\psi}} - \widetilde{\hat{\psi}}\widetilde{\overline{\Omega}} = \dot{\widetilde{\hat{\psi}}} + \widetilde{\widetilde{\overline{\Omega}}\hat{\psi}}
\end{aligned}$$

This gets us the expression for an increment in Ω as

$$\hat{\Omega} = \dot{\hat{\psi}} + \widetilde{\overline{\Omega}}\hat{\psi} \tag{G.3}$$

To find an expression for the increment in γ_α, we start with

$$\begin{aligned}
&\gamma_\alpha = C(e_\alpha + u_{,\alpha}) - e_\alpha \\
\Rightarrow\ &\overline{\gamma}_\alpha = \overline{C}(e_\alpha + \overline{u}_{,\alpha}) - e_\alpha, \\
&\overline{\gamma}_\alpha + \hat{\gamma}_\alpha = (\Delta - \widetilde{\hat{\psi}})\overline{C}(e_\alpha + \overline{u}_{,\alpha} + \hat{u}_{,\alpha}) - e_\alpha \\
\Rightarrow\ &\overline{\gamma}_\alpha + \hat{\gamma}_\alpha = \overline{C}(e_\alpha + \overline{u}_{,\alpha}) - e_\alpha + \overline{C}\hat{u}_{,\alpha} - \widetilde{\hat{\psi}}\overline{C}(e_\alpha + \overline{u}_{,\alpha})
\end{aligned}$$

Noting that $\hat{q} = \overline{C}\hat{u}$, and using $\widetilde{\overline{K}}_\alpha = -\overline{C}_{,\alpha}\overline{C}^T$, we get the expression for the increment as

$$\hat{\gamma}_\alpha = \hat{q}_{,\alpha} + \widetilde{\overline{K}}_\alpha\hat{q} + (\widetilde{e}_\alpha + \widetilde{\overline{\gamma}}_\alpha)\hat{\psi} \tag{G.4}$$

Finally, starting with

$$\begin{aligned}
&\widetilde{K}_\alpha = -C_{,\alpha}C^T \\
\Rightarrow\ &\widetilde{\overline{K}}_\alpha = -\overline{C}_{,\alpha}\overline{C}^T, \\
&\widetilde{\overline{K}}_\alpha + \widetilde{\hat{K}}_\alpha = -\left[(\Delta - \widetilde{\hat{\psi}})\overline{C}_{,\alpha} - \widetilde{\hat{\psi}}_{,\alpha}\overline{C}\right]\overline{C}^T(\Delta + \widetilde{\hat{\psi}}) \\
\Rightarrow\ &\widetilde{\overline{K}}_\alpha + \widetilde{\hat{K}}_\alpha = -\overline{C}_{,\alpha}\overline{C}^T + \widetilde{\hat{\psi}}_{,\alpha} + \widetilde{\overline{K}}_\alpha\widetilde{\hat{\psi}} - \widetilde{\hat{\psi}}\widetilde{\overline{K}}_\alpha
\end{aligned}$$

We now have the expression for the perturbation as

$$\hat{K}_\alpha = \hat{\psi}_{,\alpha} + \widetilde{\overline{K}}_\alpha \hat{\psi} \tag{G.5}$$

It is interesting to note that all of eqs. (G.2) to (G.5) look remarkably similar to their counterparts for beams (for example, as shown in [139]). Such a compact and elegant representation is made possible only in the context of a theory of Cosserat plates. So, for instance, in a generalized Reissner-Mindlin theory, one would neither have Ω_3, K_{13}, K_{23} among the primary set of variables nor have ϵ_{12} as different from ϵ_{21}. However, a Cosserat theory can always be reduced to a Reissner-Mindlin theory or even a Kirchhoff-Love theory with the right choice of elastic constants.

APPENDIX H

IN PLANE DEFORMATION OF A MICROPOLAR PLATE UNDER A DRILLING MOMENT: AN ATTEMPT

In this section, we discuss the problem of a micropolar isotropic plate subjected to a point drilling moment T. The aim of this exercise is to try and highlight the ability of micropolar elasticity to model the in plane deformation resulting from such a moment applied normal to the plate. Practically, one can imagine this problem to model a scenario where a rod, attached rigidly at right angles to a plate, is given a torque that is then transmitted to the plate, causing in plane deformation. In the limiting case of vanishing diameter, the rod can simply be replaced with a concentrated drilling moment. Plate models derived from classical elasticity (Reissner-Mindlin, Kirchhoff-Love) predict no deformation from such a moment. However, since it is physically reasonable to expect a nontrivial elastic response, micropolar elasticity is expected to be superior in providing a realistic nonlocal solution.

To simplify this process, let us restrict ourselves to a geometrically linear formulation. Also, let us look at a circular plate instead of the rectangular plates considered thus far. Doing so would make the problem axisymmetric, thereby greatly simplifying the solution procedure by reducing all the governing equations to ordinary differential equations. Let us further consider an infinite plateThe equations of equilibrium (linear) for a circular micropolar plate are given by

$$\frac{\partial N_r}{\partial r} + \frac{1}{r}\cancel{\frac{\partial N_{\theta r}}{\partial \theta}} + \frac{N_r - N_\theta}{r} = 0 \tag{H.1a}$$

$$\frac{\partial N_{r\theta}}{\partial r} + \frac{1}{r}\cancel{\frac{\partial N_\theta}{\partial \theta}} + \frac{N_{r\theta} + N_{\theta r}}{r} = 0 \tag{H.1b}$$

$$\frac{\partial M_{rz}}{\partial r} + \frac{1}{r}\cancel{\frac{\partial M_{\theta z}}{\partial \theta}} + \frac{M_{rz}}{r} + N_{r\theta} - N_{\theta r} + m_z = 0 \tag{H.1c}$$

First, from eq. (H.1b), we can write

$$N_{\theta r} = -\frac{d(rN_{r\theta})}{dr} \tag{H.2}$$

The applied drilling moment is supported solely by $M_{rz}, N_{r\theta}$ and $N_{\theta r}$. This gives $N_r = N_\theta = 0$ and a trivial satisfaction of eq. (H.1a). The distributed moment term m_z in eq. (H.1c) is mathematically a Dirac delta function enclosing an area equal in magnitude to T. Using this fact and eq. (H.2) in eq. (H.1c) gives us, after an integration,

$$rM_{rz} + r^2 N_{r\theta} = T \tag{H.3}$$

One may also arrive at eq. (H.3) directly by drawing a simple free body diagram. Since the problem is, by definition, hyperstatic, the equilibrium equations are not enough to arrive at the solution: we are one equation short. This is provided by looking at the strain compatibility equations, given by

$$\frac{\partial \epsilon_{\theta r}}{\partial r} + \frac{\epsilon_{r\theta} + \epsilon_{\theta r}}{r} - \frac{1}{r}\cancel{\frac{\partial \epsilon_r}{\partial \theta}} - K_{rz} = 0 \tag{H.4a}$$

$$\frac{\partial \epsilon_\theta}{\partial r} + \frac{\epsilon_\theta - \epsilon_r}{r} - \frac{1}{r}\cancel{\frac{\partial \epsilon_{r\theta}}{\partial \theta}} - K_{\theta z} = 0 \tag{H.4b}$$

$$\frac{\partial K_{\theta z}}{\partial r} + \frac{K_{\theta z}}{r} - \frac{1}{r}\cancel{\frac{\partial K_{rz}}{\partial \theta}} = 0 \tag{H.4c}$$

Here, eqs. (H.4b) and (H.4c) give us $\epsilon_r = \epsilon_\theta = K_{\theta z} = 0$. Equation (H.4a) provides us with the additional equation required, but needs to be expressed in terms of the stress resultants. This can be done with the help of the following constitutive relations

$$\epsilon_{r\theta} = \frac{(\mu + \kappa)N_{r\theta} - \mu N_{\theta r}}{(2\mu + \kappa)\kappa h} \tag{H.5a}$$

$$\epsilon_{\theta r} = \frac{(\mu + \kappa)N_{\theta r} - \mu N_{r\theta}}{(2\mu + \kappa)\kappa h} \tag{H.5b}$$

$$K_{rz} = \frac{1}{\gamma h \bar{\theta}} M_{rz} \tag{H.5c}$$

where $\bar{\theta}$ is the nondimensional drilling stiffness and the remaining Cosserat elastic constants are the same as given by eq. (1).

Substituting eqs. (H.5a) to (H.5c), (H.2) and (H.3) into eq. (H.4a) gives, after some simplification, a single ordinary differential equation in terms of $N_{r\theta}$:

$$l_0^2\left(r^2\frac{d^2N_{r\theta}}{dr^2}+3r\frac{dN_{r\theta}}{dr}\right)+\frac{T}{\bar{\theta}}-\frac{r^2N_{r\theta}}{\bar{\theta}}=0 \tag{H.6}$$

where l_0 is the micropolar length-scale parameter defined by eq. (38).

As a check, consider for a moment the specific case of having all micropolar effects set to zero, thereby reducing to a classical elastic plate. This implies $l_0 = 0$, reducing eq. (H.6) to

$$N_{r\theta} = N_{\theta r} = T/r^2 \tag{H.7}$$

In fact, one can arrive at this solution by simply looking at only the equilibrium equation (eq. (H.3)) for the case where $M_{rz} = 0$. Using the relevant constitutive relations, it follows that $\epsilon_{r\theta} = \epsilon_{\theta r} = T/(2\mu hr^2)$. Further, this gives a tangential displacement field

$$u_\theta = -\frac{T}{4\mu hr} \tag{H.8}$$

One can clearly see problem with the classical elasticity solution: the stress resultant field given by eq. (H.7), and hence the displacement field given by eq. (H.8), go to infinity as $r \to 0$. In fact, this is a very common behavior for a wide variety of elasticity solutions near concentrated applied loads.

The case of $l_0 \neq 0$ makes for some interesting observations. For example, the $N_{r\theta}$ distribution now depends on the specific choice of the material of the plate (reflected in l_0 and $\bar{\theta}$) and not simply on the magnitude of the applied moment. The solution to eq. (H.6) for $l_0 \neq 0$ is expected to be in terms of Bessel functions of the first and second kind. At this point, a closed form solution is not readily available and is designated as future work.

REFERENCES

[1] Aero, E. L. and Kuvshinskii, E. V., "Fundamental equations of the theory of elastic media with rotationally interacting particles," *Soviet Physics-Solid State*, vol. 2, no. 7, pp. 1272–1281, 1961.

[2] Altenbach, H. and Eremeyev, V. A., "On the linear theory of micropolar plates," *Zamm-Zeitschrift Fur Angewandte Mathematik Und Mechanik*, vol. 89, no. 4, pp. 242 – 256, 2009.

[3] Altenbach, J., Altenbach, H., and Eremeyev, V., "On generalized cosserat-type theories of plates and shells: a short review and bibliography," *Archive of Applied Mechanics*, vol. 80, no. 1, pp. 73 – 92, 2010.

[4] Ambartsumian, S. A., "The theory of transverse bending of plates with asymmetric elasticity," *Mechanics of Composite Materials*, vol. 32, no. 1, pp. 30 – 38, 1996.

[5] Ariman, T., "On circular micropolar plates," *Ingenieur-Archiv*, vol. 37, no. 3, pp. 156 – 160, 1968.

[6] Askar, A., "A model for coupled rotation-displacement modes of certain molecular crystals. illustration for KNO_3," *Journal of Physics and Chemistry of Solids*, vol. 34, no. 11, pp. 1901 – 1907, 1973.

[7] Askar, A., "Molecular crystals and the polar theories of the continua experimental values of material coefficients for KNO_3," *International Journal of Engineering Science*, vol. 10, no. 3, pp. 293 – 300, 1972.

[8] Babuška, I., d'Harcourt, J., and Schwab, C., "Optimal shear correction factors in hierarchical plate modelling," tech. rep., DTIC Document, 1991.

[9] Babuška, I. and Guo, B. Q., "The h, p and h-p version of the finite element method; basis theory and applications," *Advances in Engineering Software*, vol. 15, no. 3–4, pp. 159 – 174, 1992.

[10] Berdichevskii, V. L., "Variational-asymptotic method of constructing a theory of shells," *Journal of Applied Mathematics and Mechanics*, vol. 43, no. 4, pp. 711 – 736, 1979.

[11] Besdo, D., "Ein beitrag zur nichtlinearen theorie des cosserat-kontinuums," *Acta Mechanica*, vol. 20, no. 1-2, pp. 105 – 131, 1974.

[12] Beveridge, A. J., Wheel, M. A., and Nash, D. H., "The micropolar elastic behaviour of model macroscopically heterogeneous materials," *International Journal of Solids and Structures*, vol. 50, no. 1, pp. 246 – 255, 2013.

[13] Bigoni, D. and Drugan, W. J., "Analytical derivation of cosserat moduli via homogenization of heterogeneous elastic materials," *Journal of Applied Mechanics-Transactions of the ASME*, vol. 74, no. 4, pp. 741 – 753, 2007.

[14] Buannic, N. and Cartraud, P., "Higher-order effective modeling of periodic heterogeneous beams. I. asymptotic expansion method," *International Journal of Solids and Structures*, vol. 38, pp. 7139 – 7161, 2001.

[15] Buannic, N. and Cartraud, P., "Higher-order effective modeling of periodic heterogeneous beams. II. derivation of the proper boundary conditions for the interior asymptotic solution," *International Journal of Solids and Structures*, vol. 38, pp. 7163 – 7180, 2001.

[16] Budak, B. M., Samarskiĭ, A. A., and Tikhonov, A. N., *A collection of problems in mathematical physics*, vol. 52. Courier Corporation, 1988.

[17] Cesnik, C. E. S. and Hodges, D. H., "Variational-asymptotical analysis of initially twisted and curved composite beams," *International Journal for Engineering Analysis and Design*, vol. 1, pp. 177 – 187, Apr. 1994.

[18] Cesnik, C. E. S. and Hodges, D. H., "Stiffness constants for composite beams including large initial twist and curvature effects," *Applied Mechanics Reviews*, vol. 48, no. 11, Part 2, pp. S61 – S67, 1995.

[19] Chong, A. C. M., Yang, F., Lam, D. C. C., and Tong, P., "Torsion and bending of micron-scaled structures," *Journal of Materials Research*, vol. 16, no. 4, pp. 1052 – 1058, 2001.

[20] Chroscielewski, J. and Witkowski, W., "On some constitutive equations for micropolar plates," *Zamm-Zeitschrift Fur Angewandte Mathematik Und Mechanik*, vol. 90, no. 1, pp. 53 – 64, 2010.

[21] Claassen, R. W. and Thorne, C. J., "Vibrations of thin rectangular isotropic plates," *Journal of Applied Mechanics*, vol. 28, pp. 304 – 305, 06 1961.

[22] Cohen, H. and Desilva, C. N., "Nonlinear theory of elastic directed surfaces," *Journal of Mathematical Physics*, vol. 7, no. 6, pp. 960 – 966, 1966.

[23] Constanda, C., "On the bending of micropolar plates," *Letters in Applied Engineering and Sciences*, vol. 2, pp. 329 – 339, 1974.

[24] Constanda, C., "Complex variable treatment of bending of micropolar plates," *International Journal of Engineering Science*, vol. 15, no. 11, pp. 661 – 669, 1977.

[25] Cosserat, E. and Cosserat, F., *Théorie des corps déformables*. Hermann, Paris, 1909.

[26] Cowper, G. R., "The shear coefficient in timoshenko's beam theory," *Journal of Applied Mechanics*, vol. 33, pp. 335 – 340, 06 1966.

[27] Dawe, D., "Finite strip models for vibration of mindlin plates," *Journal of Sound and Vibration*, vol. 59, no. 3, pp. 441 – 452, 1978.

[28] Dawe, D. and Roufaeil, O., "Rayleigh-ritz vibration analysis of mindlin plates," *Journal of Sound and Vibration*, vol. 69, no. 3, pp. 345 – 359, 1980.

[29] Demasi, L. and Yu, W. B., "Assess the accuracy of the variational asymptotic plate and shell analysis using the generalized unified formulation," *Mechanics of Advanced Materials and Structures*, vol. 20, no. 3, pp. 227 – 241, 2013.

[30] DeSilva, C. N. and Tsai, P. J., "A general theory of directed surfaces," *Acta Mechanica*, vol. 18, no. 1-2, pp. 89 – 101, 1973.

[31] Diebels, S., "A micropolar theory of porous media: Constitutive modelling," *Transport in Porous Media*, vol. 34, no. 1-3, pp. 193 – 208, 1999.

[32] Diebels, S. and Steeb, H., "Stress and couple stress in foams," *Computational Materials Science*, vol. 28, no. 3 - 4, pp. 714 – 722, 2003. Twelfth International Workshop on Computational Mechanics of Materials.

[33] Diebels, S., "A macroscopic description of the quasi-static behavior of granular materials based on the theory of porous media," *Granular Matter*, vol. 2, no. 3, pp. 143 – 152, 2000.

[34] Ehlers, W., Bluhm, J., and Diebels, S., "Micropolar mixture models on the basis of the theory of porous media," in *Porous Media*, pp. 121–145, Springer, Heidelberg, 2002.

[35] Ellis, R. W. and Smith, C. W., "A thin-plate analysis and experimental evaluation of couple-stress effects," *Experimental Mechanics*, vol. 7, no. 9, pp. 372 – 380, 1967.

[36] Erbay, H., "An asymptotic theory of thin micropolar plates," *International Journal of Engineering Science*, vol. 38, no. 13, pp. 1497 – 1516, 2000.

[37] Ericksen, J. L. and Truesdell, C., "Exact theory of stress and strain in rods and shells," *Archive for Rational Mechanics and Analysis*, vol. 1, no. 1, pp. 295 – 323, 1957.

[38] Eringen, A. C., "Linear theory of micropolar elasticity," *Journal of Mathematics and Mechanics*, vol. 15, no. 6, pp. 909 – 923, 1966.

[39] Eringen, A. C., "Theory of micropolar plates," *Zeitschrift für angewandte Mathematik und Physik*, vol. 18, no. 1, pp. 12 – 30, 1967.

[40] Eringen, A. C., "Theory of micropolar elasticity," in *Microcontinuum field theories*, pp. 101–248, Springer, 1999.

[41] Fatemi, J., Van Keulen, F., and Onck, P. R., "Generalized continuum theories: Application to stress analysis in bone," *Meccanica*, vol. 37, no. 4-5, pp. 385 – 396, 2002.

[42] Fischer-Hjalmars, I., "Mechanics of micropolar media," in *Micropolar phenomena in ordered structures* (Ed. Brulin O., Hsieh, R. K. T., ed.), pp. 395–463, World Scientific, Singapore, 1982.

[43] Fischer-Hjalmars, I., "On the validity of the continuum description of molecular crystals," *International Journal of Engineering Science*, vol. 19, no. 12, pp. 1765 – 1773, 1981.

[44] Fox, D. D. and Simo, J. C., "A drill rotation formulation for geometrically exact shells," *Computer Methods in Applied Mechanics and Engineering*, vol. 98, no. 3, pp. 329 – 343, 1992.

[45] Gao, X. L., Huang, J. X., and Reddy, J. N., "A non-classical third-order shear deformation plate model based on a modified couple stress theory," *Acta Mechanica*, vol. 224, no. 11, pp. 2699 – 2718, 2013.

[46] Gauthier, R. D., "Experimental investigations of micropolar media," in *Mechanics of Micropolar Media* (Ed. Brulin O., Hsieh, R. K. T., ed.), pp. 395–463, World Scientific, Singapore, 1982.

[47] Gauthier, R. D. and Jahsman, W. E., "Quest for micropolar elastic-constants," *Journal of Applied Mechanics-Transactions of the Asme*, vol. 42, no. 2, pp. 369 – 374, 1975.

[48] Gauthier, R. D. and Jahsman, W. E., "A quest for micropolar elastic-constants .2.," *Archives of Mechanics*, vol. 33, no. 5, pp. 717 – 737, 1981.

[49] Gere, J. M. and Timoshenko, S. P., *Mechanics of Materials*. Boston, Massachusetts: PWS-Kent, 3rd ed., 1990.

[50] Gevorkyan, G. A., "The basic equations of flexible plates for a medium of cosserat," *Soviet Applied Mechanics*, vol. 3, no. 11, pp. 41 – 45, 1967.

[51] Goda, I., Assidi, M., Belouettar, S., and Ganghoffer, J. F., "A micropolar anisotropic constitutive model of cancellous bone from discrete homogenization," *Journal of the Mechanical Behavior of Biomedical Materials*, vol. 16, pp. 87 – 108, 2012.

[52] Green, A. E. and Naghdi, P. M., "The linear theory of an elastic cosserat plate," in *Proceedings of the Cambridge Philosophical Society-Mathematical and Physical Sciences*, vol. 63, pp. 537 – 550, 1967.

[53] Green, A. E. and Naghdi, P. M., "Micropolar and director theories of plates," *The Quarterly Journal of Mechanics and Applied Mathematics*, vol. 20, no. 2, pp. 183 – 199, 1967.

[54] Green, A. E., Naghdi, P. M., and Wainwright, W. L., "A general theory of a cosserat surface," *Archive for Rational Mechanics and Analysis*, vol. 20, no. 4, pp. 287 – 308, 1965.

[55] Green, A. E., Naghdi, P. M., and Wenner, M. L., "Linear theory of cosserat surface and elastic plates of variable thickness," in *Mathematical Proceedings of the Cambridge Philosophical Society*, vol. 69, pp. 227 – 254, 1971.

[56] Green, A. and Naghdi, P., "The linear elastic cosserat surface and shell theory," *International Journal of Solids and Structures*, vol. 4, no. 6, pp. 585 – 592, 1968.

[57] Grioli, G., "Elasticite asymmetrique," *Ann. di Mat. Pura et Appl. Ser. IV J*, vol. 50.

[58] Günther, W., "Zur statik und kinematik des cosseratschen kontinuums," *Abh. Braunschweig. Wiss. Ges*, vol. 10, no. 213, p. 1, 1958.

[59] Guo, J.-G. and Zhao, Y.-P., "The size-dependent elastic properties of nanofilms with surface effects," *Journal of Applied Physics*, vol. 98, no. 7, 2005.

[60] Hazell, C. R. and Mitchell, A. K., "Experimental eigenvalues and mode shapes for flat clamped plates," *Experimental Mechanics*, vol. 26, no. 4, pp. 337 – 344, 1986.

[61] Ho, J. C., Yu, W., and Hodges, D. H., "Energy transformation to generalized timoshenko form by the variational asymptotic beam section analysis," in *51st AIAA/ASME/ASCE/AHS/ASC Structures, Structural Dynamics and Materials Conference, Orlando, Florida*, April 12 – 15, 2010. Paper AIAA-2010-3017.

[62] Hodges, D. H., "Orthogonal polynomials as variable-order finite element shape functions," *AIAA Journal*, vol. 21, no. 5, pp. 796 – 797, 1983.

[63] Hodges, D. H., Atilgan, A. R., Cesnik, C. E. S., and Fulton, M. V., "On a simplified strain energy function for geometrically nonlinear behaviour of anisotropic beams," *Composites Engineering*, vol. 2, no. 5 - 7, pp. 513 – 526, 1992.

[64] Hodges, D. H., Atilgan, A. R., and Danielson, D. A., "A geometrically nonlinear-theory of elastic plates," *Journal of Applied Mechanics-Transactions of the Asme*, vol. 60, no. 1, pp. 109 – 116, 1993.

[65] Hodges, D. H., Lee, B. W., and Atilgan, A. R., "Application of the variational-asymptotical method to laminated composite plates," *AIAA Journal*, vol. 31, no. 9, pp. 1674 – 1683, 1993.

[66] Hodges, D. H., Yu, W. B., and Patil, M. J., "Geometrically-exact, intrinsic theory for dynamics of moving composite plates," *International Journal of Solids and Structures*, vol. 46, no. 10, pp. 2036 – 2042, 2009.

[67] Hodges, D. H., "A mixed variational formulation based on exact intrinsic equations for dynamics of moving beams," *International Journal of Solids and Structures*, vol. 26, no. 11, pp. 1253 – 1273, 1990.

[68] Hodges, D. H., "Geometrically-exact, intrinsic theory for dynamics of curved and twisted anisotropic beams," *AIAA Journal*, vol. 41, pp. 1131 – 1137, June 2003.

[69] Hodges, D. H., "Geometrically exact, intrinsic theory for dynamics of curved and twisted anisotropic beams," *AIAA Journal*, vol. 41, pp. 1131 – 1137, 2015/07/06 2003.

[70] Hodges, D. H., *Nonlinear Composite Beam Theory*, vol. 205 of *Progress in Astronautics and Aeronautics*. Reston, Virginia: AIAA, 2006.

[71] Hughes, T. J. R. and Brezzi, F., "On drilling degrees of freedom," *Computer Methods in Applied Mechanics and Engineering*, vol. 72, no. 1, pp. 105–121, 1989.

[72] Ibrahimbegović, A., "Stress resultant geometrically nonlinear shell theory with drilling rotations .1. a consistent formulation," *Computer Methods in Applied Mechanics and Engineering*, vol. 118, no. 3 - 4, pp. 265 – 284, 1994.

[73] Iesan, D., "The plane micropolar strain of orthotropic elastic solids(static theory of plane micropolar strain for homogeneous orthotropic elastic solids, deriving existence and uniqueness theorems and reducing boundary value problems to fredholm equations)," *Archiwum Mechaniki Stosowanej*, vol. 25, no. 3, pp. 547 – 561, 1973.

[74] Iesan, D., "Bending of orthotropic micropolar elastic beams by terminal couples," *An. Şt. Univ. Iaşi, Matematică*, vol. 20, pp. 411 – 418, 1974.

[75] Iesan, D., "Torsion of anisotropic micropolar elastic cylinders," *Zeitschrift Fur Angewandte Mathematik Und Mechanik*, vol. 54, no. 12, pp. 773 – 779, 1974.

[76] Ieşan, D. and Scalia, A., "On the deformation of orthotropic cosserat elastic cylinders," *Mathematics and Mechanics of Solids*, vol. 16, no. 2, pp. 177 – 199, 2011.

[77] Jasiuk, I. and Boccara, S., "On the reduction of constants in plane elasticity with eigenstrains," *Archives of Mechanics*, vol. 54, no. 5 - 6, pp. 425 – 437, 2002.

[78] Jomehzadeh, E., Noori, H. R., and Saidi, A. R., "The size-dependent vibration analysis of micro-plates based on a modified couple stress theory," *Physica E: Low-dimensional Systems and Nanostructures*, vol. 43, pp. 877 – 883, 2 2011.

[79] Kafadar, C. and Eringen, A. C., "Micropolar media—i the classical theory," *International Journal of Engineering Science*, vol. 9, no. 3, pp. 271 – 305, 1971.

[80] Kim, J.-S. and Wang, K. W., "Vibration analysis of composite beams with end effects via the formal asymptotic method," *Journal of Vibration and Acoustics*, vol. 132, pp. 041003–1, 2010.

[81] Koiter, W., "Couple stresses in the theory of elasticity, i and ii," in *Nederl. Akad. Wetensch. Proc. Ser. B*, vol. 67, pp. 17 – 29, 1964.

[82] Kong, S., Zhou, S., Nie, Z., and Wang, K., "The size-dependent natural frequency of bernoulliâ"euler micro-beams," *International Journal of Engineering Science*, vol. 46, pp. 427 – 437, 5 2008.

[83] Kovvali, R. K. and Hodges, D. H., "Verification of the variational-asymptotic sectional analysis for initially curved and twisted beams," *Journal of Aircraft*, vol. 49, pp. 861 – 869, 2015/07/24 2012.

[84] Kuhn, P. and Figge, I., "Unified notch-strength analysis for wrought aluminum alloys." NASA, TN D-1259, May 1962.

[85] Kumar, A., Mukherjee, S., Paci, J. T., Chandraseker, K., and Schatz, G. C., "A rod model for three dimensional deformations of single-walled carbon nanotubes," *International Journal of Solids and Structures*, vol. 48, no. 20, pp. 2849–2858, 2011.

[86] Kumar, R. and Choudhary, S., "Response of orthotropic micropolar elastic medium due to various sources," *Meccanica*, vol. 38, no. 3, pp. 349 – 368, 2003.

[87] Kuvshinskii, R. and Aero, E., "Continuum theory of asymmetric elasticity-the problem of internal rotation," *Soviet Physics-Solid State*, vol. 5, no. 9, pp. 1892 – 1897, 1964.

[88] Kvasov, R. and Steinberg, L., "Numerical modeling of bending of micropolar plates," *Thin-Walled Structures*, vol. 69, pp. 67 – 78, 2013.

[89] Lakes, R., "Experimental micro mechanics methods for conventional and negative poisson's ratio cellular solids as cosserat continua," *Journal of Engineering Materials and Technology*, vol. 113, pp. 148 – 155, 01 1991.

[90] Lakes, R., "Experimental methods for study of Cosserat elastic solids and other generalized elastic continua," *Continuum models for materials with microstructure*, pp. 1 – 25, 1995.

[91] Lakes, R. S., "Size effects and micromechanics of a porous solid," *Journal of Materials Science*, vol. 18, no. 9, pp. 2572–2580, 1983.

[92] Lakes, R., "Experimental microelasticity of two porous solids," *International Journal of Solids and Structures*, vol. 22, no. 1, pp. 55 – 63, 1986.

[93] Le, K. C., *Vibrations of Shells and Rods*. Germany: Springer, 1st ed., 1999.

[94] Lee, C.-Y. and Hodges, D. H., "Hybrid transformation to a generalized reissner–mindlin theory for composite plates," *Journal of Applied Mechanics*, vol. 82, no. 9, p. 091005, 2015.

[95] Leissa, A. W., "Vibration of plates," tech. rep., DTIC Document, 1969.

[96] Lekhnitskii, S. G., *Theory of Elasticity of An Anisotropic Body*. Holden-Day Inc., 1963.

[97] Lu, Q., Arroyo, M., and Huang, R., "Elastic bending modulus of monolayer graphene," *Journal of Physics D: Applied Physics*, vol. 42, no. 10, p. 102002, 2009.

[98] Ma, H. M., Gao, X. L., and Reddy, J. N., "A non-classical mindlin plate model based on a modified couple stress theory," *Acta Mechanica*, vol. 220, no. 1 - 4, pp. 217 – 235, 2011.

[99] McFarland, A. W. and Colton, J. S., "Role of material microstructure in plate stiffness with relevance to microcantilever sensors," *Journal of Micromechanics and Microengineering*, vol. 15, no. 5, pp. 1060 – 1067, 2005.

[100] Mindlin, R. D., "Influence of couple-stresses on stress concentrations," *Experimental Mechanics*, vol. 3, no. 1, pp. 1 – 7, 1963.

[101] Mindlin, R. D. and Tiersten, H. F., "Effects of couple-stresses in linear elasticity," vol. 11, no. 1, pp. 415 – 448, 1962.

[102] Minguet, P. and Dugundji, J., "Experiments and analysis for composite blades under large deflections. part I – static behavior," *AIAA Journal*, vol. 28, pp. 1573 – 1579, September 1990.

[103] Minguet, P. and Dugundji, J., "Experiments and analysis for composite blades under large deflections. part II – dynamic behavior," *AIAA Journal*, vol. 28, pp. 1580 – 1588, September 1990.

[104] Naghdi, P. M., "The Theory of Plates and Shells," *Handbuch der Physik*, vol. VI a/2, pp. 425 – 640, 1972.

[105] Naghdi, P. M. and Rubin, M. B., "Restrictions on nonlinear constitutive-equations for elastic shells," *Journal of Elasticity*, vol. 39, no. 2, pp. 133 – 163, 1995.

[106] Neuber, H., *Theory of notch stresses; principles for exact stress calculation.* Ann Arbor, J. W. Edwards, 1946.

[107] Nowacki, W., *Theory of Asymmetric Elasticity, 1986.* Pergamon Press, Oxford, 1986.

[108] Odegard, G. M., Gates, T. S., Nicholson, L. M., and Wise, K. E., "Equivalent-continuum modeling of nano-structured materials," *Composites Science and Technology*, vol. 62, no. 14, pp. 1869–1880, 2002.

[109] Ogden, R. W., *Non-linear elastic deformations.* Dover Publications 1997 and Ellis Horwood 1984, 1997.

[110] Pabst, W., "Micropolar materials," *Ceramics-Silikaty*, vol. 49, no. 3, pp. 170 – 180, 2005.

[111] Pal'mov, V. A., "Fundamental equations of the theory of asymmetric elasticity," *Journal of Applied Mathematics and Mechanics*, vol. 28, no. 3, pp. 496 – 505, 1964.

[112] Park, H. and Lakes, R., "Cosserat micromechanics of human bone: Strain redistribution by a hydration sensitive constituent," *Journal of Biomechanics*, vol. 19, no. 5, pp. 385 – 397, 1986.

[113] Patil, M. J. and Hodges, D. H., "Flight dynamics of highly flexible flying wings," *Journal of Aircraft*, vol. 43, no. 6, pp. 1790 – 1799, 2006.

[114] Patil, M. J. and Althoff, M., "Energy-consistent, galerkin approach for the nonlinear dynamics of beams using intrinsic equations," *Journal of Vibration and Control*, vol. 17, no. 11, pp. 1748 – 1758, 2011.

[115] Patil, M. J. and Hodges, D. H., "Variable-order finite elements for nonlinear, fully intrinsic beam equations," *Journal of Mechanics of Materials and Structures*, vol. 6, no. 1, pp. 479 – 493, 2011.

[116] Perkins, R. W. and Thompson, D., "Experimental evidence of a couple-stress effect," *AIAA Journal*, vol. 11, no. 7, pp. 1053 – 1055, 1973.

[117] Peterson, R. E., *Stress concentration Design factors.* J. Wiley and Sons, Inc., New York, 1953.

[118] Pietraszkiewicz, W. and Eremeyev, V. A., "On natural strain measures of the non-linear micropolar continuum," *International Journal of Solids and Structures*, vol. 46, no. 3-4, pp. 774 – 787, 2009.

[119] Pietraszkiewicz, W. and Konopińska, V., "Drilling couples and refined constitutive equations in the resultant geometrically non-linear theory of elastic shells," *International Journal of Solids and Structures*, vol. 51, no. 11 - 12, pp. 2133 – 2143, 2014.

[120] Popescu, B. and Hodges, D. H., "On asymptotically correct Timoshenko-like anisotropic beam theory," *International Journal of Solids and Structures*, vol. 37, no. 3, pp. 535 – 558, 2000.

[121] Pouget, J., Aşkar, A., and Maugin, G. A., "Lattice model for elastic ferroelectric crystals: Microscopic approach," *Phys. Rev. B*, vol. 33, pp. 6304 – 6319, May 1986.

[122] Rajagopal, A., Hodges, D. H., and Yu, W., "Asymptotic beam theory for planar deformation of initially curved isotropic strips," *Thin-Walled Structures*, pp. 1067 – 1072, 2011. to appear.

[123] Rajalingham, C., Bhat, R. B., and Xistris, G. D., "Vibration of rectangular plates using plate characteristic functions as shape functions in the rayleigh–ritz method," *Journal of Sound and Vibration*, vol. 193, pp. 497 – 509, 6 1996.

[124] Reissner, E., "On kinematics and statics of finite-strain force and moment stress elasticity," *Studies in Applied Mathematics*, vol. 52, pp. 97 – 101, June 1973.

[125] Reissner, E., "Linear and nonlinear theory of shells," in *Thin-shell Structures: Theory, Experiment, and Design* (Fung, Y. C. and Sechler, E. E., eds.), pp. 29–44, Prentice-Hall, Englewood Cliffs, New Jersey, 1974.

[126] Reissner, E., "Note on the equations of finite-strain force and moment stress elasticity," *Studies in Applied Mathematics*, vol. 54, pp. 1 – 8, 1975.

[127] Reissner, E., "A further note on finite-strain force and moment stress elasticity," *Zeitschrift für angewandte Mathematik und Physik*, vol. 38, no. 5, pp. 665 – 673, 1987.

[128] Roque, C. M. C., Ferreira, A. J. M., and Reddy, J. N., "Analysis of mindlin micro plates with a modified couple stress theory and a meshless method," *Applied Mathematical Modelling*, vol. 37, pp. 4626–4633, 4 2013.

[129] Rössle, A., "On the derivation of an asymptotically correct shear correction factor for the reissner-mindlin plate model," *Comptes Rendus de l'AcadÃ©mie des Sciences - Series I - Mathematics*, vol. 328, pp. 269 – 274, 2 1999.

[130] Scarpa, F., Adhikari, S., and Phani, A. S., "Effective elastic mechanical properties of single layer graphene sheets," *Nanotechnology*, vol. 20, no. 6, p. 065709, 2009.

[131] Schiavone, P., "On existence theorems in the theory of extensional motions of thin micropolar plates," *International Journal of Engineering Science*, vol. 27, no. 9, pp. 1129 – 1133, 1989.

[132] Schiavone, P., "Uniqueness in dynamic problems of thin micropolar plates," *Applied Mathematics Letters*, vol. 4, no. 2, pp. 81 – 83, 1991.

[133] Schiavone, P. and Constanda, C., "Existence theorems in the theory of bending of micropolar plates," *International Journal of Engineering Science*, vol. 27, no. 4, pp. 463 – 468, 1989.

[134] Schijve, J., "Note on couple stresses," *Journal of the Mechanics and Physics of Solids*, vol. 14, no. 2, pp. 113 – 120, 1966.

[135] Selmi, A., Hassis, H., Doghri, I., and Zenzri, H., "A cosserat-type plate theory and its application to carbon nanotube microstructure," *American Journal of Applied Sciences*, vol. 11, no. 8, p. 1255, 2014.

[136] Simmonds, J. G. and Danielson, D. A., "Nonlinear shell theory with finite rotation and stress-function vectors," *Journal of Applied Mechanics*, vol. 39, no. 4, pp. 1085 – 1090, 1972.

[137] Simo, J. C., Fox, D. D., and Hughes, T. J. R., "Formulations of finite elasticity with independent rotations," *Computer Methods in Applied Mechanics and Engineering*, vol. 95, no. 2, pp. 277 – 288, 1992.

[138] Sotoudeh, Z., "A new element for mixed plate formulation," in *56th AIAA/ASCE/AHS/ASC Structures, Structural Dynamics, and Materials Conference*, American Institute of Aeronautics and Astronautics, 2015.

[139] Sotoudeh, Z. and Hodges, D. H., "Incremental method for structural analysis of joined-wing aircraft," *Journal of Aircraft*, vol. 48, no. 5, pp. 1588 – 1601, 2011.

[140] Sotoudeh, Z. and Hodges, D. H., "Modeling beams with various boundary conditions using fully intrinsic equations," *Journal of Applied Mechanics*, vol. 78, no. 3, pp. 031010–031010–9, 2011.

[141] Srinivas, S., Rao, C. J., and Rao, A., "An exact analysis for vibration of simply-supported homogeneous and laminated thick rectangular plates," *Journal of Sound and Vibration*, vol. 12, no. 2, pp. 187 – 199, 1970.

[142] Steinberg, L., "Deformation of micropolar plates of moderate thickness," *International Journal of Applied Mathematics and Mechanics*, vol. 6, no. 17, pp. 1 – 24, 2010.

[143] Steinberg, L. and Kvasov, R., "Enhanced mathematical model for cosserat plate bending," *Thin-Walled Structures*, vol. 63, pp. 51 – 62, 2013.

[144] Steinberg, L. and Kvasov, R., "Analytical modeling of vibration of micropolar plates," *Applied Mathematics*, vol. 6, no. 05, pp. 817 – 836, 2015.

[145] Sutyrin, V. G., "Derivation of plate theory accounting asymptotically correct shear deformation," *Journal of Applied Mechanics*, vol. 64, no. 4, pp. 905 – 915, 1997.

[146] Szabo, B. A. and Babuška, I., *Finite element analysis*. John Wiley & Sons, 1991.

[147] Timoshenko, P. S., "X. on the transverse vibrations of bars of uniform cross-section," *Philosophical Magazine Series 6*, vol. 43, no. 253, pp. 125 – 131, 1922.

[148] Toupin, R. A., "Elastic materials with couple-stresses," *Archive for Rational Mechanics and Analysis*, vol. 11, no. 1, pp. 385 – 414, 1962.

[149] Toupin, R. A., "Theories of elasticity with couple-stress," *Archive for Rational Mechanics and Analysis*, vol. 17, no. 2, pp. 85 – 112, 1964.

[150] Truesdell, C. and Toupin, R., *The classical field theories*. Springer, 1960.

[151] Tsiatas, G. C., "A new kirchhoff plate model based on a modified couple stress theory," *International Journal of Solids and Structures*, vol. 46, pp. 2757 – 2764, 6 2009.

[152] Vijayakumar, K. and Ramaiah, G. K., "Analysis of vibration of clamped square plates by the rayleigh-ritz method with asymptotic solutions from a modified bolotin method," *Journal of Sound and Vibration*, vol. 56, pp. 127 – 135, 1 1978.

[153] Voigt, W., "Theoretische studien über die elasticitätsverhältnisse der krystalle," in *Abhandlungen der Königlichen Gesellschaft der Wissenschaften zu Göttingen*, vol. 24, Göttingen, 1887.

[154] Wang, F.-Y., "On the solutions of eringen's micropolar plate equations and of other approximate equations," *International Journal of Engineering Science*, vol. 28, no. 9, pp. 919 – 925, 1990.

[155] Waseem, A., Beveridge, A. J., Wheel, M. A., and Nash, D. H., "The influence of void size on the micropolar constitutive properties of model heterogeneous materials," *European Journal of Mechanics a-Solids*, vol. 40, pp. 148 – 157, 2013.

[156] Wittrick, W., "Analytical, three-dimensional elasticity solutions to some plate problems, and some observations on mindlin's plate theory," *International Journal of Solids and Structures*, vol. 23, no. 4, pp. 441 – 464, 1987.

[157] Xing, Y. F. and Liu, B., "New exact solutions for free vibrations of thin orthotropic rectangular plates," *Composite Structures*, vol. 89, pp. 567–574, 8 2009.

[158] Yang, J. F. C. and Lakes, R. S., "Transient study of couple stress effects in compact-bone - torsion," *Journal of Biomechanical Engineering-Transactions of the Asme*, vol. 103, no. 4, pp. 275 – 279, 1981.

[159] Yang, J. and Lakes, R. S., "Experimental study of micropolar and couple stress elasticity in compact bone in bending," *Journal of Biomechanics*, vol. 15, no. 2, pp. 91 – 98, 1982.

[160] Yin, L., Qian, Q., Wang, L., and Xia, W., "Vibration analysis of microscale plates based on modified couple stress theory," *Acta Mechanica Solida Sinica*, vol. 23, pp. 386 – 393, 10 2010.

[161] Young, D., "Vibration of rectangular plates by the ritz method," *Journal of Applied Mechanics-Transactions of the ASME*, vol. 17, no. 4, pp. 448 – 453, 1950.

[162] Yu, W., "Mathematical construction of a reissner-mindlin plate theory for composite laminates," *International Journal of Solids and Structures*, vol. 42, pp. 6680–6699, 2005.

[163] Yu, W. and Hodges, D. H., "Elasticity solutions versus asymptotic sectional analysis of homogeneous, isotropic, prismatic beams," *Journal of Applied Mechanics*, vol. 71, no. 1, pp. 15 – 23, 2004.

[164] Yu, W. B. and Blair, M., "GEBT: A general-purpose nonlinear analysis tool for composite beams," *Composite Structures*, vol. 94, no. 9, pp. 2677 – 2689, 2012.

[165] Yu, W., "Efficient high-fidelity simulation of multibody systems with composite dimensionally reducible components," *Journal of the American Helicopter Society*, vol. 35, no. 1, pp. 49 – 57, 2007.

[166] Yu, W., Hodges, D. H., and Volovoi, V. V., "Asymptotic construction of Reissner-like models for composite plates with accurate strain recovery," *International Journal of Solids and Structures*, vol. 39, no. 20, pp. 5185 – 5203, 2002.

[167] Yu, W., Hodges, D. H., and Volovoi, V. V., "Asymptotically accurate 3-D recovery from Reissner-like composite plate finite elements," *Computers and Structures*, vol. 81, no. 7, pp. 439 – 454, 2003.

[168] Yu, W., Hodges, D. H., Volovoi, V. V., and Cesnik, C. E. S., "On Timoshenko-like modeling of initially curved and twisted composite beams," *International Journal of Solids and Structures*, vol. 39, no. 19, pp. 5101 – 5121, 2002.

[169] Yu, W. and Tang, T., "Variational asymptotic method for unit cell homogenization of periodically heterogeneous materials," *International Journal of Solids and Structures*, vol. 44, no. 11, pp. 3738–3755, 2007.

[170] Yu, W., Volovoi, V. V., Hodges, D. H., and Hong, X., "Validation of the variational asymptotic beam sectional (VABS) analysis," *AIAA Journal*, vol. 40, pp. 2105 – 2112, Oct. 2002.

VITA

Ravi Kumar Kovvali was born on December 27, 1987 in Sheffield, England. He received a Bachelors degree in Aerospace Engineering in July 2009 from the Indian Institute of Technology Madras (IITM). He started his graduate studies in August of 2009 in the School of Aerospace Engineering at the Georgia Institute of Technology. The work presented in this thesis on Cosserat elastic plates is a result of the last three years of his research under the guidance of Prof. Dewey Hodges.